Role of REV-ERBα in the regulation of lung inflammation

A thesis submitted to the University of Manchester for the degree of
Doctor of Philosophy in the Faculty of Biology, Medicine and Health

2016

Marie Pariollaud

School of Medical Sciences

Division of Diabetes, Endocrinology & Gastroenterology

List of contents

List of figures

List of tables

List of abbreviations

-/-	knock out
AM	alveolar macrophages
AP-1	activator protein 1
ARE	antioxidant response element
BAL	bronchoalveolar lavage
BEGM	bronchial epithelial growth medium
bHLH	basic Helix-Loop-Helix
BMAL1	brain and Muscle ARNT-Like-1
BSA	bovine serum albumine
CCG	clock-controlled gene
CCSP	clara cell secretory protein
cDNA	complementary deoxyribonucleic acid
CLOCK	circadian Locomoter Output Cycles Kaput
COPD	chronic obstructive pulmonary disease
CRY	cryptochrome
CS	cigarette smoke
CT	circadian time (indicating constant conditions)
DEX	dexamethasone
FBS	fetal bovine serum
G-CSF	granulocyte colony-stimulating factor
GCL	glutamate cysteine ligase
GM-CSF	granulocyte-macrophage colony-stimulating factor
GR	glucocorticoid receptor
GRE	GR response element
HDAC3	histone deacetylase 3
H_2O_2	hydrogen peroxide
HO-1	heme oxygenase-1
IL	interleukin
i.p.	intraperitoneal
ipRGC	intrinsically photoreceptive retinal ganglion cell
KEAP1	Kelch-like-ECH-associated protein 1
LD	light-dark cycle

LPS	lipopolysaccharide
LUC	luciferase
LysM	lysozyme M
MAPK	mitogen-activated protein kinase
MARE	Maf-recognition element
mRNA	messenger deoxyribonucleic acid
NAD	nicotinamide adenine dinucleotide
NCoR1	nuclear receptor co-repressor 1
NF-κB	nuclear factor kappa b
NHBE	normal human bronchial epithelial
NK	natural killer
NQO1	NAD(P)H:quinone oxidoreductase 1
NR1D1	nuclear receptor subfamily 1, group D member 1
NR1D2	nuclear receptor subfamily 1, group D member 2
NRF2	nuclear factor erythroid 2
PAS	period-Arnt-Single-minded
PEC	peritoneal exudate cell
PER	period
PMSF	phenylmethanesulfonylfluoride
qPCR	quantitative polymerase chain reaction
RA	rheumatoid arthritis
Rev-DR2	Rev monomer sites arranged as direct repeats separated by 2 bp
RORα	retinoic acid-related orphan nuclear receptor alpha
RORE	retinoic acid-related orphan response elements
ROS	reactive oxygen species
rRNA	ribosomal ribonucleic acid
SCN	suprachiasmatic nucleus
SD	standard deviation
SEM	standard error of the mean
siRNA	small interfering ribonucleic acid
TLR	toll like receptor
TNF-α	tumor necrosis factor alpha
ZT	Zeitgeber time (indicating the presence of an external timing cue)

Abstract

The University of Manchester

Submitted by Marie Pariollaud for the degree of Doctor of Philosophy and entitled: Role of REV-ERBα in the regulation of lung inflammation, 2016.

The clock-controlled nuclear receptor REV-ERBα has emerged as a critical regulator of multiple pathways involved in metabolism, development and immunity. Recent evidence has highlighted a major role for the clock in epithelial cells regulating lung inflammation, mediated by control of neutrophil chemokine expression. In this thesis, I examined the role of REV-ERBα in pulmonary immunity, using *in-vivo* gene targeting and nebulised lipopolysaccharide (LPS), a model for gram-negative bacterial infection, *ex-vivo* cell biology approaches and *in vitro* cell models.

Initial studies of *Rev-Erbα* knock-out mice revealed an increase in pulmonary neutrophilia and inflammation upon aerosolised LPS challenge. Moreover, by selectively deleting the REV-ERBα DNA binding domain (DBD) in the mouse bronchial epithelium, I observed exaggerated inflammatory responses to LPS and augmented CXCL5 secretion. Interestingly, a dual deletion of REV-ERBα DBD and REV-ERBβ in mouse bronchial epithelium had a more dramatic effect on neutrophil recruitment and chemokine secretion than deletion of just the REV-ERBα DBD; in both basal and bacterial challenged conditions. *Ex-vivo* analysis revealed bronchial epithelial cells and macrophages both responded to novel REV-ERBα synthetic ligand GSK1362 but displayed divergent inflammatory responses in presence of this compound. Finally, I observed a striking loss of REV-ERBα protein upon pro-inflammatory challenge. Further analysis revealed this degradation was dependent on the 26S proteasome and driven by sumoylation and ubiquitination of REV-ERBα. However, by using novel REV-ERB ligand GSK1362, these post-translational modifications were blocked and the protein protected from degradation.

Collectively, my results propose a new model for a central role for REV-ERBα in conferring clock control to lung neutrophilic inflammation. I have also identified a feed-forward circuit activated by inflammatory stimuli, leading to suppression of the endogenous anti-inflammatory REV-ERBα protein. Finally, I have discovered a novel mechanism for small-molecule regulation of REV-ERBα, operating via suppression of endogenous protein ubiquitination process. These observations implicate REV-ERBα as a novel therapeutic target in human inflammatory disease.

Declaration

No portion of the work referred to in this thesis has been submitted in support of an application for another degree or qualification of this or any other university or other institute of learning.

Copyright Statement

i. The author of this thesis (including any appendices and/or schedules to this thesis) owns certain copyright or related rights in it (the "Copyright") and s/he has given The University of Manchester certain rights to use such Copyright, including for administrative purposes.

ii. Copies of this thesis, either in full or in extracts and whether in hard or electronic copy, may be made only in accordance with the Copyright, Designs and Patents Act 1988 (as amended) and regulations issued under it or, where appropriate, in accordance with licensing agreements which the University has from time to time. This page must form part of any such copies made.

iii. The ownership of certain Copyright, patents, designs, trade marks and other intellectual property (the "Intellectual Property") and any reproductions of copyright works in the thesis, for example graphs and tables ("Reproductions"), which may be described in this thesis, may not be owned by the author and may be owned by third parties. Such Intellectual Property and Reproductions cannot and must not be made available for use without the prior written permission of the owner(s) of the relevant Intellectual Property and/or Reproductions.

iv. Further information on the conditions under which disclosure, publication and commercialisation of this thesis, the Copyright and any Intellectual Property and/or Reproductions described in it may take place is available in the University IP Policy (see http://documents.manchester.ac.uk/display.aspx?DocID=24420), in any relevant Thesis restriction declarations deposited in the University Library, The University Library's regulations (see http://www.manchester.ac.uk/library/aboutus/regulations) and in The University's policy on Presentation of Theses.

Acknowledgements

I would like to thank my supervisors Professor David Ray and Professor Andrew Loudon and my advisor Professor Julian Davis for their excellent guidance and support throughout this project. David and Andrew have been mentors not only in terms of the scientific direction of the project but also with respect to career progression.

Members of the Ray and Loudon lab groups have been fantastic to work with, and I would especially like to acknowledge the technical support provided by Nicola Begley and Ryan Vonslow. They are both incredible skilled technicians who were always willing to help me with animal experiments, even in the middle of the night. Also to Dr Julie Gibbs, Dr. Shona Wood, Dr. Ben Saer, Dr. Zhenguang Zhang, Tom Hopwood and Joanna Woodburn who contributed to the work contained in this thesis either directly through their skills or indirectly through their emotional support.

I would also like to acknowledge the support of GlaxoSmithKline by providing new ligands, antibody, mice and by carrying the cigarette smoke experiments. Especially to Stuart Farrow who contributed greatly at the beginning of this project, and to Yolanda Sanchez who continuously overlooked it and who always have been a fantastic mentor and an inspirational figure as woman scientist. I am very grateful of this productive collaboration with GlaxoSmithKline through my project.

I would also like to extend my thanks to my family and especially to my mum and dad who have supported me throughout my studies and my career choices; they will be glad that I might finally stop being a student and enter the real world of work.

Finally, to my partner, Andrew, who sometimes had to bear my "crazy moods" due to non-working experiments (such as the ChIP experiments). His support over the last three years has been invaluable, particularly in respect of driving me to the lab over the weekends and cooking delicious comforting food.

Chapter 1:   Introduction

1.1 Overview of circadian rhythms

Organisms in every kingdom of life, from bacteria to humans, exhibit endogenous circadian rhythms in behaviour, physiology and metabolism. Processes such as sleep/wake cycle, feeding, core body temperature and other metabolic patterns, display circadian (from the Latin *circa diem* which means "about a day") oscillations with a period of about 24 hours which is correlated to the natural period of the Earth's rotation. Indeed, circadian rhythms are thought to have evolved in response to daily light/dark cycle and also to season cycle in order to allow organisms to be attuned to the rhythmic world (Paranjpe and Sharma, 2005).

Organisms possess an intrinsic clock system; in the absence of any environmental cues, for example by being kept in constant darkness, the free-running circadian pacemaker period is slightly offset to 24 hours. To avoid drifting off phase with the solar day, rhythmic environmental signals called zeitgebers ("synchronizer" in German) such as light for the main cue, but also availability of food, temperature and social interactions reset the internal clock period through daily phase shifts (Pittendrigh, 1993). Thanks to this process termed entrainment, circadian rhythms allow organisms to anticipate and prepare for rhythmic environmental changes adapting their physiology and behaviour.

1.1.1 A core circadian clock located in the SCN

It is now well established that the central circadian pacemaker synchronizing rhythms in mammals resides in the suprachiasmatic nucleus (SCN) in the brain (for review Takahashi, 1995; Welsh et al., 2010). The SCN is situated in the anterior hypothalamus directly above the optic chiasm (Figure 1.1). Studies have shown that complete SCN lesions eliminate many circadian rhythms and provoke arrhythmic activity (Eastman et al., 1984). The hypothesis of SCN as core clock regulating other rhythmic systems has been supported by transplant studies: transplanting the SCN from hamsters into hamsters with the lesioned SCN restored rhythms but which displayed the clock properties (period or phase) of the donor rather than of the host (Ralph et al., 1990).
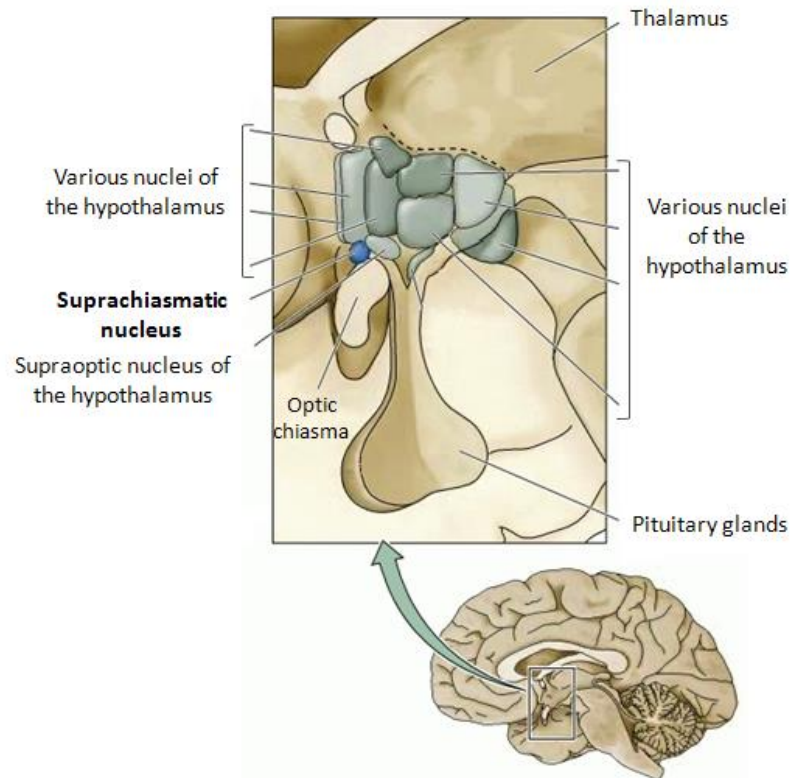
Figure 1.1: Location of the suprachiasmatic nucleus (SCN) in the mammalian brain
The name "suprachiasmatic" derives from the location of the nucleus just above the optic chiasm. Modified from Neuroscience, 2nd edition book (2001), chapter: The Circadian Cycle of Sleep and Wakefulness.

1.1.1.1 The core circadian clock is mainly entrained by light

Even if other environmental cues such as temperature and food availability can modulate circadian rhythms, the light-dark cycle of the solar day appears to be the most potent zeitgeber to entrain circadian system in mammals. Light activates a specific group of photoreceptors in the retina which send information to the hypothalamic SCN through a dedicated pathway called the retinohypothalamic tract (Rea, 1998). Recently, a photoreceptor cell type termed the intrinsically photoreceptive retinal ganglion cell (ipRGC) has emerged as a key circadian photoreceptor relaying information from the retina to the brain to control circadian photoentrainment, pupillary light reflex, and sleep (Schmidt et al., 2011).

1.1.2 Peripheral circadian oscillators

Along with the circadian pacemaker in the SCN, other circadian oscillators distributed throughout the tissues of mice, humans, and other organisms have been found. A recent study has revealed that nearly half of all genes in the mouse genome oscillate with circadian rhythm somewhere in the body (Zhang et al., 2014). Circadian clocks in the periphery were previously regarded as only "slave oscillators", requiring a regular input from the master clock in the SCN to oscillate (Reppert and Weaver, 2002). This view has been convincingly revised as circadian activity was recorded *ex vivo* in almost every organ of the body including pancreas (Peschke and Peschke, 1998), liver, heart, skeletal muscle (Zylka et al., 1998) and lungs (Bando et al., 2007). It is now recognized that the role of SCN is more to coordinate the timing of peripheral oscillators and maintain an appropriate phase relationship among them rather than driving circadian rhythms (Yoo et al., 2004). To do so, a time-of-day message is sent by the SCN to the peripheral tissues by means of hormonal rhythms, multisynaptic autonomic connections into the organs of the body and multiple other pathways (Buijs et al., 2003). Therefore, the circadian system relies on a constant exchange of timing information to maintain a good harmony between all these individual oscillators throughout the tissues. Cellular clocks respond to stimuli (inputs) from the external environment or other cells, integrate the information into their own clock system and transfer time-related information to other cells (outputs) to adjust proper metabolic and physiological processes. In turn, internal environmental signals from the tissues are returned to the clock as inputs (Figure 1.2).

1.1.3 The molecular basis of circadian rhythms

Studies over the past few years have defined an underlying genetic basis for circadian timing. A unifying theme in circadian clockwork mechanisms in both central and peripheral locations is the presence of interacting, self-sustained transcriptional and translational feedbacks loops. Major advances in understanding the molecular basis of the mammal circadian clock have been made over the past 15 years: many circadian genes have been discovered and their interaction within multiple transcriptional and translational feedbacks loops have started to be elucidated (for review Mohawk et al., 2012).
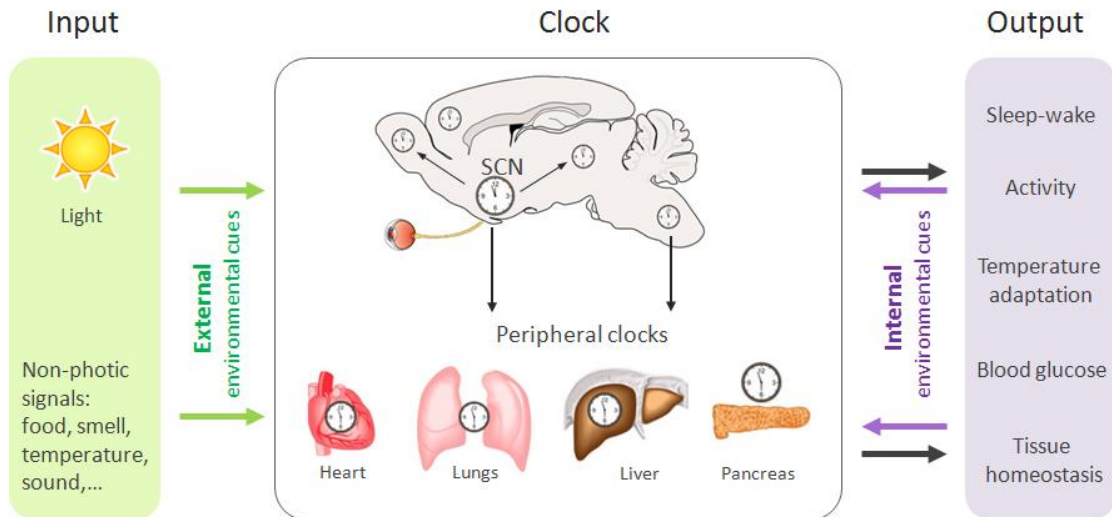
Figure 1.2: Schematic representation of the organization of the circadian system: a feedback at nearly every level

The central clock in the SCN is mainly entrained by light through retina photoreceptors but also by other external environmental cues such as food availability and temperature. The SCN then synchronizes peripheral clocks in organs which may elicit the onset of specific behaviours and tissue activities. The non-photic signals can also directly influence peripheral clocks. In turn, "outputs" such as activity, body temperature rhythms become inputs and participate in the phase entrainment of peripheral clocks.

The mechanism of the circadian clock in mammals is cell autonomous and consists of an autoregulatory positive and negative-feedback transcriptional network (Figure 1.3). The positive transcriptional elements include two basic Helix-Loop-Helix (bHLH) transcription factors, Circadian Locomoter Output Cycles Kaput (CLOCK, or its paralog NPAS2 in brain tissue) and Brain and Muscle ARNT-Like-1 (BMAL1) which bind each other through common Period-Arnt-Single-minded (PAS) domains (Reppert and Weaver, 2002). This heterodimer then binds to E-box sequences on promoters of *Periods* (*Per1*, *Per2*) and *Cryptochromes* (*Cry1*, *Cry2*) to induce their transcription. Upon translation, PER and CRY proteins accumulate in the cytoplasm, dimerize to form a complex which migrates into the nucleus to interact with CLOCK and/or BMAL1 inhibiting their own transcription and other clock-controlled gene (CCG) activation, thus forming a negative feedback loop. This cycle takes about 24
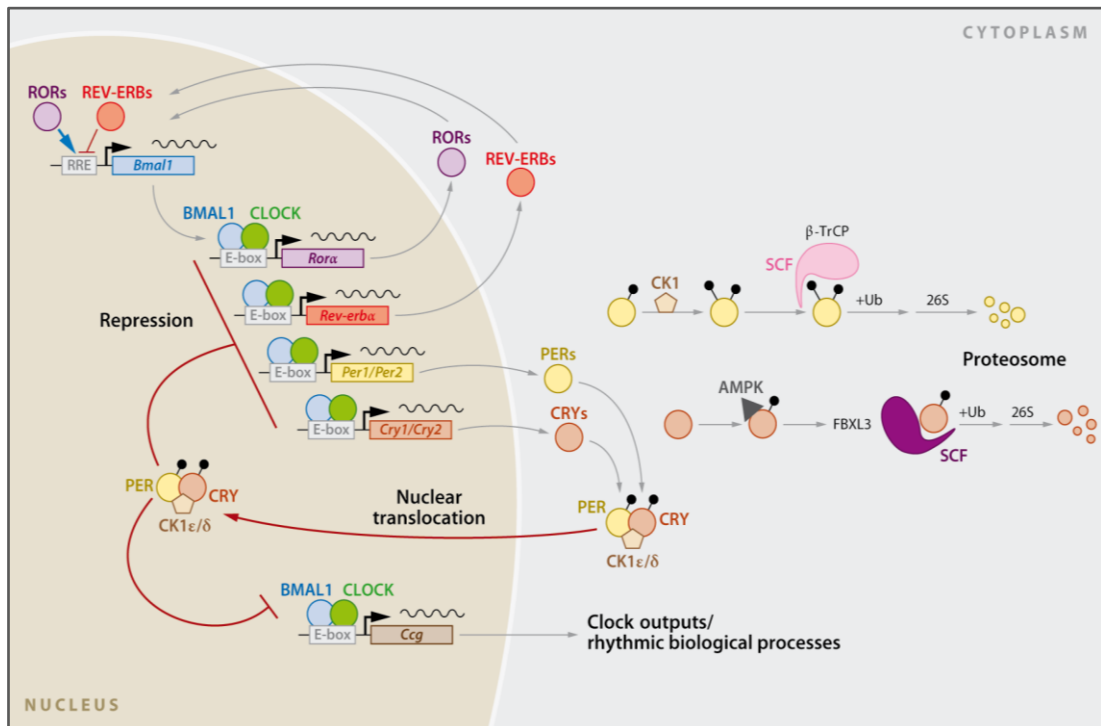
Figure 1.3: Schematic representation of the current model of the molecular mechanism of the circadian clock in mammals

This model is based on the interaction of autoregulatory positive and negative-feedback loops. The core loop involves the activators CLOCK and BMAL1 and their targets *Per1*, *Per2*, *Cry1* and *Cry2* whose proteins constitute the negative arm of the loop by inhibiting their own expression. Another feedback loop, driven also by the CLOCK:BMAL1 heterodimer, involves *Rev-erbα* and *Rora* whose gene products either repress or activate *Bmal1* transcription respectively. Many downstream genes known as clock-controlled genes (Ccg) are also activated by the CLOCK:BMAL1 heterodimer. The turnover of PER and CRY proteins is regulated by SCF (Skp1-Cullin-F-box protein) E3 ubiquitin ligase complexes involving β-TrCP and FBXL3, respectively. The kinases, casein kinase 1ε/δ (CK1ε/δ) and AMP kinase (AMPK) phosphorylate PER and CRY proteins, respectively, to promote polyubiquitination by their respective E3 ubiquitin ligase complexes targeting then PER and CRY proteins for degradation via the 26 proteasome complex. Modified from Mohawk et al. 2012.

hours and its robustness is maintained by cyclic proteolytic degradation of PER and CRY proteins. Turnover of these proteins is tightly regulated by post-translational phosphorylation which allows the recruitment of E3 ubiquitin ligase complexes and

then degradation via the 26S proteasome complex (Eide et al., 2005; Godinho et al., 2007).

Additional transcriptional-translational feedback loops are interlaced with the core BMAL1-CLOCK/PER-CRY loop to fine-tune the circadian clock. One of these loops involves *Rev-Erbα* and *Rev-Erbβ*, also known as *Nr1d1* (Nuclear receptor subfamily 1, group D member 1) and *Nr1d2* respectively, and *Rors* (RAR-related orphan receptors) whose transcriptions are also activated by the CLOCK:BMAL1 heterodimer. Both REV-ERBs and RORs bind to the same retinoic acid-related orphan response elements (ROREs) on the *Bmal1* promoter while having opposite effects on transcription: REV-ERBs repress *Bmal1* expression whereas RORs induce its activation (Guillaumond et al., 2005). Recent findings have proposed a new "facilitated repression" model indicating that RORs promote REV-ERBs loading on DNA via chromatin decondensation and thus favour its repressive activity (Zhu et al., 2015). Heme was recently found as natural ligand for both REV-ERBs (Raghuram, 2007). It allows the recruitment of the nuclear receptor co-repressor (NCoR1) which then increases REV-ERBs repressive activity (Yin and Lazar, 2005).

Although these transcriptional-translational feedback loops has been long the paradigm for the control of circadian rhythms, recent studies in red blood cells have surprisingly revealed that transcription is not required for circadian oscillations in humans, and that rhythmic modifications at post-translational level seem to be sufficient to sustain cellular circadian rhythms (O'Neill and Reddy, 2011). This suggests a more complex mechanism for the regulation of the clock but which surely also increases its stability.

1.1.4 Effects of circadian rhythm disruption

The clock system is highly regulated to be attuned with the external rhythm environment, especially with the day/night cycle. Therefore, it is not surprising that shifting phase with the natural solar day lead to disruption of circadian timing and then to negative biological consequences. Lifestyles that disrupt the inherent timing systems, such as chronic shift work, have been linked to an increased risk of many diseases such as cancer, stroke, metabolic disorders and cardiovascular disease

(Castanon-Cervantes et al., 2010). Simple experiments mimicking chronic jetlag in rodents have shown that it can provoke a faster tumor growth (Filipski et al., 2004) and early mortality in aged mice (Davidson et al., 2006). Moreover, mice housed in 20-h light/dark cycles, incongruous with their endogenous ~24-h circadian period, presented accelerated weight gain and obesity, as well as changes in neural architecture and behaviour (Karatsoreos et al., 2011). Disruption of circadian timing is now considered as an important predisposition factor to induce or exacerbate various diseases (Preuss et al., 2008).

1.2 Relationship between circadian clockwork and the immune system

1.2.1 Diseases exhibit circadian variations in the intensity of the symptoms

Nearly every physiological and metabolic process in mammals is regulated by circadian rhythms giving a circadian dimension to various diseases. The intensity of many pathologies displays rather precise timings (Smolensky and Haus, 2001). For instance, symptoms of acute pulmonary edema, congestive heart failure and asthma are most intense during the night whereas symptoms of allergic rhinitis and rheumatoid arthritis worsen in the morning. Inflammatory diseases especially exhibit strong time-of-day symptoms. Patients with rheumatoid arthritis (RA) experience strong diurnal variation in the intensity of the symptoms such as morning stiffness, joint pain and functional disability. Many studies have shown a temporal relationship between RA symptoms and levels of pro-inflammatory cytokines, in particular interleukin (IL)-6 (Cutolo et al., 2008; Yoshida et al., 2014).

1.2.2 Multiple immune parameters are under circadian control

In many organisms, including humans, many components of the immune system exhibit systemic variations over the 24-hour day (Arjona et al., 2012). In mouse liver, the expression of agents of innate immunity oscillates with a peak at the end of the subjective day, probably preparing to react efficiently in case of pathogen encounters in the early hours of activity and feeding (Panda et al., 2002). Evidence from the past

few years demonstrates that the circadian system is involved in temporal gating of immune cell function. Prominent cells in immune function, such as macrophages, natural killer (NK) cells and T-cells, are endogenously rhythmic (Arjona and Sarkar, 2005; Bollinger et al., 2011; Hayashi et al., 2007) and thus generate immune-circadian outputs. For example, cytokine secretion in macrophages displays circadian oscillations (Keller et al., 2009) and antigen-specific response of T cell depends on the timing of immunization (Fortier et al., 2011).

1.2.2.1 Emphasis on inflammation

As inflammatory diseases exhibit strong time-of-day symptoms, it is not surprising that inflammatory pathways are under circadian clock control. Expression and function of toll like receptor 9 (TLR9), a major player of activation of the cells initiating pro-inflammatory reactions, is under circadian clock control (Silver et al., 2012). Circadian clock protein CRY directly regulates the expression of pro-inflammatory cytokines such as IL-6 (Narasimamurthy et al., 2012). In mice, cytokine responses to endotoxin challenge are selectively gated by the circadian clock. A subset of cytokines exhibits significant variation in the amplitude of their response depending on the time of the challenge (Figure 1.4, Gibbs et al., 2012).
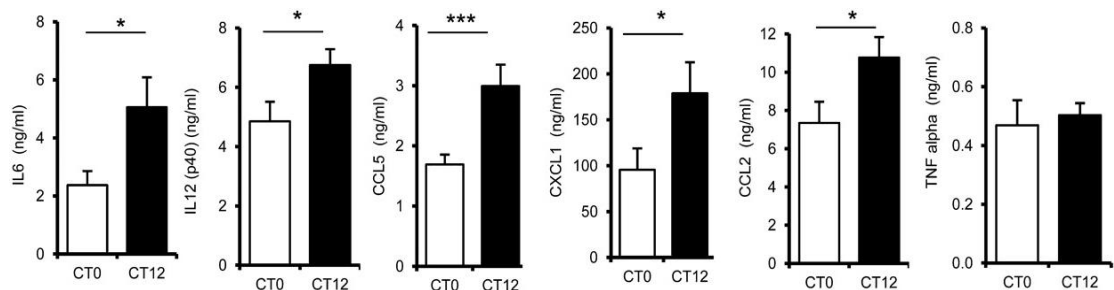
Figure 1.4: Inflammatory response to LPS gated in magnitude by the circadian clock
In mice, serum cytokines were quantified 4 h after intraperitoneal LPS administration at either CT0 (start of the rest phase) or CT12 (onset of activity). IL-6, IL-12(p40), CCL5, CXCL1, and CCL2 (but not TNF-α) showed significantly higher levels after CT12 challenge vs. CT0 ($n = 7$-9, two-way ANOVA, post hoc Bonferroni). Taken from Gibbs et al. 2012.

Host defense response to the pathogen *Salmonella enterica* Typhimurium is also altered according to circadian time in mice. The degree of intestinal inflammation and cytokine gene expression, as well as bacterial colonization, was greater in mice infected during the night (ZT16) than during the day (ZT4) (Bellet et al., 2013).

Furthermore, the clock gene *Rev-Erbα* appears to be a critical intermediary between the core clock and inflammatory pathways, especially in macrophages. Loss of the major pro-inflammatory cytokine IL6 rhythmic response to LPS challenge is seen in mice lacking the clock gene *Rev-Erbα* (Figure 1.5 A, Gibbs et al. 2012) and modulation of REV-ERBα activity by synthetic agonist ligand GSK4112 regulates LPS-induced expression of a set of cytokines in macrophages (Figure 1.5 B, Gibbs et al. 2012).
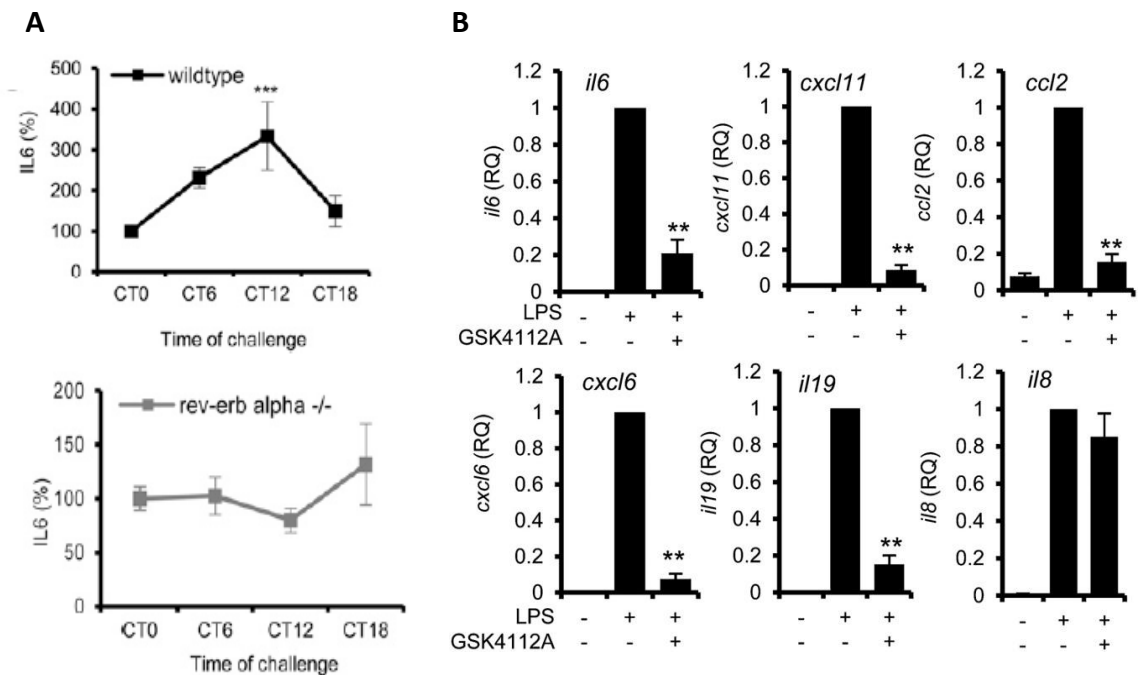
Figure 1.5: REV-ERBα is a critical component of the modulation of inflammatory response to LPS challenge

(*A*) Loss of *rev-erbα* abolishes the rhythm in IL-6 response to LPS. WT and *rev-erbα*^{−/−} mice were challenged with LPS across the circadian day, and IL-6 concentrations expressed as a percent of those detected at CT0, n = 3–7. IL-6 response at each subsequent time point was compared with CT0 (one-way ANOVA and post hoc Bonferroni). (*B*) Transcription of a selection of cytokines, but not il8, after LPS challenge is attenuated by co-application of the REV-ERB ligand GSK4112 in Human Monocyte-Derived Macrophages (MDM) (n = 6, one-way ANOVA, post hoc Bonferroni); transcript abundance is reported relative to LPS-treated cells. Modified from Gibbs et al. 2012.

To support the immune-circadian connection, experiments in rodents have shown that circadian disruption mimicking jetlag worsens the response to LPS challenge (Castanon-Cervantes et al., 2010) and causes changes in NK cells, influencing lung cancer growth (Logan et al., 2012).

1.2.2.2 Inflammation disrupts the molecular clock

While studies have highlighted the importance of the clock in modulation of inflammation, there is evidence that this connection is bidirectional and the inflammatory response itself can affect molecular clock pathways (Curtis et al., 2014; Okada et al., 2008). For example, recent findings have shown that inflammatory stimulus by TNF-α attenuates *Rev-Erbα* promoter activity and expression in the neonate (YangGuang, 2014). Using a genome-wide approach, a group has demonstrated that inflammation produces a complex re-organization of cellular and molecular circadian rhythms in mice subjected to endotoxemia (Haspel et al., 2014).

1.2.3 Optimisation of immune disease treatment using chronotherapy

Great progress to link immune function to the circadian system has been made over the last decade and it is now of utmost importance to understand the molecular mechanisms of this connection as there is a pressing need for new drugs and approaches for the treatment of many different types of inflammatory diseases. In the past few years, more investment has been made in designing drugs and treatment regimen to deliver active components at the time they are most required. This approach, termed 'chronotherapy', serves to optimise treatment efficiency – reducing the concentration of drug required and thereby reducing the risk and/or severity of side effects. For example, chronotherapy can play a vital role in the quality of life and survival rate for oncology patients (Librodo et al., 2015). Chronotherapy could be still efficiently improved by reformulating a drug so its release into the bloodstream is delayed, or using programmable pumps that deliver medicine at precise intervals. Also, new drugs are starting to be developed to directly target circadian clock components in order to modulate immune system responses (He and Chen, 2016).

1.3 Lung: a model to study the link between peripheral clockwork and inflammation

Although circadian oscillators can be found in most mammalian tissues, the battery of genes under circadian control largely depends on the tissue (Yan et al., 2008), suggesting that peripheral clocks modulate physiological processes in a rhythm specific to each organ. This project aims to look at rhythms specifically in the lung. Indeed, the lung has an unique position with respect to coping with environmental challenges which is dependent on active and rest phases. Moreover, respiratory diseases have an increasing incidence worldwide and they were the third leading cause of death in the UK in 2010. Two common respiratory diseases, asthma and chronic obstructive pulmonary disease (COPD) comprise a circadian component in their pathogenesis. Nocturnal exacerbation of asthma has been widely described and less known, night-time symptoms are also experienced by patients with COPD (Agusti et al., 2011). These observations warrant investigation of circadian rhythms in the lung and their relationship with the immune system in order to uncover effective new pharmacological targets for respiratory diseases.

1.3.1 The lung is under circadian control

Lung physiology indices such as lung resistance (Gaultier et al., 1977) and peak expiratory flow (Hetzel and Clark, 1980) exhibit circadian oscillations. Nocturnal exacerbation of asthma has been linked with these diurnal variations in lung physiology (Greenberg and Cohen, 2012). It has been also proved that the lung possesses its own endogenous circadian clock. Static explant cultures of lung tissues from clock-reporter mice (mPer2$^{Luc/Luc}$ homozygous knock-in mice) with lesions of the SCN exhibit strong circadian oscillations over a few days (Figure 1.6, Yoo et al., 2004). Furthermore, Northern blot analyses have demonstrated a significant circadian rhythmicity in the expression of the core clock genes in the murine lung (Figure 1.7, Bando et al., 2007). Moreover, circadian disruption due to chronic jetlag has been recently proved to alter mouse lung clock gene expression and also lung physiologic functions (Hadden et al., 2012).
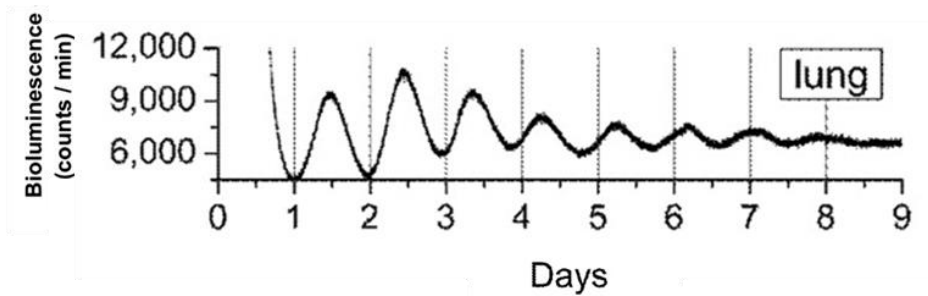
Figure 1.6: Real-time circadian oscillations in PER2 levels in lung tissues of SCN-lesioned mice

mPer2$^{Luc/Luc}$ homozygous knock-in mice with SCN-lesioned were maintained in constant darkness DD. Bioluminescence measurement of mPER::LUC protein. Modified from Yoo et al. 2004.
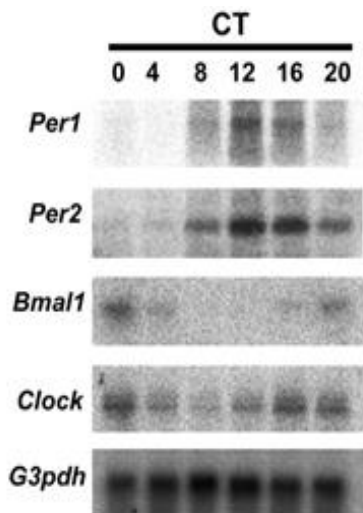
Figure 1.7: Circadian expression of *Per1*, *Per2*, *Bmal1*, and *Clock* genes in mouse lungs, as detected by Northern blot analysis

G3pdh expression was determined as a control. Samples were collected on the second day in DD at different CT (CT0, subjective day; CT12, subjective night). Note the anti-phase of gene expression between *Per1* and *Per2* on one hand (with a peak around CT12) and *Bmal1* and *Clock* on the other hand (with a peak around CT0). Modified from Bando et al. 2007.

1.3.1.1 Location of circadian pacemakers in the lung

Now that the presence of circadian clocks in lung is well-established, the question to then address is to determine whether all lung cells possess a clock or whether only a few cell types are involved, and in that case, what kind of cell-types. This question has not been totally solved yet due to the complexity of the respiratory tract which has approximately 40 different resident cell types (Cardoso and Whitsett, 2008).

In normal adult humans, epithelial cell populations vary as a function of airway level, with more cartilage cells and submucosal glands in large airways and the appearance

of bronchiolar epithelial cells, previously known as Clara cells, as the airways become smaller (Figure 1.8, Crystal et al., 2008). There is also a variety of less frequent cell types throughout the airways such as bronchoalveolar macrophages which comprise more than 95% of the immune cells found in a normal bronchial lavage fluid building up the first line of defense.
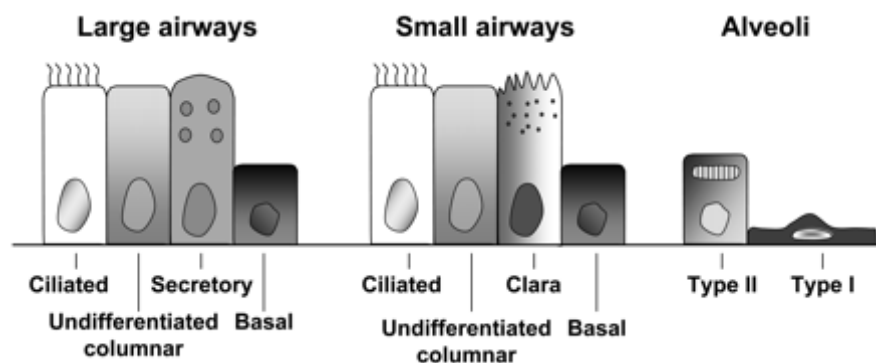
Figure 1.8: Major cell types of the lung epithelium
In the large airways, the major cells types are ciliated, undifferentiated columnar, secretory, and basal cells. In the small airways, the cell types are similar, with relatively more ciliated cells, and the secretory cells shift to the Clara cell type (tall columnar, nonciliated cells involved in detoxifying harmful inhaled substances). The airway epithelium merges with the alveolar epithelium, with type I (97%) and type II (3%) pneumocytes cells. Modified from Crystal et al. 2008.

Significant circadian rhythm have been shown in respiratory ciliary epithelial cells (Bando et al., 2007). Recent work has revealed the bronchiolar epithelial cell as a key cell type for sustaining circadian rhythms in mouse lungs as selective ablation of this cell type via naphthalene exposure results in the loss of circadian clock oscillations in mouse lung slices (Gibbs et al., 2009). Moreover, bronchoalveolar macrophages also are rhythmic (Gibbs et al., 2014) but whole lung slices from mice lacking the macrophage clock remain rhythmic (Gibbs, unpublished data). This indicates that bronchiolar epithelial cells are key lung pacemaker cells. Although progress has been made to determine which pulmonary cell types are rhythmic in mice, additional work

has to be done in humans as the composition of lung epithelium differs from mice to humans. For example, bronchiolar epithelial cells only account for 15-20% of distal airway epithelial cells in humans whereas in murine lungs bronchiolar epithelial cells comprise 70-90% (Plopper et al., 1980).

1.3.2 Role of circadian clock in the pulmonary innate immune response

The relationship between circadian clock and systemic inflammatory response has been well demonstrated but it is important to specifically look at pulmonary inflammatory response as physiological processes oscillate in a rhythm specific to each tissue. A correlation between circadian system and inflammation into the lung has been observed in subjects with asthma (Kelly et al., 2004). However, there is a lack of experimental studies to understand the underlying mechanisms which link pulmonary inflammation and circadian system. A recent study has demonstrated a time-dependent regulation of cytokine response to LPS in lungs (Gibbs et al., 2014). Wildtype mice were exposed to aerosolised LPS to directly challenge the lung and analyses of BAL fluid indicated a variation of neutrophils and inflammatory cytokine levels depending on the time of the challenge (Figure 1.9). Interestingly, peak of inflammatory cells, predominantly neutrophils, was observed at circadian time 0 (CT0, dawn) whereas major pro-inflammatory IL-6 and TNF-α showed the highest level in lung after challenge at CT6. However, the chemokine CXCL5 levels oscillated in phase with neutrophil rhythmic infiltration suggesting a coupling role between this chemokine and neutrophilic inflammation. This study also highlighted a major role for the clock in epithelial cells in regulating pulmonary inflammation. Genetic ablation of *Bmal1* in bronchiolar epithelial cells resulted in exaggerated inflammatory responses to aerosolised LPS. However, it is not clear whether these effects are mediated via central circadian clock disruption or a more general pleiotropic effect of BMAL1 disruption.

The role of resident and recruited macrophages in initiating and maintaining pulmonary inflammation in lung infection or injury has been convincingly demonstrated (Sibille, 1990). Also more than mechanical barriers, airway epithelial cells (AEC) participate actively in innate immune responses by releasing a variety of
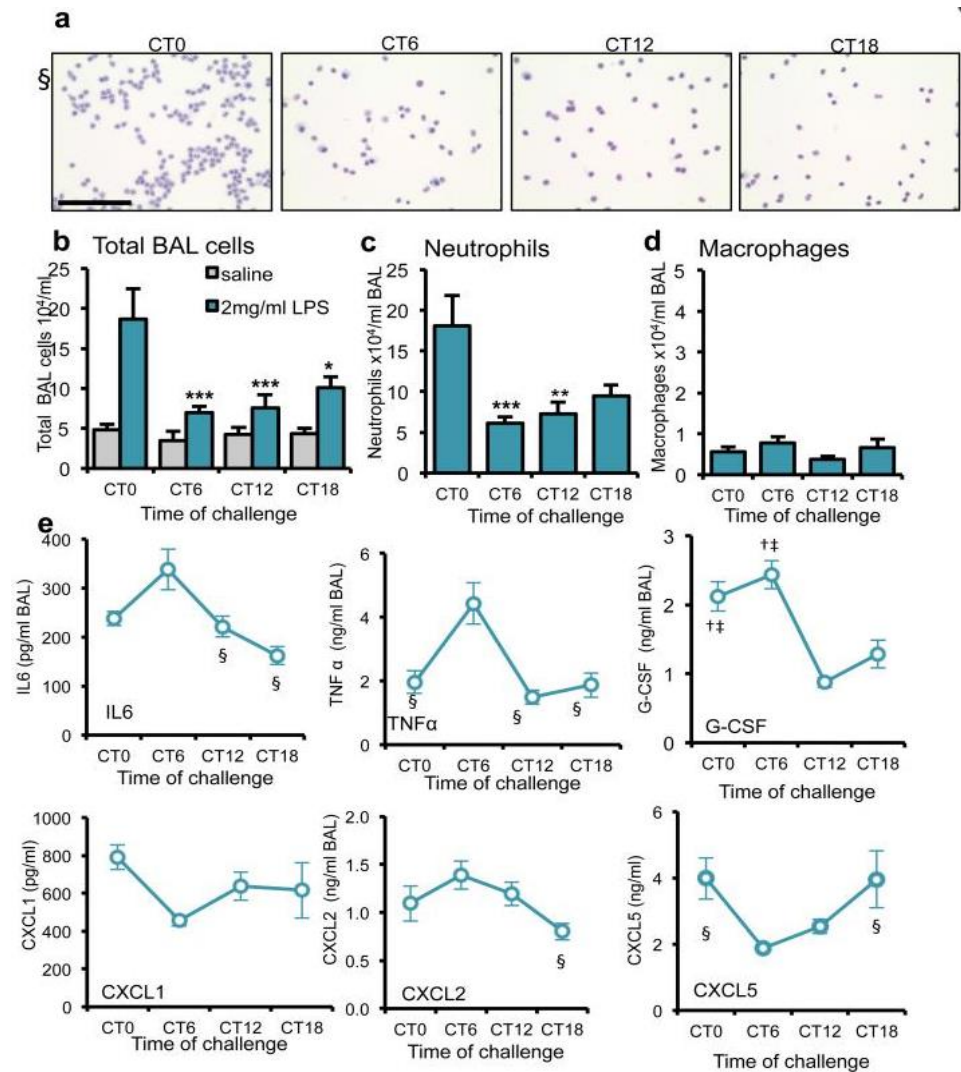
Figure 1.9: The pulmonary inflammatory response to LPS administration is gated by the circadian clock

(a) Staining of cytospins of BAL fluid from LPS-treated C57Bl/6 mice. Scale bar, 100 μm. (b) Total cell counts in BAL samples collected after LPS challenge at CT0 (n = 6), CT6 (n = 7) CT12 (n = 8) and CT18 (n = 6) or vehicle (n = 4/time point), two-way analysis of variance (ANOVA) and post hoc Bonferroni) (c) Neutrophil and (d) macrophage numbers in the same samples (one-way ANOVA and post hoc Bonferroni) (e) Cytokine levels in these BAL samples were compared between time points using one-way ANOVA and post hoc Bonferroni) § significantly different from CT6 (P≤0.05); † significantly different from CT12 (P≤0.05); ‡ significantly different from CT18 (P≤0.05).; G-CSF, granulocyte colony–stimulating factor. Modified from Gibbs et al. 2014.

cytokines/chemokines (Takizawa, 1998). It has been shown that Clara cells play an important role in the pulmonary innate immune response to LPS in mice (Elizur et al., 2007) and that their interaction with macrophages allows an effective response to challenge (Elizur et al., 2008; Snyder et al., 2010). Therefore, alveolar macrophages, Clara cells and other epithelial cells, all rhythmic cells, significantly impact the gating of the pulmonary innate immune response in mice.

Taken together, the circadian clock appears to have a fundamental role in pulmonary inflammation and it highlights the potential for a completely novel therapeutic modality in inflammatory lung disorders.

1.4 Crosstalk with oxidative stress

Oxidative stress is a critical component of lung diseases such as COPD. Studies have shown links between oxidative stress and pulmonary inflammation on one hand and between oxidative stress and circadian clock on the other hand. However, the interaction between these three elements − circadian clockwork, inflammation and oxidative stress − has been poorly investigated. Assessing whether the lung clock regulates inflammatory response induced by oxidative stress and which pathways are involved could have a dramatic benefit on respiratory disease treatment.

1.4.1 Disruption of the circadian clock in lung by cigarette smoke exposure

Cigarette smoke (CS) is a highly complex mixture of about 5,000 chemicals, most of them toxic and carcinogenic. It is recognized that the large number of oxidants contained in CS induces an oxidative burden by disturbing the oxidant:antioxidant balance and could lead to cellular damage in the lungs such as destruction of the alveolar wall, leading to airway enlargement (Arsalane et al., 2000). CS exposure is well known to strongly reduce lung function in adults (Downs et al., 2005) and is linked to a variety of lung disorders associated with a chronic inflammatory environment such as chronic obstructive pulmonary disease (COPD) (MacNee,

2005). Moreover, CS is a powerful inducer of inflammatory cell recruitment such as neutrophils and lymphocytes. Upon activation, these cells are known to generate and release a variety of cytokines and chemokines which serve as a signal for recruitment of additional inflammatory cells from blood circulation but also which are capable of causing damage to cell membranes and injury of the airway epithelium (Bhalla et al., 2008; Talhout et al., 2011).

A transcriptomics study in rat lung aiming at identifying gene expression profile upon CS exposure has confirmed the induction of the expression of genes related to antioxidant response such as *nqo1*, as well as genes involved in regulation of pro-inflammatory cell responses. It has also strikingly revealed an obvious impact of CS exposure on the expression of genes related to circadian rhythm (Gebel et al., 2006). These circadian clock genes still exhibit a specific pattern of cyclic expression after CS exposure (Figure 1.10 A). *Bmal1* expression is activated 6 h after CS exposure and is repressed 2 and 20 h after exposure, while D-site-binding protein (*dbp*) and *nr1d2* (also known as *rev-erbβ*) oscillate in an anticyclic manner. The real effect of CS exposure on clock genes becomes striking when comparison between control and smoke-exposed rats is made. In both control and CS-exposed animals, *bmal1* expression displays rhythmic oscillations but in an antiphase manner suggesting that CS exposure induces a phase shift in the circadian cycle (Figure 1.10 B).
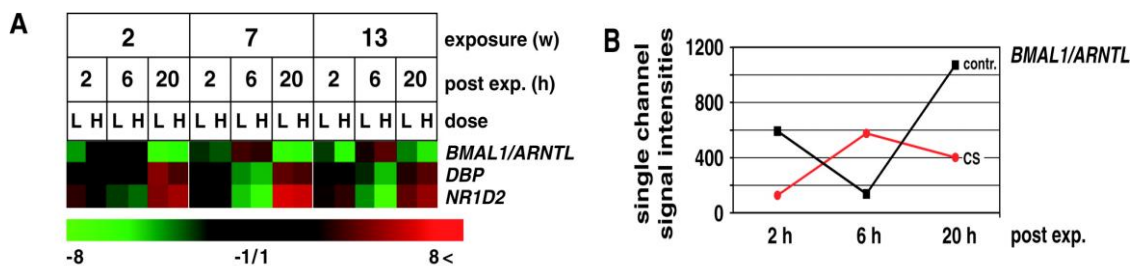
Figure 1.10: Cigarette smoke–induced changes in the expression of genes involved in circadian rhythm

(A) Dendrogram shows expression of *bmal1*/ *arntl*, *dbp*, and *nr1d2* as derived from of the PIQOR gene chip analysis. L dose = 300 µg Total Particle Matter per litre (TPM/l), H dose = 600 µg TPM/l. Color code within cluster: red = increased, green = repressed, black = unaltered. (B) Analysis of the single chain signal intensities. Figure shows data from the fluorescence signal intensities of the control samples (contr.) and of the samples of cigarette smoke–exposed animals (CS). Data are from the 600 µg TPM/l group in the 13-week exposure period. From Gebel et al. 2006.

Additional work has confirmed that CS exposure modulates expression of clock genes in lungs. A "snapshot" comparison between air and CS exposed mice has revealed a significant repression of a few clock genes, especially *Rev-erbα* (Vasu et al., 2009) and an extended study over 42 hours has validated that CS exposure affected the amplitude and phase of circadian clock gene expression in the murine lungs whilst simultaneously increasing pulmonary inflammation (Hwang et al., 2014).

As cigarette smoke contains thousands of chemicals, it is quite difficult to elucidate the mechanisms of CS on circadian clock gene regulation. Nicotine has been tested but does not significantly induce changes in circadian activity patterns (Benowitz et al., 2002). A report showed that DNA-binding activity of the BMAL1::CLOCK and BMAL1::NPAS2 heterodimers is dependent on the redox state of nicotinamide adenine dinucleotide cofactors NAD(H) and NADP(H) with enhanced binding in presence of the reduced forms of these cofactors (Rutter et al., 2001). Cigarette smoke is known to generate free radicals that disturb the oxidant:antioxidant balance and cause oxidative stress. Hence, by altering the redox potential of cells, CS exposure could influence the DNA-binding DNA-binding activity of the BMAL1::CLOCK and then shift transcription of clock-controlled genes. More recently, sirtuin1 (SIRT1), an NAD+-dependent deacetylase, has been shown to affect clock function by binding with CLOCK:BMAL1 complexes (Nakahata et al., 2008). Furthermore, CS reduces the levels and activity of SIRT1 (Yang et al., 2007), and patients with COPD have reduced lung levels of SIRT1 (Rajendrasozhan et al., 2008). Therefore, it is likely that CS-mediated reduction of SIRT1 leads to increased acetylation of circadian clock proteins and consequently to abnormal clock gene expression in the lung.

Altogether, these findings suggest that the negative effect of CS exposure on lung might be related to circadian clock disruption caused by CS-induced oxidative stress in lung. This hypothesis is worth consideration as excessive oxidative stress can trigger an enhanced release of pro-inflammatory cytokines, which are increased in the lungs of smokers and patients with COPD (see section below).

1.4.2 Oxidative stress as inducer of inflammation in lungs

Organisms are continuously exposed to oxidants, either generated endogenously as by-products of metabolic reactions (e.g. from mitochondrial electron transport chain during respiration) or exogenously, such as cigarette smoke or air pollutants. At the molecular level, reactive oxygen species (ROS) serve as important second messengers in cell signalling; however, at higher concentrations and long-term exposure, ROS, such as superoxide anion ($O_2^{\bullet-}$), hydroxyl radical ($^{\bullet}OH$) and hydrogen peroxide (H_2O_2), highly unstable molecules with unpaired electrons, are capable of initiating oxidation of proteins, DNA, lipids causing direct lung injury or inducing inflammation.

It is well documented that ROS can initiate inflammatory responses in the lungs through the activation of stress kinases (c-Jun activated kinase, extracellular signal-regulated kinase, p38) and redox-sensitive transcription factors, such as nuclear factor (NF)-kB and activator protein (AP)-1. This leads to an increased expression of variety pro-inflammatory mediators (Rahman and Adcock, 2006). A study has shown that hydrogen peroxide (H_2O_2) stimulates IL-6 mRNA expression in organotypic murine lung slices (Kida et al., 2005).

Within the lung, ROS can be endogenously produced by epithelial cells (Rochelle et al., 1998) and inflammatory cells such as alveolar macrophages, neutrophils and eosinophils via the NADPH oxidase system (Piotrowski, 2000) as part of an inflammatory-immune response towards a pathogen or irritant (cigarette smoke for example). Therefore, there is a feed-forward effect as inflammation induces recruitment of inflammatory cells which then release more ROS prolonging oxidative stress and amplifying inflammation in lung (Figure 1.11).

This is particularly relevant to explain COPD progression and increasing severity. It is now proved that oxidative burden is enhanced in patients with COPD due to ROS release by both macrophages and neutrophils which are recruited in increased numbers into the lungs of COPD patients (Shu et al., 2011). Overwhelming production of ROS then leads to an amplified inflammatory response and thus prolonged oxidative stress is thought to be a major pathogenic factor for driving disease progression (Kirkham and Rahman, 2006).
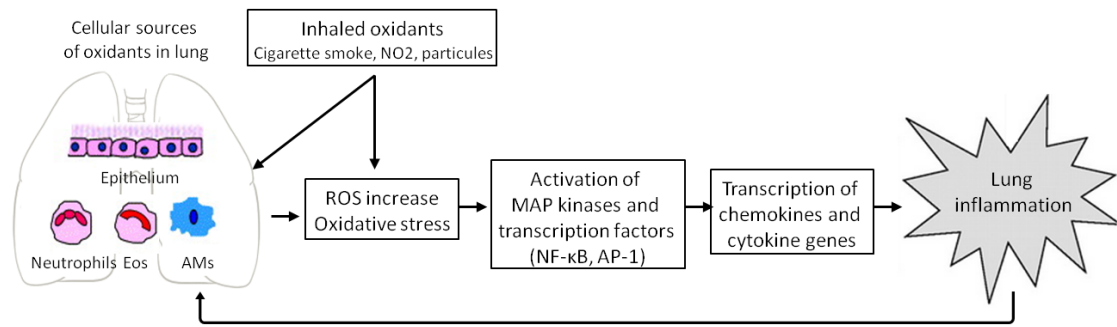
Figure 1.11: Mechanisms of reactive oxygen species (ROS)-mediated lung inflammation
Inflammatory response is mediated by oxidants either inhaled and/or released by the activated neutrophils, alveolar macrophages (AMs), eosinophils (Eos) and epithelial cells leading to production of ROS. Inflammation itself can have a feed-forward effect, triggering inflammatory cells in lungs to produce yet more oxidative stress, exacerbating and intensifying the inflammatory response.

1.4.3 Defense mechanisms to cope with excessive ROS

To prevent such an accumulation of ROS and oxidative stress, higher animals have evolved various endogenous defense strategies, comprising phase II detoxification enzymes and antioxidant proteins. The antioxidant-response element (ARE), cis-acting DNA regulatory element, plays a central role in these cytoprotective mechanisms as it is found in promoter regions of multiple phase II detoxification and antioxidant genes such as glutamate cysteine ligase (GCL), superoxide dismutase (SOD), NAD(P)H:quinone oxidoreductase 1 (NQO1), and heme oxygenase-1 (HO-1). Activation of these genes results mainly from transcriptional activation mediated by transcription factor nuclear factor erythroid 2 (Nrf2) through its interaction with the ARE (Lee and Johnson, 2004). Under normal cellular conditions, Nrf2 is sequestred into the cytosol by Kelch-like-ECH-associated protein 1 (Keap1) to be then degraded via proteasome upon ubiquitination. Thus, there is a small and steady amount of Nrf2 into the nucleus. However, in the presence of various stresses such as oxidative stress, Nrf2 is activated by phosphorylation by different kinases and escapes from Keap1 to migrate into the nucleus and to stimulate the expression of antioxidant genes (Figure 1.12).
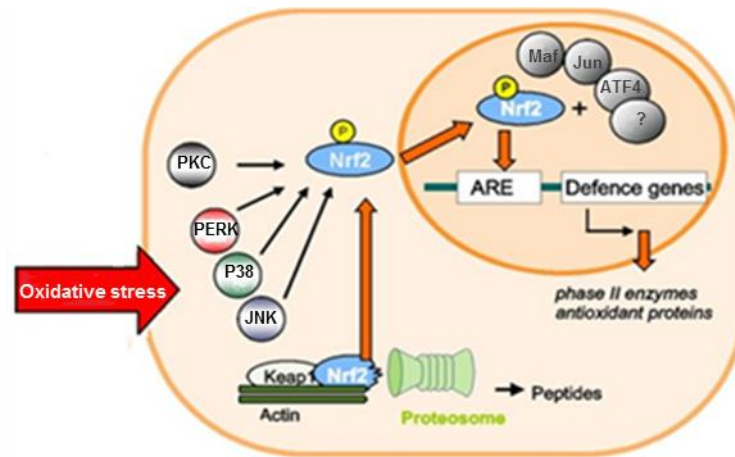
Figure 1.12: Mechanism of ARE-mediated antioxidant enzyme induction by Nrf2

Under basal conditions, the transcription factor NRF2 is sequestered within the cytosol by the repressor protein Keap1, presenting it for proteosomal degradation via ubiquitination. Oxidative stress, by disruption of the redox status, induces activation of upstream kinases including protein kinase C (PKC), and MAPKs, such as c-Jun NH_2-terminal kinase (JNK). These kinases then phosphorylate NRF2 which facilitates its dissociation from KEAP1 and thus its translocation into the nucleus. In the nucleus, NRF2 forms a heterodimer with small MAF (term derived from musuloaponeurotic-fibrosarcoma virus) and binds to the antioxidant-response element (ARE) to activate cytoprotective gene expression.

It has been demonstrated that activation of cytoprotective Nrf2 / ARE-regulated genes can suppress inflammatory responses in human endothelial cells (Chen et al., 2006). Adenovirus-mediated expression of Nrf2 in human aortic endothelial cells (HAECs) suppresses TNF-α-induced monocyte chemoattractant proteins (MCP)-1 and VCAM-1 (Chen et al., 2006). In turn, genetic ablation of *Nrf2* in mice leads to an enhanced inflammatory response to oxidant insults in murine lung (Iizuka et al., 2005).

1.4.4 Circadian fluctuations of ROS and antioxidants

To be attuned with daily light–dark cycles, it seems important that ROS levels are controlled by the circadian clock. Temporal modulation of ROS by the clock has been demonstrated in several organisms including plants (Lai et al., 2012), flies (Krishnan et al., 2008) and mice (Geyfman et al., 2012). Along with circadian fluctuation of ROS, genes involved in removal of ROS and repair of oxidative damage appear to be rhythmically expressed (Langmesser and Albrecht, 2006; Pekovic-Vaughan et al., 2014). Oxidation state of peroxiredoxins, antioxidant proteins, exhibit circadian oscillations in many organisms (Edgar et al., 2012) including humans (O'Neill and Reddy, 2011). Recently, diurnal variations and gender differences in transcript levels of *Nrf2*, *Keap1* and antioxidant genes were found in murine liver (Figure 1.13, Xu et al., 2012).
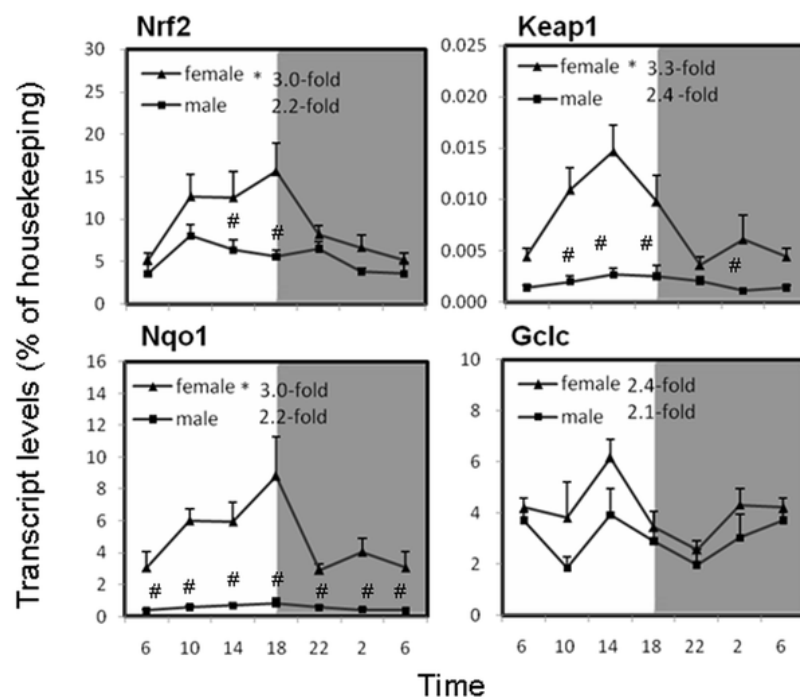
Figure 1.13: Circadian variations of mRNA levels of the Nrf2 pathway-related genes
Includes the nuclear factor erythroid-2-related factor-2 (Nrf2), Kelch-like ECH associating protein 1 (Keap1), NADPH quinone oxidase 1 (Nqo1), and glutamate-cysteine ligase catalyze subunit (Gclc) in adult female and male mouse livers (n = 4 for each time point). *Significant circadian rhythm p,0.05; #Significant sex difference p,0.05. Taken from Xu et al., 2012.

Because of this rhythmicity of cytoprotective gene expression, responses to oxidative stress may vary depending on the time of the day. Indeed, a study has shown that the time of day at which flies are exposed to hydrogen peroxide (H_2O_2) affects their ability to cope with this oxidative stressor. Flies exposed to H_2O_2 during the night had lower mortality rates than flies exposed during the day. Furthermore, this rhythmicity in response to acute oxidative stress induced by H_2O_2 is abolished in flies lacking the core clock gene *period* (Krishnan et al., 2008), suggesting that a functional clock is required for the time-of-day–specific regulation of ROS production. Moreover, a clock ''gated'' pulmonary response to oxidative injury was revealed using an *in vivo* bleomycin-induced lung fibrosis model, with a more severe fibrotic effect when bleomycin was applied at ZT12, nadir of NRF2 levels (Pekovic-Vaughan et al., 2014).

1.4.5 Effects of oxidative stress on circadian clockwork

In turn, excessive oxidative stress could disrupt the circadian clock. As said in section 1.4.1, there is some evidence that DNA-binding activity of the BMAL1::CLOCK and BMAL1::NPAS2 heterodimers is dependent on the redox state of nicotinamide adenine dinucleotide cofactors NAD(H) and NADP(H) with enhanced binding in presence of the reduced forms of these cofactors (Rutter et al. 2001). Recently, it has been shown that ROS could feed-back to affect the transcription of a clock-regulated output in plants (Lai et al., 2012). Moreover, findings suggest that oxidative stress activates Rev-erbα promoter activity via putative binding NRF2 sites (YangGuang, 2014). However, in general, the effects of oxidative stress on circadian rhythms are poorly understood.

1.4.6 More evidence to stress the relationship between antioxidant NRF2 pathway and circadian clockwork

Taken together, the findings suggest a relationship between the circadian clockwork and ROS homeostasis probably through regulation of detoxifying and antioxidant pathways such as NRF2 pathway. Intriguingly, the endogenous ligand for REV-ERBα is heme (Raghuram, 2007) which also regulates the dynamic exchange of

Bach1 and NRF2 in the Maf-recognition element (MARE) leading to activation of antioxidant gene expression (Sun et al., 2004). Bach1 acts as a nuclear repressor of Nrf2 activity by competitively binding the same MARE and repressing cytoprotective gene expression. However, increased levels of heme allow dissociation of Bach1 from enhancers, promote its migration to the cytoplasm, making MARE accessible to activators such as Nrf2 (Figure 1.14). Therefore, higher heme levels could lead to the repression of pro-inflammatory cytokine production by elevating oxidative stress through antioxidant Nrf2-dependent gene expression and also through REV-ERBα (as seen in sections 1.2.2.1 and 1.3.2). This reinforces the hypothesis of a link between circadian clock and oxidant-antioxidant balance, especially knowing that synthesis of heme exhibits a circadian rhythm (Kaasik, 2004). Therefore, the relationship between circadian clockwork and ROS homeostasis, especially in the case of pulmonary inflammation, bears investigation.
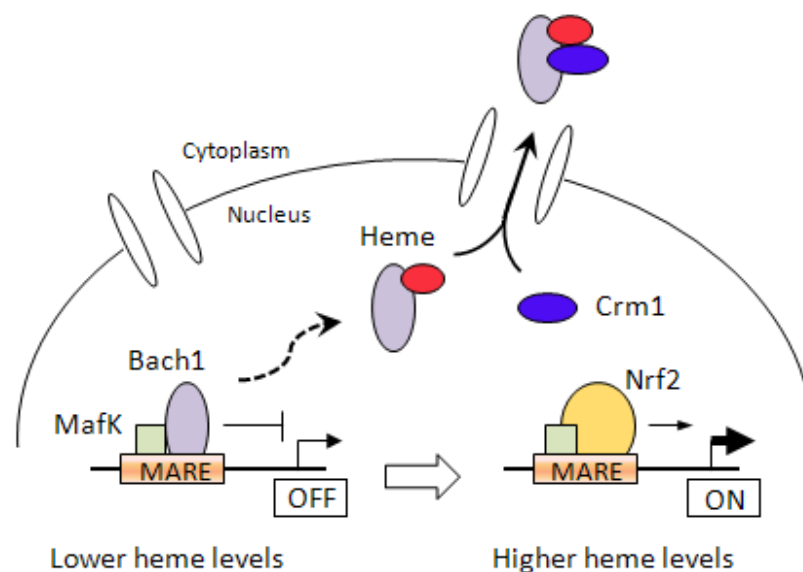
Figure 1.14: Schematic representation of the dynamic exchange of Bach1 and Nrf2 regulated by heme on the MARE

Under normal conditions, Bach1 occupies MARE enhancers to repress transcription. An increase in heme levels alleviates Bach1-mediated repression through its dissociation from MARE and its Crm1-dependent nuclear export, making MARE available for Nrf2.

1.5 Project aims, models and relevance to the research area

1.5.1 Hypotheses and objectives

The nuclear receptor REV-ERBα has been identified as a key output molecule linking inflammation and the clock, especially in macrophages. Interestingly, its natural ligand heme is involved in the activation of NRF2 antioxidant pathway. As REV-ERBα has become an attractive therapeutic target for inflammatory diseases, new drugs targeting this nuclear receptor have been developed in the past few years.

A recent study has revealed a major role for the clock in bronchiolar epithelial cells in regulating inflammation, mediated by control of neutrophil chemokine expression. In this study, BMAL1 was disrupted in the epithelial cell lineage. However, it is not clear whether these effects are mediated via central circadian clock disruption or a more general pleiotropic effect of BMAL1 disruption. Indeed, some of the anti-inflammatory effects of BMAL1 may be through regulation of its direct transactivation target REV-ERBα.

The overall aim of this project is to elucidate the role of REV-ERBα in controlling inflammatory responses in the lung. For that purpose, this thesis is based on five main hypotheses and chapters. In each section, I will highlight possible crosstalk with oxidative stress through antioxidant Nrf2 pathway activation.

Hypothesis 1: REV-ERBα plays a critical role in regulation of lung inflammation.

Objectives:

- Characterise the daily profile of clock and inflammatory gene expression and proteins in a REV-ERBα knock-out mouse model.

- Define responses of REV-ERBα knock-out mice and wild-type littermate controls to aerosolised lipopolysaccharide (LPS) or cigarette smoke, and quantify the resulting inflammatory response via quantification of cell infiltration and measurement of cytokine concentrations.

- Assess differences in antioxidant gene expression between wild-types and REV-ERBα knock-out mice in basal state or under inflammatory challenged conditions.

Hypothesis 2: The bronchiolar epithelial cells are key cells to regulate pulmonary inflammatory responses via REV-ERBα.

Objectives:

- Generate mouse strains which lack REV-ERBα DNA binding domain (DBD) in myeloid cell lineage (macrophages, monocytes, neutrophils) or bronchiolar epithelial cells by breeding *Rev-Erbα*-DBD$^{flox/flox}$ (named *Rev-Erbα*$^{fl/fl}$ afterwards) mice with *LysM*^{cre} or *Ccsp*^{icre} mice respectively, maintain on a Per2::Luc background to facilitate bioluminescence monitoring.

- Assess lung rhythmicity by monitoring organotypic lung slices from the different mouse models mice and littermate controls under photomultiplier tubes (PMTs) or camera.

- Test responses of the different mouse models mice and littermate controls to aerosolised LPS at different time points and measure any differences in the magnitude and rhythm of inflammatory response (cell infiltration and cytokine production).

Hypothesis 3: Targeting both REV-ERBα and REV-ERBβ in the bronchiolar epithelial cells has a more extensive effect on neutrophilic inflammation than deletion of the REV-ERBα DBD.

Objectives:

- Generate a mouse strain which lacks both REV-ERBα DBD and REV-ERBβ in bronchiolar epithelial cells by breeding *Rev-Erbα/β*$^{fl/fl}$ afterwards mice with *Ccsp*^{icre} mice, maintain on a Per2::Luc background to facilitate bioluminescence monitoring.

- Assess lung rhythmicity by monitoring organotypic lung slices from mutated mice and littermate controls under photomultiplier tubes (PMTs) or camera.

- Challenge the mutated mice and littermate controls with aerosolised LPS at different time points and measure any differences in the magnitude and rhythm of inflammatory response (cell infiltration and cytokine production).

Hypothesis 4: REV-ERBα repressive activity can be modulated pharmacologically with small molecules ligands.

Objectives:

- Evaluate the characteristics of new REV-ERBα ligand GSK1362 (peptide profile, toxicity)

- Assess the effects of GSK1362 on REV-ERBα protein and PER2 rhythms

- Treat different types of macrophages and epithelial cells with GSK1362 and other small molecule tool ligands and assess their effects upon inflammatory stimuli.

Hypothesis 5: Inflammation degrades REV-ERBα.

Objectives:

- Employ different inflammatory stimuli *in vivo* and *in vitro* and measure levels of REV-ERBα proteins.

 - Dissect the degradation pathway by investigating post-translational modifications of REV-ERBα.

- Assess the effect of ligand binging on the REV-ERBα degradation process.

1.5.2 Models

Bearing in mind the 3Rs (replacement, reduction and refinement) in relation to UK Home Office-licensed studies of animals, *in vitro* models were used as often as possible. Nonetheless, the immune system and the architecture of the lung are so complex that it is inevitable that *in vivo* investigations are required to account for the

local tissue and cellular context. Therefore, it is imperative to choose a suitable model, both in terms of experimental design and the organism itself.

1.5.2.1 Inflammatory models

The overall aim of this project is to elucidate the role of REV-ERBα in controlling inflammatory responses in the lung. To elicit immune responses and to target directly the lung *in vivo*, an established protocol of aerosolised lipopolysaccharide (LPS) administration will be used (Roos, 2014). LPS, derived from gram negative bacteria, induces neutrophilic inflammation in the airways and lung parenchyma of mice. LPS is a potent activator of toll-like receptor 4 (TLR4). TLR4 ligation triggers intracellular signalling cascades which ultimately promote activation of members of the nuclear factor kappa-light-chain-enhancer of activated B cells (NF-κB), interferon regulatory factor (IRF) and activator protein 1 (AP-1) families (Medzhitov and Horng, 2009). In collaboration with GlaxoSmithKline, cigarette smoke exposure was also performed in wild-type and *Rev-Erbα* knock-out mice in order to investigate the inflammatory responses to another stimulus than LPS.

1.5.2.2 Animal models

For this research, the mouse was the best experimental animal to use. As a mammal, *Mus musculus* shares our molecular clockwork and is also a powerful tool for modelling human immune function and diseases (Webb, 2014). Other advantages of the mouse model are the low maintenance costs, ease of breeding and the availability of large numbers of genetic variants. However, it is important to keep in mind the discrepancies between mice and humans in immune system activation and response to challenge.

Many aspects of circadian molecular clockwork have been revealed thanks to genetic manipulation. One of the most important valuable tools in chronobiology is the addition of the luciferase enzyme sequence (*Luc*) following the *Per2* sequence. The combination of these sequences, known as *Per2::Luc*, enables to visualise in real-time the oscillations of PER2 protein (Yoo et al., 2004). When cells containing PER2::LUC fusion proteins are cultured in a medium containing luciferin, the

luciferase enzyme catalyses a reaction which produces light. As light is produced only in presence of PER2 protein, rhythms of PER2 proteins can be recorded by measuring luminescence using photomultiplier tubes. Therefore, this construct allows to assess whether genetic mutations or *ex vivo* pharmacological manipulations induce a perturbation of the circadian clock rhythms. All the mice generated during this project were bred on a background of this *Per2::Luc* reporter.

Along with insertion of the *Per::Luc* reporter, knock-outs of the REV-ERBs in specific cell types were required. For that purpose, the Cre-loxP recombination system was used. It involves the targeting of a specific sequence of DNA and splicing it with an enzyme called Cre recombinase. The Cre recombinase catalyses the recombination of DNA between two loxP (locus of X-over P1) sites. The loxP sites comprise two palindromic 13 base-pair sequences and an asymmetric 8 base-pair sequence in the centre which confers directionality. The result of the Cre-mediated recombination is dependent upon the relative orientations of the two loxP sites (Figure 1.15). Temporal or tissue-specific control on where to have this Cre recombination occurring is achieved by regulating where Cre is expressed. For that, a Cre sequence is inserted after a gene known to be expressed only at the desired time or in the region of interest – a 'driver' gene. Therefore, whenever cells transcribe the driver gene, they will also produce the Cre recombinase which will catalyse the recombination of DNA between any floxed sequences present. For this project, cell specific knock-outs of the REV-ERBs were performed in myeloid cell lineage and bronchiolar epithelial cells using the *LysM* (Clausen et al., 1999) and *Ccsp* (Li et al., 2008a) drivers respectively.

Previous studies have highlighted the role of the macrophage clock in circadian responses to endotoxin (Gibbs et al., 2012; Keller et al., 2009). In order to determine the contribution of REV-ERBα in macrophages in regulating pulmonary inflammation *in vivo,* mutation of *Rev-Erbα* was introduced in myeloid cells using the LysM driver. Although this approach targets macrophages, mutation of REV-ERBα is also introduced in the other myeloid cells such as neutrophils and monocytes. The choice of this LysM driver over other more macrophage specific drivers was mainly based on its availability within my group.

The airway epithelium plays a critical role in mediating pulmonary inflammatory responses. Both alveolar epithelial cells and bronchiolar epithelial cells produce cytokines in response to LPS, including CXCL1 and CXCL5 (Elizur et al., 2007; Gibbs et al., 2014; Jeyaseelan et al., 2005) and expression of TLR4 has been detected in these two groups of lung epithelial cells (Sender and Stamme, 2014; Tomita et al., 2011). I focused my work on the bronchiolar epithelial cells, which express the surfactant protein CCSP, as previous work has uncovered a critical role of these non-ciliated epithelial cells in maintaining circadian rhythm within the lung. Indeed, after selective depletion of these cells via naphthalene exposure *in vivo*, lung slices taken from treated mice are arrhythmic when cultured (Gibbs et al., 2009). Therefore, bronchiolar epithelial cells are key targets for investigations into rhythmic pulmonary physiology and pathology.
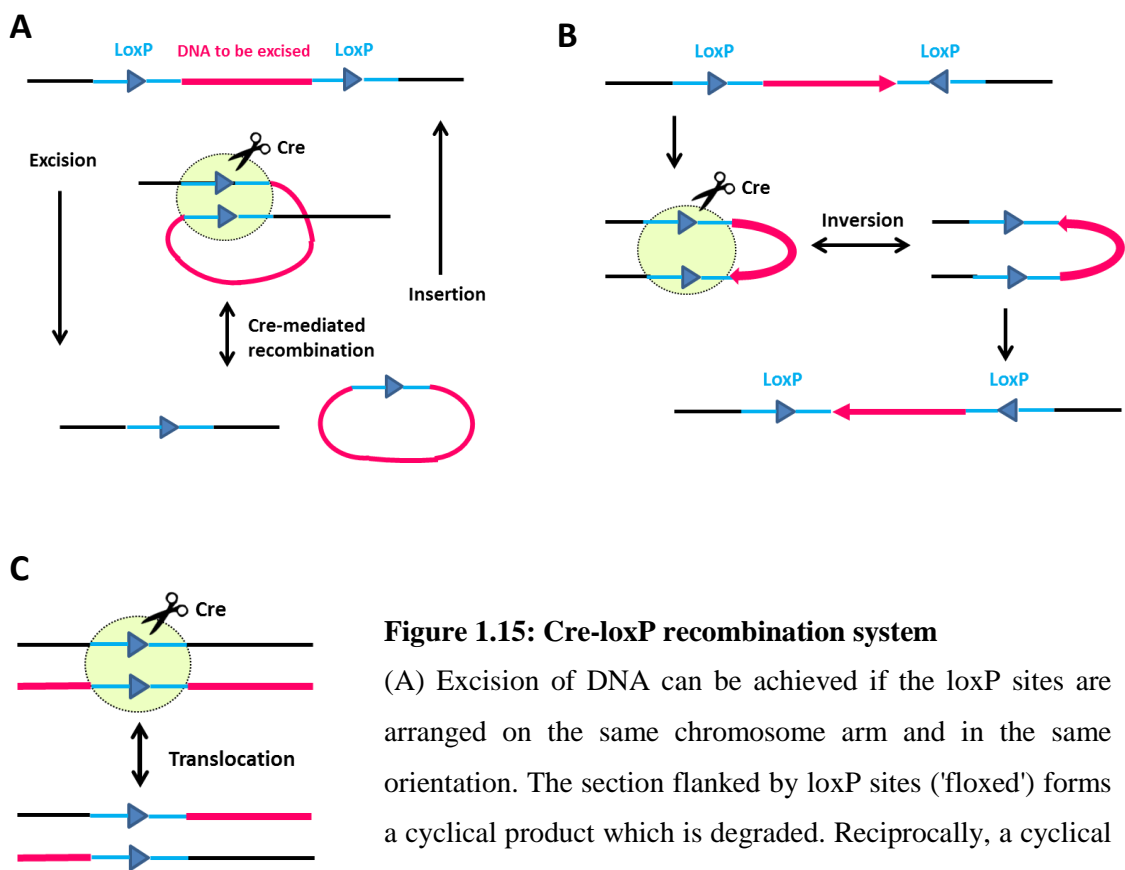
Figure 1.15: Cre-loxP recombination system
(A) Excision of DNA can be achieved if the loxP sites are arranged on the same chromosome arm and in the same orientation. The section flanked by loxP sites ('floxed') forms a cyclical product which is degraded. Reciprocally, a cyclical fragment containing a loxP site can be integrated into a gene with a single loxP site. However, this is much less common due to degradation of the cyclical fragments. (B) Inversion occurs between inverted loxP sites on the same chromosome. (C) Translocation occurs between loxP sites on non-homologous chromosomes.

1.5.2.3 Experiments at ZTs versus CTs

As described previously, organisms possess an intrinsic clock system; in the absence of any environmental cues, for example by being kept in constant darkness, organisms still display rhythm with a free-running circadian pacemaker period slightly offset to 24 hours. Light, as main Zeitgeber, allows to entrain organisms so the period of their rhythms is in phase with the solar day. Therefore, when designing experiments, it is fundamental to choose between performing experiments following the light-dark cycles of the animal housing conditions or carrying out experiments in constant darkness, in order to avoid the confounding effects of the external light-dark cycle and test for a true circadian rhythm which persists in constant conditions. In the latter case, animals are housed in constant darkness at least 24 hours prior to any experiment which is carried out in constant darkness (Figure 1.16A). By convention, the onset of activity of diurnal organisms defines circadian time zero (CT 0) and the onset of activity of nocturnal organisms defines circadian time twelve (CT 12). All my experiments were performed following the light/dark cycle of the housing condition at Zeitgeber Times (ZTs), ZT0 being the light on-set and ZT12 the light off-set (Figure 1.16B).
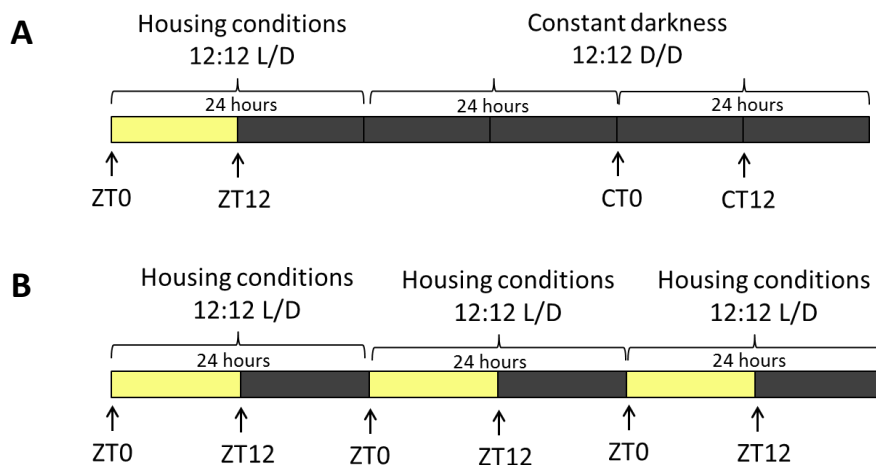
Figure 1.16: Schematic representation of experiments performed at CTs or ZTs

(A) For experiments carried out at Circadian Times (CTs), animals are moved from the 12h:12h light/dark cycle conditions to constant darkness for at least 24 hours prior to the beginning of the experiments. For mice, CT0 is the beginning of the resting phase and CT12 the on-set of activity. (B) For experiments carried out at Zeitgeber Times (ZTs), animals are kept under the 12h:12h light/dark cycle conditions, ZT0 being the light on-set and ZT12 the light off-set.

Experiments from ZT0 (included) to ZT12 (excluded) were performed under normal light whereas experiments from ZT12 (included) to ZT0 (excluded) were performed in darkness, using infrared goggles to view animals or red light as specified in each chapter. This implicates the animals were constantly entrained by light. I chose to keep the mice under light-dark cycle conditions for my experiments rather than constant darkness as it is more representative of the real-life environmental conditions.

1.5.3 Relevance of the project to the research area

There is a pressing need for new drugs and approaches for treatment of airway diseases, especially COPD whose incidence is increasing worldwide. Many current agents lack specificity, causing side-effects, and also often lack efficacy. Pulmonary inflammation and oxidative stress play key contributory roles in pathology of many lung diseases. Recent discoveries have revealed the circadian clock to be a potent regulator of inflammation and immune responses suggesting novel mechanisms to target. Moreover, evidence has linked circadian system to oxidant:antioxidant balance control. It is therefore of utmost importance to gain new knowledge into how clocks modulate lung inflammatory responses and how oxidative stress pathways are involved in order to uncover effective new pharmacological targets.

Chapter 2:   Methods

2.1 Animal husbandry

All work within this project was carried out under Home Office licence, in accordance with the Animals (Scientific Procedures) Act of 1986 or in collaboration with GlaxoSmithKline (GSK) in accordance with the GSK Policy on the Care, Welfare and Treatment of Laboratory Animals reviewed by the Institutional Animal Care and Use Committee at GSK. All animals were housed in a 12hr light − 12hr dark (12:12 LD) lighting schedule with food and water available *ad libitum*. Mice bred in-house were used at approximately the same age, between 6 and 12 weeks. In general mice were killed using anaesthetic overdose with 0.2 mL pentobarbital intraperitoneal injection per mouse, in order to maintain the trachea. All killing was done in accordance with the schedule 1 licensing act 1981. Carcasses were destroyed by incineration.

2.1.1 Mouse strains

Male C57BL/6J mice aged 8 weeks were purchased from Harlan Laboratories, UK. Global Rev-Erbα knock-out *Nr1d1^{tm1Schb}* mice (subsequently known as *Rev-Erbα$^{-/-}$*) were provided by Professor Ueli Schibler (University of Geneva, Switzerland) (Preitner et al., 2002). These animals are on a C57/BL6 background and were created by replacing exons 3 and 4 (encoding the DNA binding domain) and part of exons 2 and 5 of the *Rev-erbα* gene by an in-frame LacZ allele. Animals were bred as a heterozygous colony, and offspring genotyped to identify knock-out (KO) and wild-type (WT) animals.

Nr1d1^{tm1Ics} and *Nr1d2 $^{tm1.1Rev}$* (hereafter known as *Rev-Erbα$^{fl/fl}$* and *Rev-Erbβ$^{fl/fl}$* respectively) transgenic mice were purchased from the Mouse Clinical Institute – Institut Clinique de la Souris (ICS) as frozen embryos and re-derived by Harlan Laboratories, UK.

The *Rev-Erbα$^{fl/fl}$* mouse strain was first described as a model of REV-ERBα conditional deletion (Cho et al., 2012; Lam et al., 2013). However, a recent study has demonstrated that the targeting strategy − the chosen position for the two loxP- leads to in-frame deletion of the DNA-binding domain (DBD) of REV-ERBα (Zhang et al., 2015). REV-ERBα protein without its DBD is still translated and maintains

"DBD-independent" functions. Therefore, this model is actually a knock-in of a DBD mutation, rather than a complete knockout of the REV-ERBα protein (Figure 2.1). Crossing of this strain with a Cre-driver line will result in impairment of REV-ERBα DBD function in specific cell types.
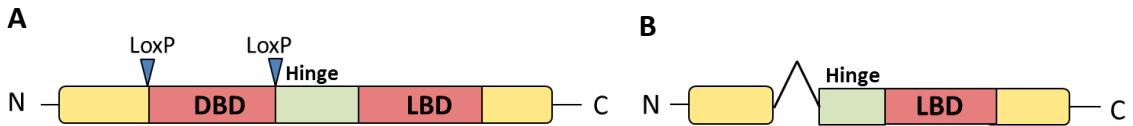
Figure 2.1: Schematic representation of conditional Rev-Erbα allele deletion resulting in an in-frame DNA binding domain mutant (DBDm)

(A) In *Rev-Erbα^{fl/fl}* mice, the two loxP sites are positioned upstream of exon3 and downstream of exon 4, flanking the DNA binding domain of the Rev-erbα locus. (B) In presence of Cre recombinase, deletion of the floxed region maintains the open reading frame and REV-ERBα protein without its DBD is translated.

The *Rev-Erbβ^{fl/fl}* (*Nr1d2^{tm1.1Rev}*) mouse strain, described by Ronald Evans and colleagues (Cho et al., 2012), contains an insertion of two loxP sites which flank exon 4 leading to non-functional protein.

Rev-Erbα^{fl/fl}Ccsp^{icre/+}/PER2::Luc and *Rev-Erbα^{fl/fl}Rev-Erbβ^{fl/fl}Ccsp^{icre/+}*/PER2::Luc (subsequently called *Ccsp-Rev-Erbα*-DBD^m and *Ccsp-Rev-Erbα*-DBD^m/*Rev-Erbβ^{-/-}*) strains were bred on site using the *Rev-Erbα^{fl/fl}* and *Rev-Erbβ^{fl/fl}* lines and an already established *Ccsp^{icre/+}*/PER2::Luc strain. Similarly, *Rev-Erbα^{fl/fl}LysM^{cre/+}*/PER2::Luc (subsequently called *LysM-Rev-Erbα*-DBD^m) mice were bred on site by crossing the *Rev-Erbα^{fl/fl}* line with an already established *LysM^{cre/+}*/PER2::Luc strain.

2.1.2 Genotyping

Mice from transgenic lines were ear punched for identification and the ear clips used for DNA extraction and genotyping. Tissue samples were stored at -20°C prior to DNA extraction using a QiaAmp kit (Qiagen).

DNA extraction began with incubation of tissue samples in 50μl animal tissue lysis (ATL) buffer and 10μl proteinase K (both part of kit) at 56°C for 1 hour. Samples

were vortexed after 30 minutes to ensure thorough mixing and digestion. Following incubation, 4μl RNase A (20mg/ml, Roche) was added, the solutions were mixed by vortexing and incubated at room temperature for 2 minutes. 100μl buffer AL (part of kit) was added and the mixture incubated at 70°C for 10 minutes. To precipitate DNA, 100μl 100% ethanol was added and solutions vortexed for 15 seconds. The resulting mixture was added to a spin column (part of kit), which was centrifuged at 8,000 rpm for 1 minute. The filtrate was discarded and 250μl of wash buffer AW1 (part of kit) added. The columns were spun again at 8,000 rpm for 1 minute. The filtrate was discarded again, and 250μl of wash buffer AW2 (part of kit) added. Columns were then spun for 3 minutes at 14,000 rpm to thoroughly wash the membrane. The top of the spin column was removed from the outer filtrate tube and placed into a clean 1.5ml Eppendorf tube and 100μl buffer AE (part of kit) was added to the membrane. Tubes were left to sit at room temperature for 1 minute to allow the elution buffer to soak the entire membrane and then spun at 8,000 rpm for 1 minute to elute the DNA. DNA samples were then stored at -20°C prior to use in genotyping PCR reactions.

Genotyping was carried out using GoTaq® Hot Start Polymerase (Promega). All primer sequences, reaction mixes and cycling conditions are given in appendix 1.

Genotyping of the Rev-Erbαflox alleles was undertaken using primers targeting the excision of the floxed exons resulting in the detection of a wild-type (769 base pairs), flox/conditional knock-out (956bp), and/or total knock-out (420 bp) fragments.

Genotyping of the Rev-Erbβflox alleles was undertaken using primers targeting the excision of the floxed exons resulting in the detection of a wild-type (983 bp), flox/conditional knock-out (1182 bp), and/or total knock-out (443 bp) fragments.

Assessment of Ccspicre status was performed using primers directed at the iCre sequence, resulting in a binary outcome of Cre positive (500bp) or Cre negative (no amplification). Animals were always bred as heterozygotes to wild-types, so no animals were produced that were homozygous for the Ccspicre allele.

Similarly, assessment of LysMcre status was performed using primers directed at the Cre sequence, resulting in a binary outcome of Cre positive (700bp) or Cre negative (no amplification). Animals were also always bred as heterozygotes to wild-types.

Genotyping for PER2::Luc was performed as a triplex reaction using primers targeting the normal and modified Per2 gene, such that wild type (230bp) and Luciferase positive (650bp) alleles could both be detected. Heterozygotes yielded both products.

All PCR products were run on a 2% agarose-TBE gel containing Safeview (NBS Biologicals) to visualise DNA bands. Electrophoresis was performed in 0.5× TBE buffer at 70V for 40 minutes. HyperLadder™ 50bp (Bioline) was used to determine fragment sizes. TBE buffer recipe is given in appendix 1.

2.2 *In vivo* experimental procedures and sample collection

All experiments were performed at Zeitgeber Times (ZTs), ZT0 being the light on-set and ZT12 the light off-set. This implicates the animals were constantly entrained by light. Experiments from ZT0 (included) to ZT12 (excluded) were performed under normal light whereas experiments from ZT12 (included) to ZT0 (excluded) were performed in constant darkness, using infrared goggles to view animals or red light as specified in each chapter.

2.2.1 Intranasal compound administration

Compound solution was made 2 hours prior intranasal dosing. 9.95 mg of compound GSK3824 was re-suspended in 4 ml vehicle (0.9% saline with 0.2% Tween 80, Sigma) for a final concentration of 2.49 mg/ml. As the solubility of the compound in the vehicle was very poor, the compound solution was sonicated using EpiShear Probe Sonicator (Active Motif, UK) at 45% amplitude, pulse for 30 seconds on and 30 seconds off for a total sonication "on" time of 10 minutes (or 20 minutes elapsed time). This resulted in having a compound suspension rather a proper dissolved compound solution.

Male C57BL6J mice were lightly anaesthetized using isoflurane delivered via a breathing system. Oxygen flow rate was set at 0.5l/min with an isoflurane concentration of 5% for induction and 2-3% for maintenance. Mice were placed in the "induction chamber" for about 3 minutes until breathing was slow and regular. Mice were then manually restrained and held in a supine position with the head elevated. The end of the micropipette was placed at the external nares, and 50µl of compound in suspension or vehicle was poured in dropwise. Mice were transferred back to their home cages. This dosing was repeated one more time 4 hours later. For each dose, animals received 0.124 mg of compound, so about 4.96 mg/kg.

2.2.2 Aerosolised lipopolysaccharide challenge

Before challenge, mouse tails were marked with ink to indicate home cage. At the indicated time points (specified in each chapter), mice were transferred to a Perspex exposure chamber. The lid was then sealed and the chamber transferred to a biological safety cabinet with a flow rate of 0.579m/s. Approximately 7ml of 2mg/ml lipopolysaccharide (isolated from *E.Coli* 0127:B8, L3129, Sigma) in 0.9% saline vehicle, or vehicle alone, was added to a jet nebuliser and inserted into the exposure chamber. The nebuliser was switched on for 20 minutes, after which the lid of the chamber was removed to quickly vent remaining vapours. Once the vapours had cleared, the exposure chamber was removed from the biological safety cabinet. Mice were transferred back to their home cages, using the markings for identification. 5 hours following challenge, mice were sacrificed via intraperitoneal injection of 200 µl pentobarbitone (Pentoject).

2.2.2.1 Bronchoalveolar lavage

The mouse chest cavity was opened and a hole made in the trachea using microdissecting scissors. A cannula, made from a 23G needle (BD Microlance 3, Becton Dickinson) inserted into plastic tubing (Fine bore, 0.58mm internal diameter, 0.96 external diameter, Smiths), was then inserted into the trachea. 1ml of chilled bronchoalveolar lavage (BAL) fluid, consisting of 3.72g/l EDTA and 0.1% w/v BSA in dH2O, was instilled into the lungs using a 1ml syringe. The fluid was then

withdrawn using the same syringe, and exudate transferred to 1.5ml Eppendorf tube. Samples were stored on ice before further processing.

2.2.2.2 Total cell counting

After a quick vortex to re-suspend the cells, 19µl of BAL fluid was transferred into a 200µl tube and mixed with 1µl of fluorescent dye solution 18 (Chemometec, Denmark). This dye contains Acridine Orange (AO) and DAPI. AO is used as a counterstain staining all living and dead cells thus providing a total count whereas DAPI stains the dead cells. Having the total number of cells and the number of dead cells makes it possible to provide with the viability, total count, the concentration of nonviable and viable cells. 11µl of the cell suspension and dye mixture was loaded to the chambers in A8 slides and slides inserted in NucleoCounter® NC-250™ (ChemoMetec, Denmark). NucleoView™ software for NucleoCounter® NC-250™ gives total cell number automatically expressed as cells/ml.

2.2.2.3 Flow cytometry

Staining

BAL samples were spun for 7 minutes at 1,400 rpm to pellet cells and debris. The supernatants were transferred to fresh 1.5ml tubes and stored at -80°C for cytokine analysis. Cell pellets were re-suspended in 200µl PBA (PBS with 1% BSA and 0.1% sodium azide) and transferred to a 96-well U bottom plate on ice, one sample per well. For the "unstained control" sample, 30µl of 6 random samples were transferred to an additional well. All samples were spun at 2,000 rpm for 2 minutes at 4°C in an Eppendorf 5804R plate spinner and supernatants were flicked off.

30µl of no fluorochrome anti-CD16/32 antibody (eBioscience, 14-0161-85) diluted 1:100 in PBA was added to each well to block the FC-receptors. After 20 minute incubation on ice, 150µl PBA was added to each well, the plate spun at 2,000 rpm for 2 minutes at 4°C and supernatant flicked off.

An antibody cocktail was then used to simultaneously stain for multiple markers (see table 2.1 for fluorochromes and dilutions). 30µl antibody cocktail was added to each well, except for the unstained control sample, and the plate incubated at 4°C for 20 minutes protected from the light. Following incubation, 150µl PBA was added to

each well, the plate spun at 2,000 rpm for 2 minutes at 4°C and supernatants flicked off.

Cells were re-suspended in 50μl/well PBA and 50μl/well fix solution (3.6% formaldehyde in PBA). The plate was incubated at room temperature for 20 minutes in darkness and then spun at 2,000 rpm for 2 minutes at 4°C. Supernatants were flicked off and the pellets re-suspended in 200μl PBA. The plate was spun again, supernatants flicked off and cells re-suspended in 100μl PBA.

Stained cells were stored at 4°C and protected from light for up to one week until run on flow cytometer.

Antibody	Fluorophore	Dilution	Supplier (ID)
Ly-6G (Gr-1)	AlexaFluor-488	1:100	eBioscience (53-5931)
CD11c	APC	1:200	eBioscience (17-0114)
SiglecF	PE	1:100	BD Biosciences (552126)

Table 2.1: Antibody dilutions and fluorophores used for flow cytometry

Analysis of cell populations

BD Biosciences LSR II flow cytometer was used to process suspensions, along with FACSDiva software to collect data and FlowJo software to analyse cell populations.

The unstained control sample was used to adjust FSC and SSC voltages to place the total cell population on scale. Appropriate gating of positive and negative populations was set up using compensations beads (OneComp eBeads, eBioscience) for each fluorophore to correct for spill-over into other channels. Cell suspensions were analysed using a medium to high flow rate and an automated stop at 10,000 counts. Neutrophils were counted as the proportion of single cells which were Ly-6G positive. Alveolar macrophages were counted as the proportion of single cells which were SiglecF and Cd11c positive whereas eosinophils were counted as the proportion of cells which were SiglecF and Cd11c negative.

2.2.2.4 Tissue for protein or RNA extraction

Tissue samples taken for RNA and protein extraction were snap frozen on dry ice and stored at -80°C.

2.2.3 Diurnal time series

At 6 time points across the day (ZT0, 4, 8, 12, 16 and 20), animals were sacrificed by anaesthetic overdose using 0.2 mL pentobarbital intraperitoneal injection per mouse. At ZT0, 4 and 8 animals were sacrificed under normal light. At ZT12, 16 and 20, animals were sacrificed under red light.

2.2.3.1 Tissue for protein and RNA extraction

Tissue samples taken for RNA and protein extraction were snap frozen on dry ice and stored at -80°C.

2.2.4 Cigarette smoke exposure

Cigarette smoke exposure was performed at GlaxoSmithKline (Upper Merion, Pennsylvania, USA) as previously described (Podolin et al., 2013). Briefly, beginning at 3-4 months of age, *Rev-Erbα*$^{-/-}$ mice and littermate controls (n = 9-10 per treatment group) received a single 2 hour nose-only exposure to 4% cigarette smoke from 3R4F cigarettes (College of Agriculture, Reference Cigarette Program, University of Kentucky). Smoke was generated by a Baumgartner-Jaeger CSM 2070i Smoking Machine (CH Technologies Inc., Westwood, NJ) containing a circular head that holds 30 cigarettes and performs one revolution per minute. A 4% concentration of smoke was produced via a 2 second, 35 ml puff of smoke taken from each cigarette once per minute; the resulting 1 liter of smoke was then mixed with 24 liters of air, and delivered to the exposure tower. During exposure to smoke or air only (sham controls), mice were maintained in restraining tubes containing stainless steel nose cone inserts. Twenty hours following the final smoke exposure, mice were anesthetized with isoflurane and then euthanized via cardiac exsanguination followed by cervical dislocation, and BAL fluid and lung tissue were

collected as previously described. All animal studies were ethically reviewed and carried out in accordance with European Directive 86/609/EEC and the GSK Policy on the Care, Welfare and Treatment of Animals.

2.3 *Ex vivo* experimental procedures

2.3.1 Isolation and treatment of mouse macrophages

2.3.1.1 Alveolar macrophages

Mice were euthanized by anaesthetic overdose using 0.2 mL pentobarbital intraperitoneal injection per mouse. Animal fur was dampen with 70% ethanol and using scissors, skin was pealed and tissue dissected to exposed trachea. Small incision was made into trachea and a cannula made from a 23G needle (BD Microlance 3, Becton Dickinson) inserted into plastic tubing (Fine bore, 0.58mm internal diameter, 0.96 external diameter, Smiths) was inserted into trachea. Cannula and trachea were stabilized with forceps throughout the procedure. 1 mL chilled bronchoalveolar lavage (BAL) fluid, consisting of 3.72g/l EDTA and 0.1% w/v BSA in dH2O, was infused into the lungs using 1 mL syringe fitted with the cannula and then gently aspirated back into the syringe. This lavage fluid was placed into 15 mL tube on ice. This process was repeated once and lavages were pooled on ice. BAL samples were then centrifuged at 1,400 rpm for 7 min at 4°C. Supernatant was discarded and cells were re-suspended into RPMI containing Penicillin/Streptomycin (P0781, Sigma − 1% v/v) before counting. Cells were seeded at ~800,000 cells/well in 6-well plates and directly treated with REV-ERBα ligand GSK1362 at 10μM followed by LPS at 100ng/ml. Plates were incubated in a humidified atmosphere (5% CO_2, 37°C) for 4 hours.

2.3.1.2 Peritoneal exudate cells (PECs)

Mice were euthanized by neck dislocation. Animal fur was dampen with 70% ethanol. Using scissors and forceps, the outer skin of the peritoneum was cut and gently pulled back to expose the inner skin lining the peritoneal cavity. 5 ml of ice cold PBS (with 3% FBS) were injected into the peritoneal cavity using a 25G needle (BD Microlance 3, Becton Dickinson). After injection, the peritoneum was gently

massaged to dislodge any attached cells into the PBS solution. The 25 g needle, attached to a 5 ml syringe was inserted again, bevel up, in the peritoneum and the fluid was collected while moving the tip of the needle gently to avoid clogging by the fat tissue or other organs. Collected cell suspension was kept in tubes on ice. This process was repeated once. If visible blood contamination was detected then the contaminated sample was discarded. Collected cell suspension was then centrifuged at 1,500 rpm for 8 minutes at 4°C. Supernatant was discarded and cells were re-suspended into RPMI containing Penicillin/Streptomycin (P0781, Sigma – 1% v/v) before counting. Cells were seeded at about 1×10^6 cells/well in 24-well plates and incubated in a humidified atmosphere (5% CO_2, 37°C). After a couple of hours, medium was changed in order to remove any residual blood cells and plates were incubated overnight. The following day, cells were treated with REV-ERBα ligand GSK1362 at 10μM or LXR agonist GW3965 at 2μM followed by LPS at 100ng/ml. Plates were incubated in a humidified atmosphere (5% CO_2, 37°C) for 4 hours before cell lysis.

2.3.2 Bioluminescence real-time recording

2.3.2.1 Preparation of precision cut ectopic lung slices

Ex vivo lung slices were prepared essentially as described before (Gibbs et al., 2009). Mice on a PER2::Luc background were sacrificed using an intraperitoneal injection of 200μl pentobarbitone (Pentoject) and the trachea and diaphragm exposed. A small incision was made in the upper trachea and a cannula made from a 23G needle (BD Microlance 3, Becton Dickinson) inserted into plastic tubing (Fine bore, 0.58mm internal diameter, 0.96 external diameter, Smiths), was then inserted into the trachea. 1ml of warmed (35°C) 2% agarose (type IXA, Sigma, UK) in Hanks' Balanced Salt Solution (HBSS, H6648, Sigma) was perfused through the tubing to inflate the lung. The trachea was then clamped below the insertion point with tissue clamps to prevent leakage and the cannula removed. Following this, the mouse was placed face down onto ice for 15 minutes to allow the agarose to set. Once the agarose had set, lungs and heart were dissected out *en bloc* and placed in ice cold HBSS to rinse. Lung lobes were separated prior to slicing, so that individual lung lobes could be used.

One by one, lung lobes were attached to the chuck of a vibratome (Campden Instruments Integraslice 7550MM) using superglue (Permabond 102 industrial cyanoacrylate adhesive). Once the glue had set, the chuck was immersed into the vibratome tank, which contained HBSS. An integrated liquid cooling system was used to maintain a tank/HBSS temperature of 4°C. 275μm sections were cut using a stainless steel blade (Campden Instruments) at 80Hz, 0.2mm/s. Sections were transferred to 1ml warmed (37°C) DMEM medium with Penicillin/Streptomycin (P0781, Sigma − 1% v/v) and L-glutamine (G7513, Sigma − 1% v/v); one slice per well of a 24-well cell culture plate (Corning). Plated tissue slices were incubated at 37°C, 5% CO_2 for 30 minutes. Medium was changed four times every 30 min to remove any traces of agarose. The tissue was incubated overnight to ensure the tissue was infection-free prior to rhythm measurement, and prepared for bioluminescence recording the next day.

2.3.2.2 Photomultiplier tube experiments

One hour before bioluminescence recordings, lung slices were synchronized by serum shock (50% FBS in DMEM). One hour later, the tissue was transferred onto a Millicell insert (Millipore Corp., Billerica, MA) within a 35-mm culture dish containing 1 ml recording medium (recipe in appendix 2). Vacuum grease (Dow Corning) was applied to the rim of the 35mm dish base, and a 50mm diameter glass coverslip (VWR) applied. Slight pressure was used to seal the coverslip to the dish, and the dish was then transferred to a 37°C incubator housing the photomultiplier tubes (PMTs - H6240 MOD1; Hamamatsu Photonics, Shizuoka, Japan). Each tissue slice was enclosed in an individual monitor (Channel), and multiple monitors were housed in each incubator (8 or 16-channels incubators). The PMTs were set to record in 60s bins, counting number of photons detected in this time.

2.3.2.3 Camera recording experiments

As described above, lung slices were placed onto cell culture inserts (Millicell) within 35-mm dishes containing 1 ml recording medium, sealed with a coverslip. They were then placed under a self-contained Olympus LV200 luminescence microscopy system fitted with a cooled Hamamatsu C9100-13 EM-CCD camera

(Olympus, Japan) as previously described (Guilding et al., 2013). Bioluminescence intensity was calculated from individual regions of interest using ImageJ software (v1.41o) and normalised to a 24 hour moving average.

2.3.2.4 Rhythm analysis

Bioluminescence data was recorded as photon counts per minute and normalised using a 24 hour moving average to produce oscillations about a mesor of 0counts/min. Normalised data was then entered into cosinor rhythm analysis software (Refinetti, 1993) to assess periods.

2.3.3 *In situ* hybridisation

In situ hybridisation (ISH) was used to visualise and quantify mRNA expression of *Rev-Erbα* (using probes targeting either the DNA binding domain or the ligand binding domain), *Rev-Erbβ* and *Cxcl5* in the lung of *Ccsp-Rev-Erbα*-DBD^m, *Ccsp-Rev-Erbα*-DBD^m/*Rev-Erbβ*$^{-/-}$ mice and their littermate controls. Due to the precise nature of this protocol and the use of radioactive isotopes, this work was performed by another lab member, Dr. Ben Saer, who is already proficient at this technique.

2.3.3.1 Preparation of tissue sections

Mice were sacrificed using an intraperitoneal injection of 200μl pentobarbitone (Pentoject) and the trachea and diaphragm exposed. A small incision was made in the upper trachea and a cannula made from a 23G needle (BD Microlance 3, Becton Dickinson) inserted into plastic tubing (Fine bore, 0.58mm internal diameter, 0.96 external diameter, Smiths), was then inserted into the trachea. The lungs were inflated with a 50/50 mix of 1xPBS and OCT (Optimum cutting temperature solution) to aid with sectioning. The trachea was then clamped below the insertion point with tissue clamps to prevent leakage and the cannula removed. Lungs and heart were dissected out *en bloc* and were snap frozen on autoclaved foil. Once frozen solid, the lung lobes were wrapped in the tin foil, labelled, and stored at -80ºC prior to slide preparation.

Frozen lungs were sectioned using a Leica CM3050 cryostat with object temperature set to -21ºC and chamber temperature set to -23ºC. The right lobe was sectioned at 12 μm and placed onto polysine slides. To preserve both tissue morphology and mRNA, mounted cryosections were fixed in 4% paraformaldehyde (PFA, Sigma) for 15 minutes and washed twice in 0.1 M PBS (Sigma) for 5 minutes. Triethanolamine (TEA, Sigma) and Acetic anhydride (AA, Sigma) was used to acetylate the sections. This prevents unspecific binding, and consequently minimises any background signal. The TEA/AA solution was prepared fresh for each batch of slides using 200 ml of 0.9% NaCl (Promega Ltd, Chilworth, UK), 3 ml of TEA and 520 μl of AA. The slides were treated for 10 minutes, whilst on a magnetic stirrer. The slides were then placed into 0.1 M PBS for a further 5 minutes. Slides were then dehydrated in sequentially increasing grades of ethanol at 70%, 80% and 90% for 5 minutes, followed by 10 minutes in 95% and 100%. Finally, the slides were placed into chloroform for 5 minutes and left to air-dry.

2.3.3.2 Preparation of plasmids containing sequences of interest

In order to obtain a probe for *in situ* hybridisation targeting a specific sequence of the gene of interest, primers were designed by retrieving mRNA sequence from the NCB1 nucleotide database and using the following criteria: 18 to 22bp long, GC content close to 50%, melting temperature (T_m) above 50ºC with a variance smaller than 0.5ºC between each primer. The T_m of each primer was calculated using the Vector NTI software (Invitrogen Ltd, Paisley, UK). Primer sequences and probe alignment to the gene of interest are given in appendix 3. The DNA sequences of interest were amplified from wild-type mouse lung cDNA by PCR reaction using 100ug of cDNA, with 2 μl forward primer at 10 μM, 2 μl reverse primer at 10 μM, 10 μl 10x buffer, 2 μl dNTP 10 mM, 2 μl Sahara DNA Polymerase (Bioline, London, UK). Samples were placed in a PCR machine with the following cycling conditions: 10 min at 95˚C, 35 times (30 sec at 95˚C, 30 sec at 60˚C, 30 sec at 68˚C) and 5 min at 68˚C. The final reaction product was loaded on a 1% agarose gel with SafeView (2μL in 50mL, NBS Biologicals Ltd, Cambridgeshire, UK) and submitted to a migration at 50 V for 80 min. 5μL of DNA HyperLadder 100bp (Bioline) was used to check band size. The gel was viewed on a UV Transilluminator (Biorad) and the

gel portion containing the amplified fragment was then excised and purified using a QIAquick gel extraction kit (Qiagen). In a microcentrifuge tube, three volumes of Buffer QG was added to 1 volume of the excised gel and incubated at 50˚C for 10 minutes. After incubation, 1 gel volume of isopropanol was added and vortexed. Once dissolved, the sample was purified using a QIAquick spin column and centrifuged for 1 minute at 13,000 × g. The flow-through was discarded before adding 0.5 ml of Buffer QG and centrifuged for 1 minute at 13,000 × g to remove all traces of the agarose gel. The flow-through was discarded and DNA washed using 0.75 ml of Buffer PE by centrifugation for 1 minute at 13,000 × g. The DNA was eluted using 50 µl of Buffer EB into a clean microcentrifuge tube by centrifuging the column for 1 minute at 13,000 × g.

Ligation and Transformation

The amplified fragment or insert (3 µl) was ligated into the pGEMT-easy vector (1 µl; Promega Ltd) with 2 µl of 10x Buffer, 0.5 µl of T4 DNA Ligase (Roche Diagnostics) in a final volume of 20 µl using nuclease-free water. The sample was left to incubate at ~10ºC overnight.

The ligation product was transformed into DH5α *E.coli* competent cells (Invitrogen) to select for a positive plasmid construct; 2 µl of the ligation mix was incubated with 25 µl of DH5α cells for 30 min on ice. The bacteria were heat shocked for 45 sec at 42ºC and incubated for a further 5 min on ice. The bacteria were gently resuspended in 500µL of SOC medium (Invitrogen), incubated for 1 hour at 37ºC and spread on pre-warmed LB agar plates with 100 µg/ml of Ampicillin (Sigma-Aldrich). After an overnight incubation at 37ºC, the plate was removed from the incubator and placed at 4°C to halt bacterial growth. Prior to inocculation, 50ul of x-gal (ThemoFisher) was spread on each plate before pre-warming. Consequently, positive colonies will appear white whilst self-ligated colonies appear as blue (due to activation of the lac-z gene encoding the enzyme β-galactosidase present in the pGEMT-easy vector cloning site).

Plasmid Preparation

From the incubated plate, individual colonies were chosen and placed individually into 2 ml of LB medium containing 100 µg/ml of Ampicillin. The tubes were then

incubated under agitation (300rpm) at 37°C overnight. Plasmidic DNA was extracted from the bacteria using a Qiagen Midiprep kit (Qiagen) following the manufacturer's recommendations. The DNA was finally eluted with 50 µl of EB buffer and spun for 2.5 minutes.

Sequencing

Plasmidic DNA extracted from each clone was prepared for sequencing using the BigDye 3.1 system (Applied Biosystems) using 2 µl of BigDye polymerase enzyme, 3 µl of 5x reaction buffer, 2 µl of pUC M13 sequencing primer (10 µM; Eurofin MWG Operon, Germany) and 12 µl of water. PCR cycling conditions were as follows: 4 min at 96ºC, 35 times (30 sec at 98ºC, 15 sec at 50ºC, 4 min at 60ºC). The final reaction samples were then precipitated by adding 68µL of H_2O, 11 µl of 3M Sodium Acetate, 2µl of EDTA 125mM, 1 µl of glycogen 20 mg/ml and 300 µl of 100% EtOH. The samples were centrifuged at $13,000 \times g$ for 30 min at 4ºC. The supernatant was removed and the pellet washed with 100 µl of 70% EtOH and spun for a further 5 min. The supernatant was removed and the pellet left to air-dry for 15 min. The samples were sent to the University of Manchester DNA sequencing facility. The sequence data was analysed using the NCBI Blast database software. One bacterial clone containing the insert was kept and grown overnight in 200 ml of LB medium containing 100 µg/ml of Ampicillin to obtain more DNA (Qiagen Maxiprep kit, Qiagen).

2.3.3.3 Preparation of Radiolabelled Probes

Plasmids were linearised using restriction enzymes (Roche Diagnostics) to generate templates for sense (using NCOI) and antisense (using SALI) transcripts. Reactions were setup using 20 µg of plasmid, 10 µl of 10x reaction buffer (Roche Diagnostics), 10 µl of restriction enzyme (500-1000u) and completed with nuclease-free water to a final volume of 100 µl. Samples were mixed by vortexing and incubated at 37ºC for 4 hours. To ensure the plasmid was fully linearised, 5µl of each reaction mix was run on a 1% agarose TBE gel using a non-linearised plasmid as a control.

Linearised plasmids were then purified using a phenol chloroform based extraction. This procedure removes enzymes and salts used during linearisation, and increases

the final concentration through precipitation. For this, 400µl of phenol chloroform (Sigma-Aldrich) and 300µl nuclease-free water were added to the remaining linearised product and the mixture was vortexed and centrifuged at 13,000 × g for 5 minutes. The upper aqueous phase was transferred to a new Eppendorf tube along with 350µl of chloroform (Sigma-Aldrich), and centrifuged at 13,000 × g for a further 5 minutes. The upper aqueous phase was transferred to a new Eppendorf tube along with 1/10 volume of 3 M Sodium Acetate and 1 µl of 20 mg/ml glycogen (Roche Diagnostics). The samples were vortexed and mixed with 2 × volume of 100% cold ethanol and were left to precipitate at -80°C for 1 hour. Following precipitation, samples were centrifuged at 13,000g for 45 minutes at 4ºC to pellet the DNA. The supernatants were discarded and DNA pellets were washed with 100 µl of 70% EtOH followed by centrifugation at 13,000 × g for 5 minutes. The supernatants were discarded and DNA pellets were left to air-dry before resuspension in 15 µl of nuclease-free water. The samples were then quantified using a Nanodrop® 2000 (Thermo Scientific).

Prior to radiolabelling, cold transcription (non-radiolabelled) was performed for both sense and anti-sense probes to ensure a transcriptional product could be obtained from the reaction. 1µg linearised template was added to 2µl DTT, 4µl 5x transcription buffer, 1µl each of rATP, rCTP, rGTP and rUTP (all 10mM) and 1µl RNase inhibitor (all Promega). For the sense construct, 2.5µl SP6 RNA polymerase (Promega) was added whereas 1.5µl T7 RNA polymerase (Promega) was added for the anti-sense construct. Each mixture was made up to 20µl with nuclease-free water and then incubated at 37ºC for 45 minutes. Following incubation, 3µl RQ1 DNase (Promega) was added and incubated for a further 10 minutes to degrade the DNA template. To assess successful transcription, solutions were run on a 1% agarose-TBE gel.

The synthesis of the radiolabelled probes follows the same protocol as the cold transcription. However, rUTP was replaced by Uridine 5'-triphosphate alpha-^{33}P (PerkinElmer). All radioactive work followed the rules and regulations associated with ionising radiation, including both protection and waste disposal. Radiolabelled probes were purified prior to use by running through illustra ProbeQuant G-50 micro columns (GE Healthcare). Columns remove unincorporated ^{33}P-UTP, which may

have the potential to bind unspecifically. The gel matrix was resuspended by vortexing followed by centrifugation at 735g for 1 minute to remove the equilibration buffer and re-establish the matrix bed. The buffer was discarded and the column placed into a new microcentrifuge tube. Sample volumes were made up to 50μl with DEPC-treated water and then added to the columns (one column per sample). Samples were spun at 735g for 2 minutes. 50μl deiodinised formamide 99.5% (Sigma-Aldrich) was added to each elute and samples were denatured on a 65°C heat block for 5 minutes and then quenched on ice for 2 minutes. To assess radioactivity counts, 1μl of each probe was added to 4ml scintillation fluid (National Diagnostics) and measured using a Tri-Carb 2100CA Liquid Scintillation Analyser (Perkin Elmer). To ensure an even coverage of probe per slide, a measure of 15×10^5 cpm was mixed in 100 μl of Hybridisation Buffer. This ensured the amount of radiolabelled probe was consistent across all slides. For each probe, a measure of 15×10^5 counts per minute was added per 100μl hybridisation buffer (Appendix 2 for recipe and preparation).

2.3.3.4 Hybridization

Once the radiolabelled probe was mixed with the required amount of hybridisation buffer, 100μl hybridisation buffer/probe solution (pre-heated to 60°C) was dispensed over each slide and covered with a hybrid-slip (Sigma-Aldrich). Hybridisation was performed overnight at 60°C in a humidified chamber.

The following morning, hybrid-slips were removed and slides washed in 2x SSC buffer (Promega) with 50% formamide at room temperature for 10 minutes, followed by 2 x 30 minute incubations at 60ºC in 2x SSC-50% formamide buffer pre-heated to 60ºC. The slides were then incubated in RNase A (20μg/ml in TEN buffer, recipe in appendix 2) at 37ºC for 30 minutes to degrade all unbounded riboprobes. The slides were then placed into 2xSSC-50% formamide at 60ºC for 2×15 min followed by 0.5xSSC at 60ºC for 30 min. Finally the slides were placed into increasing grades of ethanol (70%, 95% and 100%) for 5 minutes each time.

2.3.3.5 Imaging and analysis

Slides were fixed, tissue side up, onto development cassettes using masking tape and covered with Kodak Biomax MR film (Sigma-Aldrich) for signal visualisation. The cassettes were left at -80°C for 1 or 2 weeks, depending on the probes, before development using a JP-33 Film Processor (JPI Healthcare).

After development, the film was scanned using a CoolSNAP-Pro camera (Photometrics) while placed on a light box (Jencons Scientific Ltd). Signal intensity was determined by measuring the optical density of regions of interest in Image Pro Plus 6.0 software (Media Cybernetics). Relative optical density was calculated for bronchioles for each animal (n=2/genotype) using the following formula:

$$ROD = (-Log10(ROI/LB)) - (-Log10(C/LB))$$

Where:
ROD = relative optical density
ROI = region of interest
LB = light box
C = control region

The formula takes into account the optical density of the film, light box and the area being quantified through subtraction. 2-3 bronchioles on each lung section were analysed per animal. Relative optical densities of each were averaged per animal, to give 2/genotype, and values are expressed as proportions of the littermate control mean.

2.3.4 Histology staining and immunohistochemistry

2.3.4.1 Preparation of tissue sections

Mice were sacrificed using an intraperitoneal injection of 200μl pentobarbitone (Pentoject) and the trachea and diaphragm exposed. A small incision was made in the upper trachea and a cannula made from a 23G needle (BD Microlance 3, Becton Dickinson) inserted into plastic tubing (Fine bore, 0.58mm internal diameter, 0.96 external diameter, Smiths), was then inserted into the trachea. The lungs were inflated with1ml ice cold 4% paraformaldehyde (PFA). The trachea was then clamped below the insertion point with tissue clamps and the cannula removed. The

lungs and heart were removed en bloc, and transferred to a 50ml Falcon tube containing 20 ml ice cold 4% PFA for fixation. Tissue in PFA was incubated overnight at 4°C on a rocker.

Following fixation overnight, the tissue was transferred into 70% ethanol to avoid over-fixation. Tissue processing was performed overnight in a Microm Spin Tissue Processor, moving through a series of incubations in 70% IMS (7 hours), 90% IMS (45 mins), 95% IMS (45 mins), 100% IMS (45 mins x 3), xylene (30 mins x 3) and finally molten paraffin wax (1 hour x 2).

A final incubation of 1 hour was performed in molten wax in a vacuum oven (65°C, -0.8bar) to facilitate evaporation and improve infiltration. Lung tissues were then embedded in paraffin wax blocks and left to set.

Tissue sections were cut to a thickness of 5 μm using a Leica 2255 microtome, mounted onto glass slides (X-tra Adhesive, Leica Biosystems) and allowed to dry for a minimum of 48 hours.

2.3.4.2 H&E staining

This staining was performed using the automatic carousel-type slide stainer Shandon Varistain 24-4 (Thermo Scientific™). Briefly, slides were incubated in xylene (5 mins), xylene (3 mins), xylene (3 mins), ethanol (3 mins), ethanol (2 mins), 90% IMS (2 mins), 70% IMS (2 mins), tap water (2 mins), Haematoxylin Gills 2 (2 mins), tap water (1 min), 5% acetic acid (10 secs), tap water (1 min), blueing agent/ Scott's tap water substitute (30 secs), tap water (2 mins), 70% IMS (1 min), 90% IMS (1 min), ethanol (1 min), eosin alcoholic (1.5 min), ethanol (2 mins), ethanol (2 mins), ethanol (2 mins), xylene (2 mins), xylene (3 mins), xylene (5 mins). Slides were then coverslipped using entellan (Merck Millipore). Images were collected using Zeiss axio imager a1 at 10x objective magnification and Zen software.

2.3.4.3 Picro Sirius Red Staining

Slides first underwent rehydration via incubation in xylene 1 (3 mins), xylene 2 (3 mins), 100% ethanol (2 mins) and 90% ethanol (2 mins). Slides were rinsed in dH2O

and PBS, followed by incubation in Picrosirius red stain (0.1% Sirius red F3b , 0.1% Fast green C.I. 42053, Fischer F-99, in saturated aqueous solution of picric acid) for 1 hour minimum in order to reach equilibrium. Slides were dunked one by one into 0.5% acetic acid solution for 2seconds in order to prevent loss of dye and blotted between 2 blotting papers to dry. Slides finally underwent dehydration by dipping them 3 times in 100 % ethanol, followed by another 3 dips in a separate 100% ethanol and a final incubation in xylene, before applying cover slips using entellan (Merck Millipore). Images were collected using Zeiss axio imager a1 at 10x objective magnification and Zen software. Quantification of percentage of Sirius red staining was performed using ImageJ software (v1.41o) following instructions given at https://imagej.nih.gov/ij/docs/examples/stained-sections/index.html. A first threshold was set to have all lung tissue coloured in red and therefore determine the total area. A second threshold was set to highlight only the red-stained areas. The percentage of Sirius red staining to total tissue was then calculated by dividing the area of red staining by the total area. By this means, the empty alveolar or bronchiolar space was not taken into account in the measurement of total area.

2.4 Cell culture

2.4.1 Maintenance of cell lines

2.4.1.1 Primary normal human bronchial epithelial (NHBE) cells

NHBE cells from a 40-year old healthy male donor were purchased from Lonza (Walkersville, MD). NHBE cells were expanded, cryopreserved, and cultured as monolayers in standard tissue culture flasks (Costar) in serum-free bronchial epithelium basal media supplemented with growth factors (BEGM®, Lonza). Reagentpack™ subculture reagents (Trypsin/EDTA, Trypsin Neutralizing Solution and Hepes-buffered saline solution), all purchased from Lonza, were used for subculture according to the suppliers instructions. Briefly, to harvest the cells, medium was removed and cells washed once with 10 ml HBSS (Lonza) per T175 flask. 10 ml of Trypsin/EDTA solution (Lonza) was added to each flask and cells incubated at 37°C/5% CO2 for 4-5 min. After cells were released, trypsin was neutralized by adding 10 ml of TNS (Trypsin Neutralizing solution, Lonza) to each

flask. Cells were pelleted by centrifugation at 850 rpm for 5 min at room temperature, re-suspended in growth medium, counted and seeded at the desired density in plates/ flasks. Cells were incubated in a humidified atmosphere (5% CO_2, 37°C), the culture medium was changed every 2-3 days and the cell viability was monitored routinely. For experiments, NHBE cells were seeded in 24-well culture plates at $5-7 \times 10^4$ cells/well and allowed to attach overnight before any treatment. Cells from the same batch of culture were pooled for each individual experiment and never used after passage 5. The cells from the same donor were used in all assays for assay consistency.

2.4.1.2 LA-4 cells

LA-4 cells are epithelial-like cells isolated from an urethan-induced lung adenoma of a 28 week old A/He strain mouse. LA-4 cells, purchased from Sigma, were expanded, cryopreserved, and cultured as monolayers in standard tissue culture flasks (Costar) in Ham′s F12 medium supplemented with 2mM Glutamine, 1% Non-Essential Amino Acids (NEAA) and 15% FBS. For subculture, cells were detached using 1ml or 3 ml of 10× Trypsin/EDTA (Sigma) to a T75 or T225 flask respectively. To stop the action of trypsin, 4 volumes of culture medium was added and cells were spun at 1,250 rpm for 5 minutes at room temperature. Cells were re-suspended in growth medium, counted and seeded at the desired density in plates/ flasks. Cells were incubated in a humidified atmosphere (5% CO_2, 37°C), the culture medium was changed every 2-3 days and the cell viability was monitored routinely. For experiments, LA-4 cells were seeded at 1×10^5 cells/well in 24-well culture plates or at 5×10^6 cells/dish into 150mm dishes and allowed to attach overnight before any treatment.

2.4.1.3 Human Embryonic Kidney (HEK) 293 cells

HEK 293 cells, purchased from European Collection of Authenticated Cell Cultures (ECACC), were expanded, cryopreserved, and cultured as monolayers in standard tissue culture flasks (Costar) in Dulbecco's Modified Eagle's Medium (DMEM) supplemented with 10% FBS. For subculture, cells were detached using 1ml of 10× Trypsin/EDTA (Sigma) to a T75 flask. To stop the action of trypsin, 4 volumes of

culture medium was added and cells were spun at 1,250 rpm for 5 minutes at room temperature. Cells were re-suspended in growth medium, counted and seeded at the desired density in plates/ flasks. Cells were incubated in a humidified atmosphere (5% CO_2, 37°C), the culture medium was changed every 2-3 days and the cell viability was monitored routinely. For experiments, HEK 293 cells were seeded at 4×10^5 cells/well in 12-well culture plates or at 8×10^5 cells/well in 6-well culture plates and allowed to attach overnight before any treatment.

2.4.2 Cell synchronisation

At time = 0, medium in plates was exchanged with serum-rich medium (50% Fetal Bovine Serum (FBS) in serum-free culture medium (v/v)). After 1 hour at 37°C, 5% CO_2, this medium was replaced by serum-free culture medium. For experiments in NHBE cells involving pro-inflammatory or oxidant agents, BEGM without hydrocortisone was used.

2.4.3 Cell transfection

2.4.3.1 Rev-Erbα siRNA transfection

NHBE cells were transfected with SMARTpool: ON-TARGETplus Human NR1D1 siRNA (Thermo Scientific) at 25 nM using DharmaFECT 1 (Thermo Scientific) as transfection reagent (0.25% v/v per well). ON-TARGETplus Non-targeting Pool siRNA (Thermo Scientific) was used as control at 25 nM. Briefly, siRNAs were mixed in Gibco Opti-MEM® (Thermo Fisher Scientific) in one tube and DharmaFECT 1 was mixed in Gibco Opti-MEM® in a second tube. After 5 minutes incubation at room temperature, the contents of both tubes were pooled and mixed by pipetting carefully up and down. After 30 min incubation at room temperature, BEGM was added. The culture medium was removed from the plates and the transfection solution added to each well. Transfection was performed for 48 hours by incubating NHBE cells at 37°C, 5% CO_2.

2.4.3.2 Plasmid transfection

HEK 293 cells were transfected with plasmids as indicated in each chapter. Polyethylenimine (PEI, Polysciences) was used as transfection vehicle on a 3:1 ratio of PEI (μg):total DNA (μg) (Longo et al., 2013). Plasmids were mixed in Gibco Opti-MEM® (Thermo Fisher Scientific) in one tube and PEI was mixed in Gibco Opti-MEM® in a second tube. After 5 minutes incubation at room temperature, the contents of both tubes were pooled and mixed by pipetting carefully up and down. After 20 min incubation at room temperature, the transfection solution was added dropwise to each well. Transfection was performed overnight for about 18 hours by incubating HEK 293 cells at 37°C, 5% CO_2.

2.4.4 Cell treatment

Cells were treated with compounds, pro-inflammatory or oxidant agents as indicated in each chapter. The different compounds and agents were directly added to the medium in each well or dish. Cells were incubated at 37°C, 5% CO_2 for indicated hours.

2.5 Proliferation Assay: MTT protocol

Proliferation assay was carried out following the protocol from Wallert and Provost Lab. It relies on the use of yellow MTT (3-(4,5-Dimethylthiazol-2-yl)-2,5-diphenyltetrazolium bromide, a tetrazole) which is reduced to purple formazan in the mitochondria of living cells. The absorbance of this coloured solution can be then quantified by measuring at a certain wavelength (usually between 500 and 600 nm) by a spectrophotometer. In brief, HEK 293 cells were seeded at 10,000 cells per well in a 96-well plate. A blank containing complete culture medium without cells was including. The following day, cells were treated with compounds at 10 μM or with 0.1% DMSO as control for 24 hours. Final volume was 100 μl per well. The next day, 20 μl of Thiazolyl Blue Tetrazolium Bromide (MTT), dissolved at 5 mg/ml in PBS was added to each well and cells were incubated at 37°C, 5% CO_2 for 3.5 hours. Media was then carefully removed from each well and 150 μl of MTT solvent (4 mM HCl, 0.1% Nondet P-40 (NP40) all in isopropanol) was added to each well. After 15-

minute incubation at room temperature on orbital shaker in foil paper, absorbance was read at 600 nm.

2.6 Bmal1 luciferase assay

This assay was performed using the Dual-Light® Luciferase & β-Galactosidase Reporter Gene Assay System (ThermoFisher Scientific, cat. #T1003) according to manufacturer's instructions. It allows rapid and sensitive sequential detection of firefly luciferase and β-galactosidase, enabling experimental and control reporter gene enzymes to be measured in the same cell extract sample. In brief, cell supernatants were discarded. Cells were rinsed once with PBS and were lysed using 90 μl of Tropix lysis solution (per well of a 12-well plate). After 10-minute incubation on ice, cell lysates were transferred into 1.5 ml tubes and centrifuged for 2 minutes at full speed at 4°C. 10 μl of each extract was transferred to luminometer microplate wells and 25 μl of Buffer A was added to each well. Within 10 minutes, 100 μl of Buffer B containing Galacton-Plus substrate was injected to each well and after 2 second delay, the luciferase signal was read for 1 second/well. After 45 minutes incubation at room temperature in the dark, 100 μl of Accelerator-II was injected to each well and after 2 second delay, the β-galactosidase signal was read for 1 second/well. Automatic injections of Buffer B and Accelerator-II and signal readings were carried out using GloMax®-Multi Detection System (Promega).

2.7 His-purification

Supernatants from the wells were discarded, HEK 293 cells lysed with either RIPA buffer supplemented with protease and phosphatase inhibitors for input samples or Guanidinium/HCl buffer I for His-purified samples (recipes in appendix 2). Lysates were transferred into 1.5 ml tubes and input samples were stored at -80C° while processing his-purified samples. Lysates were first sonicated using EpiShear Probe Sonicator (Active Motif, UK) at 35% amplitude, pulse for 10 seconds on and 10 seconds off for a total sonication "on" time of 40 seconds (or 80 seconds elapsed time). Samples were then centrifuged at full speed for 10 minutes at 4°C. Supernatants were added to Ni-NTA Agarose beads (Qiagen), previously washed with buffer I and partially bound with BSA at 50ng/μl (Sigma). Imidazole was added

for a final concentration of 5mM in order to interfere with the weak binding of other proteins and to elute any proteins that weakly bind. β-mercaptoethanol was also added for a final concentration of 10mM. Samples were incubated by rotation at room temperature for 2-3 hours. Samples were centrifuged at 2,000 rpm for 1.5 minutes, supernatants discarded and beads washed with buffer I supplemented with 5 mM imidazole. Samples were incubated by rotation at room temperature for 20 minutes and the wash step with buffer I and imidazole was repeated. Beads were then washed with urea buffer 3 (recipe in appendix 2) containing 5mM imidazole by rotating for 10 minutes, followed by another wash with buffer 3 containing 5mM imidazole and 0.2% TritonX100 (Sigma). Beads were finally washed with PBS by rotation for 10 minutes. After 1.5 minutes centrifugation at 1,000 rpm, supernatants were discarded. Beads were mixed with 4 × NuPAGE® LDS Sample Buffer (Life technologies) containing 10% β-mercaptoethanol (v/v) (Sigma) to obtain a final 1 × NuPAGE® LDS Sample Buffer and boiled 10 minutes at 70°C. Samples were stored at -80°C until run for Western blotting.

2.8 Immuno-precipitation

Supernatants from the wells were discarded, HEK 293 cells lysed with immunoprecipitation (IP) buffer (recipes in appendix 2). Lysates were transferred into 1.5 ml tubes, incubated on ice for 20 minutes and centrifuged at full speed at 4°C for 5 min. Supernatants were transferred to new 1.5 ml tubes and 80 μl were taken out for input and stored at -80°C. 1 μg of anti-HDAC3 antibody (rabbit polyclonal, Santa Cruz H-99) or 1 μg of rabbit IgG (Sigma) was incubated with protein lysates for 1 hour on a rotating wheel at 4°C. Antibody complexes were captured by addition of 50 μl magnetic beads formerly washed in IP buffer (Sure beads Protein G magnetic beads, BioRad) and incubation for 45 minutes at 4°C. Beads were washed three times with 500 μl IP buffer. After the final wash, beads were resuspended in 32 μl IP buffer containing loading buffer (4 × NuPAGE® LDS Sample Buffer, Life Technologies) and 10% β-mercaptoethanol (v/v, Sigma). Samples were boiled for 10 minutes at 70°C. Beads were cleared using magnetic separator and supernatants transferred to fresh tubes.

2.9 RNA analyses

2.9.1 RNA extraction

2.9.1.1 From cells

Cells were lysed by adding 350 µl RLT buffer (QIagen), containing 1% β-mercaptoethanol (v/v). Lysates were placed into QIAshredder (QIAgen) columns, spun at full speed for 2 minutes to thoroughly lyse the cells and remove cells debris. Total RNA was extracted using RNeasy Mini kit (QIAgen) according to manufacturer's instructions and on-column DNase digestion step was included. Briefly, lysates were well mixed with 350 µl 70% ethanol by pipetting up and down and transferred to an RNeasy spin column placed in a 2 ml collection tube. Columns were centrifuged at 10,000 rpm for 30 seconds and the flow-through was discarded. 350 µl buffer RW1 was added to the RNeasy spin columns. Columns were then centrifuged and the flow-through was discarded. For each sample, 10 µl of DNase I stock solution was mixed with 70 µl Buffer RDD (RNase-Free DNase Set, QIagen). 80 µl of DNase I incubation mix was directly applied to the RNeasy spin column membrane, and placed on the benchtop (20–30°C) for 15 min. 350 µl buffer RW1 was added and the columns were centrifuged at 10,000 rpm for 30 seconds. The flow-through was discarded, 500 µl of buffer RPE was added and the columns were spun at 10,000 rpm for 30 seconds. The flow-through was discarded, 500 µl of buffer RPE was added and the columns were spun at 10,000 rpm for 2 minutes. The flow-through was discarded, the columns were placed in a new 2 ml collection tube and centrifuged at full speed for 1 minute in order to remove any residual buffer. The columns were placed in a new 1.5 ml collection tube and 50 µl of RNase-free water was applied to the RNeasy spin column membrane. Columns were centrifuged at 10,000 rpm for 1 minute to elute RNA. RNA concentration (ng/µl) and purity ($A_{260/280}$ ratio of 1.9-2.1) was determined using Nanodrop 2000 spectrophotometer (Thermo Scientific). RNA samples were stored at -80°C.

2.9.1.2 From mouse tissues

RNA extraction from frozen tissue was performed using 1 ml Trizol reagent (Invitrogen) per piece of tissue and mechanical homogenisation at a speed of 6.0m/s, 3x 40s cycles (Lysing matrix D tube and FastPrep machine, MP Bio). Following homogenisation, 200 µl of chloroform was added and the mixture centrifuged at 12,000g for 15 minutes at 4°C. The aqueous phase (about 500 µl) was transferred to a new 1.5 ml tube and 500 µl of isopropanol was added. Tubes were incubated on ice for 10 minutes before being centrifuged at 12,000g for 10 minutes at 4°C. The pelleted RNA was washed with 1 ml of 75% ethanol, vortexed and spun at 12,000g for 5 minutes at 4°C. The supernatant was discarded and the pellet left to air dry for 10 minutes before being re-suspended in 200µl Nuclease-free water. RNA concentration (ng/µl) and purity ($A_{260/280}$ ratio of 1.9-2.1) was determined using Nanodrop 2000 spectrophotometer (Thermo Scientific). RNA samples were stored at -80°C.

2.9.2 Reverse transcription (RNA to cDNA)

For RNA extracted from mouse tissue, 500ng RNA was treated with 0.5 unit of RQ1 DNase (Promega) and incubated at 37°C for 30 minutes. To terminate the reaction, RQ1 DNase stop solution was added and the mixture incubated at 65°C for 10 minutes to inactivate the DNase. This DNase step was not performed for RNA extracted from cells as DNase was added directly to the column during the extraction. cDNA was prepared using High-Capacity RNA-to-cDNA^{TM} kit (Applied Biosystems) following manufacturer's instructions. Briefly, the 500 ng RNA was converted into cDNA in a 20 µl reaction volume containing 2× buffer and 20× enzyme. The reverse transcription reaction was performed at 37°C for 60 minutes, then stopped by denaturing the enzyme at 95°C for 5 minutes and held at 4°C. The incubation was performed in a thermal cycler. cDNA samples were stored at -20°C prior to use in quantitative PCR (qPCR).

2.9.3 Quantitative Real-time PCR (qPCR)

qPCR was carried out in 96-well MicroAmp Optical reaction plates (Life technologies) in 20 μl volume with 25 ng of cDNA using 2× FAST BLUE qPCR MaterMix (Eurogentec) and Taqman primers and probes. Amplification reactions were performed in duplex using eukaryotic 18s rRNA (VIC/MGB Probe, Life technologies) as endogenous control and the primer/probe set of the gene of interest. Primer/probe sets were either sequenced by MWG, Germany and used at 200 nM or purchased as pre-made primer/probe mixes from Life technologies. Sequences, references and master mix recipes are given in appendix 4. qPCR reactions in duplex were performed on StepOnePlus™ System (Life technologies) with an holding stage at 50°C for 2 minutes and at 95°C for 6 minutes to activate the *Taq* polymerase, followed by 40 cycles at 95°C for 15 seconds and at 60°C for 60 seconds. Relative gene expression were determined using the comparative CT (threshold cycle) method, which consists of the normalization of the number of target gene copies to the endogenous reference (18s rRNA) and untreated cell sample was used as the calibrator. A common threshold for both endogenous control and target gene was set in the exponential phase of the amplification curves. The relative changes of gene expression were calculated using the following formula: Fold change in gene expression, $2^{-\Delta\Delta Ct} = 2^{-[\Delta Ct \text{ (treated samples)} - \Delta Ct \text{ (untreated control)}]}$, where $\Delta Ct = Ct$ (detected gene) - Ct (18s rRNA) and Ct represents threshold cycle number. Each sample was run in duplicate.

2.10 Protein analyses

2.10.1 Protein extraction

2.10.1.1 From cells

Cells were lysed with RIPA buffer supplemented with protease and phosphatase inhibitors unless stated otherwise (recipe in appendix 2). After a few minutes of incubation at room temperature, plates were scrapped with tips to remove and lyse residual cells. The lysates were stored directly at -80°C or placed on ice for protein quantification.

2.10.1.2 From mouse tissues

Tissues were lysed in RIPA buffer supplemented with protease and phosphatase inhibitors using a tissue Ruptor (Qiagen). Briefly, frozen tissue was placed in a 50 ml tube on ice containing 500 μl of lysis buffer and homogenise for about 1 minute using a tissue Ruptor. Thes lysates were transferred into new 1.5 ml tubes on ice and 2 μl of benzonase nuclease (Novagen) were added. After a quick vortex, samples were incubated on ice for at least 5 minutes. The lysates were stored directly at -80°C or placed on ice for protein quantification.

2.10.2 Protein quantification

Protein lysates were centrifuged at $8,000 \times$ g for 10 minutes at 4°C for cells and at full speed for 2 minutes at 4°C for tissues in order to pellet cell debris. Bradford assay was performed to determine the amount of proteins in each sample using Protein Assay Dye Reagent (BioRad) and following manufacturer's instructions. Briefly, a standard curve was made by diluting BSA (Sigma) in distilled deionised water (ddH$_2$O) with an equal amount of lysis buffer as used in the samples for testing. An 8 point BSA dilution series was made: 0, 1, 2, 4, 6, 8, 10, and 12 μg/ml. Protein lysates from cells were diluted 1:200 in ddH$_2$O and 1:2,000 for lysates from tissue to have values in the standard curve range. Dye reagent was added and absorbance was read at 595 nm. Standards and samples were run in duplicate. Total protein concentration was calculated using standard curve equation which fitted a linear regression.

2.10.3 Immuno (Western) blotting

Total protein was quantified as described previously and 10-20 μg proteins were immuno-blotted against the respective antibodies following standard procedures. 4 × NuPAGE® LDS Sample Buffer (Life technologies) containing 10% β-mercaptoethanol (v/v) (Sigma) was added to protein lysates to obtain a final 1 × NuPAGE® LDS Sample Buffer in the tubes. Proteins were denatured at 70°C for 10 minutes and loaded into Mini Protean TGX Precast Gels 4-15% (BioRad). In

parallel, Precision plus Protein-Dual color standards (BioRad) which range 15 to 250 kDa, were loaded into each gel. Proteins were separated by SDS polyacrylamide gel electrophoresis (SDS-PAGE) passing 110V for 10 minutes and 150V for about 30 minutes through the system. The resolved proteins were transferred to a 0.2 μm pore size Protran nitrocellulose membrane (Whatman) for 70 minutes at 100V at 4°C in a methanol based transfer buffer (see buffer recipes in appendix 2). Membranes were then rinsed with Tris-HCl pH 7.6 buffered saline (TBS) solution supplemented with 0.1% Tween-20 (Sigma) (TBST) and blocked with 5% skim milk powder (Sigma) in TBST for 1 hour at room temperature with gentle agitation. Membranes were blotted with primary antibody diluted at the proper concentration in 0.5% skim milk powder in TBST, overnight at 4°C shaking gently. Antibodies and concentrations used are reported in Table 2.2. Membranes were washed 3×10 minutes with TBST to remove unbound antibody and secondary HRP-linked antibody was added diluted in 0.5% skim milk powder in TBST. After 1 hour of gentle agitation, excess antibody was washed off with 3×10 minute TBST washes. Blots were developed using Supersignal West Dura (ThermoScientific) detection reagent, Kodak BioMax MR or XAR Film and JP-33 Film Processor (JPI Healthcare). After developing, membranes were rinsed twice and wash 10 min with TBST to remove ECL detection reagent. Blots were stripped using 37°C pre-warmed Restore Western Blot stripping buffer (ThermoScientific) with gentle shaking for 15 min at room temperature. After two quick rinses and a 10 min wash with TBST, blots were blocked again as previously described and re-probed for beta-actin detection following the previous procedure.

After development, films were scanned using a HP Scanjet G4010 (HP) and signal intensity was determined by measuring the optical density of band using ImageJ software (v1.41o). Relative intensity was calculated using the following formula:

$$RI = \frac{\text{Protein of interest band intensity} - \text{background intensity}}{\text{ACTIN band intensity} - \text{background intensity}}$$

Relative intensities were averaged per genotype or treatment and values were normalised to controls.

Protein	Species	Source	Dilution
REV-ERBα	Mouse monoclonal	GlaxoSmithKline GSK6F05-2	1:1,000
Uteroglobin (CCSP)	Rabbit polyclonal	Abcam #ab40873	1:5,000
HO-1	Rabbit polyclonal	Enzo Life Sciences #ADI-SPA-895	1:2,000
HA	Mouse monoclonal	Roche #12CA5	0.12μg/ml
HDAC3	Rabbit polyclonal	Santa Cruz (H-99) #sc-11417	1:500
β-ACTIN	Rabbit polyclonal	Abcam #ab8227	1:5,000
Anti-mouse IgG	Sheep	GE Healthcare #NA931V	1:10,000
Anti-rabbit IgG	Donkey	GE Healthcare #NA934V	1:20,000

Table 2.2: List of antibodies used for Western blotting

GSK6F05-2 (Biocat 137359) antibody was developed in collaboration with GlaxoSmithKline at Stevenage, UK. The antibody was generated by conventional 3 month immunisation of SJL mice, with his-tagged Rev-ErbA alpha ligand-binding domain (aa 281-614), purified from *E. Coli*. Protein-specific monoclonal antibodies were identified by ELISA and Western Blot screening of single-cell derived clones. I carried out further validation and characterisation of this antibody. It detects both murine and human REV-ERBα by Western blotting and it does not bind to REV-ERBβ (Appendix 5 Figure A5.1). As this is a mouse monoclonal antibody, non-specific bands were expected to be detected by the anti-mouse secondary antibody when running mouse tissue samples. Indeed, by probing mouse lung lysates directly with the anti-mouse secondary antibody, multiple bands were detected (Appendix 5 Figure A5.2).

2.10.4 Magnetic Luminex Assay

The Magnetic Luminex Assay is analogous to an ELISA but measures multiple analytes simultaneously by using colour-coded superparamagnetic microparticles for each analyte. When the plate is read, a magnet in the analyser captures and holds the superparamagnetic microparticles in a monolayer. Two spectrally distinct Light Emitting Diodes (LEDs) illuminate the microparticules. One LED identifies the analyte being detected (colour of particle, pre-determined by kit) and the second LED measures the magnitude of the PE-derived signal, which is in direct proportion to the amount of analyte bound. The kit used in this work was a magnetic luminex

screening assay from R&D systems (LXSAMSM-23), which was read on a Bio-Rad Bio-Plex 200 system with Bio-Rad software. All bronchoalveolar lavage fluid samples were run neat unless stated otherwise. All buffers and reagents were provided as part of the R&D Systems assay kit.

Standards were prepared from three stock vials provided. Each vial was reconstituted with calibrator diluent RD6-52 as per instructions. Each vial was allowed to sit for 15 minutes with gentle agitation prior to making dilutions. A high standard cocktail was then made from 100μl of each standard stock vials, along with 700μl calibrator diluent RD6-52 to make 1ml total volume. This served as standard 1. Serial 3-fold dilutions were then performed from 100μl previous standard + 200μl calibrator diluent RD6-52. At each step, standards were mixed thoroughly before proceeding with the next dilution. 6 standards were made in total.

Next, the microparticles were re-suspended by a brief centrifugation (to spin down liquid from inside the cap) and a gentle vortex. For a full 96-well plate, 500μl microparticle cocktail was mixed with 5ml assay diluent RD1W in the opaque mixing bottle provided. 50μl of the diluted microparticle solution was added to each well of the 96-well plate provided. Standards and samples were then added to the appropriate wells, 50μl/well, along with 2 wells containing 50μl calibrator diluent RD6-52 to serve as a blank control. Standards and blank were run in duplicate and samples were run individually. The plate was then sealed using the foil plate sealer provided and incubated for 2 hours at room temperature on an orbital shaker set at 800 rpm.

Wash buffer was prepared by adding 20ml wash buffer concentrate to distilled water to prepare 500ml of wash buffer. The plate was washed using a magnetic micro-plate washer (Bio-Rad), which was attached to the underside of the plate while the plate was inverted to remove liquid. The magnet was removed before adding wash buffer (100μl/well), to allow resuspension of the microparticles and a more thorough wash. The magnet was then re-applied and the plate inverted to remove wash buffer. This process was repeated twice for a total of three washes. With the magnet still in place, the plate was gently blotted against absorbent paper to remove as much liquid as possible before proceeding with the assay.

Biotin antibody was then prepared by a brief centrifugation and a gentle vortex. 500μl antibody cocktail was mixed with 5ml assay diluent RD1W. 50μl of the diluted biotin antibody solution was added to each well and the plate was sealed with a fresh foil plate sealer. The plate was placed back on the orbital shaker at 800rpm for a further 1 hour at room temperature.

Three washes were repeated as described previously. Streptavidin-PE was prepared by brief centrifugation and a gentle vortex, and diluted to working concentration by adding 220μl concentrate to 5.35ml of wash buffer. 50μl working streptavidin-PE was added to each well and the plate was sealed with a foil plate sealer. The plate was placed back on the orbital shaker at 800rpm for 30 minutes at room temperature. During this time, lasers of the Bio-Rad Bio-Plex 200 machine were warmed up and the analyser calibrated. These processes were performed according to the on-screen instructions provided by the machine.

A final wash step (3x washes) was performed and microparticles resuspended with 100μl wash buffer per well. The plate was incubated for 2 minutes on the orbital shaker at 800rpm to ensure a thorough mixing and resuspension. The plate was then read on a Bio-Rad Bio-Plex 200 machine with the following settings (specified by the R&D Systems kit):

> Microparticle regions: See table 2.3
> Events/bead: 50
> Flow rate: 60μl/minute (fast)
> Sample size: 50μl
> Doublet discriminator gates: 8,000 and 16,500
> Collect: Median fluorescence intensity (MFI)

Concentrations of samples were calculated automatically by the software using blank-subtracted median fluorescence intensity values and a 5-parameter logistic (5-PL) curve for each analyte.

Analyte	Bead region	High Standard Value pg/ml
GM-CSF	12	4,975
TNF-α	14	822
CCL2	18	100,769
CXCL2	20	1,406
IL-5	26	2,601
IL-10	28	8,646
IL-17A	30	33,909
CXCL10	37	37,169
G-CSF	39	11,820
CCL3	46	2,640
CCL4	51	69,360
CCL11	74	4,530
CXCL1	13	17,573
IL-12p70	15	15,041
IL-1β	19	73,174
IL-2	22	2,644
IL-6	27	13,668
IL-13	29	33,272
IFN-γ	33	4,817
CCL5	38	26,770
M-CSF	45	2,460
IL-1α	47	15,240
CXCL5	66	15,370

Table 2.3: Standard values and bead regions for bioplex assay

Standards were provided pre-mixed as part of the magnetic luminex screening assay (R&D systems). A 6 point standard curve was generated from serial 3-fold dilutions. 'Bead regions' denote the unique colour attributed to each analyte and serve as a way of identifying which protein is being measured.

2.11 ChIP-seq

2.11.1 Cell treatment

For ChIP-seq experiments, LA-4 cells were seeded at 10×10^6 cells per 15-cm dish. The following day, cells were synchronised by serum shock as described in 2.4.2. Seventeen hours after serum shock, cells were treated with 10 μM GSK1362 or DMSO as control. One hour later, at +18h post serum shock, cells were challenged with 1 ng/ml IL-1β or PBS as control for an additional hour.

2.11.2 DNA-protein crosslinking and cell collection

Following treatment, LA-4 cells were fixed at +19h post serum shock by adding formaldehyde in PBS directly in medium for a final concentration of 1% formaldehyde. Cells were incubated 10 minutes at room temperature with occasional manual agitation to enable fixation. The formaldehyde crosslinking was quenched by adding 125mM glycine (final concentration) and incubating at room temperature for 5 minutes. The crosslinked cells were then collected using a rubber policeman scraper and transferred to a 50-ml conical tube on ice. Cells were centrifuged for 3 minutes at $1{,}250 \times g$ at 4°C. Supernatant was discarded and cell pellet was washed with 10 ml ice-cold PBS. This wash step was repeated a second time. After centrifugation for 3 minutes at $1{,}250 \times g$ at 4°C, supernatant was discarded and cell pellet was frozen and stored at -80°C.

2.11.3 Nuclei isolation and chromatin shearing

Nuclei isolation has appeared to be a critical step for efficient chromatin shearing in cells. This step was performed as previously described with a few minor changes (Arrigoni et al., 2015). Briefly, thawed cell pellet was re-suspended in 0.5 ml of Farnham Lab (FL) buffer (5 mM PIPES pH 8; 85 mM KCl; 0.5% Igepal CA-630) supplemented with protease inhibitor cocktail. Re-suspended cells were transferred into a 1.5 ml Eppendorf tube and briefly sonicated using EpiShear Probe Sonicator (Active Motif, UK) at 20% amplitude, pulse for 10 seconds on and 30 seconds off for a total sonication "on" time of 40 seconds. To ensure cell lysis and nuclei isolation, 10 μl of the cell lysate was used to look at it under a phase contrast microscope using

a hemocytometer. In lysed cells, the nuclei appear as dark dots with no surrounding halo of cytoplasm. Nuclei were then centrifuged for 5 minutes at 1,000 × g at 4°C. Supernatant was discarded and nuclei washed with 1 ml FL buffer. Nuclei were again centrifuged for 5 minutes at 1,000 × g at 4°C and supernatant was discarded. Nuclei pellet was re-suspended in 0.5 ml of ChIP buffer tC1 (True MicroChIP kit, Diagenode) supplemented with protease inhibitor cocktail. Samples were then sonicated to shear the chromatin using EpiShear Probe Sonicator (Active Motif, UK) at 37% amplitude, pulse for 30 seconds on and 30 seconds off for a total sonication "on" time of 20 minutes (or 40 minutes elapsed time). During all the sonication time, samples were kept in a tube cooler to prevent from the samples to get too warm during the process. After the shearing, samples were centrifuged at full speed for 2 minutes at 4°C and supernatant which contained the sheared chromatin was collected and stored at -80°C.

2.11.4 Magnetic immunoprecipitation and washes

This step was performed using True MicroChIP kit (Diagenode) and following manufacturer instructions. Briefly, 200 µl of thawed sheared chromatin was placed into a new 1.5 ml tube and specific antibody added to the tube. Antibodies and concentrations used are reported in table 2.4. The IP tube was then placed on a rotating wheel at 4°C and incubated overnight (for about 15 hours).

The following day, Protein A-coated magnetic beads (11 µl per IP sample) were resuspended in Beads Wash buffer tBW1 (55 µl per IP sample) and placed on a magnetic rack. The supernatant was discarded and the beads washed again using 55 µl tBW1 buffer. After removing the supernatant, beads were resuspended in 11 µl tBW1 buffer per IP sample and 10 µl of these pre-washed beads were added to each IP tubes. The tubes were then incubated on a rotating wheel for 2 hours at 4°C. After incubation, IP tubes were briefly spun to collect liquid from inside of the cap and placed on a magnetic rack. Supernatants were removed and beads were washed. To wash the beads, 100 µl of Wash Buffer tW1 was added; the tubes were gently shaken to resuspend the beads and incubated for 4 minutes on a rotating wheel at 4°C. This wash step was repeated with Wash Buffer tW2, tW3 and tW4, respectively.

Protein	Species	Source	Quantity per IP
H3K27Ac	Rabbit polyclonal	Active Motif # 39133	4 µg
REV-ERBα	Rabbit polyclonal	Ronald Evans' lab (Cho et al., 2012)	2 µg

Table 2.4: List of antibodies used for immunoprecipitation

2.11.5 DNA elution, reverse cross-linking and DNA purification

This step was still performed using True MicroChIP kit (Diagenode) and following manufacturer instructions. After the last wash with tW4, 200 µl of Elution Buffer tE1 was added to the beads and the tubes were incubated for 30 minutes on a rotating wheel at room temperature. In the meantime, 175 µl of Elution Buffer tE1 was added to 25 µl of sheared chromatin for the input sample. After incubation, IP tubes were briefly spun and placed on the magnetic rack. The supernatant which contained the eluted DNA-ptotein complex was transferred into a new tube. 8 µl of Elution Buffer tE2 was added to the IP and input samples and tubes were incubated for 4 hours in a thermomixer at 1,300 rpm and 65°C. This step allows to reverse the cross-linking and to digest proteins by the help of Proteinase K contained in buffer tE2. DNA was subsequently purified using MicroChIP DiaPure columns (Diagenode) following manufacture instructions. After reverse cross-linking, 5 volumes of ChIP DNA Binding buffer were added to each tubes (IP and input samples). The mixture, well mixed, was transferred to the provided Spin column in collection tubes. Columns in tubes were centrifuged at $10,000 \times g$ for 30 seconds and the flow-through was discarded. 200 µl DNA Wash buffer was added to each column. Columns in tubes were centrifuged at $10,000 \times g$ for 30 seconds and the flow-through was discarded. This wash step was repeated once. The columns were transferred into new 1.5 ml tubes and 25 µl of DNA Elution buffer was directly applied to the column matrix. After one minute of incubation, the columns in tubes were centrifuged at $10,000 \times g$ for 30 seconds to elute DNA. Quantification of DNA from IP'd and input samples was performed using Qubit™ fluorometric quantitation (Life Technologies). The Qubit® Fluorometer utilizes a fluorescent dye that is specific to DNA. This fluorescent dye emits only when bound to DNA, even at low concentrations, which

minimizes the effects of contaminants. The Qubit® 3.0 Fluorometer is more sensitive than UV absorbance, which measures anything absorbing at 260 nm—DNA, RNA, protein, free nucleotides, or excess salts. Qubit dsDNA HS Assay Kit (Life Technologies) was used following manufacturer's protocol. Briefly, a few microliters (from 1 µl for input samples to 5 µl for IP'd samples) were added to Qubit® working solution containing the dye for a total volume of 200 µl. Standards provided by the kit were also mixed with Qubit® working solution. After brief vortexing and 2 minute incubation at room temperature, standard and sample concentrations were read on the Qubit® 3.0 Fluorometer.

2.11.6 Sheared chromatin analysis

This step is crucial to validate chromatin shearing efficiency. For that purpose, 175 µl of Elution Buffer tE1 was added to 25 µl of sheared chromatin along with 10 µg of RNase A (Active Motif). After incubation at 37°C for 30 minutes, 8 µl of Elution Buffer tE2 was added and samples were incubated overnight in a thermomixer at 1,300 rpm and 65°C to allow reserve cross linking. The next day, sodium acetate was added to the samples for a final concentration of 0.3 M, followed by 0.7 volumes of isopropanol. Samples were stored at -20°C for about an hour to help the DNA precipitation. After centrifugation at 13,000 × g for 15 minutes at 4°C, DNA pellets were washed with 1 ml of 70% ethanol. Samples were centrifugation at 13,000 × g for 5 minutes at 4°C and the supernatants were removed. The DNA pellets were air-dried for about 5 minutes and resuspended in 25 µl of nuclease-free water.

Samples (10 µl of precipitated DNA + 2.5 µl of 5 × loading dye) were run in a 1.5% agarose gel at 50 V for about 2 hours along with DNA size marker to analyze chromatin size.

2.11.7 Quantitative PCR analysis

Before sequencing the samples, the IP'd DNA was analyzed by qPCR using one positive and one negative control target. The primer controls and concentrations are reported in appendix 4. qPCR was carried out in 96-well MicroAmp Optical reaction plates (Life technologies) in 20 µl volume using 2× SYBR Green master mix (Promega). A standard curve on known DNA quantities of Input DNA was produced

using five samples that are 10-fold dilutions (50, 5, 0.5, 0.05 and 0.005 ng). The IP'd samples were run along with the dilution series of the Input DNA standards using both positive and negative control primers. qPCR reactions were performed on StepOnePlus™ System (Life technologies) with an holding stage at 95°C for 10 minutes to activate the polymerase, followed by 40 cycles at 95°C for 15 seconds and at 60°C for 60 seconds. A melt curve stage was added with three consecutive steps at 95°C for 15 seconds, 60°C for 60 seconds and 95°C for 15 seconds respectively. The quantity of DNA in the qPCR IP'd samples was assigned by the instrument based on the standard curve. As 1 µl of IP'd samples was used for the qPCR reaction, the total amount of DNA in the IP'd sample was calculated by multiplying the elution volume of the ChIP reaction by the qPCR quantity of DNA assigned by the instrument. To express data as percent of input, the total amount of DNA in the IP'd sample calculated above was divided by the amount of DNA that went into the ChIP reaction (measured by Qubit® Fluorometer) and then multiply by 100.

2.12 Statistics

Data was plotted and analysed using Prism 6 (GraphPad). Data is presented as mean +/- standard error of the mean (SEM) or as mean +/- standard deviation (SD), and a significance value of $p < 0.05$ was used as standard. Where multiple comparisons were made, One-Way ANOVA or Two-Way ANOVA with Bonferroni post-hoc correction test was applied. In some experiments, outliers were removed using the Median Absolute Deviation (MAD). Briefly, the median value is determined for each data set. MAD is defined as followed: $MAD = b\ M_i\ (|x_i - M_j(x_j)|)$ where the x_j is the n original observations and M_i is the median of the series. In other words, the MAD is the median of the absolute values of the residuals (deviations) from the data's median. Usually, $b = 1.4826$, a constant linked to the assumption of normality of the data. The MAD is then used as a measure of whether an individual data point can be considered an outlier. If a data point fell outside of the median +/- 2.5x MAD, then it was excluded. This measure is very similar to the common mean +/- 2.5x standard deviation protocol, but is less affected by outliers themselves and is therefore a more reliable test (Leys, 2013). Where outliers were removed, this is made explicit in figure legends.

Chapter 3: Consequences of global REV-ERBα deletion on pulmonary inflammation

3.1 Introduction

The core clock component REV-ERBα (also known as NR1D1) is a member of the nuclear receptor superfamily of ligand-regulated transcription factors (Mangelsdorf et al., 1995). It lacks the C-terminal helix that is critical for ligand dependent recruitment of co-activators and transcriptional activation by nuclear receptors. As result, REV-ERBα is a potent repressor of transcription (Harding and Lazar, 1995) and it has found to interact constitutively with the nuclear co-repressor 1 NCoR and histone deacetylase 3 (HDAC3) (Downes et al., 1996; Yin and Lazar, 2005). REV-ERBα has emerged as a critical regulator of multiple pathways involved in metabolism, development and immunity. It has shown to be a critical intermediary between the core clock and inflammatory pathways, especially in macrophages. Loss of rhythmic response of the major pro-inflammatory cytokine IL6 to peritoneal LPS challenge is observed in mice lacking the clock gene *Rev-Erbα* and modulation of REV-ERBα activity by synthetic agonist ligand GSK4112 regulates LPS-induced expression of a set of cytokines in macrophages (Gibbs et al., 2012). REV-ERBα also represses *Ccl2* expression directly through a REV-ERBα–binding motif in the *Ccl2* promoter region in murine macrophage cell line (Sato et al., 2014). In addition, REV-ERBs regulate their target genes by inhibiting the functions of distal enhancers that are selected by macrophage-lineage-determining factors, thereby establishing a macrophage-specific program of repression (Lam et al., 2013). In this chapter, the lung is used as a model to investigate the role of REV-ERBα in regulating inflammation in order to take into account the local tissue and cellular context.

3.2 Hypothesis tested and experimental approaches

Hypothesis: REV-ERBα plays a critical role in regulation of lung inflammation.

Objectives:

- Characterise the daily profile of clock and inflammatory gene expression and proteins in a REV-ERBα knock-out mouse model.

- Define responses of REV-ERBα knock-out mice and wild-type littermate controls to aerosolised lipopolysaccharide (LPS) or cigarette smoke, and quantify the

resulting inflammatory response via quantification of cell infiltration and measurement of cytokine concentrations.

- Assess differences in antioxidant gene expression between wild-types and REV-ERBα knock-out mice in basal state or under inflammatory challenged conditions.

3.3 Results

3.3.1 REV-ERBα deletion does not suppress clock gene rhythms in the lung but it dampens *Bmal1* expression

First, I confirmed the absence of REV-ERBα at transcript and protein levels over 24 hours in the knock-out animals by sampling lungs from wild-type and *Rev-Erbα$^{-/-}$* mice every 4 hours (Figure 3.1). As previously reported in wild-type mice, *Rev-Erbα* mRNA peaked during the late light period at ZT8 (Sukumaran et al., 2011). In collaboration with GlaxoSmithKline, a novel monoclonal anti-REV-ERBα antibody (GSK6F05) was developed (Chapter 2.10.3 and Appendix 5). With this antibody, I detected REV-ERBα rhythmic expression at protein levels (Figure 3.1B). This was in phase with the transcript rhythms, suggesting a rapid translation process and a quick turnover of the protein.

Although diurnal rhythms of other clock genes were not perturbed in lung tissue from knock-out animals (Figure 3.1), there was a lower amplitude in *Bmal1* transcript oscillations, being at least 16-fold in wild-type animals, but less than 3-fold in *Rev-Erbα* knock-outs. Diurnal rhythm of *Cxcl5*, a critical clock-controlled lung chemokine signal, was not affected by REV-ERBα deletion whereas *G-csf* transcript levels were significantly lower in *Rev-Erbα* knock-out mice at ZT4 and ZT8. Other non-rhythmic inflammatory gene transcripts were measured and no difference between wild-types and knock-outs was observed (Appendix 6 Figure A6).
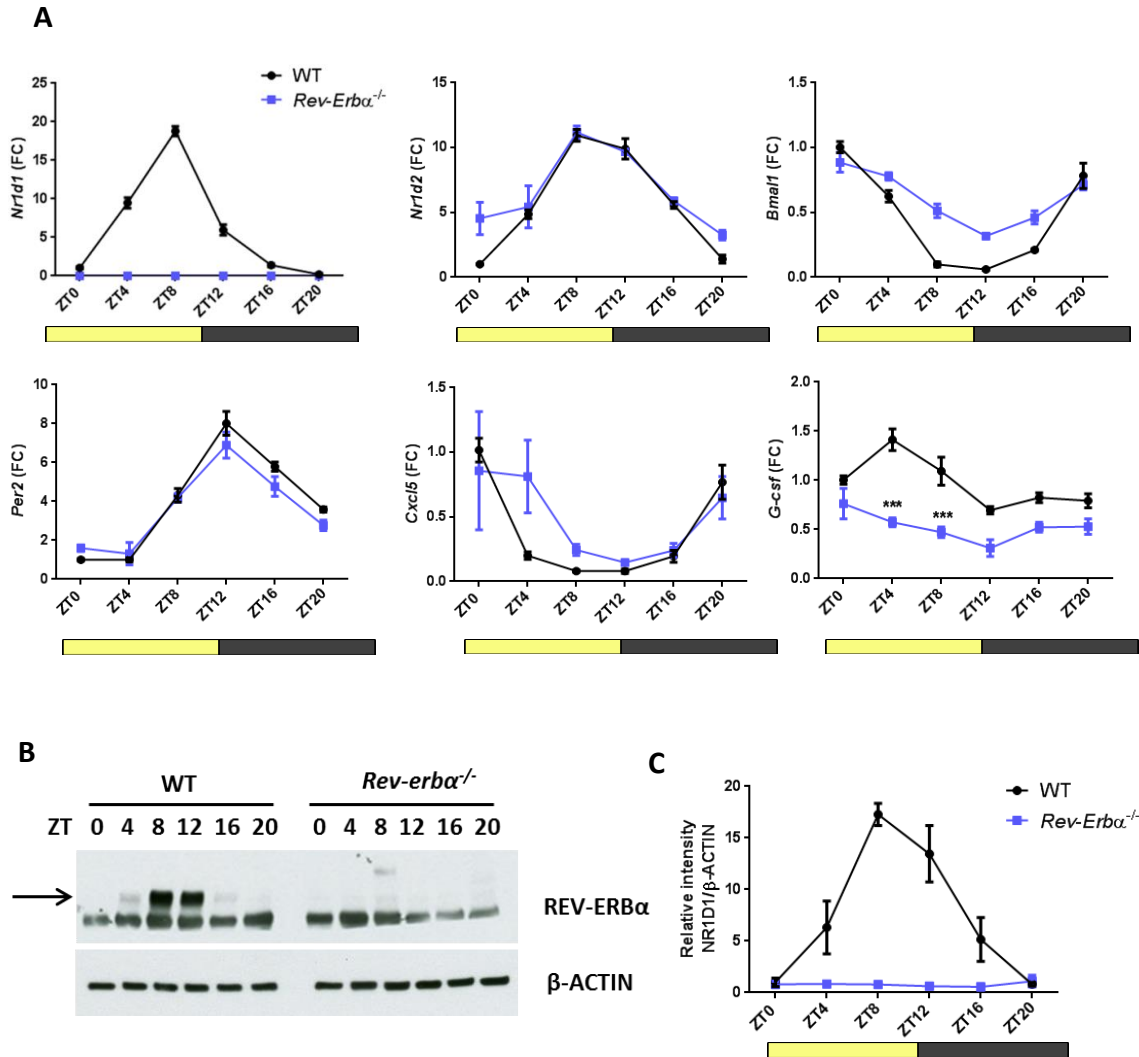
Figure 3.1: Profile of clock and inflammatory gene expression and proteins across a diurnal period in wild-type and *Rev-Erbα*^{-/-} mice

Lung tissues from *Rev-Erbα*^{-/-} and wild-type littermate control mice were collected at different time points across the day (ZT0 being the light on-set and ZT12 the light off-set). (A) mRNA levels in total lung tissues were determined by Real-Time qPCR and normalized to WT at ZT0. Data are presented as mean ± SEM; $n = 5$-6 for WT and $n = 3$-5 for KO, ****P <0.001*, significantly different to wild-type (Two-way ANOVA, post hoc Bonferroni). (B) Levels of REV-ERBα proteins were measured by Western blotting using monoclonal GSK6F05 anti-REV-ERBα antibody. (C) REV-ERBα densitometry (mean ± SEM) was normalised to β-ACTIN and to WT at ZT0; $n = 5$ per time point for WT and $n = 3$ per time point for KO.

3.3.2 Loss of REV-ERBα exacerbates neutrophilic inflammation upon aerosolised LPS

To investigate the pulmonary inflammatory responses in *Rev-Erbα*^{-/-} mice, males and females were first challenged with aerosolized lipopolysacchararide (LPS). Prior to the start of the project, members of the laboratory carried out a pilot study in collaboration with GlaxoSmithKline at Stevenage, UK. Different concentrations of LPS were nebulized at ZT4 and mice were culled 5 hours later. Thus, this experiment was carried out when REV-ERBα levels were rising, under light condition. Total cell count from bronchoalveolar lavage (BAL) fluid revealed an enhanced inflammatory cell infiltration in *Rev-Erbα*^{-/-} mice compared to wild-type in a dose-dependent manner (Figure 3.2A).
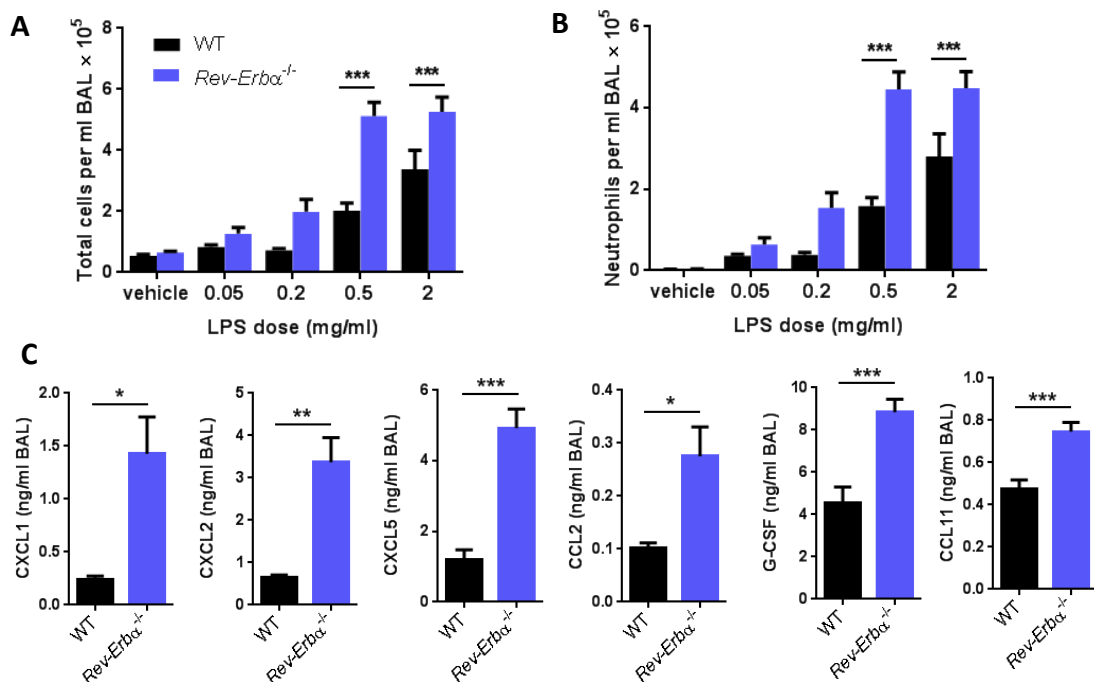
Figure 3.2: Pulmonary inflammatory response to lipopolysaccharide challenge at ZT4 in wild-type and *Rev-Erbα*^{-/-} mice

Mice were exposed to different doses of aerosolised LPS in saline for 20 minutes at ZT4 and culled 5 hours later. (A) Total cell counts per ml BAL. (B) Neutrophils were quantified in BAL using flow cytometry. Data are presented as mean ± SEM; *n*=6-8 per genotyping per dose, *P <0.05, ***P <0.001 (Two-way ANOVA, post hoc Bonferroni). (C) A select group of pro-inflammatory cytokines/chemokines, measured by bioplex analyses, are up-regulated in the broncho-alveolar lavage fluid after aerosolised LPS challenge (2mg/ml). *n*=8 per genotype, t-tests with Welch's correction.

Flow cytometry analyses showed these cells were predominantly neutrophils (Figure 3.2B). Release of pro-inflammatory chemokines and cytokines in BAL fluid was also elevated in *Rev-Erbα*^{-/-} mice compared to wild-type (Figure 3.2C).

In order to assess the effects of the time of challenge on inflammatory responses in this model, I repeated this experiment at both ZT0 and ZT12 using a LPS dose of 2 mg/ml.

Both male and female *Rev-Erbα*^{-/-} mice and littermate controls were then exposed to nebulised LPS at 2 mg/ml for 20 minutes at either ZT0 or ZT12 and culled 5 hours later at ZT5 or ZT17 respectively. As expected (Gibbs et al., 2014), infiltration of cells into the lungs of wild-type mice was significantly higher when animals were challenged at ZT0 than when challenged at ZT12 (Figure 3.3A). Interestingly, a significant increase of cell numbers was observed in knock-out mice compared to wild-type mice only when challenged at ZT12. Moreover, total cell numbers in BAL fluids from *Rev-Erbα*^{-/-} mice were statistically similar for both time points.

The composition of BAL cells was calculated as a percentage, using flow cytometry, and showed that macrophages were predominant in saline groups whereas neutrophils represented on average 98% of total cells in LPS-exposed groups (Figure 3.3B). The proportion of eosinophils was insignificant in all groups (about 0.1% of total cells). However, the number of total cells was so low in many BAL samples from unchallenged mice that the proportion of alveolar macrophages was not as elevated as expected (percentage of alveolar macrophages varied from 40 to 90 % depending on the total cell numbers). Therefore, the presence of debris and dead cells could lower the percentage of alveolar macrophages in BAL samples with few cells from unchallenged mice. A live/dead staining was not performed but it would have probably allowed to negatively gate for debris and dead cells. As neutrophils represented about 98% of total cell numbers, neutrophil numbers in LPS-exposed animals closely reflected the phenotype observed in total cell number analysis (Figure 3.3C). Wild-type males had a trend for greater neutrophilic recruitment than wild-types females at both ZT0 and ZT12. However, numbers of neutrophils in *Rev-Erbα*^{-/-} mice were similarly elevated in both sexes (Figure 3.3D). Macrophage numbers remained low at both time points and for both genotypes (Figure 3.3E). As LPS induced a massive recruitment of neutrophils into the lungs, the proportion of

macrophages in LPS-exposed groups was minor, and explained the reduction of macrophages numbers in the LPS-treated groups compared to the saline groups.
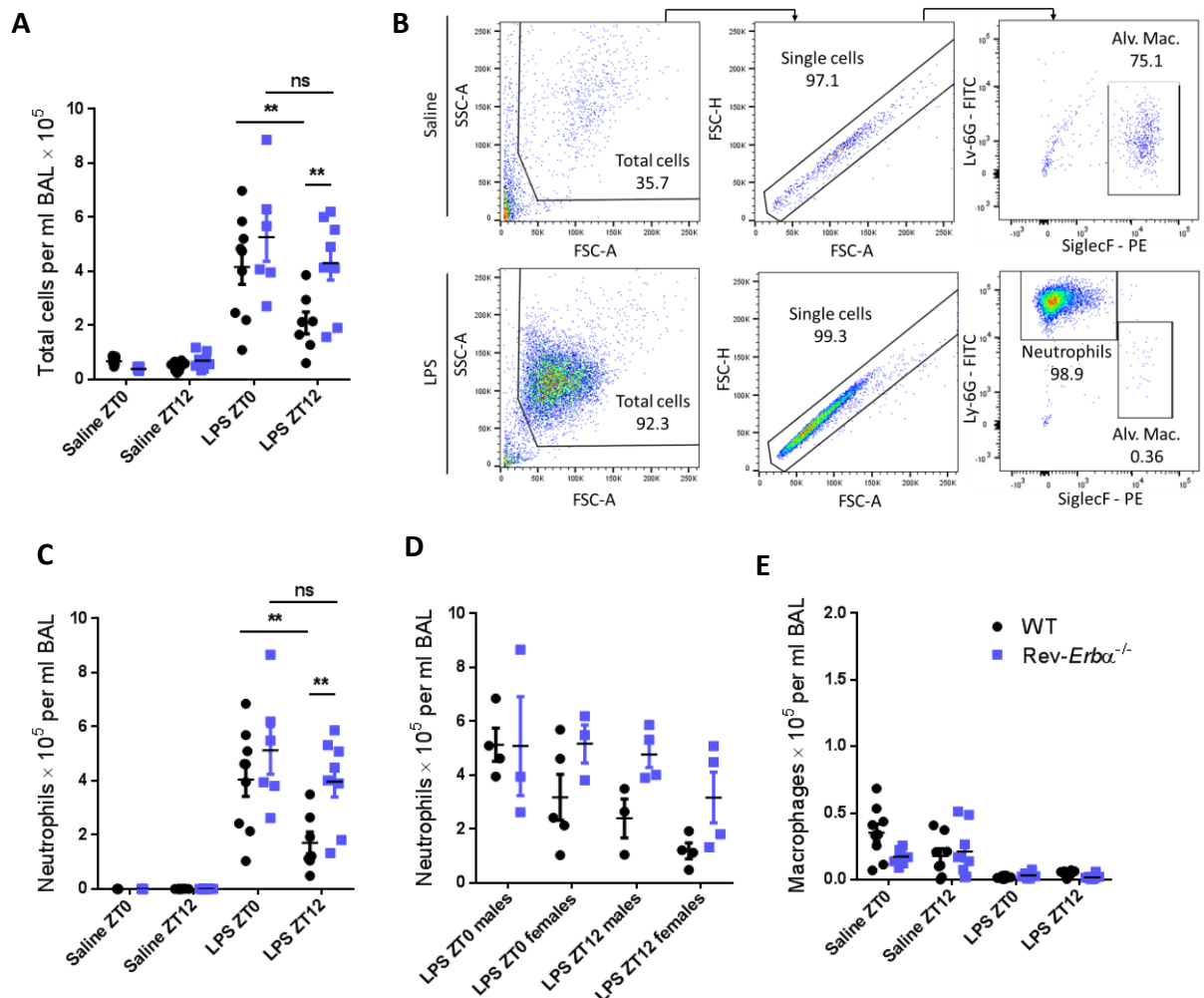
Figure 3.3: Inflammatory cell numbers recovered by BAL after LPS challenge at ZT0 or ZT12 in wild-type and *Rev-Erbα*^{-/-} mice

Mice were exposed to aerosolised LPS at 2mg/ml or to saline for 20 minutes at ZT0 or ZT12 and culled 5 hours later. (A) Total cell counts per ml BAL. Neutrophils (B,C,D) and macrophages (B,E) were quantified in BAL fluid using flow cytometry. Two data points representing two male wild-type mice exposed to LPS at ZT0 and ZT12 respectively with high measured total cell numbers were excluded using the median absolute deviation method. Data are presented as mean ± SEM; n = 6-10, *P <0.05, **P <0.01, ***P <0.001 (Two-way ANOVA, post hoc Bonferroni).

The levels of 23 cytokines/chemokines in BAL supernatants were measured by luminex assay. Twelve of them were detectable in samples from LPS-exposed mice

but only CXCL5 could be detected in BAL samples from unchallenged mice. This luminex analysis showed significantly elevated levels of CXCL1, CXCL2 and G-CSF in *Rev-Erbα*[^-/-] mice compared to wild-type controls, only when LPS exposure was presented at ZT12 (Figure 3.4, Appendix 7 Table A7). In contrast, release of CXCL5 in BAL fluid from *Rev-Erbα*[^-/-] mice was up-regulated compared to wild-types only when mice were challenged at ZT0 (Figure 3.4). Consistently with previous findings, gender analysis confirmed this phenotype was driven by males (Appendix 7 Figure A7). Moreover, only G-CSF levels in wild-type animals mimicked the gating of inflammatory responses observed in total cell and neutrophil recruitment with lower levels when mice were exposed at ZT12 compared to ZT0. In contrast, levels of chemokines CXCL1, CXCL2 and CXCL5 were similar at both time points in wild-type mice.

Eight other cytokines detected by luminex assay were up-regulated upon LPS exposure (Appendix 7 Table A7). However, no differences were measured between genotypes at neither time points, except for CCL5 which was reduced in *Rev-Erbα*[^-/-] mice compared to littermate controls when mice were exposed at ZT12.
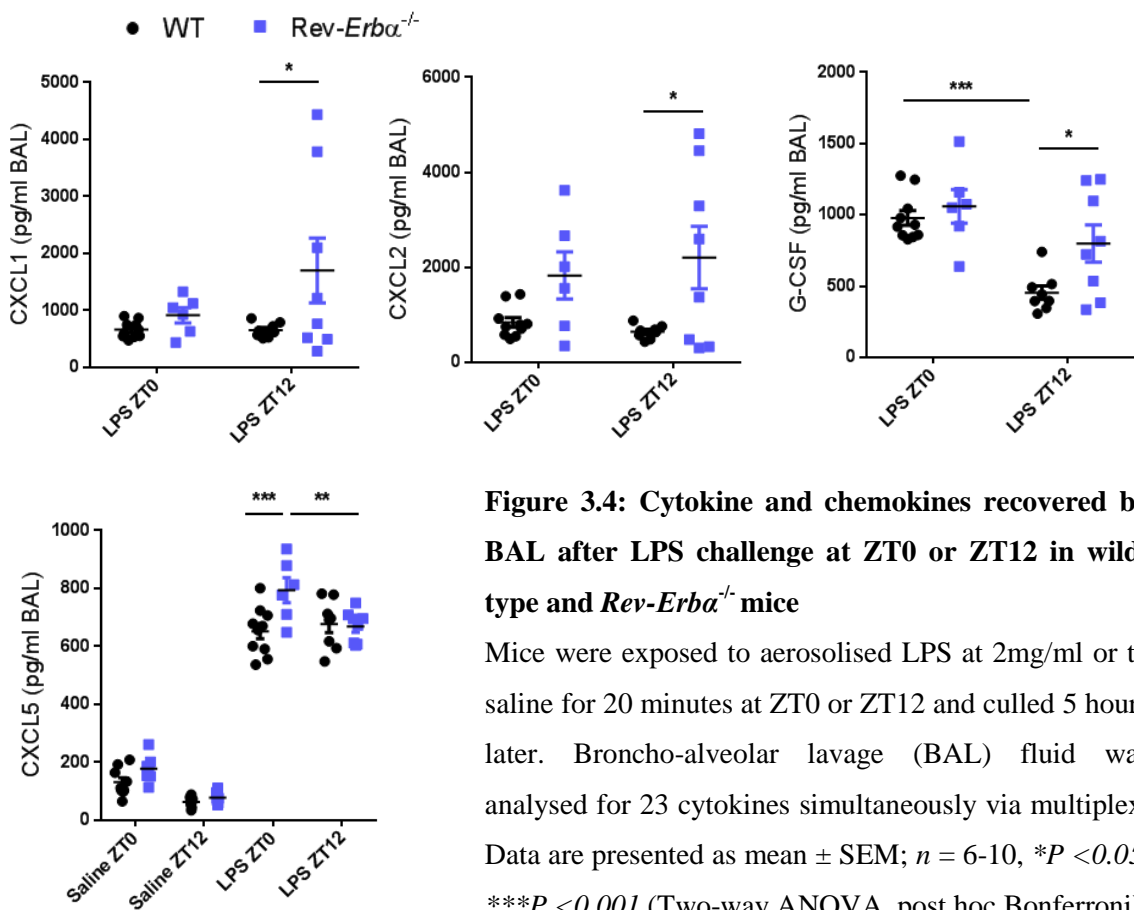
Figure 3.4: Cytokine and chemokines recovered by BAL after LPS challenge at ZT0 or ZT12 in wild-type and *Rev-Erbα*[^-/-] mice

Mice were exposed to aerosolised LPS at 2mg/ml or to saline for 20 minutes at ZT0 or ZT12 and culled 5 hours later. Broncho-alveolar lavage (BAL) fluid was analysed for 23 cytokines simultaneously via multiplex. Data are presented as mean ± SEM; *n* = 6-10, *P <0.05, ***P <0.001 (Two-way ANOVA, post hoc Bonferroni).

Transcript levels of inflammatory genes in whole lung were also measured by real-time qPCR (Figure 3.5). Profile of *G-csf* transcript perfectly corresponded to the protein levels in BAL samples with an increase in knockout animals compared to wild-types only when subjected to LPS at ZT12. Moreover, lower levels of *G-csf* mRNA were measured in wild-type mice exposed to LPS at ZT12 compared to ZT0, matching the protein profile. Interestingly, LPS-induced *Ccl2* increase was repressed in *Rev-Erbα*$^{-/-}$ mice compared to wild-type animals when exposed to LPS at ZT12. In contrast with proteins in BAL samples, *Cxcl5* transcript levels in wild-type mice were higher when animals were challenged at ZT12 compared to ZT0 whereas no time difference was observed in knockout mice. *Cxcl1*, *Cxcl2, Il-6* mRNA levels were elevated upon LPS challenges but no difference was observed between genotypes or between time points.
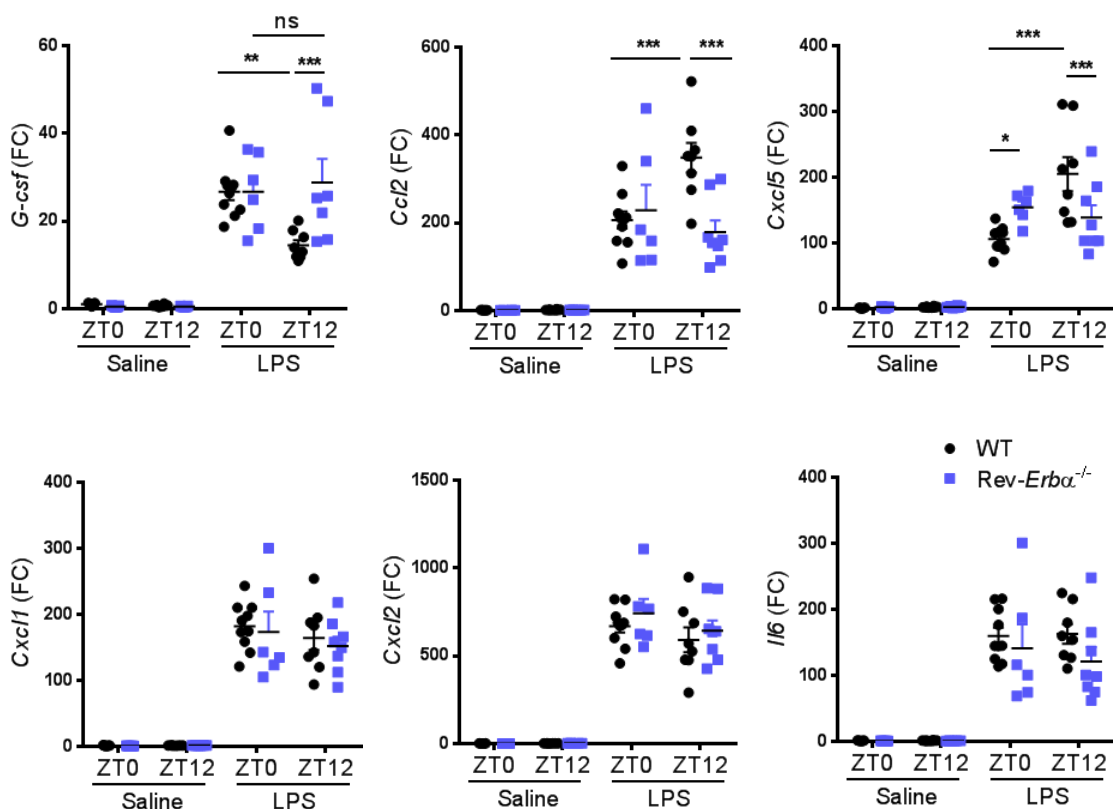
Figure 3.5: Transcript levels of inflammatory genes in response to LPS challenge at ZT0 and ZT12 in wild-type and *Rev-Erbα*$^{-/-}$ mice

Mice were exposed to aerosolised LPS at 2mg/ml or to saline for 20 minutes at ZT0 or ZT12 and culled 5 hours later. RNA was extracted from whole lung and transcript levels were measured by Taqman Real-Time qPCR and normalized to ZT0 wild-type saline group. Data are presented as mean ± SEM; *n* = 6-10, (Two-way ANOVA, post hoc Bonferroni).

3.3.3 Loss of REV-ERBα worsens pulmonary inflammation upon cigarette smoke challenge

3.3.3.1 Single smoke exposure

LPS drives inflammatory responses via multiple pathways but predominated by TLR-4 mediated signalling. To assess the wider spectrum of inflammatory responses, *Rev-Erbα*$^{-/-}$ and wild-type mice were also exposed to cigarette smoke, in collaboration with GlaxoSmithKline (USA). Single cigarette smoke (CS) exposure was carried out between ZT8 and ZT10 – when REV-ERBα levels peak - and mice were culled 24 hours later. BAL analyses revealed no difference in total cell, neutrophil or macrophage numbers between the two genotypes and between CS or sham exposure, despite two *Rev-Erbα*$^{-/-}$ mice having an increased neutrophil recruitment to the lung upon cigarette smoke (Figure 3.6A,B,C). Two-way ANOVA analysis of *Cxcl5* transcript levels in whole lung revealed a significant increase in *Rev-Erbα*$^{-/-}$ mice upon CS exposure compared to wild-type mice, despite a large standard deviation (Figure 3.6D). Elevated *Cxcl1* and *Cxcl2* mRNA levels were measured upon smoke exposure but no difference was detected between the two genotypes (Figure 3.6 E,F). Consistently with findings in 3.3.1, *G-csf* transcript levels were significantly down-regulated in *Rev-Erbα*$^{-/-}$ mice (Figure 3.6G). Interestingly, cigarette smoke caused a diminution of *G-csf* transcript levels in the wild-type mice. Levels of chemokines and cytokines in BAL fluids were either non detectable by multiplex analyses or very low and no significant changes were observed between genotypes. These results could be explained by the fact that a single CS exposure operates as a modest inflammatory challenge. Therefore, a multiple CS exposure study was carried out by exposing the mice once a day, for 10 days.

3.3.3.2 Multiple smoke exposures

Rev-Erbα$^{-/-}$ and wild-type mice were exposed to CS between ZT8 and ZT10 every day for 10 days and they were culled about 20 hours after the last exposure. Throughout this study, three *Rev-Erbα*$^{-/-}$ mice out of a total of nine died, two during smoke exposure and one sometime after exposure, resulting in a 33 % loss. In contrast, all the wild-type mice exposed to CS were fine. BAL analyses revealed no
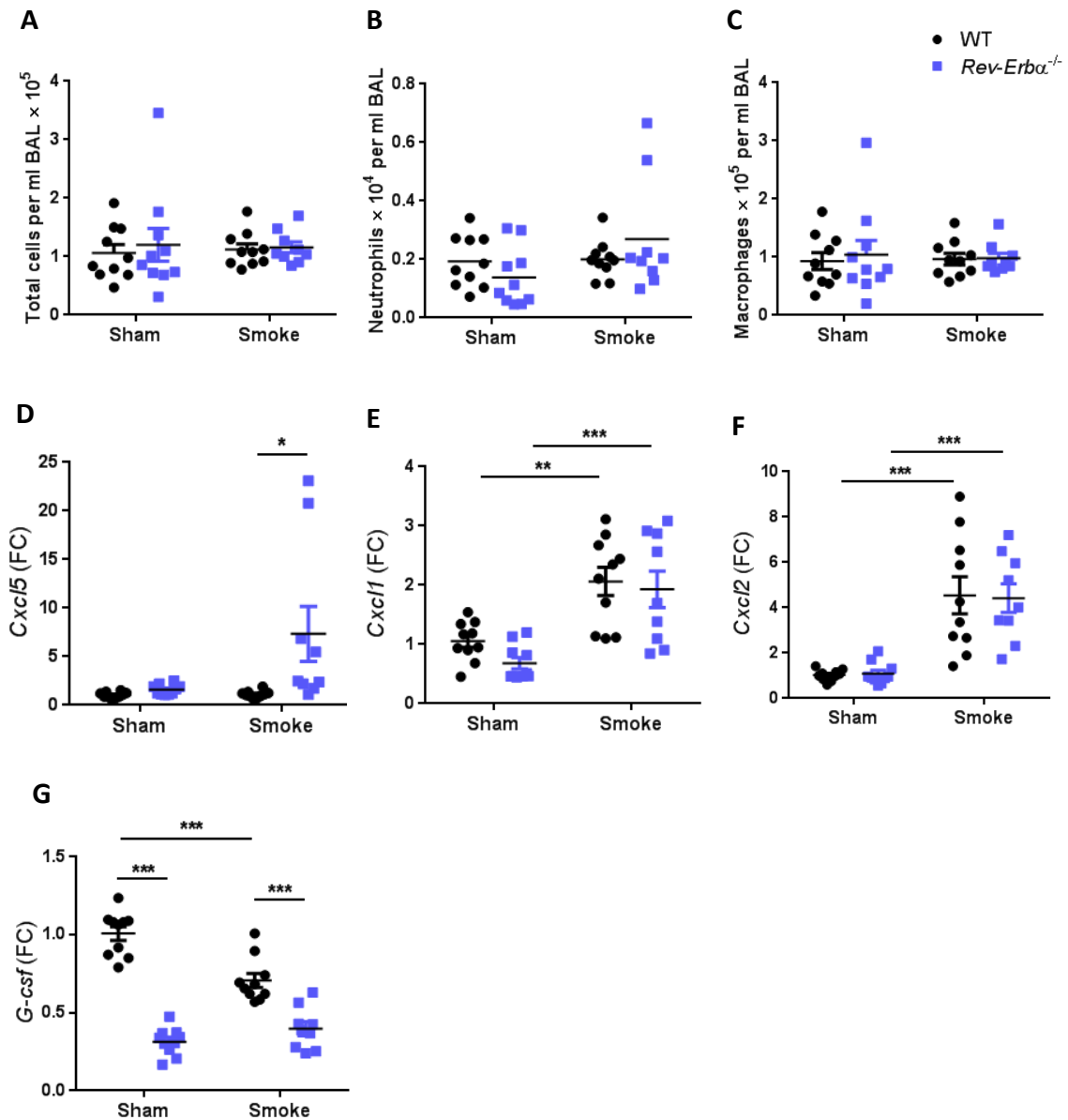
Figure 3.6: Pulmonary inflammatory responses after a single cigarette smoke exposure at ZT8 in wild-type and *Rev-Erbα*^{-/-} mice

Mice were exposed to cigarette smoke between ZT8 and ZT10 and culled 24 hours later. (A) Total cell counts per ml BAL. Neutrophils (B) and macrophages (C) were quantified in BAL using flow cytometry. (D) RNA was extracted from whole lung and transcript levels were measured by Taqman Real-Time qPCR and normalized to WT-sham group. Data are presented as mean ± SEM; n = 9-10, *P <0.05 (Two-way ANOVA, post hoc Bonferroni).

difference in total cell when both genders were plotted together (Figure 3.7A). However, gender analyses showed a significant increase in total cell numbers in BAL

fluid in females knock-out exposed to CS compared to the wild-types whereas no difference was observed in males (Figure 3.7B). Neutrophil numbers in BAL fluid were not different between genotypes despite a significant increase upon smoke exposures (Figure 3.7C). However, two-way ANOVA analysis showed elevated macrophage numbers in *Rev-Erbα⁻/⁻* mice compared to wild-type mice upon CS exposure (Figure 3.7D). Gender analyses revealed that the principal contribution to this phenotype was from females (Figure 3.7E).
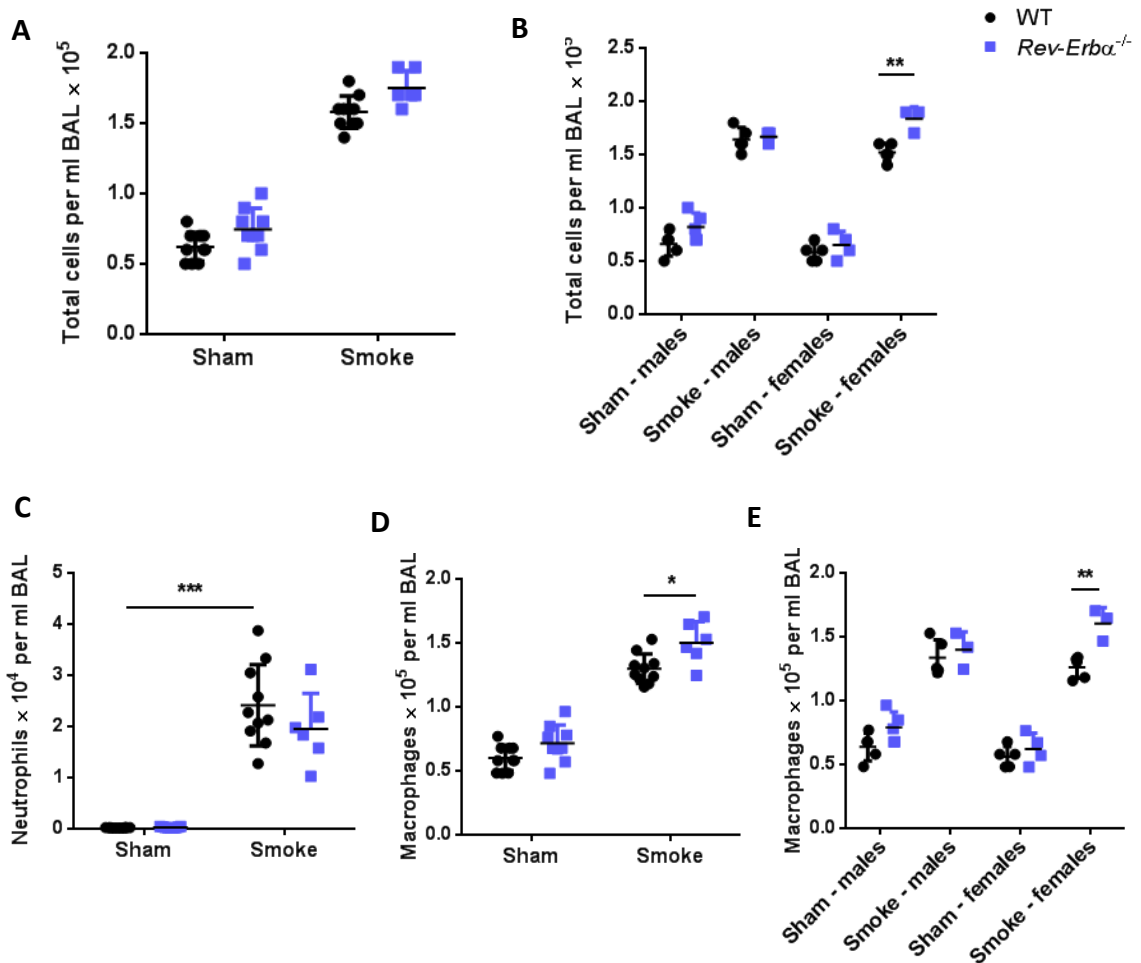
Figure 3.7: Pulmonary cell infiltration after multiple cigarette smoke exposures at ZT8 in wild-type and *Rev-Erbα⁻/⁻* mice

Mice were exposed to cigarette smoke between ZT8 and ZT10 for 10 days and culled 20 hours after the last exposure at ZT6. (A,B) Total cell counts per ml BAL. Neutrophils (C) and macrophages (D,E) were quantified in BAL using flow cytometry. Data are presented as mean ± SEM; n = 6-10, *P <0.05, **P <0.01, ***P <0.001 (Two-way ANOVA, post hoc Bonferroni).

Multiplex assay could only detect CXCL1, CXCL2 and CXCL5 in BAL samples (Appendix 8 Table 8A). CXCL1 levels were elevated in CS-exposed animals compared to sham controls and a significant increase was measured in *Rev-Erbα*^{-/-} mice compared to wild-type mice upon smoke exposures (Figure 3.8A). Again, gender analyses showed that this phenotype was driven by the females (Figure 3.8B). Despite a rise of CXCL2 levels in CS-exposed animals compared to sham controls, no difference was observed between genotypes (Figure 3.8C). CXCL5 levels were unaltered by CS exposures or by REV-ERBα deletion (Figure 3.8D). The same multiplex assay was also performed on lung homogenates. More cytokines and chemokines were then detected but only CXCL1, CXCL2, IL-6 and IL-1α levels were significantly increased in *Rev-Erbα*^{-/-} mice compared to wild-type mice upon smoke exposures (Appendix 8 Table 8A).
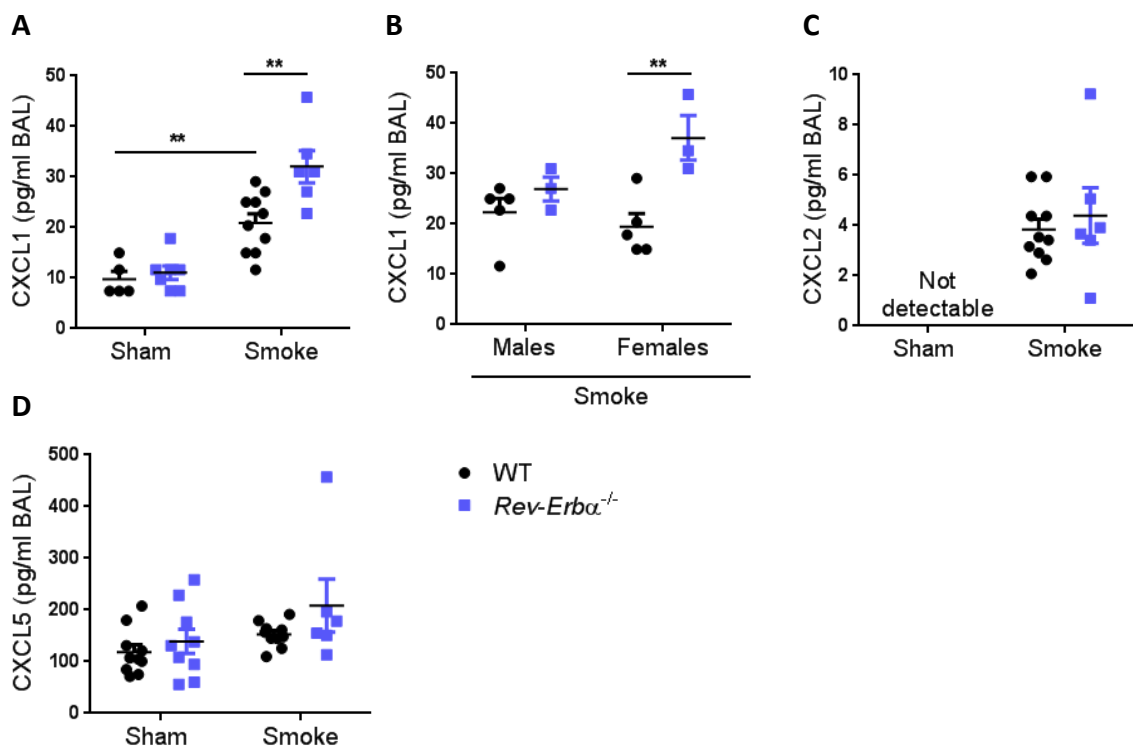
Figure 3.8: Chemokine release into lungs after multiple cigarette smoke exposures at ZT8 in wild-type and *Rev-Erbα*^{-/-} mice

Mice were exposed to cigarette smoke between ZT8 and ZT10 for 10 days and culled 20 hours after the last exposure at ZT6. A select group of pro-inflammatory cytokines/chemokines were measured by bioplex analyses. Only CXCL1 (A,B), CXCL2 (C) and CXCL5 (D) were detectable. Data are presented as mean ± SEM; n = 6-10, *$P <0.05$, **$P <0.01$, ***$P <0.001$ (Two-way ANOVA, post hoc Bonferroni).

Measurement of transcript levels in whole lung indicated that 10-day CS exposure induced an increase of multiple pro-inflammatory cytokines and chemokines such as *Cxcl5*, *Cxcl2*, *Cxcl1*, *Ccl2* and *Il-6* (Figure 3.9). Moreover, *Cxcl5* and *Cxcl2* were significantly increased in *Rev-Erbα*$^{-/-}$ mice compared to wild-type mice upon smoke exposures. As previously observed upon a single CS exposure, *G-csf* transcript was significantly down-regulated in *Rev-Erbα*$^{-/-}$ mice and cigarette smoke caused a diminution of *G-csf* transcript levels in the wild-type mice.
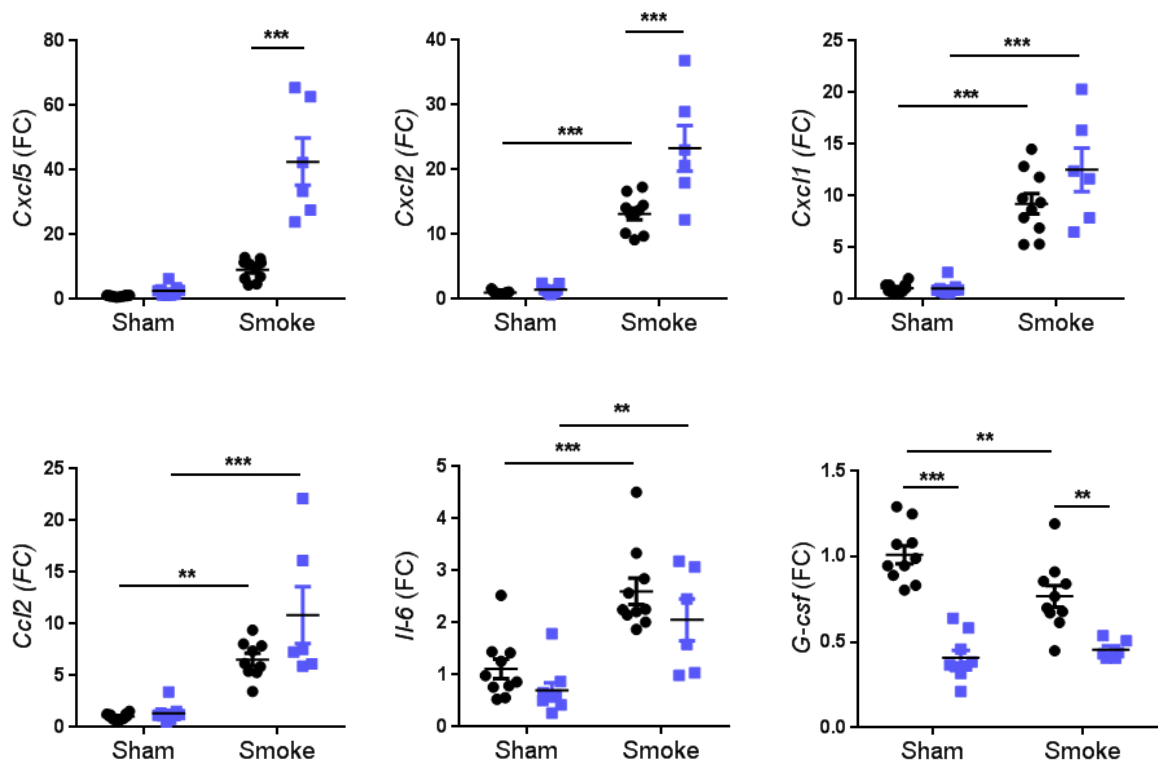
Figure 3.9: Inflammatory gene transcript levels in whole lung after multiple cigarette smoke exposures at ZT8 in wild-type and *Rev-Erbα*$^{-/-}$ mice

Mice were exposed to cigarette smoke between ZT8 and ZT10 for 10 days and culled 20 hours after the last exposure at ZT6. Gene expression was determined by Real-Time qPCR and normalized to wild-type sham group. Data are presented as mean ± SEM; *n* = 6-10, **P* <0.01, ***P* <0.001 (Two-way ANOVA, post hoc Bonferroni).

3.3.4 Deletion of REV-ERBα affects expression of a set of NRF2 regulated antioxidant genes

Nuclear factor erythroid 2-related factor 2 (NRF2) controls several different antioxidants pathways. Each of the NRF2 gene targets studied in this thesis was chosen as it plays a key role in one of these different antioxidants pathways. The glutamate–cysteine ligase complex catalytic subunit (GCLC) is a key element of glutathione production and regeneration whereas thioredoxin reductase 1 (TXNRD1) is involved in thioredoxin production, regeneration and utilisation. Additional antioxidants that are controlled by NRF2 include NAD(P)H:quinone oxidoreductase 1 (NQO1) and enzymes regulating iron sequestration, such as haem oxygenase (HMOX1).

3.3.4.1 In basal conditions

First, diurnal profiles of *Nrf2* and target gene transcripts in whole lung were assessed by sampling tissues from wild-type and *Rev-Erbα$^{-/-}$* mice every 4 hours (Figure 3.10). No diurnal rhythmicity was observed for *Nrf2*, *Txnrd1* and *Gclc* transcripts in neither wild-type or *Rev-Erbα$^{-/-}$* mice. A small amplitude rhythm could be measured for *Ho-1* and *Nqo1* in wild-types peaking respectively at ZT8 and ZT12 whereas transcripts levels were similar across the day in knockout animals. Moreover, when looking further at gender differences, *Nqo1* transcript levels were higher in males than in females and *Nqo1* rhythmicity became significant in male wild-types. This could suggest a major difference between genders in regulation of oxidative stress by *Nqo1* and males could be more sensitive to any dysregulation of REV-ERBα in coping with oxidative burden.

Then, effects of REV-ERBα deletion on *Nrf2* and its target gene expression were investigated upon inflammatory and oxidative challenges. I capitalised on samples collected after LPS exposures at ZT0 or ZT12 and after the 10-day smoke exposure carried out in collaboration with GlaxoSmithKline.
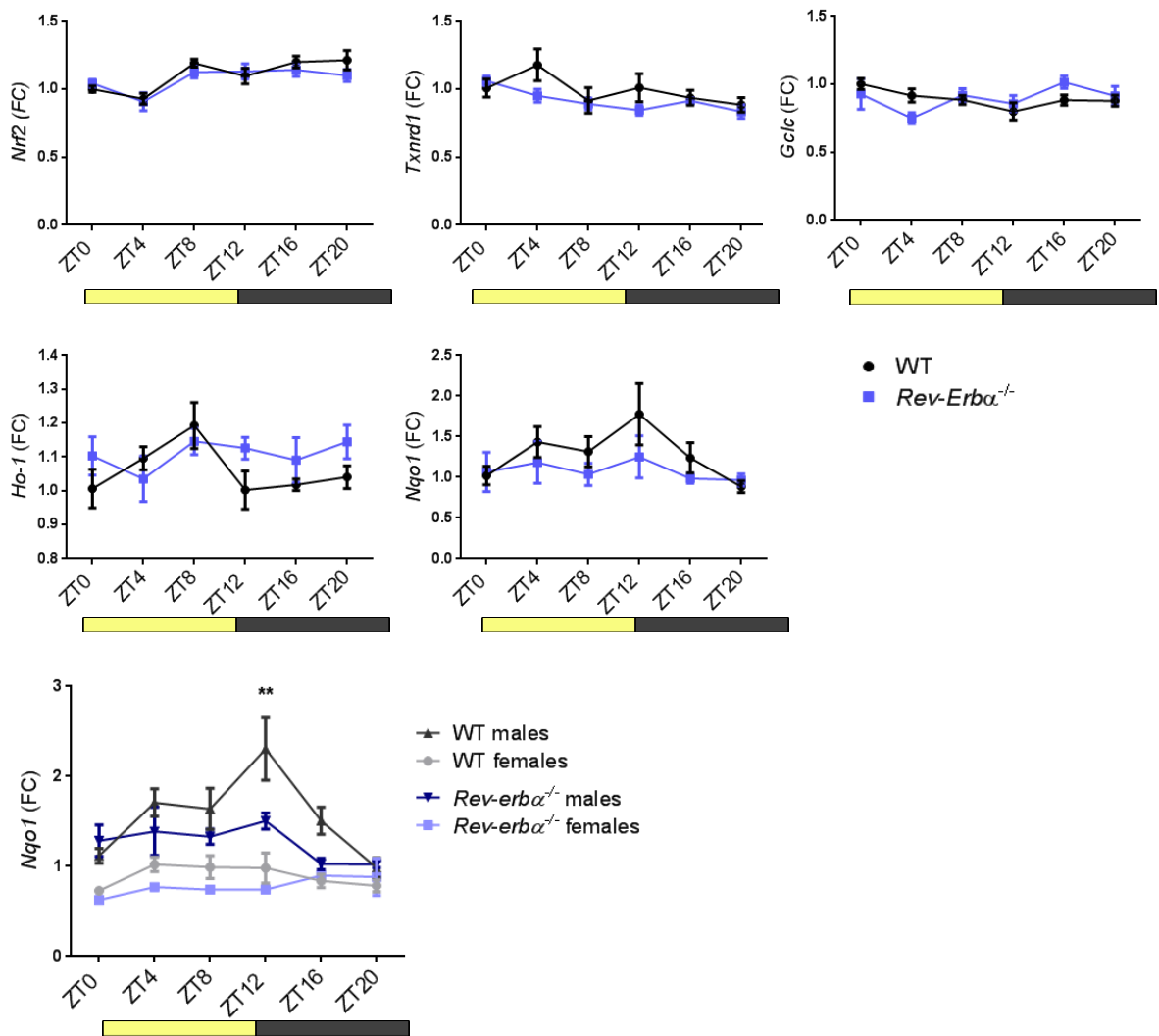
Figure 3.10: Profile of antioxidant gene expression across a diurnal period in wild-type and *Rev-Erbα*^{-/-} mice

Lung tissues from *Rev-Erbα*^{-/-} and wild-type littermate control mice were collected at different time points across the day. mRNA levels in total lung tissues were determined by Real-Time qPCR and normalized to WT at ZT0. Data are presented as mean ± SEM; $n = 5$-6 for WT and $n = 3$-5 for KO per time point. **(P <0.01)* significantly different from ZT0 and ZT20 (One-way ANOVA, post hoc Bonferroni).

3.3.4.2 Upon endotoxin challenge

Exposure to LPS at either ZT0 or ZT12 induced an up-regulation of *Txnrd1*, *Gclc* and *Ho-1* transcript levels in both *Rev-Erbα*^{-/-} and wild-type mice (Figure 3.11). However, a difference between genotypes was observed only for *Txnrd1* and *Gclc* with a significant increase in knockout animals compared to wildtypes at both time

points. No significant differences were measured in levels of *Nrf2* and *Nqo1* between time points and genotypes. These results indicated that bacterial challenge leaded to induction of specific antioxidant pathways and that REV-ERBα contributed in their repression.
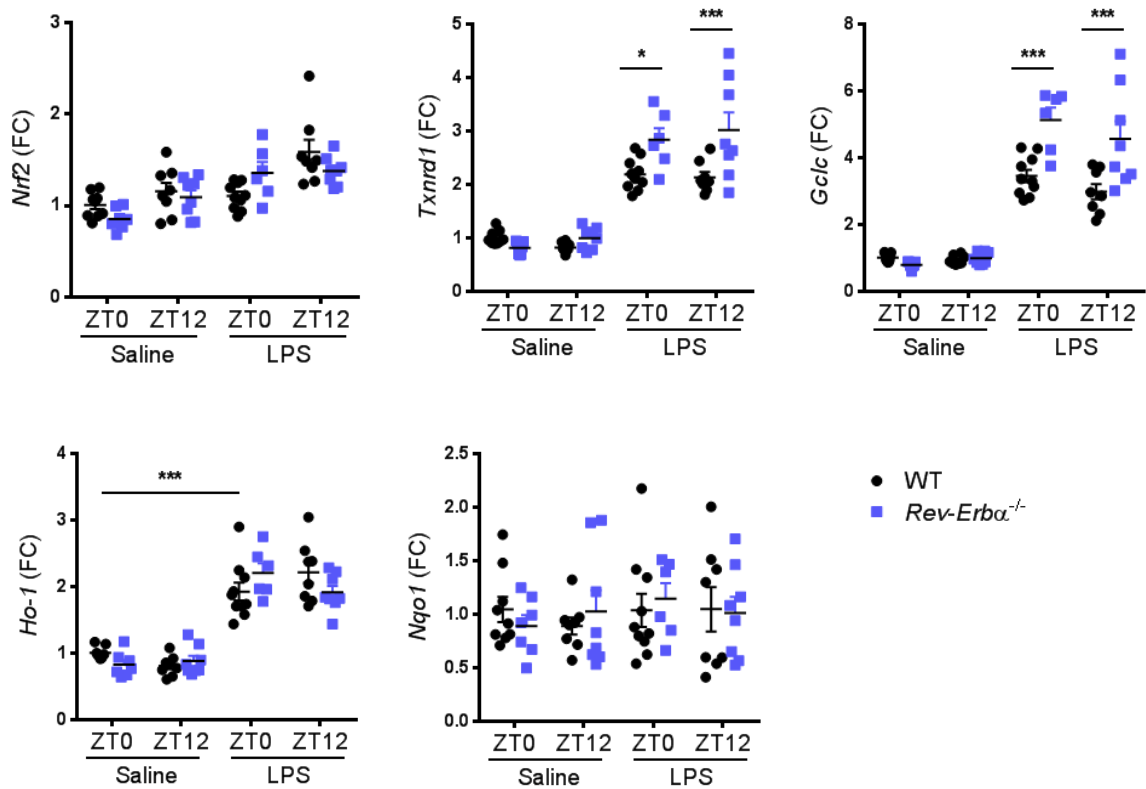
Figure 3.11: Transcript levels of Nrf2 and its target genes in response to LPS challenge at ZT0 and ZT12 in wild-type and *Rev-Erbα*^-/- mice

Mice were exposed to aerosolised LPS at 2mg/ml or to saline for 20 minutes at ZT0 or ZT12 and culled 5 hours later. RNA was extracted from whole lung and transcript levels were measured by Taqman Real-Time qPCR and normalized to ZT0 wild-type saline group. Data are presented as mean ± SEM; $n = 6$-10, *P <0.05, ***P <0.001 (Two-way ANOVA, post hoc Bonferroni).

3.3.4.3 Upon cigarette smoke exposures

Except for a slight elevation of *Gclc* transcript upon smoke exposure in *Rev-Erbα*^-/- mice compared to wild-types, no differences were observed in antioxidant gene
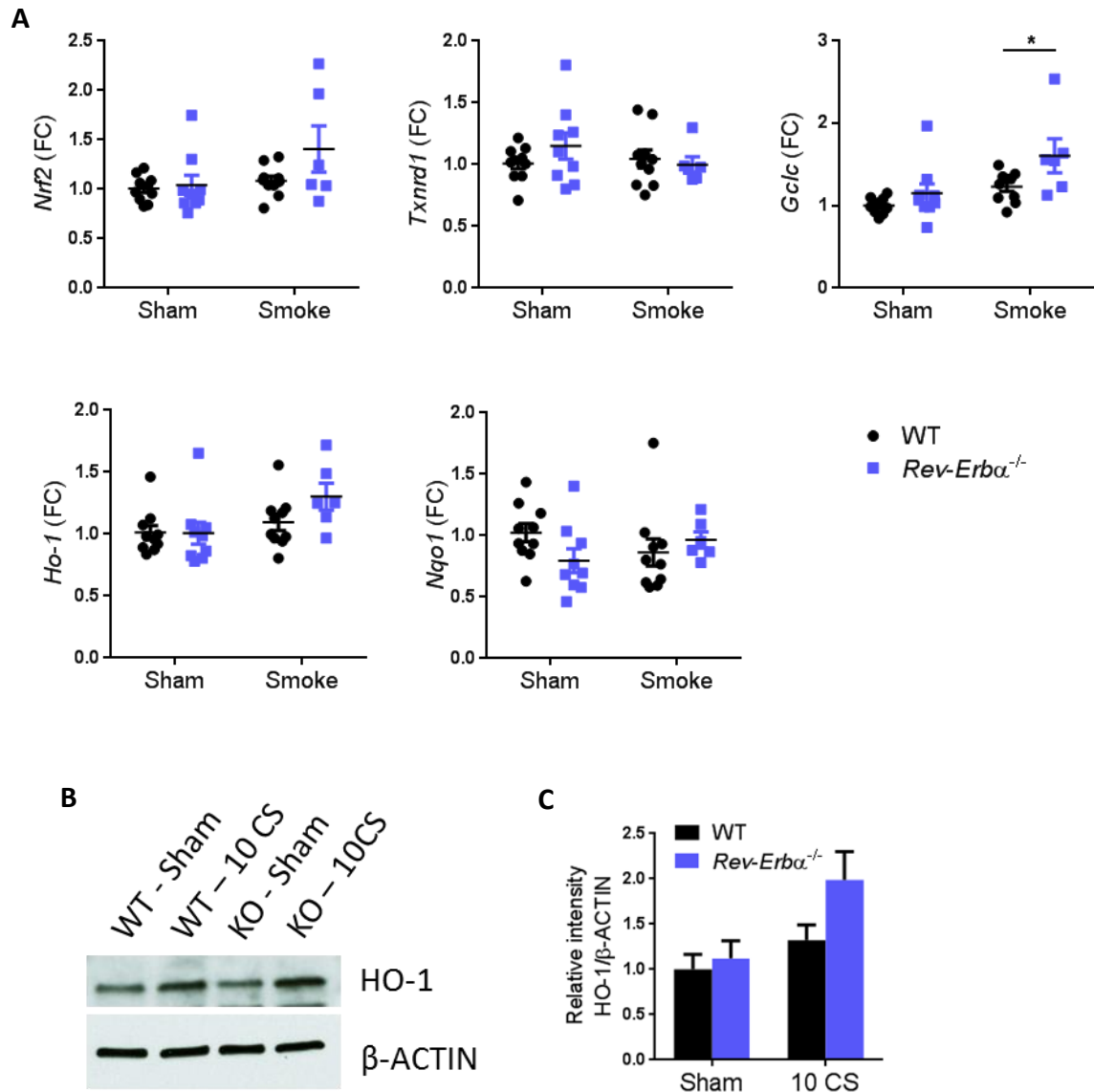
Figure 3.12: Antioxidant gene response in whole lung after multiple cigarette smoke exposures at ZT8 in wild-type and *Rev-Erbα*-/- mice

Mice were exposed to cigarette smoke between ZT8 and ZT10 for 10 days and culled 20 hours after the last exposure at ZT6. (A) Gene expression was determined by Real-Time qPCR and normalized to wild-type sham group. Data are presented as mean ± SEM; n = 6-10, *$P <0.05$ (Two-way ANOVA, post hoc Bonferroni). (B) Levels of HO-1 proteins were measured by Western blotting. (C) HO-1 densitometry (mean ± SEM) was normalised to β-ACTIN and to WT exposed to air; n = 6.

expression between the two genotypes (Figure 3.12A). Moreover, *Nrf2* and its target antioxidant genes did not display any increase in their transcript levels upon 10-day CS exposures compared to air-exposed control groups. These results could be

explained by the timing of the cull which occurred 20 hours after the last exposure. After that time, it was likely that the smoke-induced increase of antioxidant gene transcription would be repressed and mRNA levels would return to basal levels. Indeed, even after 22 months of cigarette smoke exposures, *Nqo1* levels, 10-fold increased four hours after the last exposure, were reduced to nearly basal levels 16 hours after last exposure (Appendix 9, Figure A9).

Levels of HO-1 proteins in whole lung were also assessed by Western blotting (Figure 3.12B). Despite a trend in increase HO-1 levels upon CS exposures, especially in *Rev-Erbα*$^{-/-}$ mice, no significant difference between genotypes was measured by a two-way ANOVA statistical analysis (Figure 3.12B).

3.4 Discussion

3.4.1 Daily profile of clock and inflammatory gene expression in *Rev-Erbα*$^{-/-}$ mice

Over the past few years, it has been shown that deletion of REV-ERBα from cells, tissues or entire organisms does not abolish rhythms of other clock proteins. This is likely due to the redundant contribution from REV-ERBβ. Indeed, my results confirmed persistence of rhythms in *Per2*, *Bmal1* and *Rev-Erbβ* transcripts in global REV-ERBα knockout mice (Figure 3.1A). However, the amplitude of *Bmal1* mRNA oscillations was more than four times higher in wild-type mice compared to *Rev-Erbα* mutant mice, consistently with previous findings (Preitner et al., 2002). *Cxcl5* transcript daily rhythms were also maintained in *Rev-Erbα*$^{-/-}$ mice whereas *G-csf* mRNA levels were significantly lower in *Rev-Erbα* knockout mice at ZT4 and ZT8 compared wild-types. G-CSF (Granulocyte-colony stimulating factor) is a glycoprotein that stimulates the bone marrow to produce granulocytes and release them into the bloodstream. It has been shown that G-CSF also stimulates the survival, proliferation, differentiation, and function of neutrophil precursors and mature neutrophils (Roberts, 2005). Mice lacking G-CSF or its receptor, G-CSFR, demonstrate chronic severe neutropenia, a reduced ability to make new white blood cells. Many tissues can produce G-CSF when appropriately stimulated, with inflammatory agents such as LPS and TNF-α, inducing expression in endothelial cells, macrophages, epithelial cells and fibroblasts (Bendall and Bradstock, 2014).

The lower levels of *G-csf* transcripts in the lung of *Rev-Erbα*$^{-/-}$ mice may suggest impairment of homeostatic neutrophil numbers and/or functions in these mice. It would be interesting to analyse bone marrow and blood samples from *Rev-Erbα* knockout mice to determine whether there are any homeostatic differences in neutrophils at the periphery compared to wild-type animals.

3.4.2 Lung inflammatory responses to endotoxin challenge in *Rev-Erbα*$^{-/-}$ mice

Previous unpublished work showed that loss of REV-ERBα resulted in an increase in neutrophilic inflammation in response to LPS at ZT4 (Figure 3.1). My own findings confirmed these results and also highlight a loss of the normal evening nadir in inflammatory responses in *Rev-Erbα* knockout mice (Figure 3.3). It is also interesting to stress that the amplitude of inflammatory responses to LPS tended to be greater in males than in females for both genotypes, suggesting stronger protective mechanisms to endotoxin challenge in female mice. This could be due to differences in hormones, lung function or weight and further work would be warranted to determine the source of these gender variations.

Moreover, it was notable that the increased chemokine and cytokine response was far greater in the evening than at dawn, which in wild-type mice is the peak phase for inflammatory reaction (Figure 3.4). A select group of inflammatory mediators showed these evening (ZT12) differences, including CXCL1, CXCL2 and G-CSF. However, differences between genotypes in CXCL5 levels were greater when animals where challenged at dawn. This result was unexpected as CXCL5 was previously found to be required for the time of day variation in neutrophilic inflammation (Gibbs et al., 2014).

Transcript levels quantification in whole lung confirmed the BAL samples protein analysis for G-CSF, showing a loss of the normal evening nadir in inflammatory responses in *Rev-Erbα* knockout mice (Figure 3.5). However, transcript results for the other cytokines and chemokines showed disparities with levels of the proteins in BAL samples. For instance, similar levels of *Cxcl2* transcripts were measured between time points and genotypes whereas higher levels of CXCL2 in BAL fluid were quantified in *Rev-Erbα* knockout mice compared to wild-types. This could be

explained by the timing of the experiment; five hours after exposure, LPS-induced increase of inflammatory gene transcripts may decline to basal levels, whereas the translated proteins may still persist in the alveolar space. Another explanation could be that the proteins secreted in the alveolar space come from a small subset of cells whereas the transcripts were measured from the whole lung, and therefore from multiple different cell types, in which REV-ERBα deletion may have distinct effects upon an endotoxin challenge. An interesting observation from the transcript analysis was a lower induction of *Ccl2* in *Rev-Erbα* knockout mice when subjected to LPS at

ZT12 compared to wild-types. As Sato et al. showed that REV-ERBα represses *Ccl2* expression in murine macrophages, this highlights the importance of considering the local environment.

3.4.3 Lung inflammatory responses to cigarette smoke in *Rev-Erbα*$^{-/-}$ mice

Further analysis of the pulmonary inflammatory responses in *Rev-Erbα* knockout mice used cigarette smoke exposure, a prevalent real-world environmental challenge to the lung. After a single exposure no cellular inflammatory mediators were found to change indicating that a single CS exposure remains a mild attack (Figure 3.6). However, it induced pro-inflammatory chemokine gene activation and *Cxcl5* transcript levels were significantly elevated in the *Rev-Erbα*$^{-/-}$ lung compared to the wild-type. Therefore, responses to multiple smoke exposures (10 days) were tested. This resulted in the death of three of the nine *Rev-Erbα*$^{-/-}$ mice, and none of the ten controls, indicating before any further investigation a limited capacity of the knock-out mice to recover from the consequences of multiple cigarette smoke exposures. This 10-day CS study also showed elevated inflammatory mediators in knockout animals (CXCL1 at protein levels, *Cxcl5* and *Cxcl2* at transcript levels), but only minimally elevated macrophage infiltrates (Figures 3.7-9). Gender analysis revealed the majority of the increase was seen in *Rev-Erbα*$^{-/-}$ females. This observation was consistent with findings showing that female mice exposed to cigarette smoke develop emphysematous-like changes in alveolar structure and related alterations of pulmonary function more rapidly than males (March et al., 2006).

3.4.4 Nrf2-regulated antioxidant gene expression in *Rev-Erbα*^{-/-} mice

Daily profiles of *Nrf2* and a subset of its target genes revealed no significant effect of REV-ERBα deletion, except for a down-regulation of *Nqo1* but only in males (Figure 3.10). Moreover, the transcripts levels even in wild-type animals did not appear to be highly rhythmic. In my study, *Gclc* mRNA levels were similar across the day which contradicts with previous findings showing robust oscillations of NRF2-regulated antioxidant genes involved in glutathione homeostasis (Pekovic-Vaughan et al., 2014). Interestingly, gender analysis of *Nqo1* transcript revealed higher expression in males than in females. This result contrasts from expression of *Nqo1* in liver which is higher in female mice than in males (Xu et al., 2012). However, it could explain that *Rev-Erbα*^{-/-} female mice were more susceptible to cigarette smoke exposure.

Moreover, upon endotoxin challenge, loss of REV-ERBα resulted in an up-regulation of *Gclc* and *Txnrd1* at both dawn and dusk (Figure 3.11). It is known that LPS-stimulated leukocytes produce pro-inflammatory cytokines, which trigger reactive oxygen species (ROS) production through NAD(P)H oxidase (Nox) activation (DeLeo et al., 1998). ROS are essential for bacterial killing, but may also induce oxidative stress within the tissues. To cope with this stress, lung parenchymal cells activate NRF2 that regulates the expression antioxidant genes. Therefore, the increase in *Gclc* and *Txnrd1* observed in *Rev-Erbα*^{-/-} mice could be a direct consequence of exaggerated inflammatory responses and ROS production to LPS in the whole lung. Besides, it has been demonstrated that *Txnrd1* transcription is induced in macrophages upon LPS challenge via intracellular signaling pathways mediated by p38 MAP kinase and IκB kinase (Carlson et al., 2011). This leads to the translation of the selenoprotein thioredoxin reductase 1 (TR1) protein involved in selenium metabolism, suggesting a regulatory link between immune function and metabolic state.

In the multiple CS exposures study, no major difference in antioxidant gene expression was observed between wild-type and KO mice (Figure 3.12). As explained in 3.3.4.3, this was probably due to the timing of the cull which occurred 20 hours after the last exposure; smoke-induced transcripts could be repressed and returned to basal levels.

3.5 Conclusions

Studies have shown that loss of BMAL1 leads to augmented pulmonary inflammatory responses but no published work has addressed the effects of direct REV-ERBα deletion. This chapter clearly demonstrates that REV-ERBα is critical repressor of lung inflammation upon both endotoxin challenge and cigarette smoke exposure. Activation of NRF2-dependent pathways was significantly up-regulated in absence of REV-ERBα but only in challenged conditions, highlighting the interplay between immune function and antioxidant pathways. In order to localize the action of REV-ERBα to single cell type, mice with cell specific mutation of REV-ERBα were generated and studied in chapter 4.

Chapter 4: Targeted impairment of the DNA binding function of REV-ERBα in different cell types

4.1 Introduction

Alveolar macrophages (AM) and the airway epithelium provide the first lines of defense against respiratory pathogens. Besides their phagocytic functions, AMs also secrete numerous chemical mediators upon stimulation, thereby playing a role in regulating inflammatory reactions in the lung. Previous studies have suggested that AMs possess robust anti-inflammatory effects upon endotoxin-induced lung injury (Beck-Schimmer et al., 2005). Moreover, REV-ERBα in macrophages has been shown to play a critical role to repress inflammation after systemic administration of LPS (Gibbs et al., 2012). As for the airway epithelium, it acts as a frontline defense against respiratory pathogens, not only as a physical barrier and through the mucociliary apparatus but also through its immunological functions. A major role for bronchiolar epithelial cells in modulating airway inflammatory response to LPS has been demonstrated (Elizur et al., 2007). In addition, these bronchiolar epithelial cells are essential to maintain circadian rhythmicity in the lung (Gibbs et al., 2009) and genetic ablation of the core clock gene *Bmal1* within these cells results in exaggerated neutrophilic inflammation (Gibbs et al., 2014). However, it is not clear whether these effects are mediated via core circadian clock disruption or a more general pleiotropic effect of BMAL1 disruption. In this chapter, I investigated which cell type between myeloid cells or bronchiolar epithelial cells, is the key cell type for REV-ERBα to regulate pulmonary inflammation *in vivo*.

4.2 Hypothesis tested and experimental approaches

Hypothesis: The bronchiolar epithelial cells are key cells to regulate pulmonary inflammatory responses via REV-ERBα.

Objectives:

- Generate mouse strains which lack REV-ERBα DNA binding domain (DBD) in myeloid cell lineage (macrophages, monocytes, neutrophils) or bronchiolar epithelial cells by breeding *Rev-Erbα*-DBD$^{flox/flox}$ (named *Rev-Erbα*$^{fl/fl}$ afterwards) mice with *LysM*^{cre} or *Ccsp*^{icre} mice respectively, maintain on a Per2::Luc background to facilitate bioluminescence monitoring.

- Assess lung rhythmicity by monitoring organotypic lung slices from the different mouse models mice and littermate controls under photomultiplier tubes (PMTs) or camera.

- Test responses of the different mouse models mice and littermate controls to aerosolised LPS at different time points and measure any differences in the magnitude and rhythm of inflammatory response (cell infiltration and cytokine production).

4.3 Results

4.3.1 Gene targeting strategy impaired expression of REV-ERBα DNA binding domain in specific cell types

Assessment of successful knockout of REV-ERBα DBD in bronchiolar epithelial cells ($Ccsp^{icre}$ positive cells) or myeloid cells ($LysM^{cre}$ positive cells) was performed using multiple approaches. First, the genotyping strategy used allowed identification of floxed, wild-type and null (recombined, 'knockout') fragments (Figure 4.1A,B). Null fragments were observed in ear punches (which are routinely used for genotyping) only from LysMcre^{+ve} animals as ear tissues contain myeloid cells but naturally no bronchiolar epithelial cells (Figure 4.1A,B). However, null fragments were observed in lung samples from Ccspicre^{+ve} animals (Figure 4.1B).

Loss of REV-ERBα DBD at protein level was initially tested using Western Blot on whole lung tissue from *Rev-Erbα*$^{fl/fl}$, *Ccsp-Rev-Erbα*-DBD^{m} and *LysM-Rev-Erbα*-DBD^{m} animals collected at ZT9, peak of REV-ERBα protein. It was expected to detect two bands in LysMcre^{+ve} and Ccspicre^{+ve} mice; a first one at 75 kDa, the molecular weight of the full REV-ERBα, and another one just under 75 kDa corresponding to the protein lacking its DBD (Zhang et al., 2015). A clear band at 75 kDa was detected for all the animals (Figure 4.1C,D). However, observation of a second lower band was very difficult as non-specific bands were also detected just below 75 kDa (chapter 2.10.3, appendix 5). Moreover, the potential masking effect of the other cell types in the whole lung, which express the full length of REV-ERBα has to be taken into account. Interestingly, lower levels of CCSP were detected in the *Ccsp-Rev-Erbα*-DBD^{m} mice (Figure 4.1D). This down-regulation of CCSP was also
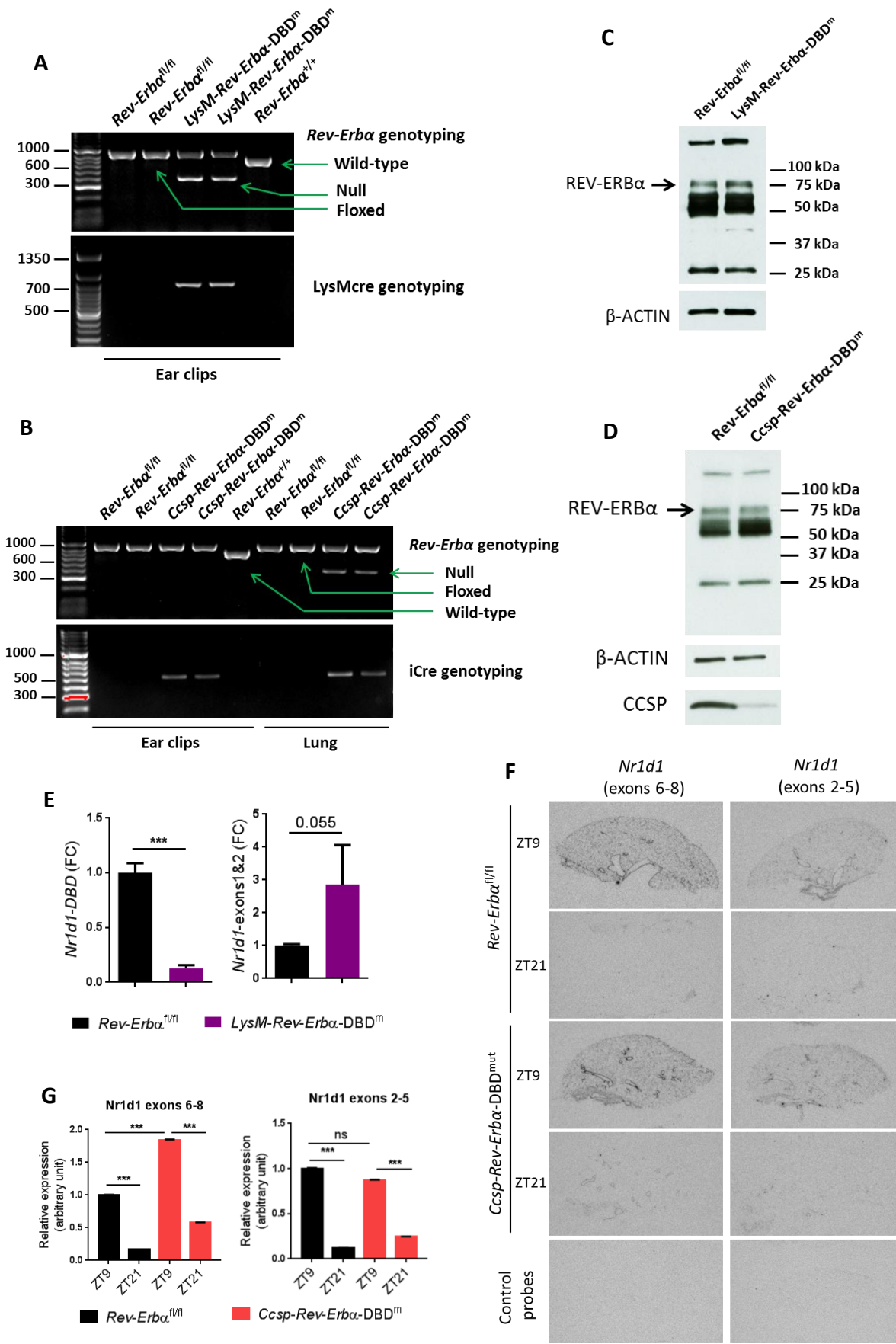
Figure 4.1: Testing for REV-ERBα DBD loss in myeloid or bronchiolar epithelial cells of the mouse models (legend on next page)

(A,B) Example of genotyping results from ear clips and lungs of *LysM-Rev-Erbα*-DBD^m, *Ccsp-Rev-Erbα*-DBD^m and *Rev-Erbα*^fl/fl littermate controls. *Rev-Erbα*^+/+ samples were included for comparison. (C,D) Western blot analysis of whole lung from *LysM-Rev-Erbα*-DBD^m, *Ccsp-Rev-Erbα*-DBD^m and *Rev-Erbα*^fl/fl littermate controls. Membranes were stained for REV-ERBα using monoclonal GSK6F05 antibody (75 kDa), β-ACTIN (42kDa) and CCSP (10kDa). (E) PECs from *LysM-Rev-Erbα*-DBD^m mice and *Rev-Erbα*^fl/fl littermate controls were collected at ZT9, seeded into plates and let to attach for 2 hours before lysis. Gene expression was determined by Real-Time qPCR and normalized to *Rev-Erbα*^fl/fl littermate control group. Data are presented as mean ± SD; *n* = 3. ***P <0.001 (Student's *t*-test). (F) Example images of lung sections probed for *Rev-Erbα* mRNA via *in situ* hybridisation using two set of primers. Control probes were sense probes for each gene targeting region and were hybridised on lung sections from *Rev-Erbα*^fl/fl littermate control mice, collected at ZT9. (G) Relative quantification of *Rev-Erbα* mRNA abundance from multiple lung sections measured via *in situ* hybridisation. Data are presented as mean ± SEM; *n* = 2/genotype/time point. ***P <0.001 (One-way ANOVA, post hoc Bonferroni).

detected at transcript levels. This was later found to be the result of the icre sequence knock-in in *Ccsp* gene which disrupted one of the Ccsp alleles. Indeed, this was also observed in non-floxed *Ccsp*^icre control mice (Appendix 10).

Detection of REV-ERBα by Western Blot in peritoneal or alveolar macrophages from *Rev-Erbα*^fl/fl and *LysM-Rev-Erbα*-DBD^m mice was attempted but without success suggesting that the nuclear receptor is expressed at low levels in these cells. However, transcript levels of *Rev-Erbα* in peritoneal macrophages from *Rev-Erbα*^fl/fl and *LysM-Rev-Erbα*-DBD^m mice were detected by Real-time qPCR using two sets of primers; one targeting the DNA binding domain (exons 3 and 4) and the other one targeting exons 1 and 2. Levels of *Rev-Erbα* DBD were significantly lowered in *LysM-Rev-Erbα-DBD*^m mice whereas an up-regulation of transcripts containing exons 1 and 2 was measured (Figure 4.1E), consistently with previous findings (Zhang et al., 2015).

Assessment of deletion of the *Rev-Erbα* DBD at transcript levels in the bronchiolar epithelial cells of CcspiCre^+ve mice was attempted via *in situ* hybridisation (performed by Dr. Ben Saer). Two probes were used; one targeting exons 2 to 5 (containing the DBD) and the other targeting exons 6 to 8 (containing the LBD). As expected, a significant time-of-day difference of *Rev-Erbα* was observed in the

bronchioles of both genotypes (Figure 4.1F,G). When using the probe targeting the ligand binding domain (LBD) sequence, a significant increase in *Rev-Erbα* mRNA was measured in the bronchioles of *Ccsp-Rev-Erbα*-DBD[m] mice compared to the littermate controls at ZT9. Again, this was consistent with previous findings (Zhang et al., 2015). However, when using primers targeting the DBD sequence, no difference in *Rev-Erbα* mRNA was measured between the two genotypes whereas a significant decrease was expected in the bronchioles of *Ccsp-Rev-Erbα*-DBD[m] mice compared to the littermate controls at ZT9.

4.3.2 Lung rhythmicity is not affected by deletion of REV-ERBα DBD in myeloid cells or bronchiolar epithelial cells

Organotypic lung slices from *Ccsp-Rev-Erbα*-DBD[m], *LysM-Rev-Erbα*-DBD[m] and *Rev-Erbα*^{fl/fl} mice all exhibited rhythmic oscillations of PER2::Luc-driven bioluminescence for several days (Figure 4.2). Cosinor analysis of data from hours 24-72 showed an average period of 25.17 $\pm$ 0.6 hours for *Rev-Erbα*^{fl/fl} mice, 25.92 $\pm$ 0.3 hours for *Ccsp-Rev-Erbα*-DBD[m] mice and 27.3 $\pm$ 1.4 hours for *LysM-Rev-Erbα*-DBD[m] mice (Figure 4.2B). Statistical analysis using unpaired *t*-test showed no significant difference between groups.

Isolated peritoneal exudate cells (PECs) from *LysM-Rev-Erbα*-DBD[m] mice and *Rev-Erbα*^{fl/fl} littermate controls both also exhibited rhythmic oscillations of PER2::Luc-driven bioluminescence for several days (Figure 4.2C). Cosinor analysis of data from hours 24-72 showed an average period of 26.3 $\pm$ 1.6 hours for controls and 25.2 $\pm$ 0.6 hours for *LysM-Rev-Erbα*-DBD[m] mice. Statistical analysis using unpaired *t*-test showed no significant difference between groups.

In order to assess rhythms in the airway epithelial cells of *Ccsp-Rev-Erbα*-DBD[m] mice and littermate controls, a recording camera was used to focus on the bronchioles of ectopic lung slices. Surprisingly, luciferase signal intensity from bronchioles of *Rev-Erbα*^{fl/fl} mice was weak whereas it was very strong in bronchioles from *Ccsp-Rev-Erbα*-DBD[m] mice (Figure 4.2D). Nonetheless, by measuring the intensity in a selected part of a bronchiole over time, rhythms could be detected in both genotypes and cosinor analysis of data from all the hours recorded showed an average period of 23.05 $\pm$ 0.9 hours and 21.8 for $\pm$ 1 hours for control and mutant mice respectively (Figure 4.2E).
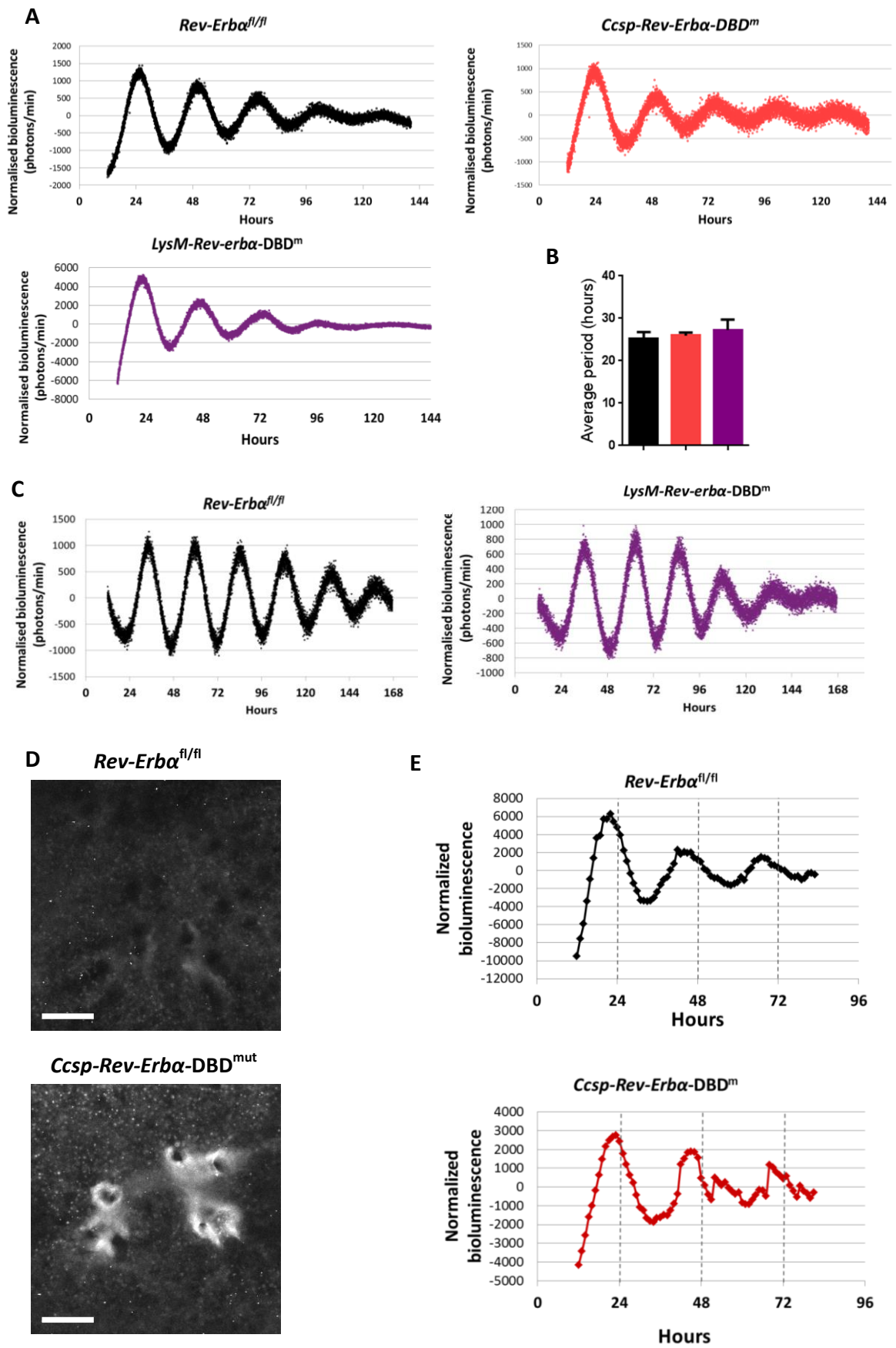
Figure 4.2: Oscillations of PER2::Luc-driven bioluminescence in organotypic lung slices and alveolar macrophages (legend on next page)

(A) Example bioluminescence recordings from *Rev-Erbα*^{fl/fl} (black), *Ccsp-Rev-Erbα*-DBD^m (red) and *LysM-Rev-Erbα*-DBD^m (purple) precision cut lung slices. Photon counts per minute are normalised to a 24 hour moving average and traces are representative of 3 biological replicates (B) Average oscillation period of bioluminescence recording, determined by cosinor analysis of individual traces. (C) Example bioluminescence recordings from *Rev-Erbα*^{fl/fl} (black) and *LysM-Rev-Erbα*-DBD^m (purple) PECs. Photon counts per minute are normalised to a 24 hour moving average and traces are representative of 2 biological replicates (D) Snapshots of recording oscillations of PER2 of precision cut lung slices from *Rev-Erbα*^{fl/fl} and *Ccsp-Rev-Erbα*-DBD^m mice. Scale bars, 500 μM. (E) Bioluminescence intensity from bronchioles was quantified, normalised to a 24 hour moving average. Traces are representative of 2 biological replicates.

4.3.3 Deficiency of CCSP in *Ccsp*^{icre/+} mice does not promote elevated pulmonary responses to LPS

As described above in 4.3.1, CCSP levels were about 50% lower at both transcript and protein levels in *Ccsp-Rev-Erbα*-DBD^m mice. This is caused by the knock-in of the iCre sequence in the *Ccsp* gene leading to a non-viable copy of the gene and thus the absence of the transcript and protein. Studies in CCSP gene-targeted (CCSP−/−) mice have suggested that CCSP plays a protective role by modulating lung inflammatory responses to infection or injury (Harrod et al., 1998; Watson et al., 2001). Therefore, it was absolutely necessary to carry out a control experiment subjecting *Ccsp*^{icre/+} and *Ccsp*^{+/+} control mice to inflammatory stimuli to assess whether decrease in CCSP proteins leaded to alteration of inflammatory responses and therefore would be a confounding factors in experiments involving any Ccsp-targeted knockouts, such as the *Ccsp-Rev-Erbα*-DBD^m line.

Male and female *Ccsp*^{icre/+} mice and littermate controls *Ccsp*^{+/+} mice were challenged to aerosolised LPS at 2mg/ml for 20 min at ZT4. Mice were culled 5 hours after endotoxin challenge at ZT9. Lung content was washed out by bronchoalveolar lavage (BAL) and lung tissues were taken out for further RNA and protein analyses. No difference in total cell or neutrophil numbers was measured in BAL samples between the two genotypes (Figure 4.3A,B). Also, transcripts levels of cytokines and chemokines were similar for both genotypes (Figure 4.3C). However, as expected,

Ccsp mRNA and CCSP protein levels were 50% lower in the *Ccsp*[icre/+] mice than in the control group (Appendix 10, Figure A10).

Altogether, this control experiment confirms the absence of a pro-inflammatory phenotype in *Ccsp*[icre/+] mice upon aerosolised LPS challenge in spite of a 50% reduction in CCSP levels.
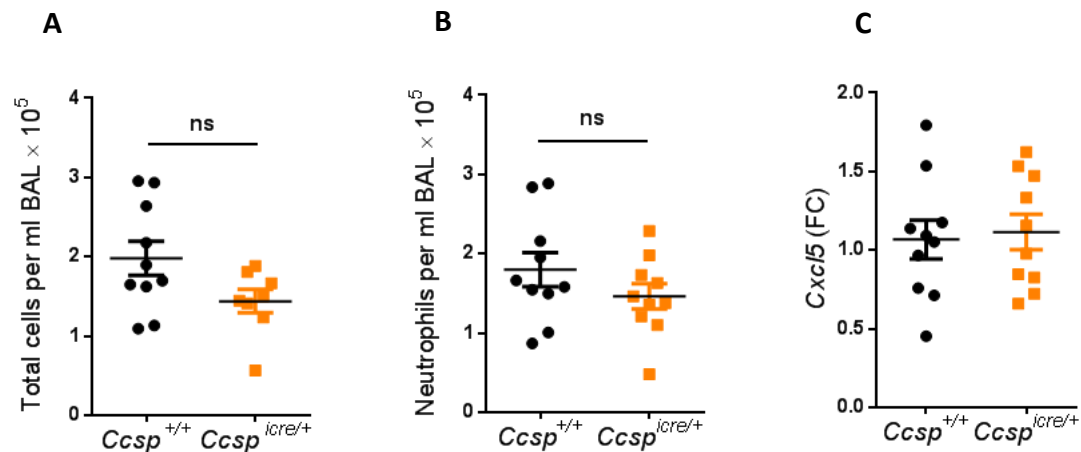
Figure 4.3: Pulmonary inflammatory response to LPS challenge at ZT4 in *Ccsp*[icre/+] mice and *Ccsp*^{+/+} littermate controls

Mice were exposed to aerosolised LPS at 2mg/ml or to saline for 20 minutes at ZT4 and culled 5 hours later. (A) Total cell counts per ml BAL. (B) Neutrophils were quantified in BAL fluid using flow cytometry. (C) *Cxcl5* mRNA levels in total lung tissues were determined by Real-Time qPCR and normalized to *Ccsp*^{+/+} control group. Data are presented as mean ± SEM; $n = 10$ (Two-way ANOVA, post hoc Bonferroni).

4.3.4 Impairment of DNA binding function of REV-ERBα in bronchiolar epithelial cells enhances pulmonary responses to LPS

Male and female *Ccsp-Rev-Erbα*-DBD[m] mice and *Rev-Erbα*^{fl/fl} littermate controls were challenged with aerosolised LPS at 2mg/ml or saline as control, for 20 minutes at ZT4. This time point was chosen to match the first study done in the global *Rev-Erbα* knockout mice. Mice were culled 5 hours after endotoxin challenge at ZT9. Lung content was washed out by bronchoalveolar lavage (BAL) and lung tissues were taken out for further RNA and protein analyses. BAL sample analyses revealed
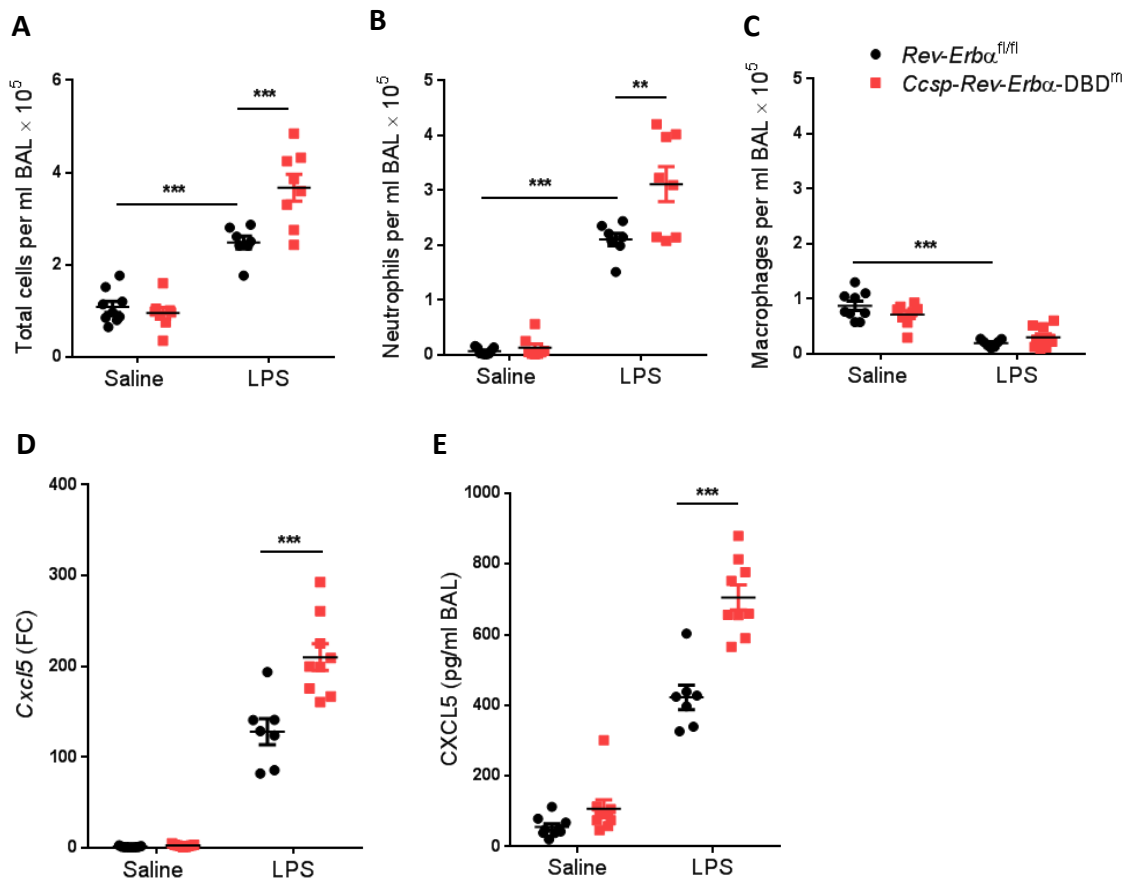
Figure 4.4: Pulmonary inflammatory response to LPS challenge at ZT4 in *Ccsp-Rev-Erbα*-DBD^m mice and *Rev-Erbα*^fl/fl littermate controls

Mice were exposed to aerosolised LPS at 2mg/ml or to saline for 20 minutes at ZT4 and culled 5 hours later. (A) Total cell counts per ml BAL. Neutrophils (B) and macrophages (C) were quantified in BAL fluid using flow cytometry. One data point corresponding to a *Ccsp-Rev-Erbα*-DBD^m male with high measured total cell numbers and neutrophils was excluded using the median absolute deviation method. (D) Cxcl5 mRNA levels in total lung tissues were determined by Real-Time qPCR and normalized to saline control group. (E) CXCL5 protein levels in BAL samples were assessed by Bioplex analyses. Data are presented as mean ± SEM; $n = 7$-9, **$P <0.01$, ***$P <0.001$ (Two-way ANOVA, post hoc Bonferroni).

an increase in infiltration of inflammatory cells, predominantly neutrophils for mice lacking REV-ERBα within bronchiolar epithelial cells, compared to the control group (Figure 4.4A,B). Pulmonary macrophage numbers remained low for both genotypes (Figure 4.4C). Mirroring neutrophil recruitment profile, *Cxcl5* transcript levels were higher in *Ccsp-Rev-Erbα*-DBD^m mice than in the control group upon LPS challenge (Figure 4.4D). Transcript levels for other pro-inflammatory cytokines and chemokines such as *Il-6*, and *Cxcl1* were also elevated upon LPS challenge but

no difference between the genotypes was observed (Appendix 11, Figure A11). As previously reported, cytokine mRNA levels were higher in males than in females but differences between genotypes were similar in both genders (Appendix 11, Figure A11). Moreover, out of 23 different inflammatory and chemotactic cytokines measured in BAL fluid by luminex assay, only CXCL5 showed a difference between the two genotypes upon LPS exposure with a significant increase in mice lacking REV-ERBα DBD in bronchiolar epithelial cells compared to littermate controls (Figure 4.4E and Appendix 11 Table A11). A significant decrease in GM-CSF and CXCL10 levels could be also detected in *Ccsp-Rev-Erbα*-DBD^m mice compared to the control group upon LPS challenge. However, the levels of these two analytes remained in the bottom range of the respective standard curves.

Time of day effect of LPS challenge in *Rev-Erbα*$^{fl/fl}$ and *Ccsp-Rev-Erbα*-DBD^m mice

Next, I wanted to assess whether the gating in pulmonary inflammation (previously demonstrated by Gibbs et al, 2014) was abolished in *Ccsp-Rev-Erbα*-DBD^m mice. For that purpose, male and female *Ccsp-Rev-Erbα*-DBD^m mice were challenged with aerosolised LPS at 2mg/ml or saline as control, for 20 minutes at ZT0 and ZT12. BAL sample analyses revealed a significant increase in infiltration of inflammatory cells, predominantly neutrophils for mice lacking REV-ERBα DBD within bronchiolar club cells, compared to the control group, at ZT0 only (Figure 4.5A,B). Although BAL fluids from *Ccsp-Rev-Erbα*-DBD^m mice contained more neutrophils at ZT0 than at ZT12, this was not observed for the littermate control group. This contradicts my own findings and published results showing greater neutrophil recruitment at ZT0 than at ZT12 upon aerosolised LPS challenge (Chapter 3 and Gibbs et al., 2014), for reasons that are unclear.

Multiplex analyses of the same 23 cytokines and chemokines as above revealed that again, only CXCL5 levels were different between the genotypes with significant increase in the BALs from *Ccsp-Rev-Erbα*-DBD^m mice, and only at ZT0, which was consistent with the neutrophil data (Figure 4.5C). Although no difference was observed between genotypes, a few cytokines exhibit higher levels at ZT0 than at ZT12 such as G-CSF, TNFα, IL-6, CCL2 (Figure 4.5C, Appendix 12 Table A12).

However, no gating and no genotype differences were observed for CXCL1 and CXCL2 (Figure 4.5C, Appendix 12 Table A12). Interestingly, even in un-challenged conditions, CXCL5 levels were enhanced in *Ccsp-Rev-Erbα*-DBD[m] mice compared to littermate controls, both at ZT0 and ZT12 (Figure 4.5C). In this saline condition, CXCL5 levels were higher at ZT0 than at ZT12 for both genotypes, which this time, is consistent with my own findings (Chapter 3) and reported data (Gibbs et al., 2014).
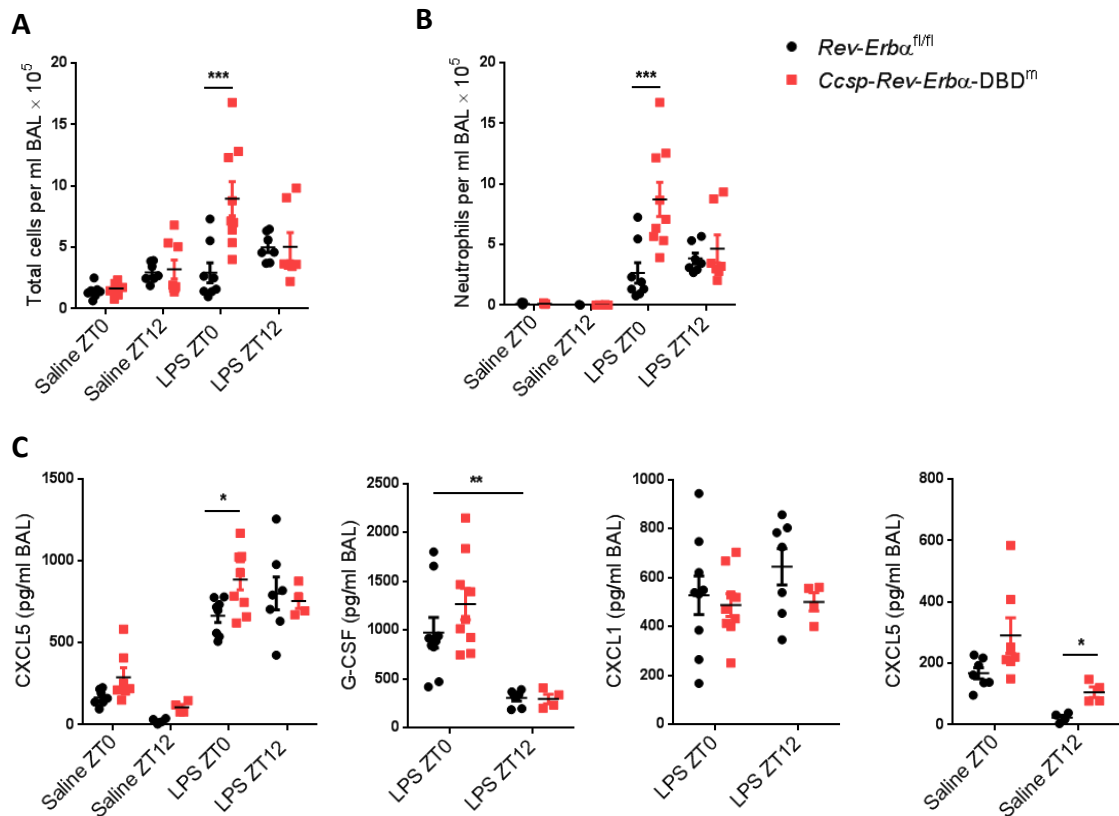
Figure 4.5: Effect of impaired REV-ERBα DBD in CCSP-expressing cells on the pulmonary response to aerosolised LPS at different time points

Ccsp-Rev-Erbα-DBD[m] and littermate control mice were exposed to aerosolised LPS at 2 mg/ml or saline at ZT0 or ZT12 for 20 min. (A) Total cell counts in BAL samples collected at 5 hours after challenge. (B) Neutrophil numbers in the same sample were determined by flow cytometry analyses. A few data points with high measured total cell numbers and neutrophils were excluded using the median absolute deviation method. (C) Cytokine and chemokine protein levels in BAL samples were assessed by luminex assay. During the cull at ZT12, a few BAL samples collected were bloody. These samples were excluded for the multiplex analyses. Data are presented as mean ± SEM; n = 7-9, *P <0.05, **P <0.01, ***P <0.001 (Two-way ANOVA, post hoc Bonferroni).

RNA analyses of inflammatory genes in whole lungs confirmed the results obtained by multiplex assay for *Cxcl5* and revealed elevation of transcript levels of *Cxcl2* and *G-csf* in *Ccsp-Rev-Erbα*-DBD[m] mice compared to littermate controls when challenged at ZT0 (Appendix 12, Figure A12). Moreover, *Bmal1* transcript levels were up-regulated at ZT0 in mice lacking REV-ERBα DBD within bronchiolar club cells compared to control mice.

These results indicate that the lack of REV-ERBα DBD in the bronchiolar epithelial cells enhances pulmonary inflammation but it does not affect its temporal gating. This suggests that impairment of the DNA binding function of REV-ERBα is not sufficient to disrupt the clock control of lung inflammation.

Impairment of DNA binding function of REV-ERBα in bronchiolar epithelial cells does not affect macrophage responses to LPS *ex vivo*

Growing evidence has demonstrated a critical interplay between epithelial cells and alveolar macrophages (Westphalen et al., 2014). Therefore, I wanted to assess whether loss of REV-ERBα DBD in bronchiolar epithelial cells affected isolated alveolar macrophage responses to inflammatory stimulus. For that purpose, alveolar macrophages were collected by performing broncho-alveolar lavages from *Ccsp-Rev-Erbα*-DBD[m] mice and *Rev-Erbα*^{fl/fl} littermate controls and the cells were subjected to LPS *ex vivo.* Unpaired *t*-test analysis revealed no genotype difference in transcript abundance in response to LPS (Figure 4.6). This indicated that alveolar macrophage immune function was not remodelled due to the effects of REV-ERBα DBD mutation in bronchiolar epithelial cells.
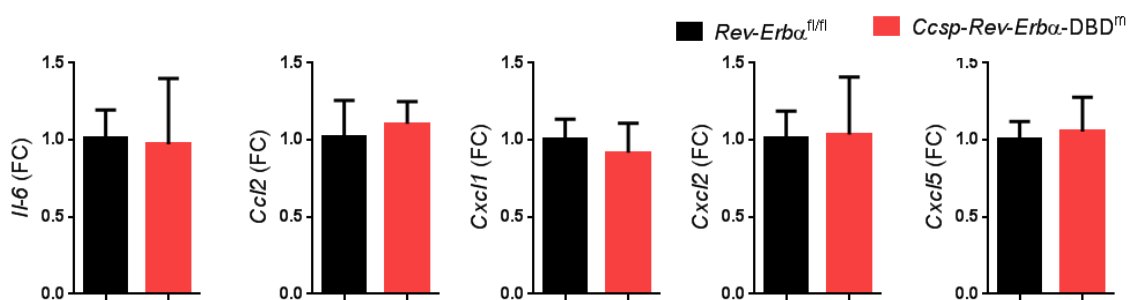
Figure 4.6: Effect of impaired REV-ERα DBD in CCSP-expressing cells on alveolar macrophage responses to *ex vivo* LPS (legend on next page)

Alveolar macrophages from *Ccsp-Rev-Erbα*-DBD[m] and littermate control mice were collected at ZT8, seeded into plates and directly treated with LPS at 100 ng/ml for 2 hours. Gene expression was determined by Real-Time qPCR and normalized to *Rev-Erbα*^{fl/fl} control group. Data are presented as mean ± SD; n = 3. Student's *t*-test.

4.3.5 Impairment of DNA binding function of REV-ERBα in myeloid cells has no impact on modulating pulmonary responses to LPS *in vivo*

Male and female *LysM-Rev-Erbα*-DBD[m] mice and *Rev-Erbα*^{fl/fl} littermate controls were challenged with aerosolised LPS at 2mg/ml or saline as control, for 20 min at ZT4. Mice were culled 5 hours after endotoxin challenge at ZT9. Lung content was
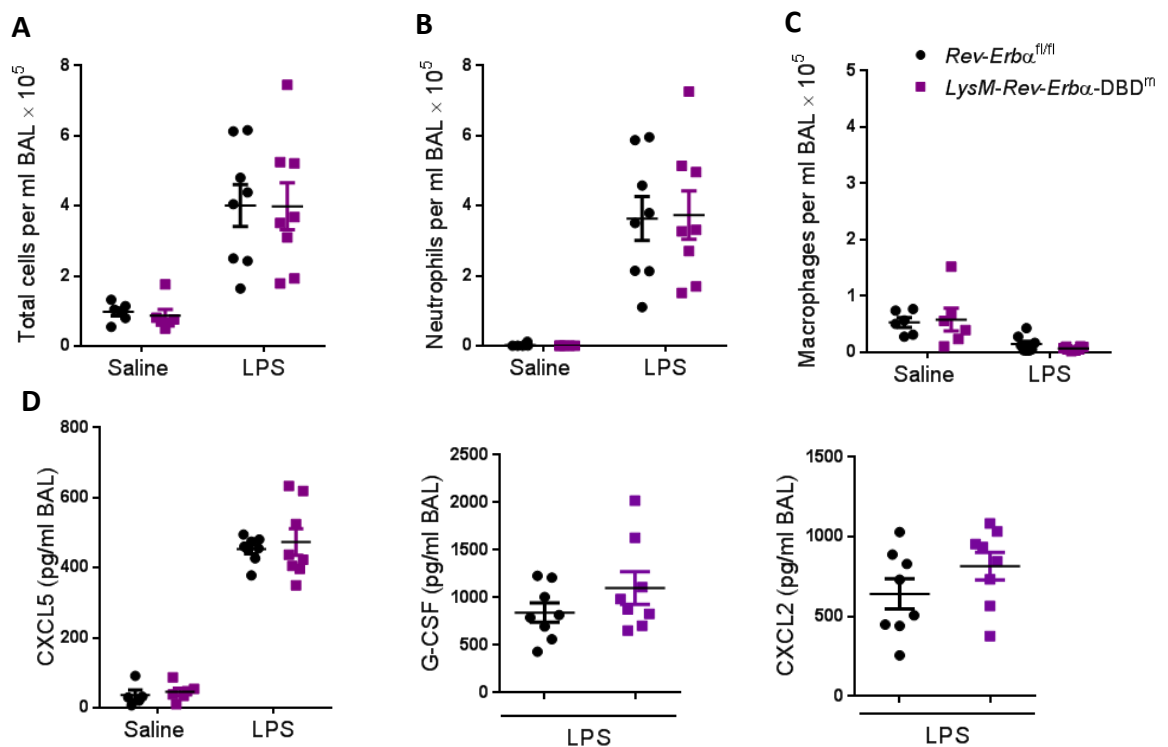
Figure 4.7: Pulmonary inflammatory response to LPS challenge at ZT4 in *LysM-Rev-Erbα*-DBD[m] mice and *Rev-Erbα*^{fl/fl} littermate controls

Mice were exposed to aerosolised LPS at 2mg/ml or to saline for 20 minutes at ZT4 and culled 5 hours later. (A) Total cell counts per ml BAL. Neutrophils (B) and macrophages (C) were quantified in BAL fluid using flow cytometry. (D) Chemokine and cytokine levels in BAL samples were assessed by Bioplex analyses. Data are presented as mean ± SEM; *n* = 8 (Two-way ANOVA, post hoc Bonferroni).

washed out by bronchoalveolar lavage (BAL) and lung tissues were taken out for further RNA and protein analyses. *LysM-Rev-Erbα*-DBD[m] mice exhibited similar pulmonary responses to LPS than *Rev-Erbα*^{fl/fl} littermate controls. Two-way ANOVA statistical analyses revealed no difference in total cell counts, neutrophils and macrophages between the two genotypes (Figure 4.7A,B,C). Out of 23 chemokines and cytokines measured by luminex assay, 12 were upregulated in response to LPS challenge (Appendix 13, Table A13). However, similar levels were measured in both *LysM-Rev-Erbα*-DBD[m] mice and *Rev-Erbα*^{fl/fl} littermate controls (Figure 4.7D). Transcript levels of pro-inflammatory genes in whole lung were also elevated upon LPS exposure but no difference was observed between the two strains (Appendix 13, Figure A13).

These results suggest that the myeloid cells are not the key cell types by which REV-ERBα mediates control of pulmonary inflammation through its DNA binding function in an *in vivo* context.

4.3.6 Impairment of DNA binding function of REV-ERBα in myeloid cells leads to moderate elevated inflammatory responses to LPS *ex vivo*

As demonstrated above, mutation of REV-ERBα DBD in alveolar macrophages has no impact on regulation of pulmonary inflammation in an *in vivo* context. In order to measure inflammatory responses of macrophages removed by broncho-alveolar lavage, alveolar macrophages from *LysM-Rev-Erbα*-DBD[m] mice and *Rev-Erbα*^{fl/fl} littermate controls were subjected to LPS *ex vivo*. Overall, cytokine and chemokine expression was moderately elevated in alveolar macrophages from *LysM-Rev-Erbα*-DBD[m] mice compared to controls and increased expression reached significance only for *Cxcl1* and *Cxcl2* when *t*-test statistical analysis was performed (Figure 4.8).
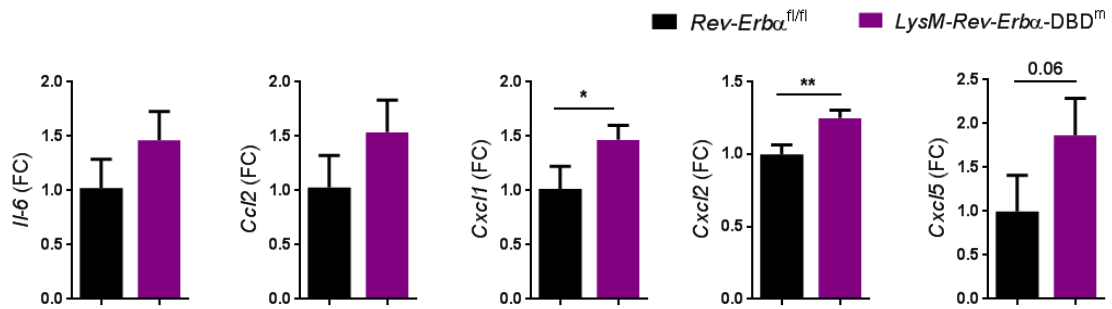
Figure 4.8: Effect of impaired REV-ERBα DBD in myeloid cells on alveolar macrophage responses to *ex vivo* LPS

Alveolar macrophages from *LysM-Rev-Erbα*-DBD[m] and littermate control mice were collected at ZT8, seeded into plates and directly treated with LPS at 100 ng/ml for 2 hours. Gene expression was determined by Real-Time qPCR and normalized to *Rev-Erbα*^{fl/fl} control group. Data are presented as mean ± SD; *n = 3, *P <0.05, **P <0.01* (Student's *t*-test).

4.3.7 Impairment of DNA binding function of REV-ERBα in either bronchiolar epithelial cells or myeloid cells has no effect on NRF2-dependent antioxidant gene expression

The effects of REV-ERBα DBD deletion in either bronchiolar epithelial cells or myeloid cells on NRF2-regulated gene expression were evaluated in both basal and LPS-challenged conditions.

In whole lung from *Ccsp-Rev-Erbα*-DBD[m] and *LysM-Rev-Erbα*-DBD[m] mice, transcript levels of *Nrf2* and its target genes were equivalent to the ones measured in the respective littermate controls in both basal and challenged conditions despite a significant activation of these genes in response to LPS exposure (Figure 4.9A). At protein levels, LPS exposure induced an increase in HO-1 but a two-way ANOVA statistical analysis of relative intensity of HO-1 to β-ACTIN bands revealed no significant difference between genotypes and exposures (Figure 4.9B,C).
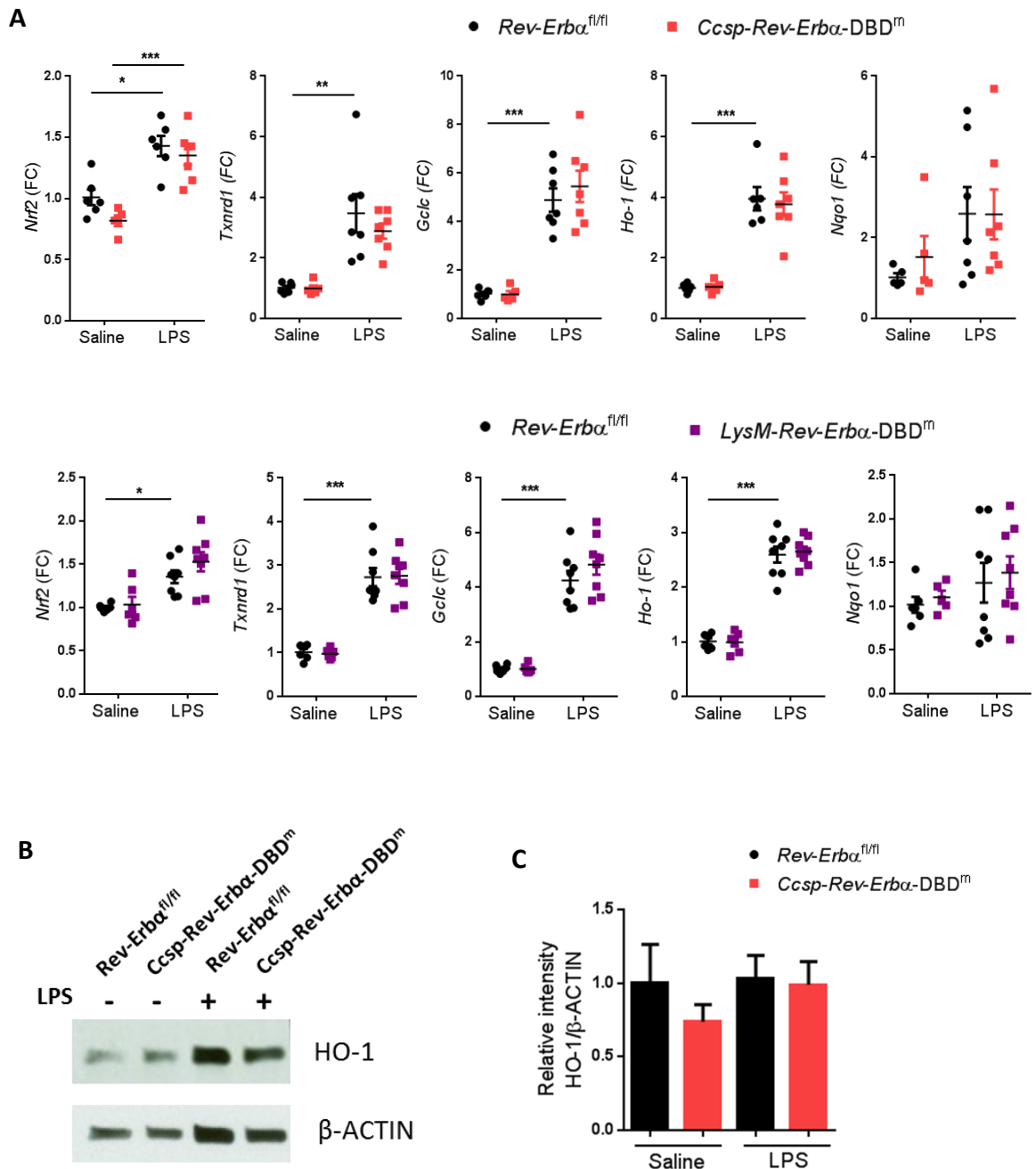
Figure 4.9: Antioxidant gene response in whole lung after aerosolised LPS exposures at ZT4 in *Ccsp-Rev-Erbα*-DBD[m], *LysM-Rev-Erbα*-DBD[m] mice and *Rev-Erbα*^{fl/fl} littermate controls

Mice were exposed to aerosolised LPS at 2mg/ml or to saline for 20 minutes at ZT4 and culled 5 hours later. (A) Gene expression was determined by Real-Time qPCR and normalized to *Rev-Erbα*^{fl/fl} saline group. Data are presented as mean ± SEM; n = 5-8, *P <0.05, **P <0.01, ***P <0.001   (Two-way ANOVA, post hoc Bonferroni). (B) Levels of HO-1 proteins were measured by Western blotting. (C) HO-1 densitometry (mean ± SEM) was normalised to β-ACTIN and to *Rev-Erbα*^{fl/fl} saline group; n = 6.

4.4 Discussion

4.4.1 Choice of the mouse models

In order to determine the contribution of REV-ERBα in macrophages in regulating pulmonary inflammation *in vivo,* mutation of *Rev-Erbα* was introduced in myeloid cells using the LysM driver. Although this approach targets macrophages, mutation of REV-ERBα is also introduced in the other myeloid cells such as neutrophils and monocytes. The choice of this LysM driver was mainly based on the availability within my group and even if it is not specific to macrophages, it still allowed me to conclude that macrophages were not the key cells for REV-ERBα to exert its anti-inflammatory action in an *in vivo* context. Another option to target more specifically macrophages would have been to use a Cx3cr1 driver although it also targets monocytes (Yona et al., 2013), or to use a Cd11c driver, which targets alveolar macrophages and dendritic cells .

As described in the introduction, mutation of REV-ERBα was introduced in bronchiolar epithelial cells, which express the surfactant protein CCSP, rather than in alveolar epithelial cells because these non-ciliated bronchiolar epithelial cells are the key lung pacemaker cells (Gibbs et al., 2009). However, an overlap between alveolar epithelial type II (AEII) cells and bronchiolar epithelial cells exists, as recent research has found a subset of CCSP+ cells expressing also the AEII marker surfactant protein-C (SP-C) with stem cell capacities (Wang et al., 2012). Thus, the genetic strategy employed using the CCSP driver could also target a sub-population of AEII cells and immunostaining for CRE on lung sections would be required to assess accurately which cells of the lung possess the REV-ERBα mutation.

4.4.2 Generation of *LysM-Rev-Erbα*-DBD[m] and *Ccsp-Rev-Erbα*-DBD[m] mouse lines

Assessment of REV-ERBα DBD knock-out using genotyping PCR from ear clip or lung tissue clearly revealed the presence of a null (recombined) fragment in Cre[+ve] animals (Figure 4.1A,B). However, this was not sufficient to show that REV-ERBα proteins in the specific cell types no longer expressed the DBD. Western Blot results from whole lung tissue were inconclusive, as abundance of protein relative to β-

ACTIN did not vary between genotypes (Figure 4.1C,D). Also, bronchiolar epithelial cells or myeloid cells are a relatively small proportion of whole lung cells and the selective loss of REV-ERBα DBD only in these cell types may be masked by the high expression of REV-ERBα throughout the rest of the lung. Quantification of CCSP protein abundance (relative to β-ACTIN) shows a 50% decrease in *Ccsp-Rev-Erbα*-DBD[m] compared with *Rev-Erbα*^{fl/fl} littermate controls (Figure 4.1D). Further investigation into the genetics of the *Ccsp*[icre/+] mice revealed that the insertion of the iCre sequence in the *Ccsp* gene yields to a non-viable copy of the gene. Therefore, *Ccsp*[icre/+] animals have only one normal copy of the *Ccsp* gene and this haploinsufficiency causes a reduced quantity of protein product by 50%. As CCSP is an important regulator of pulmonary immune barrier function (Watson et al., 2001), this raises important questions regarding the response of *Ccsp*[icre/+] mice to inflammatory challenge, but a control experiment showed these mice do not display elevated neutrophilic inflammation compared to *Ccsp*^{+/+} mice in response to aerosolised LPS challenge at ZT4 (Figure 4.3). Thus, disruption of the *Ccsp* gene was not a confounding factor in experiments where Ccsp-targeted knockouts, such as the *Ccsp-Rev-Erbα*-DBD[m] line, were subjected to aerosolised LPS.

REV-ERBα DBD disruption in myeloid cells from *LysM-Rev-Erbα*-DBD[m] mice was confirmed at the transcript levels by measuring mRNA in peritoneal exudate cells (PECs) which are mainly macrophages after plate seeding and attachment. When using primers targeting the DBD, *Rev-Erbα* mRNA levels were decrease by 85% in *LysM-Rev-Erbα*-DBD[m] mice compared to littermate controls (Figure 4.1E). However, *Rev-Erbα* mRNA levels in these mutated mice were nearly two fold increased when primers targeting exons 1 and 2 were used. These results were consistent with previous findings showing an up-regulation of the truncated version of REV-ERBα (Zhang et al., 2015). Multiple attempts to detect these changes at protein levels were unfortunately unsuccessful maybe due low REV-ERBα protein abundance in macrophages.

In situ hybridisation was employed to assess deletion of the DBD within *Rev-Erbα* transcript in the bronchioles of *Ccsp-Rev-Erbα*-DBD[m] mice. Consistently with findings in PECs, when using primers targeting exons 6 to 8, an up-regulation of the transcript was observed in *Ccsp-Rev-Erbα*-DBD[m] mice. However, when targeting

exons 2 to 5, which contain the DBD, no significant change was measured whereas a decrease of the transcript was expected in the mutant mice. This contradicts genotyping results and could be due to an inadequate probe design for the *in situ*; the sequence targeted, between exons 2 to 5 (455 bp), might be too long and the radiolabelled probe could still detect the 200 bp targeted part of exon 5 (Appendix 3). Hence, this warrants further work to confirm loss of the *Rev-Erbα* DBD at transcript levels in the bronchioles of *Ccsp-Rev-Erbα*-DBD[m] mice, by either designing a new probe to target only exons 3 and 4, or by collecting bronchiolar epithelial cells from lung slices using laser capture.

Moreover, further work would also be required to evaluate the lack of REV-ERBα DBD at protein levels in both mouse lines.

4.4.3 Rhythmic bioluminescence in the mouse models

Over the past few years, it has been well demonstrated that deleting REV-ERBα from cells, tissues or entire organisms does not abolish rhythms of other clock proteins. Therefore, persistence of PER2::Luc rhythmic oscillations observed in ectopic lung slices from mice lacking REV-ERBα DBD in either myeloid cells or bronchiolar cells was expected (Figure 4.2). Similarly, isolated PECs from *LysM-Rev-Erbα*-DBD[m] mice exhibited circadian oscillations of PER2::Luc comparable to littermate controls (Figure 4.2).

The bronchiolar epithelial cells are a key cell type to sustain rhythms within the lung as deletion of these cells using naphthalene renders lung slices arrhythmic in culture (Gibbs et al., 2009). Moreover, targeted disruption of *Bmal1* in *Ccsp*[icre] positive cells abolishes PER2::Luc oscillations in the bronchial epithelium (Gibbs et al., 2014). In contrast, PER2::Luc oscillations were recorded in bronchioles of *Ccsp-Rev-Erbα*-DBD[m] mice, which is consistent with the fact that presence of REV-ERBα is not necessary for sustaining rhythms (Figure 4.2). However, for still non-elucidated reason, the luciferase signal from bronchioles of the *Rev-Erbα*^{fl/fl} littermate controls was very weak. It is also important to take into account that I may compare signals from slices cut at different position in the lung and thus from different pulmonary cell types.

4.4.4 Pulmonary inflammatory phenotype in *Ccsp-Rev-Erbα*-DBD^m mice

Previous work has shown that ablation of the core clock gene *Bmal1* within bronchiolar epithelial cells results in exaggerated neutrophilic inflammation (Gibbs et al., 2014). *Ccsp-Bmal1$^{-/-}$* mice also lose circadian gating of their neutrophilic response to aerosolised lipopolysaccharide and the key neutrophil attractor chemokine CXCL5 is constantly up-regulated in these animals. However, one of the effects of *Bmal1* knock-out is to suppress Rev-Erbα and Rev-Erbβ expression. Therefore, it is important to investigate whether the pro-inflammatory phenotype observed in *Ccsp-Bmal1$^{-/-}$* mice is mediated by circadian clock disruption within the bronchiolar epithelial cells or by a more general pleiotropic effect of BMAL1 disruption.

The results from LPS exposures in *Ccsp-Rev-Erbα*-DBD^m mice showed increased neutrophilia compared to littermate controls when mice were challenged at ZT0 and ZT4 but not at ZT12 (Figures 4.4 and 4.5). This suggests that REV-ERBα in bronchiolar epithelial cells possesses an anti-inflammatory function which is operated by its ability to bind DNA. This result is even more interesting knowing that Lazar's group has demonstrated that REV-ERBα contributes to regulation of liver metabolism through a DBD-independent function (Zhang et al., 2015). It is well known that the nuclear receptor REV-ERBα has other functions than being only a core clock component. Its role in metabolism has been well characterised (Bugge et al., 2012; Duez and Staels, 2009). Zhang et al. (2015) have shown that REV-ERBα in liver binds directly to DNA through RORE elements to exert his core repressive function of the cell autonomous clock whereas it is tethered to chromatin by liver-lineage determining transcription factor hepatocyte nuclear factor 6 (HFN6) to regulate metabolic genes. Other nuclear receptors such as the glucocorticoid receptor have also DBD-independent activities through protein-protein interactions with other transcription factors (Glass and Saijo, 2010). In contrast, my data suggests that the anti-inflammatory role of REV-ERBα in the lung is DBD-dependent. It has been reported that REV-ERBα modulates the inflammatory function of macrophages through direct DNA binding in the Ccl2 promoter region (Sato et al., 2014). As my experimental work was carried out targeting the bronchiolar epithelial cells, further

investigation involving ChIP-sequencing would be required to elucidate the DNA sites and motifs bound by REV-ERBα upon inflammatory stimuli in my pulmonary model.

Moreover, my results showing increased neutrophilia in *Ccsp-Rev-Erbα*-DBD^m mice after LPS exposure at ZT0 and ZT4 but not at ZT12 indicate that the circadian gating of inflammation is preserved in mice lacking REV-ERBα DBD in the bronchiolar epithelial cells. Indeed, Gibbs et al. (2014) showed that severity of neutrophilic inflammation upon aerosolised LPS depends on the timing of the exposure. Mice exposed at dawn exhibit higher inflammatory burden than mice challenged at dusk. Therefore, impairment of REV-ERBα DBD in bronchiolar epithelial cells is not sufficient to abolish circadian clock control of pulmonary inflammation. It would be interesting to investigate whether knock-out of the entire REV-ERBα in CCSP-expressing cells would exacerbate the pro-inflammatory phenotype observed in *Ccsp-Rev-Erbα*-DBD^m mice and whether the gating of the inflammation would be still maintained.

However, an important caveat of this work is the absence of circadian gating of inflammation in the *Rev-Erbα*^fl/fl littermate controls. As described above, I expected these mice to exhibit more neutrophilic inflammation at ZT0 than at ZT12 (Figure 4.5). In contrast, the levels of neutrophils were similar at both time points. Comparing with similar studies, it seemed that *Rev-Erbα*^fl/fl littermate control mice did not respond to LPS as greatly as expected when challenged at ZT0. Unfortunately, I cannot explain these results, but it is noteworthy to relate them to the weak PER2::Luc bioluminescence signal observed in the bronchial epithelium of these mice (Figure 4.2) which may reflect unexpected core clock amplitude dampening. As this time-of-day LPS challenge study was performed once, it would be worth repeating it.

Previous findings have demonstrated that CXCL5 expression during lung inflammation is predominantly produced by the alveolar epithelium and that the expression of this neutrophil attractor chemokine in the lung is regulated by the Toll-like receptor 4 (TLR4) (Jeyaseelan et al., 2005). More recently, Gibbs et al. (2014) showed that bronchiolar epithelial cells are also capable of secreting CXCL5 when

challenged *ex vivo* with LPS. My own data confirms the importance of CXCL5 in driving neutrophils upon nebulized LPS challenges and highlights the regulatory role of REV-ERBα in controlling the expression of this chemokine. Indeed, out of 23 different cytokines and chemokines measured in BAL samples, only CXCL5 was significantly increased in *Ccsp-Rev-Erbα*-DBD[m] mice at the same time points than elevated neutrophil numbers were measured. As for neutrophils, CXCL5 levels upon LPS challenge were up-regulated in BAL samples from *Ccsp-Rev-Erbα*-DBD[m] mice compared to littermate controls only when mice were challenged at ZT0 and ZT4. Therefore, impairment of REV-ERBα DBD in bronchiolar epithelial cells is not sufficient to reproduce the constant elevation of CXCL5 observed in *Ccsp-Bmal1*^{-/-} mice (Gibbs et al., 2014).

Finally, alveolar macrophages from *Ccsp-Rev-Erbα*-DBD[m] mice did not exhibit any inflammatory changes upon *ex vivo* endotoxin challenge compared to macrophages from the littermate controls. This indicates that mutation of *Rev-Erbα*-DBD in the bronchiolar epithelial cells does not alter the intrinsic immune properties of the alveolar macrophages. Westphalen et al. (2014) have shown intercellular communication between sessile alveolar macrophages and the pulmonary epithelium to have immunosuppressive effects. In my experiments, collection of alveolar macrophages was performed by broncho-alveolar lavage and it is more likely to collect free-moving alveolar macrophages than sessile ones.

4.4.5 Absence of exaggerated pulmonary inflammatory phenotype in *LysM-Rev-Erbα*-DBD[m] mice

Whilst REV-ERBα has been shown to be a critical intermediary between the core clock and inflammatory pathways in macrophages (Gibbs et al., 2012; Lam et al., 2013; Sato et al., 2014), mutation of REV-ERBα DBD in myeloid cells had no impact on pulmonary inflammatory responses in an *in vivo* model (Figure 4.7). These results were not surprising as previous findings showed no changes in neutrophil and cytokine responses after administration of aerosolised LPS in *LysM-Bmal1*^{-/-} mice compared to controls (Gibbs et al., 2014). However, alveolar macrophages from *LysM-Rev-Erbα*-DBD[m] mice, when dissociated from the tissue environment,

displayed moderate pro-inflammatory responses (Figure 4.8). For all cytokines and chemokines measured, expression was increased by 1.5 fold change and significance was reached only for *Cxcl1* and *Cxcl2*. Sato et al. (2014) previously showed that REV-ERBα regulates inflammation in macrophages through direct DNA binding in the *Ccl2* promoter region. However, my own data revealed only a small and non-significant elevation of *Ccl2* transcripts in alveolar macrophages from *LysM-Rev-Erbα*-DBD[m] mice, subjected *ex vivo* to LPS. This could be explained by the different type of macrophage used for the experiments; Sato et al. used peritoneal macrophages and RAW264 cells.

4.4.6 No effect of loss of REV-ERBα DBD on NRF2-regulated pathway activation

In Chapter 3, I showed that global knockout of REV-ERBα leaded to an up-regulation of *Txnrd1* and *Gclc* transcripts upon endotoxin challenge. In contrast, deletion of REV-ERBα DBD in either bronchiolar epithelial cells or myeloid cells did not result in any increased antioxidant gene expression. This could be a consequence of the minor difference between mutated mice and the littermate controls in terms of inflammatory responses and cytokine recruitment to the lung. Indeed, no pro-inflammatory phenotype was observed in mice with impaired REV-ERBα DBD in myeloid cells compared to control animals and only the chemokine CXCL5 showed increased levels in mice with impaired REV-ERBα DBD in bronchiolar epithelial cells. This is probably not sufficient to produce greater quantity of ROS and thus greater levels of antioxidants.

4.5 Conclusions

As other nuclear receptors, REV-ERBα controls gene expression by either direct binding to the genome or by DBD-independent tether through transcription factors. This chapter clearly demonstrates that REV-ERBα regulates pulmonary

inflammation through direct DNA binding. Moreover, this chapter highlights the importance of the bronchiolar epithelium as part of a cell specific mechanism controlling pulmonary immune responses. This mechanism involves CXCL5, a chemokine mainly expressed by epithelial cells. Therefore, my results suggest that neutrophil recruitment to the lung upon bacterial challenge is driven by CXCL5 of which the expression may depend to the ability of REV-ERBα to bind DNA in the bronchiolar epithelial cells.

Chapter 5: Impact of REV-ERBα DBD mutation and REV-ERBβ deletion in bronchiolar epithelial cells

5.1 Introduction

REV-ERBβ, also known as NR1D2, was identified in 1994 as a paralog of REV-ERBα by multiple groups (Bonnelye et al., 1994; Dumas et al., 1994). REV-ERBβ is highly similar to REV-ERBα in its protein structure by also lacking the activation function 2 helix (AF2-helix) required for ligand-dependent activation by other members of nuclear receptors, making it a repressor of transcription (Burke et al., 1996). The intrinsic repressive activities of both REV-ERBs are believed to control the rhythmic expression of target genes such as *Bmal1*. Depletion of either one of the REV-ERB proteins has a minimal effect on the cell-autonomous circadian clock in mouse embryonic fibroblasts, but loss of both REV-ERBα and β abrogated circadian gene expression in this system (Bugge et al., 2012). Moreover, genetic ablation of both Rev-Erbα and β in adult mice resulted in arrhythmic wheel running behaviour, in both the presence or absence of light entrainment cues, and disrupted circadian expression of core circadian clock genes (Cho et al., 2012). These findings demonstrate that both REV-ERBs are required for functional clock machinery, although REV-ERBα is considered to be more important, because its absence results in mild disruptions to circadian rhythms, in contrast to the relatively inconsequential loss of REV-ERBβ alone (Bugge et al., 2012; Cho et al., 2012). Various groups have highlighted the importance of REV-ERBα on regulation of metabolism and inflammation, however only a few of studies looked at the effects of the dual depletion of both REV-ERBα and β (Bugge et al., 2012; Cho et al., 2012; Lam et al., 2013). In the previous chapter, I demonstrated the importance of DNA binding function of REV-ERBα in the bronchiolar epithelial cells to regulate pulmonary inflammation. In this chapter, I examined the consequences of depletion of both REV-ERBα DBD and REV-ERBβ in bronchiolar epithelial cells on lung immune response.

5.2 Hypothesis tested and experimental approaches

Hypothesis: Targeting both REV-ERBα and REV-ERBβ in the bronchiolar epithelial cells has a more extensive effect on neutrophilic inflammation than deletion of the REV-ERBα DBD.

Objectives:

- Generate a mouse strain which lacks both REV-ERBα DBD and REV-ERBβ in bronchiolar epithelial cells by breeding *Rev-erbα/β*[fl/fl] mice with *Ccsp*[icre] mice, maintain on a Per2::Luc background to facilitate bioluminescence monitoring.

- Assess lung rhythmicity by monitoring organotypic lung slices from mutated mice and littermate controls under photomultiplier tubes (PMTs) or camera.

- Challenge the mutated mice and littermate controls with aerosolised LPS at different time points and measure any differences in the magnitude and rhythm of inflammatory response (cell infiltration and cytokine production).

5.3 Results

5.3.1 Assessment of deletion of REV-ERBα DBD and REV-ERBβ in bronchiolar epithelial cells

As in chapter 4, confirmation of successful knockout of both REV-ERBα DBD and REV-ERBβ in bronchiolar epithelial cells (*Ccsp*[icre] positive cells) was attempted using multiple approaches. First, the genotyping strategy used allowed identification of floxed, wild-type and null (recombined, 'knockout') fragments (Figure 5.1A). As expected, null fragments were only observed in lung samples from Ccspicre[+ve] animals and not in ear clips which obviously do not possess bronchiolar epithelial cells.

As described in chapter 4.3.1, confirmation of loss of REV-ERBα DBD at protein level using Western Blot on whole lung tissue was ineffective. It was expected to detect two bands in Ccspicre[+ve] mice; a first one at 75 kDa, the molecular weight of the full REV-ERBα, and another one just under 75 kDa corresponding to the protein lacking its DBD (Zhang et al., 2015). A clear band at 75 kDA was detected for all the animals (Figure 5.1B). However, observation of a second lower band was difficult or rather impossible as non-specific bands were also detected just below 75 kDA (chapter 2.10.3, appendix 5). Moreover, the potential masking effect of the other cell types in the whole lung, which express the full length of REV-ERBα has to be taken into account. As for assessment of REV-ERBβ loss, I could not find a commercial
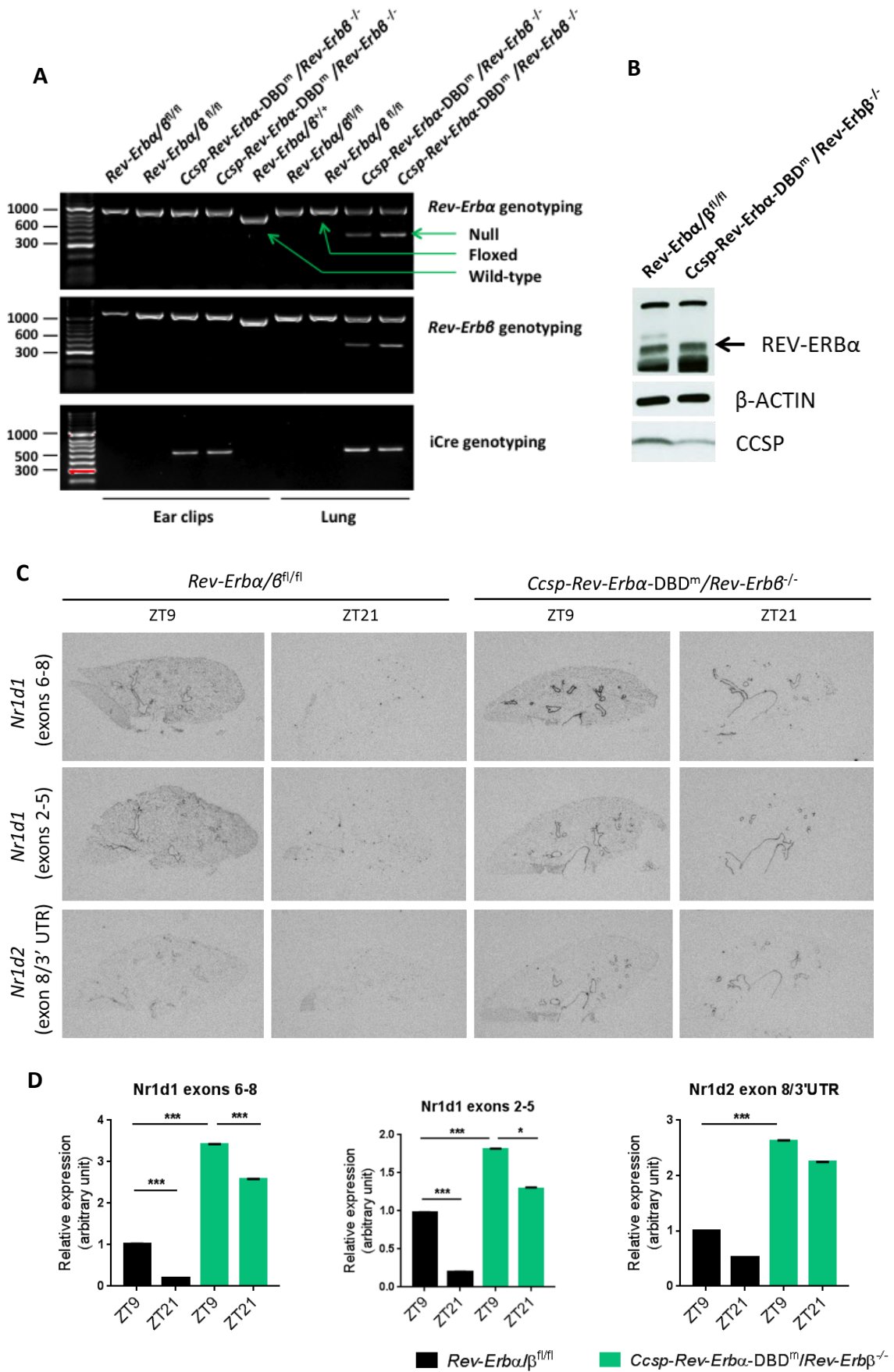
Figure 5.1: Testing for REV-ERBα DBD and REV-ERBβ loss in bronchiolar epithelial cells of *Ccsp-Rev-Erbα*-DBD^m/*Rev-Erbβ*^{-/-} mice   (legend on next page)

(A) Example of genotyping results from ear clips and lungs of *Ccsp-Rev-Erbα*-DBD^m/*Rev-Erbβ*^-/- mice and *Rev-Erbα/β*^fl/fl littermate controls. *Rev-Erbα/β*^+/+ samples were included for comparison. (B) Western blot analysis of whole lung from *Ccsp-Rev-Erbα*-DBD^m/*Rev-Erbβ*^-/- mice and *Rev-Erbα/β*^fl/fl littermate controls. Membranes were stained for REV-ERBα using monoclonal GSK6F05 antibody (75 kDa), β-ACTIN (42kDa) and CCSP (10kDa). (C) Example images of lung slices probed for *Rev-Erbα* and *Rev-Erbβ* mRNA via *in situ* hybridisation. (D) Relative quantification of mRNA abundance from multiple lung slices measured via *in situ* hybridisation. Data are presented as mean ± SEM; $n = 2$/genotype/time point. *P <0.05, ***P <0.001 (One-way ANOVA, post hoc Bonferroni).

antibody which detects the endogenous protein by Western blotting. Consistently with findings in chapter 4.3.1, lower levels of CCSP were detected in the *Ccsp-Rev-Erbα*-DBD^m/*Rev-Erbβ*^-/- mice (Figure 5.1B) resulting from the iCre sequence insertion in the *Ccsp* gene (Appendix 10).

As in chapter 4.3.1, *in situ* hybridisation was performed in attempt to confirm successful knock-out of both *Rev-Erbα* DBD and *Rev-Erbβ* in the bronchioles of CcspiCre^+ve mice (Figure 5.1 C,D). The same two set of probes were used to detect *Rev-Erbα* transcript and a probe targeting exon 8/3'UTR region of *Rev-Erbβ* were also employed. As in chapter 4, when using the probe targeting the *Rev-Erbα* LBD sequence (exons 6-8), a significant increase in *Rev-Erbα* mRNA was measured in the bronchioles of *Ccsp-Rev-Erbα*-DBD^m/*Rev-Erbβ*^-/- mice compared to the littermate controls at ZT9 (3.4 fold change increase). In contrast with findings from Chapter 4, a significant up-regulation of the transcript in the mutant mice at ZT9 was also measured when using the probe targeting the *Rev-Erbα* DBD sequence (exons 2-5), although the increase was less important than with the probe targeting exons 6-8 (1.8 fold change increase). In the case of *Rev-Erbβ,* a significant up-regulation of mRNA levels was measured in the bronchioles of *Ccsp-Rev-Erbα*-DBD^m/*Rev-Erbβ*^-/- mice compared to the littermate controls at ZT9 (2.6 fold change increase). This indicates that the *Rev-Erbβ* targeting strategy (flanking exon 4 with two loxP sites) leads to a viable transcript, still including the exon 8/3'UTR region. Another probe has to be designed to target specifically exon 4 to confirm the absence of this exon in *Rev-Erbβ* mRNA in the bronchioles of *Ccsp-Rev-Erbα*-DBD^m/*Rev-Erbβ*^-/- mice.

Nonetheless, the up-regulation of this potential exon 4-truncated *Rev-Erbβ* transcript could be explained by a negative/positive regulation; if the *Rev-Erbβ* targeting strategy employed leads to a non-functional protein as reported previously (Cho et al., 2012), the molecular clock machinery may try to compensate the low levels of REV-ERBβ protein by enhancing the transcription of *Rev-Erbβ*. Another important observation from these *in situ* hybridisations was that the night repression of the *Rev-Erbα* and *β* transcripts observed in the bronchioles of the littermate controls was less important in the bronchioles of the double mutant mice; the mRNA levels remained elevated at ZT21, which was not the case in mice lacking only the REV-ERBα DBD (Figure 4.1F,G). Moreover, this diminished night repression was restricted to the bronchioles as transcripts were clearly absent from the lung parenchyma of the double mutant mice at ZT21 (Figure 4.1F). This suggests an impairment of the clock machinery in the bronchioles of the *Ccsp-Rev-Erbα*-DBD^{m}/*Rev-Erbβ*$^{-/-}$ mice.

5.3.2   Bronchiole but not lung rhythmicity is affected by deletion of REV-ERBα DBD and REV-ERBβ in bronchiolar epithelial cells

Organotypic lung slices from *Ccsp-Rev-Erbα*-DBD^{m}/*Rev-Erbβ*$^{-/-}$ and *Rev-Erbα/β*$^{fl/fl}$ mice all exhibited rhythmic oscillations of PER2::Luc-driven bioluminescence for several days (Figure 5.2A). Cosinor analysis of data from hours 24-72 shows an average period of 25.5 ± 0.5 hours for control mice and 25.5 ± 0.2 hours for *Ccsp-Rev-Erbα*-DBD^{m}/*Rev-Erbβ*$^{-/-}$ mice. Statistical analysis using unpaired *t*-test showed no significant difference between means.

In order to assess rhythms specifically in the airway epithelial cells, a recording camera was used to focus on the bronchioles of ectopic lung slices. PER2 bioluminescence signal could be observed in bronchioles from both *Rev-Erbα/β*$^{fl/fl}$ and *Ccsp-Rev-Erbα*-DBD^{m}/*Rev-Erbβ*$^{-/-}$ mice (Figure 5.2B). However, if robust rhythmic signal could be observed in bronchioles of control animals, the amplitude of PER2: Luc oscillations in mutant bronchioles was very low (Figure 5.2C). This again suggests an impairment of the clock machinery in the bronchioles of the *Ccsp-Rev-Erbα*-DBD^{m}/*Rev-Erbβ*$^{-/-}$ mice.
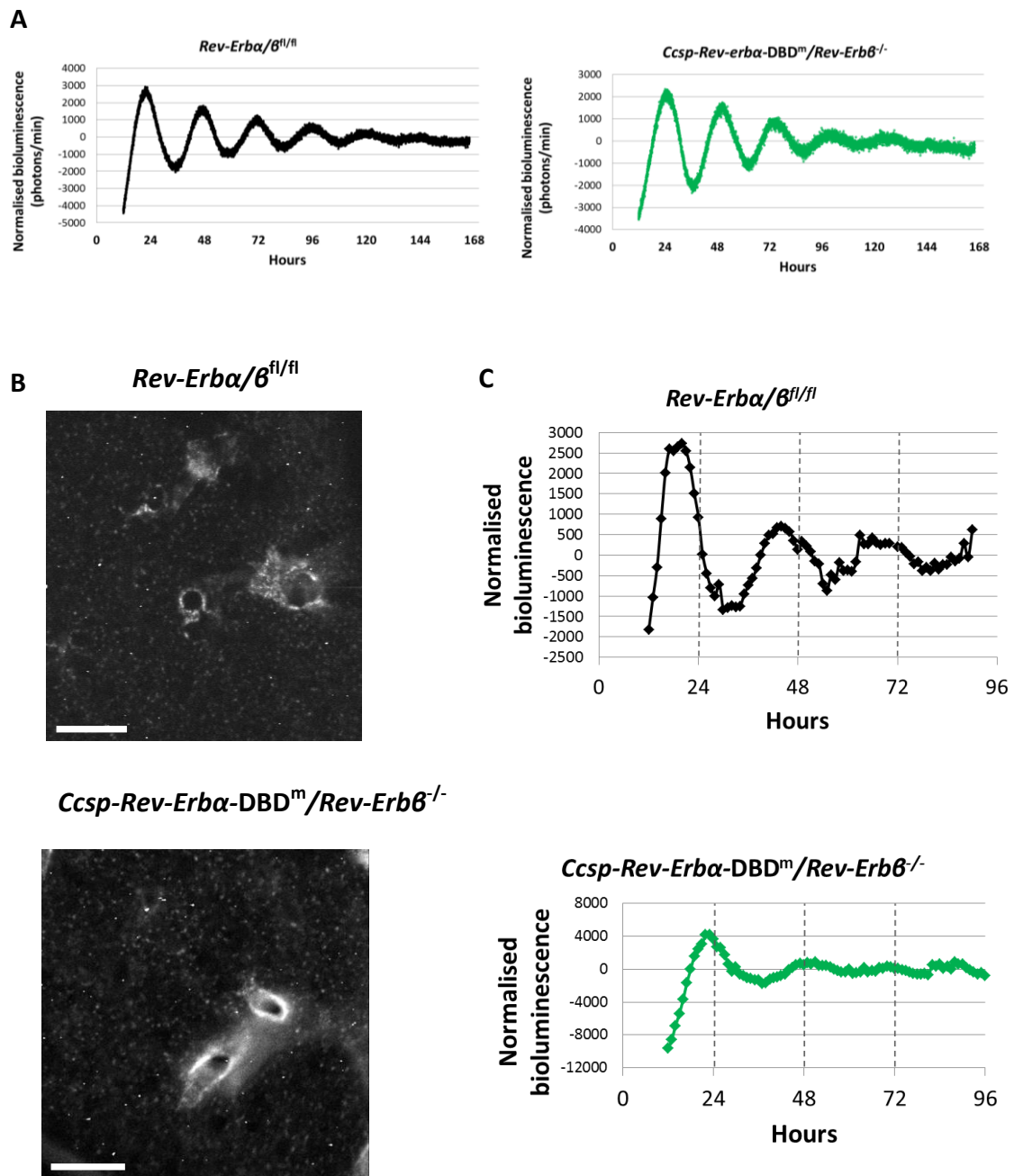
Figure 5.2: Oscillations of PER2::Luc-driven bioluminescence in organotypic lung slices and alveolar macrophages

(A) Example bioluminescence recordings from *Rev-Erbα/β*[fl/fl] (black) and *Ccsp-Rev-Erbα-*DBD[m]/*Rev-Erbβ*^{-/-} (green) precision cut lung slices. Photon counts per minute are normalised to a 24 hour moving average and traces are representative of 3 biological replicates. (B) Snapshots of recording oscillations of PER2 of precision cut lung slices from *Rev-Erbα/β*[fl/fl] and *Ccsp-Rev-Erbα-*DBD[m]/*Rev-Erbβ*^{-/-} mice. Scale bars, 500 μM. (C) Bioluminescence intensity from bronchioles was quantified, normalised to a 24 hour moving average. Traces are representative of 2 biological replicates.

5.3.3 Impairment of both REV-ERBs in bronchiolar epithelial cells has a greater impact on inflammation than just deletion of REV-ERBα DBD

To compare effects of mutations in both REV-ERB paralogs to mutation in REV-ERBα DBD only upon inflammation, male and female *Ccsp-Rev-Erbα-DBD*[m] mice, their littermate controls *Rev-Erbα*^{fl/fl}, *Ccsp-Rev-erbα-DBD*[m]*/Rev-Erbβ*^{-/-} mice and their littermate controls *Rev-Erbα/β*[fl/fl] were challenged with aerosolised LPS at 2mg/ml or saline as control, for 20 minutes at ZT4. Mice were culled 5 hours after endotoxin challenge at ZT9. Lung content was washed out by bronchoalveolar lavage (BAL) and lung tissues were taken out for further RNA and protein analyses. BAL analyses revealed a significant increase in infiltration of inflammatory cells, predominantly neutrophils for *Ccsp-Rev-erbα-DBD*[m]*/Rev-Erbβ*^{-/-} mice compared to their littermate controls. An increase was also observed for *Ccsp-Rev-Erbα-DBD*[m] mice compared to their control group but it did not reach significance (Figure 5.3A, B). Pulmonary macrophage numbers remained low for all genotypes (Figure 5.3C).

Legend:
- *Rev-Erbα*^{fl/fl} (black circle)
- *Rev-Erbα/β*[fl/fl] (grey circle)
- *Ccsp-Rev-Erbα-DBD*[m] (red square)
- *Ccsp-Rev-Erbα-DBD*[m]*/Rev-Erbβ*^{-/-} (green square)
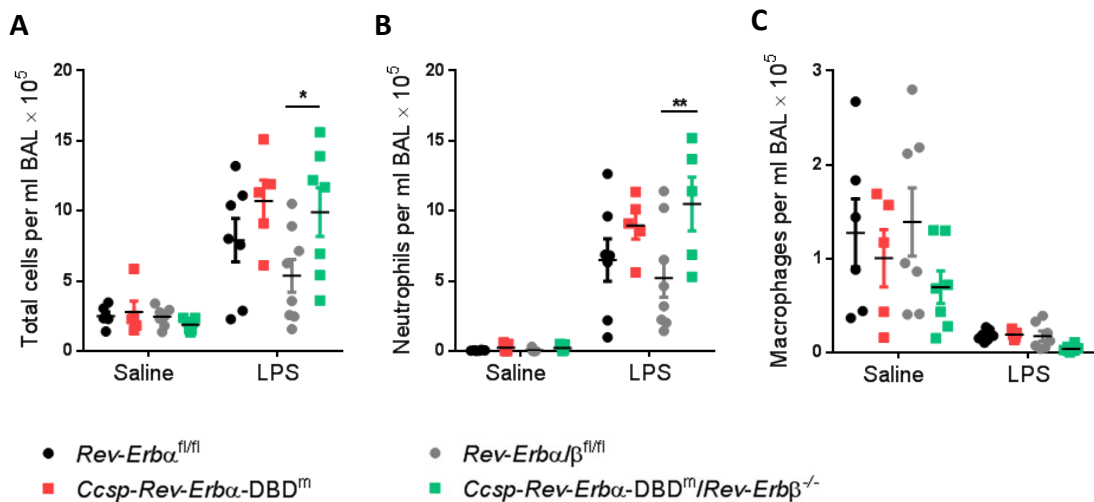
Figure 5.3: Pulmonary inflammatory response to LPS challenge at ZT4 in *Ccsp-Rev-Erbα-DBD*[m], *Ccsp-Rev-Erbα-DBD*[m]*/Rev-Erbβ*^{-/-} mice and *Rev-Erbα*^{fl/fl}, *Rev-Erbα/β*[fl/fl] littermate controls

Mice were exposed to aerosolised LPS at 2mg/ml or to saline for 20 minutes at ZT4 and culled 5 hours later. (A) Total cell counts per ml BAL. Neutrophils (B) and macrophages (C) were quantified in BAL fluid using flow cytometry. One data point corresponding to a *Ccsp-Rev-Erbα-DBD*[m] male and another one corresponding to a *Ccsp-Rev-Erbα-DBD*[m] */Rev-Erbβ*^{-/-} male, both exposed to LPS, with high measured total cell (legend continued on next page)

numbers and neutrophils were excluded using the median absolute deviation method. Two samples from *Ccsp-Rev-Erbα*-DBD^m */Rev-Erbβ^-/-* group exposed to LPS were run improperly during flow cytometry and were then excluded. Data are presented as mean ± SEM; *n* = 5-8, **P <0.05, **P <0.01* (Two-way ANOVA, post hoc Bonferroni).

Quantification of 23 inflammatory and chemotactic cytokines in BAL fluid was also performed by Multiplex analyses (Appendix 14, Table A14). Only levels in CXCL5 were different between *Ccsp-Rev-Erbα*-DBD^m mice and their littermate controls (Figure 5.4A), consistently with previous findings. Interestingly, CXCL5 levels were even higher in *Ccsp-Rev-erbα*-DBD^m*/Rev-Erbβ^-/-* mice compared to their littermate controls upon LPS challenge (Figure 5.4). More strikingly, levels of CXCL5 in saline treated *Ccsp-Rev-erbα*-DBD^m*/Rev-Erbβ^-/-* mice were as high as levels in LPS treated control groups, suggesting a possible chronic inflammatory state for these mice (Figure 5.4).

Although no difference for the other cytokines/chemokines was observed between mice lacking REV-ERBα DBD in CCSP-expressing cells and their littermate controls, CXCL1, CXCL2, G-CSF and CCL11 levels were augmented in *Ccsp-Rev-erbα*-DBD^m*/Rev-Erbβ^-/-* mice compared to their littermate controls upon LPS challenge (Figure 5.4). These results indicate that the double deletion of REV-ERBα DBD and REV-ERBβ in CCSP-expressing cells has a more dramatic effect than the single deletion of REV-ERBα DBD in both basal and bacterial challenged conditions.

Transcript levels of different cytokines and chemokines in total lung were also measured and were consistent with protein levels measured in BAL fluids. For example, *Cxcl5* transcript levels were dramatically increased in *Ccsp-Rev-Erbα*-DBD^m*/Rev-Erbβ^-/-* mice upon LPS challenge whereas a more moderate increase was observed in *Ccsp-Rev-Erbα*-DBD^m mice compared to littermate controls (Figure 5.5A). Again, a significant increase of the *Cxcl5* mRNA was observed in saline condition for mice lacking both Rev-Erbα DBD and Rev-Erbβ in CCSP-expressing cells (Figure 5.5B). *Cxcl2* and *G-csf* mRNA were also significantly up-regulated in
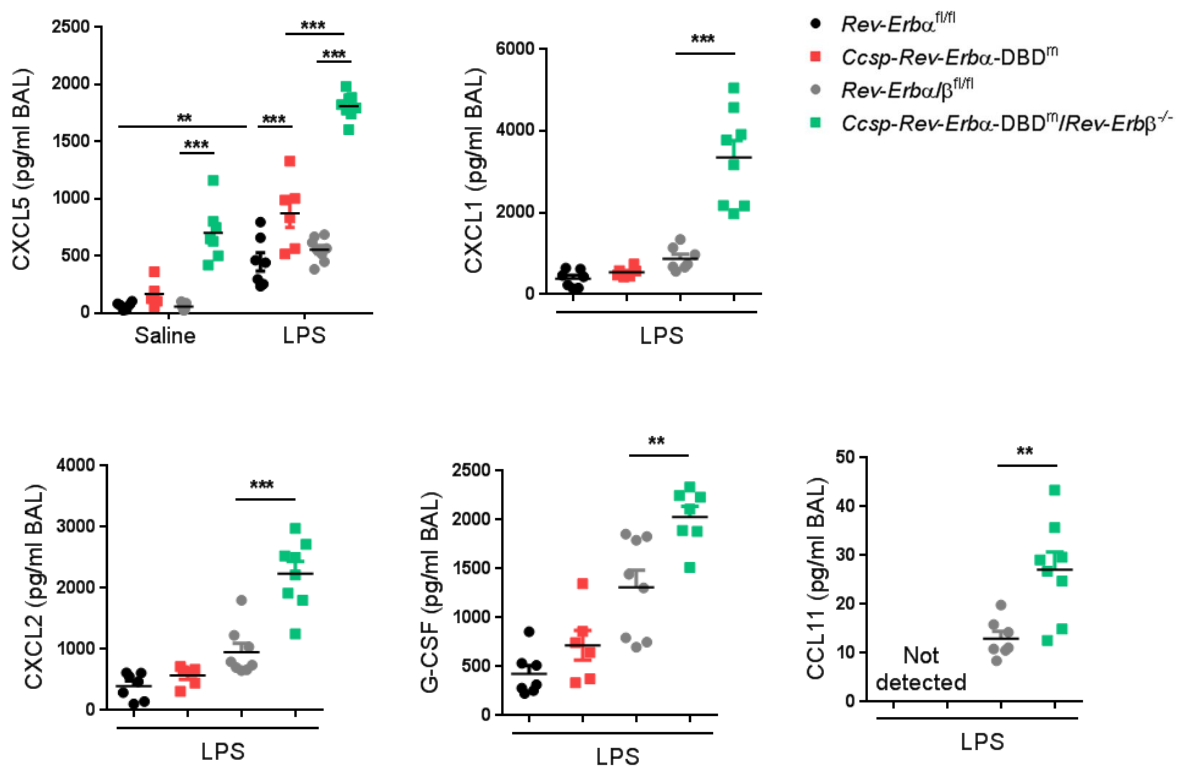
Figure 5.4: Cytokines and chemokines recovered by BAL after LPS challenge at ZT4 in *Ccsp-Rev-Erbα*-DBD^m, *Ccsp-Rev-erbα*-DBD^m/*Rev-Erbβ*^{-/-} mice and *Rev-Erbα*^{fl/fl}, *Rev-Erbα/β*^{fl/fl} littermate controls

Mice were exposed to aerosolised LPS at 2mg/ml or to saline for 20 minutes at ZT4 and culled 5 hours later. Cytokine and chemokine protein levels in BAL samples were assessed by luminex assay. Data are presented as mean $\pm$ SEM; $n = 5\text{-}8$, $**P <0.01$, $***P <0.001$ (Two-way ANOVA, post hoc Bonferroni).

Ccsp-Rev-Erbα-DBD^m/*Rev-Erbβ*^{-/-} mice upon LPS challenge compared to *Rev-Erbα/β*^{fl/fl} control mice (Figure 5.5C,D). Interestingly, LPS-induced *Ccl2* increase was repressed in the double mutated mice compared to *Rev-Erbα/β*^{fl/fl} animals (Figure 5.5E). Beside, *Bmal1* transcript levels in these double mutant mice were significantly augmented (Figure 5.5F) suggesting both impairment of the DNA binding function of REV-ERBα and the absence of REV-ERBβ in the CCSP-expressing cells leads to the absence of repression of *Bmal1*. However, no large difference was seen in *Bmal1* transcription between *Ccsp-Rev-Erbα*-DBD^m mice and

their littermate controls. This indicates that REV-ERBβ compensates the impairment of the DNA binding function of REV-ERBα to repress *Bmal1*.
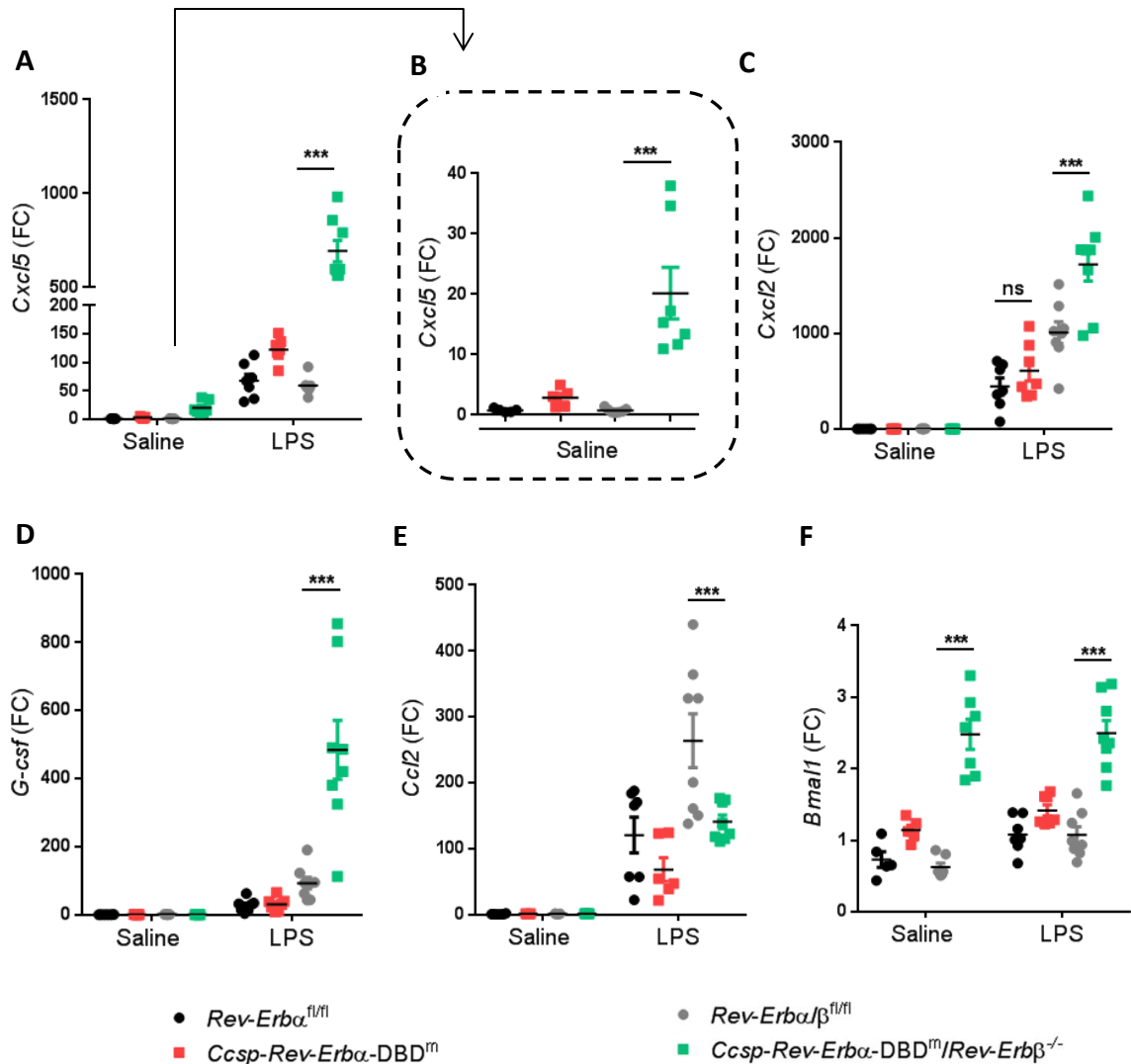
Figure 5.5: Transcript levels in whole lung from *Ccsp-Rev-Erbα*-DBD^m, *Ccsp-Rev-Erbα*-DBD^m/*Rev-Erbβ*^/- mice and *Rev-Erbα*^fl/fl, *Rev-Erbα/β*^fl/fl littermate controls exposed to LPS at ZT4

Mice were exposed to aerosolised LPS at 2mg/ml or to saline for 20 minutes at ZT4 and culled 5 hours later. mRNA levels in total lung tissues were determined by Real-Time qPCR and normalized to saline *Rev-Erbα*^fl/fl group. Data are presented as mean ± SEM; *n* = 5-8, ****P <0.001* (Two-way ANOVA, post hoc Bonferroni).

5.3.4 Gating of inflammatory responses is lost in mice with impairment of both REV-ERBα and β in bronchiolar epithelial cells

Next, I wanted to assess whether the gating in pulmonary inflammation (previously demonstrated by Gibbs et al, 2014) was abolished in mice lacking both REV-ERBα DBD and REV-ERBβ in CCSP-expressing cells. Male and female *Ccsp-Rev-Erbα-*DBD^m*/Rev-Erbβ^-/-* mice and *Rev-Erbα/β*^fl/fl littermate controls were challenged with aerosolised LPS at 2mg/ml or saline as control, for 20 minutes at ZT0 and ZT12. BAL sample analyses revealed a significant increase in infiltration of inflammatory cells, predominantly neutrophils for double mutated mice compared to the control group, at both time points (Figure 5.6A,B). Interestingly, *Ccsp-Rev-Erbα-*DBD^m*/Rev-Erbβ^-/-* mice exhibited exaggerated neutrophil numbers in basal condition at ZT0 compared to littermate control (Figure 5.6B). No difference in macrophage numbers was observed between genotyping and time points (Figure 5.6C).

Multiplex analyses of the same 23 cytokines and chemokines as above revealed that CXCL5 levels in BAL samples were up-regulated at both time points (Figure 5.6D, Appendix 15, Table A15). Other analytes such as CXCL1, CXCL2, G-CSF and CCL11 were significantly increased in the double mutant mice compared to the littermate controls only when challenged at ZT12 but their levels in BALs from *Ccsp-Rev-Erbα-*DBD^m*/Rev-Erbβ^-/-* mice were equivalent at both time points (Figure 5.6D, Appendix 15, Table A15). This indicates that the gating in pulmonary inflammation previously demonstrated (Gibbs et al., 2014) was lost in these animals. Interestingly, even in un-challenged conditions, CXCL5 levels were enhanced in *Ccsp-Rev-Erbα-*DBD^m*/Rev-Erbβ^-/-* mice compared to littermate controls, both at ZT0 and ZT12 (Figure 5.6D).

RNA analyses of inflammatory genes in whole lungs supported the results obtained by multiplex assay (Appendix 15, Figure A15). They also revealed an up-regulation of *Il-6* transcript in *Ccsp-Rev-Erbα-*DBD^m*/Rev-Erbβ^-/-* mice exposed to LPS at ZT12 compared to littermate controls. As seen in section 5.3.3, LPS-induced *Ccl2* increase was repressed in the double mutated mice compared to *Rev-Erbα/β*^fl/fl animals. Moreover, *Bmal1* increase observed previously at ZT4 in double mutated mice was also measured in un-challenged animals but only at ZT12.
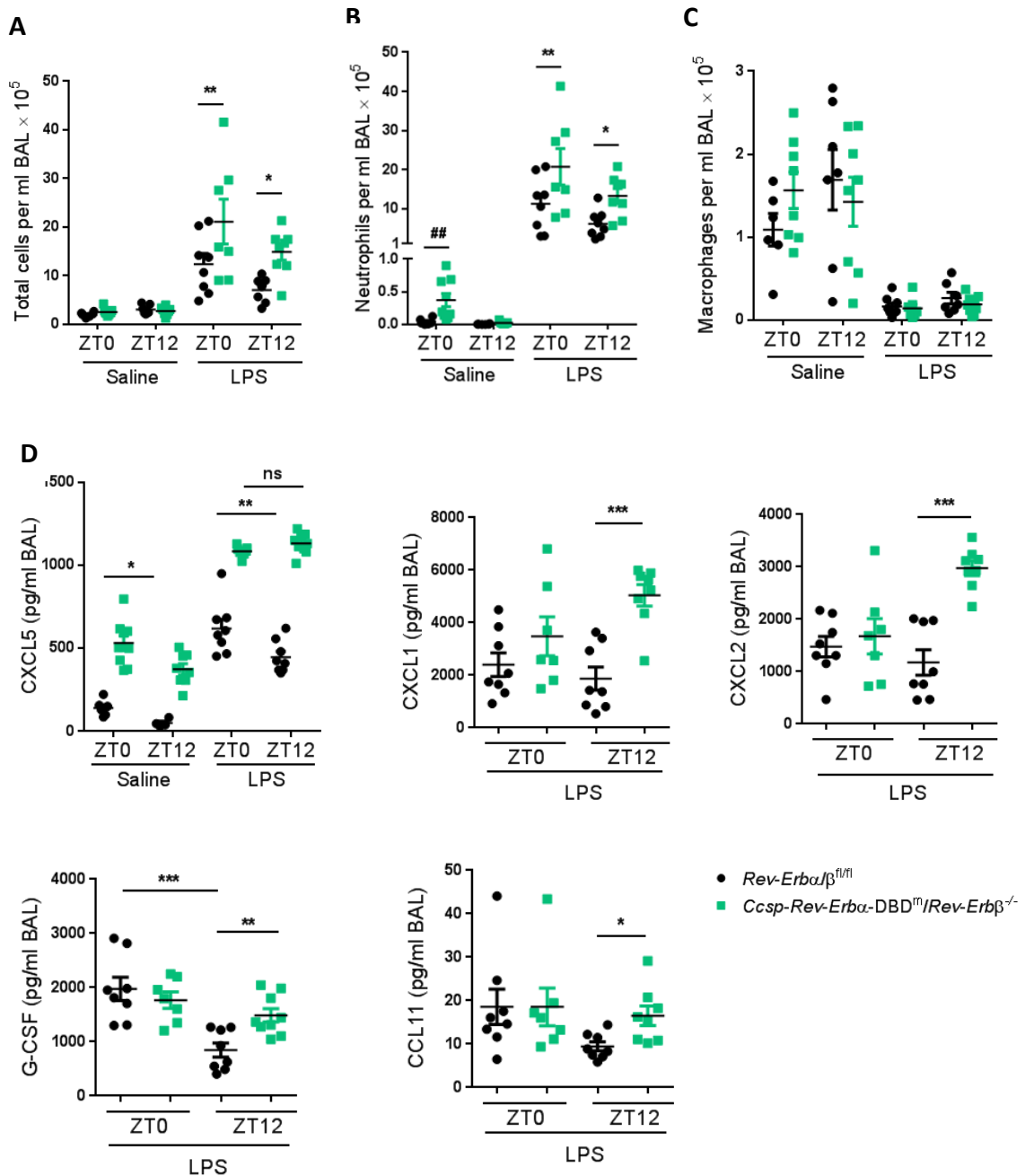
Figure 5.6: Effect of impaired REV-ERα DBD and loss of REV-ERBβ in CCSP-expressing cells on the pulmonary response to aerosolised LPS at different time points

Ccsp-Rev-Erbα-DBD[m]*/Rev-Erbβ^{-/-}* and littermate control mice were exposed to aerosolised LPS at 2 mg/ml or saline at ZT0 or ZT12 for 20 min. (A) Total cell counts in BAL samples collected at 5 hours after challenge. Neutrophil (B) and (C) macrophage numbers in the same sample were determined by flow cytometry analyses. (D) Cytokine and chemokine protein levels in BAL samples were assessed by luminex assay. Data are presented as mean ± SEM; n = 7-9, *P <0.05, **P <0.01, ***P <0.001 (Two-way ANOVA, post hoc Bonferroni), ##P<0.01 (Two-way ANOVA, post hoc Bonferroni, on saline samples only).

RNA analyses also confirmed a constant elevation of *Cxcl5* transcript levels in lung of *Ccsp-Rev-Erbα*-DBD[m]*/Rev-Erbβ*^{-/-} mice compared to littermate control animals even in un-challenged condition (Appendix 15, Figure A15). To determine the source of this enhanced *Cxcl5* expression, *in situ* hybridisation was performed on lung sections. It demonstrated that *Cxcl5* expression was confined to the bronchioles and was low in *Rev-Erbα/β*[fl/fl] control mice whereas in *Ccsp-Rev-Erbα*-DBD[m]*/Rev-Erbβ*^{-/-} mice, it was elevated at both time points (Figure 5.7).
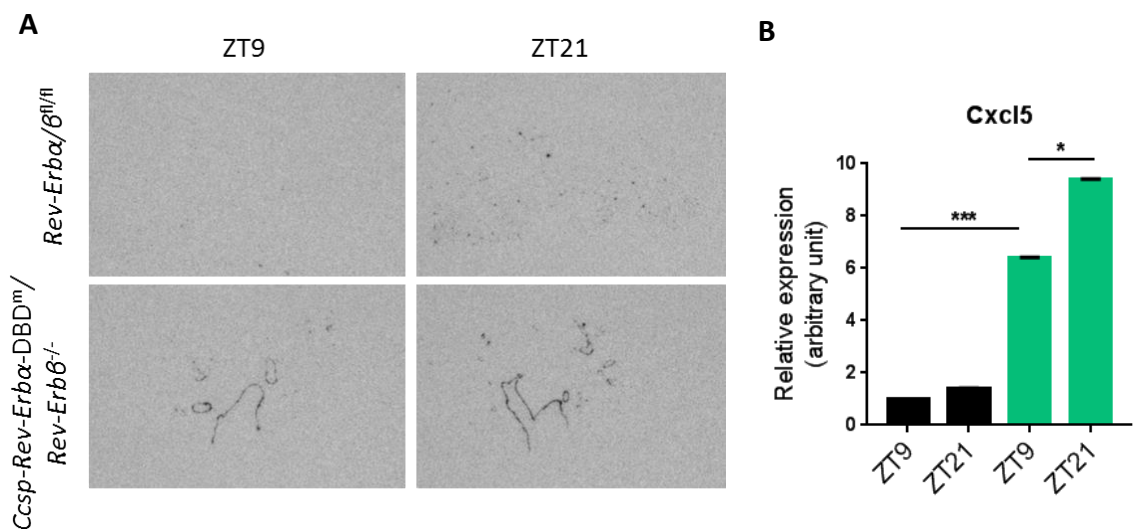
Figure 5.7: Localisation of Cxcl5 expression in lung of *Ccsp-Rev-Erbα*-DBD[m]/*Rev-Erbβ*^{-/-} mice and *Rev-Erbα/β*[fl/fl] littermate controls

(A) Example images of lung slices probed *Cxcl5* mRNA via *in situ* hybridisation. (B) Relative quantification of mRNA abundance from multiple lung slices measured via *in situ* hybridisation. Data are presented as mean ± SEM; *n* = 2/genotype/time point. *P <0.05, ***P <0.001 (One-way ANOVA, post hoc Bonferroni).

All together, these results indicate that the lack of REV-ERBα DBD and REV-ERBβ in the bronchiolar epithelial cells enhances pulmonary inflammation and affects its temporal gating.

5.3.5 Impairment of both REV-ERBα and β in bronchiolar epithelial cells does not induce changes in lung architecture or fibrosis

Because of the constant elevation of CXCL5 levels in the lung of *Ccsp-Rev-Erbα-*DBD^m/*Rev-Erbβ$^{-/-}$* mice under normal conditions and exaggerated neutrophil numbers at the onset of day (Figures 5.6, 5,7), I wanted to assess whether the lung architecture of these double mutant was altered in the long term and whether any fibrosis developed in older mice. To that end, lungs from 11-month old *Ccsp-Rev-Erbα-*DBD^m/*Rev-Erbβ$^{-/-}$* mice and *Rev-Erbα/β$^{fl/fl}$* littermate controls were collected at the beginning of the day for histology. Staining of paraffin-embedded lung sections with haematoxylin and eosin (H&E) revealed no major differences in lung architecture between the two genotypes (Figure 5.8A). Staining with Picro Sirius red did not show a difference in collagen deposition between the two genotypes when imaging the lung sections (Figure 5.8A), but quantification of the red staining and statistical analysis indicated a slight but significant increase of collagen fibres in *Ccsp-Rev-Erbα-*DBD^m/*Rev-Erbβ$^{-/-}$* mice compared to littermate controls (Figure 5.8B), suggesting potential development of fibrosis in the mutant mice.
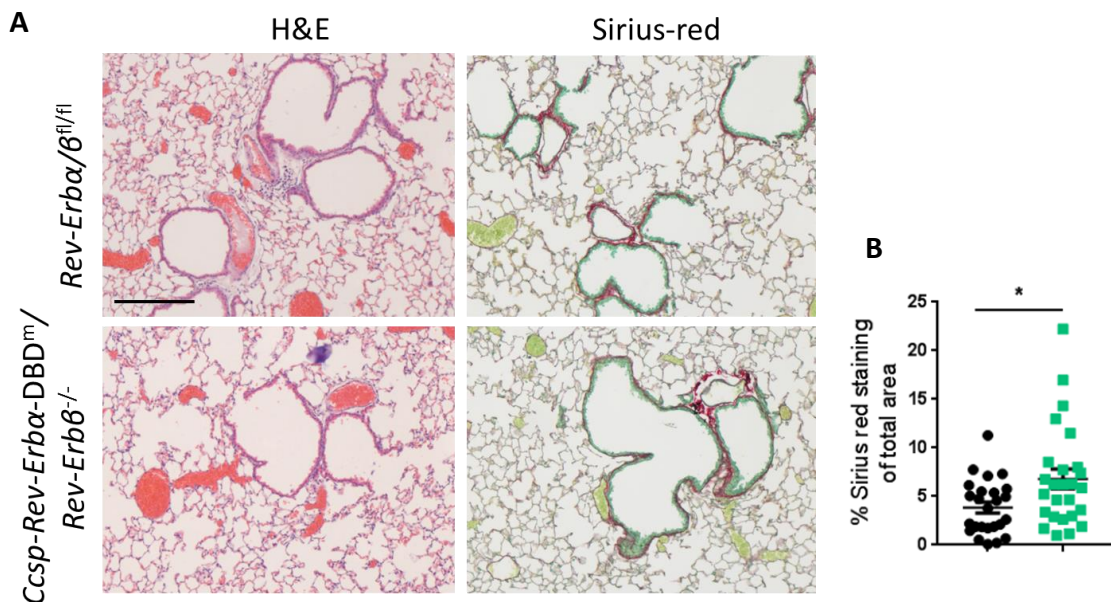
Figure 5.8: H&E and sirius-red staining of lung section from *Ccsp-Rev-Erbα-*DBD^m/*Rev-Erbβ$^{-/-}$* mice and *Rev-Erbα/β$^{fl/fl}$* littermate controls

11-month old mice were culled at ZT2, lungs were inflated with 4 % PFA and collected for histology. (A) Paraffin-embedded lung sections were stained with H&E and sirious-red. Scale bar = 200 μm. Images representative of *n* = 3 mice/genotype. (legend continued on next page)

(B) Quantification of Sirius red staining was calculated as described in chapter 2.3.4.3 using 9 images per animal. Black dots = *Rev-Erbα/β*$^{fl/fl}$ mice, green dots = *Ccsp-Rev-Erbα*-DBD^m*/Rev-Erbβ*$^{-/-}$ mice. Data are presented as mean ± SEM, unpaired *t*-test with Mann-Whitney test.

5.3.6 Alveolar macrophages from *Ccsp-Rev-Erbα*-DBD^m*/Rev-Erbβ*$^{-/-}$ mice displayed increased *Cxcl5* expression in response to LPS *ex vivo*

As in chapter 4, I wanted to assess whether dual mutation of REV-ERBα and β in bronchiolar epithelial cells affected isolated alveolar macrophage responses to inflammatory stimulus. Alveolar macrophages were collected by performing broncho-alveolar lavages from *Ccsp-Rev-Erbα*-DBD^m*/Rev-Erbβ*$^{-/-}$ mice and *Rev-Erbα/β*$^{fl/fl}$ littermate controls and the cells were subjected to LPS *ex vivo*. Unpaired *t*-test analysis revealed increased *Cxcl5* transcript levels in macrophages from double mutated mice compared to littermate controls (Figure 5.9). This result was surprising as published data demonstrated that alveolar macrophages do not secrete CXCL5 (Jeyaseelan et al., 2005) and my own data confirmed that CXCL5 could not be detected in the supernatants of cultured alveolar macrophages stimulated with LPS. No genotype difference in expression of other inflammatory genes was observed.
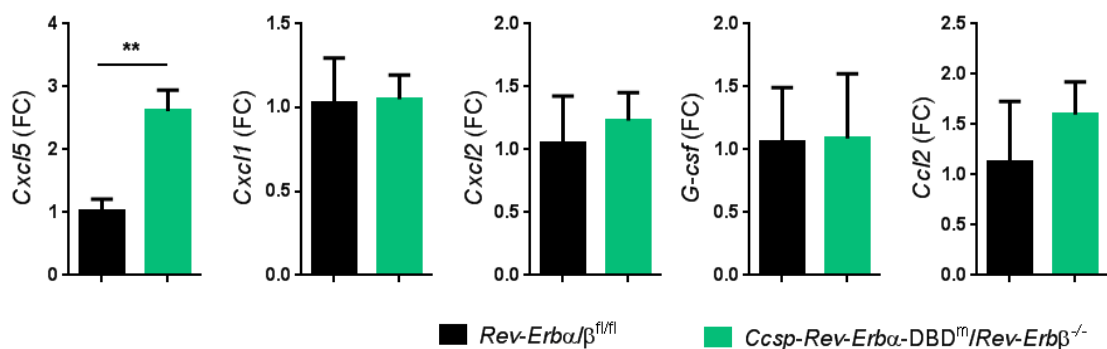
Figure 5.9: Effect of impaired REV-ERBα DBD and REV-ERBβ deletion in CCSP-expressing cells on alveolar macrophage responses to *ex vivo* LPS

Alveolar macrophages from *Ccsp-Rev-Erbα*-DBD^m*/Rev-Erbβ*$^{-/-}$ and *Rev-Erbα/β*$^{fl/fl}$ control mice were collected at ZT8, seeded into plates and directly treated with LPS at 100 ng/ml for 2 hours. Gene expression was determined by Real-Time qPCR and normalized to *Rev-Erbα/β*$^{fl/fl}$ control group. Data are presented as mean ± SD; $n = 3$. Student's *t*-test.

5.3.7   Impairment of both REV-ERBα and β in bronchiolar epithelial cells activate Nrf2-dependent antioxidant gene expression upon LPS exposure

In unchallenged conditions, mutation of both *Rev-Erb*s in CCSP-expressing cells had no impact on *Nrf2* and its target gene expression. However, upon an aerosolised LPS challenge, a significant up-regulation of NRF2 regulated gene expression was observed in *Ccsp-Rev-Erbα*-DBD^m*/Rev-Erbβ*^-/- mice compared to *Rev-Erbα/β*^fl/fl littermate controls (Figure 5.10A). At protein level, LPS exposure seemed to induce an increase in HO-1, especially in double mutant mice but a two-way ANOVA statistical analysis of relative intensity of HO-1 to β-ACTIN bands revealed no significant difference between genotypes and exposures (Figure 5.10B,C).
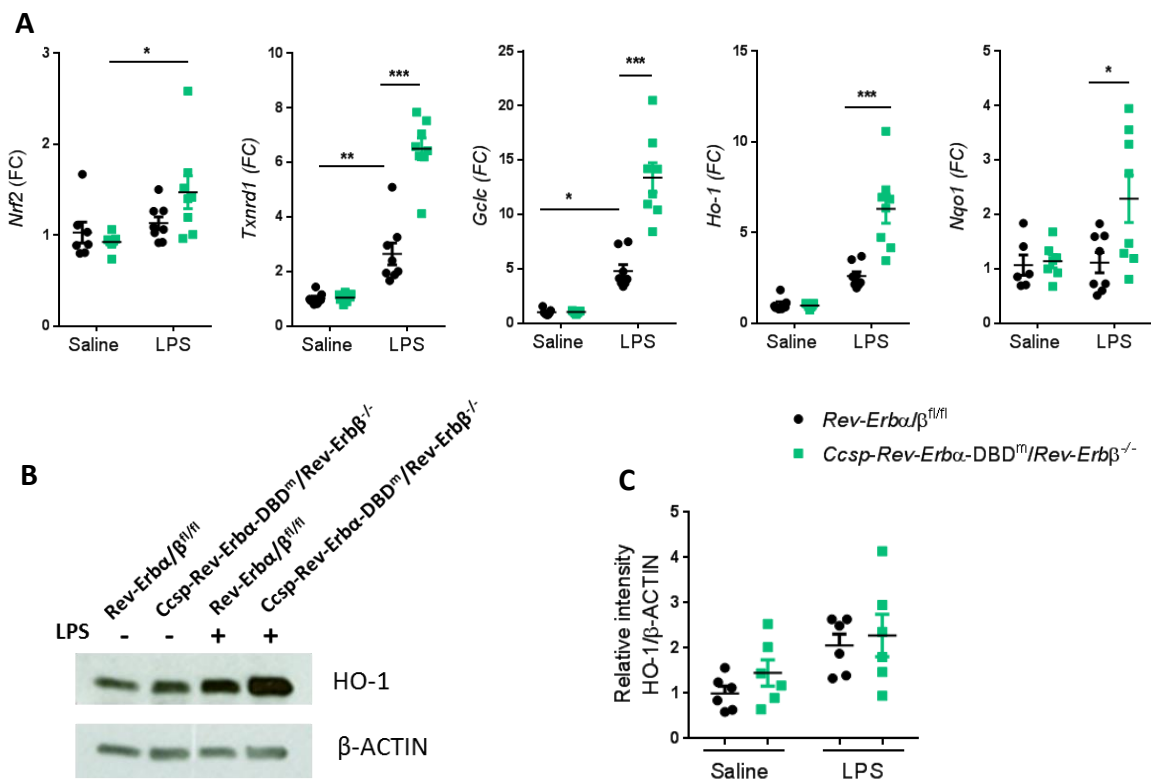
Figure 5.10: Antioxidant gene response in whole lung after aerosolised LPS exposures at ZT4 in *Ccsp-Rev-Erbα*-DBD^m*/Rev-Erbβ*^-/- mice and *Rev-Erbα/β*^fl/fl littermate controls
Mice were exposed to aerosolised LPS at 2mg/ml or saline for 20 minutes at ZT4 and culled 5 hours later. (A) Gene expression was determined by Real-Time qPCR and normalized to *Rev-Erbα/β*^fl/fl saline group. Data are presented as mean ± SEM; n = 7-8, *P <0.05, **P <0.01, ***P <0.001   (Two-way ANOVA, post hoc Bonferroni). (B) Levels of HO-1 protein were measured by Western blotting. (C) HO-1 densitometry (mean ± SEM) was normalised to β-ACTIN and to *Rev-Erbα*^fl/fl saline group; *n*=6.

5.4 Discussion

5.4.1 Generation of *Ccsp-Rev-Erbα*-DBD^m/*Rev-Erbβ*^{-/-} mouse line

Assessment of REV-ERBα DBD knockout was already discussed in chapter 4.4.1. Confirmation of loss of REV-ERBβ was attempted using the same techniques. Genotyping PCR from lung tissue clearly revealed the presence of a null (recombined) fragment in iCre^{+ve} animals (Figure 5.1A,B). *In situ* hybridisation data revealed the existence of a viable *Rev-Erbβ* transcript comprising exon8/3'UTR region in the bronchioles of the double mutant mice. However, the up-regulation of this transcript in the double mutant mice compared to littermate controls could be the consequence of the loss of REV-ERBβ at protein levels, consistently with the known function of REV-ERB protein to repress its own gene expression (Adelmant et al., 1996). Moreover, *in situ* data also revealed loss of the night nadir of *Rev-Erbα* and *β* transcript abundance in the bronchioles of the double mutant mice. This indicates a dysfunction of the molecular oscillator within the bronchioles of *Ccsp-Rev-Erbα*-DBD^m/*Rev-Erbβ*$^{-/-}$ mice, which was not observed in mice lacking the REV-ERBα DBD.

In order to confirm *Rev-Erbβ* deletion in bronchiolar epithelial cells, another probe, targeting specifically the loxP flanked exon, has to be designed for *in situ* hybridisation. Another alternative would be to perform laser capture to collect bronchiolar epithelial cells from lung slices and carry out qPCR using primers targeting exon 4. Finally, confirmation of REV-ERBβ deletion at protein levels is not possible at the moment, due to the lack of an antibody able to detect endogenous REV-ERBβ.

5.4.2 Rhythmic bioluminescence in the double mutated mouse model

Examination of the effects of dual depletion of REV-ERBα and REV-ERBβ on circadian rhythms has led to contradictory findings. Liu et al. (2008) have showed that cells deficient in both REV-ERBα and β function, or those expressing constitutive BMAL1, were still able to generate and maintain normal PER2 rhythmicity. In contrast, another group found that mouse embryonic fibroblasts were rendered arrhythmic by depletion of both REV-ERBs (Bugge et al., 2012). These

later findings were confirmed by Cho et al. (2012) who demonstrated a profound disruption of circadian expression of core clock genes in livers of mice with specific knockout of both REV-ERBs in liver. My data revealed that whole lung slices from *Ccsp-Rev-Erbα*-DBD^m*/Rev-Erbβ*^{-/-} mice exhibited circadian oscillations of PER2::Luc comparable to littermate controls (Figure 5.2A). The maintenance of these rhythms could be explained by the contribution of other cell types than the bronchiolar epithelial cells. Indeed, when focusing on the bronchioles which mainly contain CCSP expressing cells, PER2::Luc signal did not display strong rhythms as in the control mice (Figure 5.2B). Therefore, my findings confirmed that REV-ERBα and β function are necessary to maintain robust PER2 circadian oscillations. The faint rhythm of PER2::Luc signal in the bronchioles of the double mutant mice could be explained by a potential transmission of timing cues from surrounding, non-targeted cells. The knowledge about how lung cells interact and communicate timing signals remains poor and would certainly be an interesting area of research for the chronobiology field.

5.4.3 Pulmonary inflammatory phenotype in *Ccsp-Rev-Erbα*-DBD^m*/Rev-Erbβ*^{-/-} mice

As both REV-ERBα and REV-ERBβ show major physiological redundancy, the question of REV-ERBβ compensation on regulating pulmonary required analysis. In a comparative study, the double mutated mice had an exaggerated inflammatory reaction to LPS compared to *Ccsp-Rev-Erbα*-DBD^m mice. Indeed, only CXCL5 concentration differed between *Ccsp-Rev-Erbα*-DBD^m and littermate control mice (Figure 5.4), consistently with previous experiment described in chapter 4.3.4. In contrast, *Ccsp-Rev-erbα*-DBD^m*/Rev-Erbβ*^{-/-} mice also exhibited elevated CXCL1, CXCL2, G-CSF and even higher concentrations of CXCL5 upon LPS challenge. Interestingly, even in the absence of inflammatory challenge, CXCL5 in the double mutant mice was up-regulated to the same level achieved post LPS in intact mice.

Further analysis of responses to LPS by time of day in the double knockout mice revealed exaggerated neutrophilic inflammation at both ZT0 and ZT12 (Figure 5.6). Moreover, CXCL1, CXCL2, G-CSF and CXCL5 reached similar levels upon LPS challenge at either ZT0 and ZT12, respectively peak and nadir for inflammatory

reaction in intact mice. Therefore, loss of REV-ERBα DBD and REV-ERBβ in bronchiolar epithelial cells resulted in both a loss of the normal evening nadir in inflammatory response, and an overall increase in neutrophilic inflammation in response to LPS.

Under un-challenged conditions, CXCL5 was elevated at transcript and protein levels at different time points in *Ccsp-Rev-erbα*-DBD^m/*Rev-Erbβ*^-/- mice compared to littermate controls (Figures 5.6D, 5.7, A15). However, neutrophil numbers were increased in the double mutant mice compared to controls only at the onset of the day (Figure 5.6B). Although CXCL5 is a critical chemokine for recruitment of neutrophils to the lung, this suggests that another parameter is required at basal level for neutrophil invasion. Identification of such parameter would warrant further investigation but it could be correlated to permeability of the endothelial barrier.

The constant elevation of CXCL5 at protein and transcript levels in both basal and challenged conditions reproduced exactly the phenotype observed in *Ccsp-Bmal*^-/- mice (Gibbs et al., 2014). In that model, *Bmal1* was knocked out in the bronchiolar epithelial cells whereas in *Ccsp-Rev-erbα*-DBD^m/*Rev-Erbβ*^-/- mice, *Bmal1* transcript levels in lung were up-regulated due to the absence of the functional repressors (Figure 5.5). Thus, this suggests that the pro-inflammatory phenotype seen in *Ccsp-Bmal*^-/- mice was actually the result of the indirect deletion of both REV-ERBs.

It has been demonstrated that two REV-ERBα molecules are required for interaction with the co-repressor NCoR (Zamir et al., 1997). This can occur as two REV-ERBα monomers bound independently to two separate ROREs or, more strongly, as a dimer bound to a repeat of ROREs separated by 2 base pairs, referred to as RevDR2 (Harding and Lazar, 1995; Hu and Lazar, 1999). Because of the redundancy of REV-ERBα and REV-ERBβ, we could hypothesize that formation of a heterodimer could occur between a molecule of REV-ERBα and a molecule of REV-ERBβ. Therefore, in absence of REV-ERBβ and REV-ERBα DBD, formation of a dimer able to bind DNA on RORE or RevDR2 elements is impossible and NCoR cannot be recruited. This could thus explain the more dramatic pro-inflammatory phenotype observed in *Ccsp-Rev-erbα*-DBD^m/*Rev-Erbβ*^-/- mice compared to mice lacking only REV-ERBα DBD in bronchiolar epithelial cells. Indeed, in *Ccsp-Rev-erbα*-DBD^m mice, REV-

ERBβ is still expressed and may form a dimer capable of recruiting NCoR to repress inflammation. The fact that CXCL5 is still up-regulated in *Ccsp-Rev-erbα*-DBD^m mice upon endotoxin challenge may be explained by a predominant role of REV-ERBα compared to its paralog. If this hypothesis is correct, we could predict that deletion of REV-ERBβ in bronchiolar epithelial cells would not result in a pro-inflammatory phenotype (or a very mild one) in response to aerosolised LPS as it would be compensated by REV-ERBα which could form dimers, recruit NCoR and repress pulmonary inflammation.

Finally, alveolar macrophages from *Ccsp-Rev-erbα*-DBD^m/*Rev-Erbβ*$^{-/-}$ mice exhibited an increase in *Cxcl5* transcript levels upon *ex vivo* endotoxin challenge compared to macrophages from the littermate controls (Figure 5.9). As communication between macrophages and epithelium in the lung has been reported (Westphalen et al., 2014), the constant CXCL5 elevation in the bronchiolar epithelium of the double mutant mice in basal condition might alter the intrinsic immune properties of the alveolar macrophages. However, it was surprising to detect a change in *Cxcl5* transcripts as my own and other published data demonstrated that alveolar macrophages do not secrete CXCL5 (Jeyaseelan et al., 2005).

5.4.4 NRF2-regulated pathway activation in *Ccsp-Rev-Erbα*-DBD^m/*Rev-Erbβ*$^{-/-}$ mice

In chapter 4, I showed that deletion of REV-ERBα DBD in bronchiolar epithelial cells did not result in any increased antioxidant gene expression even in challenged conditions. In contrast, dual impairment of REV-ERBα and β function in bronchiolar epithelial cells leaded to exaggerated expression of NRF2 regulated antioxidant gene expression but only upon endotoxin challenge (Figure 5.10). As described in chapter 4, this could be a consequence of the significant increase in inflammatory responses and cytokine recruitment to the lung in the double mutant mice compared to the littermate controls. Increase in pro-inflammatory cytokines and chemokines within the lung probably triggers greater production of ROS and thus greater levels of antioxidants to cope with it. Although the expression of NRF2 regulated antioxidant genes was significant up-regulated upon LPS exposure, *Nrf2* transcript levels

remained nearly unaffected. This is consistent with previous studies showing that the oxidative stress does not induce expression of *Nrf2* but rather elicits the translocation of NRF2 protein from the cytoplasm into the nucleus in order to activate the transcription of its antioxidant target genes (Nguyen et al., 2009).

5.5 Conclusions

This chapter reveals a significant compensatory role for REV-ERBβ, in that impairment of both REV-ERBα and β in the bronchiolar epithelium resulted in greatly exaggerated inflammatory responses to LPS, involving more chemokines, and also, intriguingly, led to augmented chemokine CXCL5 production under basal conditions. Moreover, time-of-day gating of inflammation was lost in this cell specific double knockout model, which was consistent with disruption of circadian expression of core clock components in the bronchioles. Generating a new mouse model lacking only REV-ERBβ in bronchiolar cells would allow to fully understand its contribution in regulating lung inflammation.

Chapter 6:   Effects of REV-ERBα ligands in different cell types

6.1 Introduction

Nuclear receptors are generally classified as ligand-regulated transcription factors, as the activities of many of them are regulated by direct binding of specific lipophilic molecules, including both endogenous compounds and drugs. These small molecules target the ligand-binding pocket of the nuclear receptor which causes a conformational change of the protein resulting in a cascade of downstream events (Moore et al., 2006). The porphyrin heme was identified as endogenous ligand of both REV-ERBα and REV-ERBβ. It enhances the thermal stability of the proteins and the recruitment of the co-repressor NCoR, leading to repression of target genes including *BMAL1* (Raghuram, 2007). The crystal structure of heme-bound REV-ERBβ identified the ligand-binding pocket (Pardee et al., 2009) and this consequently has stimulated the development of synthetic ligands. Indeed, over the past few years, several synthetic ligands for REV-ERBα/β, both agonists and antagonists, have been synthesized (Grant et al., 2010; Kojetin et al., 2011; Shin et al., 2012; Trump et al., 2013) and have been shown to modulate REV-ERBs repressive functions. The first non-porphyrin synthetic ligand synthesised was GSK4112. This small tool agonist molecule has been shown to mimick the action of heme, in cell-based assays and it was able to reset the circadian rhythm in a phasic manner (Meng et al., 2008). Moreover, GSK4112 appeared to be a potent repressor of many cytokines upon LPS challenge in macrophages (Gibbs et al., 2012). However, it appeared that GSK4112 was not specific to the REV-ERBs and exhibited LXRα activities (Trump et al., 2013). As activation of LXRα has been reported to have diverse effects on inflammation, GSK4112 anti-inflammatory effect could not be entirely attributed to REV-ERB activation. Therefore, a key goal was to improve the selectivity over LXRα to allow clear and precise interpretations of subsequent data. In collaboration with GlaxoSmithKline, novel REV-ERBα ligands lacking LXRα activity have been generated. In this chapter, novel ligand GSK3201362A (hereafter called GSK1362) was used along with GSK4112 and natural ligand hemin. These ligands were tested in different types of macrophages as well as in both murine and human epithelial cells.

6.2 Hypothesis tested and experimental approaches

Hypothesis: REV-ERBα repressive activity can be modulated pharmacologically with small molecules ligands.

Objectives:

- Evaluate the characteristics of new REV-ERBα ligand GSK1362 (peptide profile, toxicity)

- Assess the effects of GSK1362 on REV-ERBα protein and PER2 rhythms

- Treat different types of macrophages and epithelial cells with GSK1362 and other small molecule tool ligands and assess their effects upon inflammatory stimuli.

6.3 Results

6.3.1 Initial assays suggest GSK1362 to be an antagonist ligand

In an effort to identify small molecule nonporphyrin ligands of REV-ERBα, GSK1362 was synthesized among other molecules as part of an oxazole series. As this compound has not been yet published GSK1362, GlaxoSmithKline is not ready to disclose the structure beforehand. However, they have agreed to allow the disclosure of the core scaffold (Figure 6.1A). In collaboration with Nicholas Tomkinson at University of Strathclyde, a model for GSK1362 docked in the ligand binding domain (LBD) of REV-ERBα was also developed (Figure 6.1B).

The recruitment of different peptides to REV-ERBα protein in presence of GSK1362 was determined by GlaxoSmithKline using an already characterised FRET assay (Trump et al., 2013) (Figure 6.1C). This peptide recruitment profile was compared to the one using GSK4112. Full curve analysis of compound GSK1362 demonstrated a dose-dependent increased distance of NCOR1 and SMRT2, two repressive coregulatory factors, with REV-ERBα. The interaction of RIP140 with REV-ERBα was also repressed in a dose-dependent manner in presence of GSK1362. RIP140 is a nuclear protein which interacts with most, if not all, nuclear receptors and it is also capable of binding several other transcription factors and histone modifying enzymes, such as HDAC3. In addition, RIP140 acts as a coactivator for NF-κB/RelA
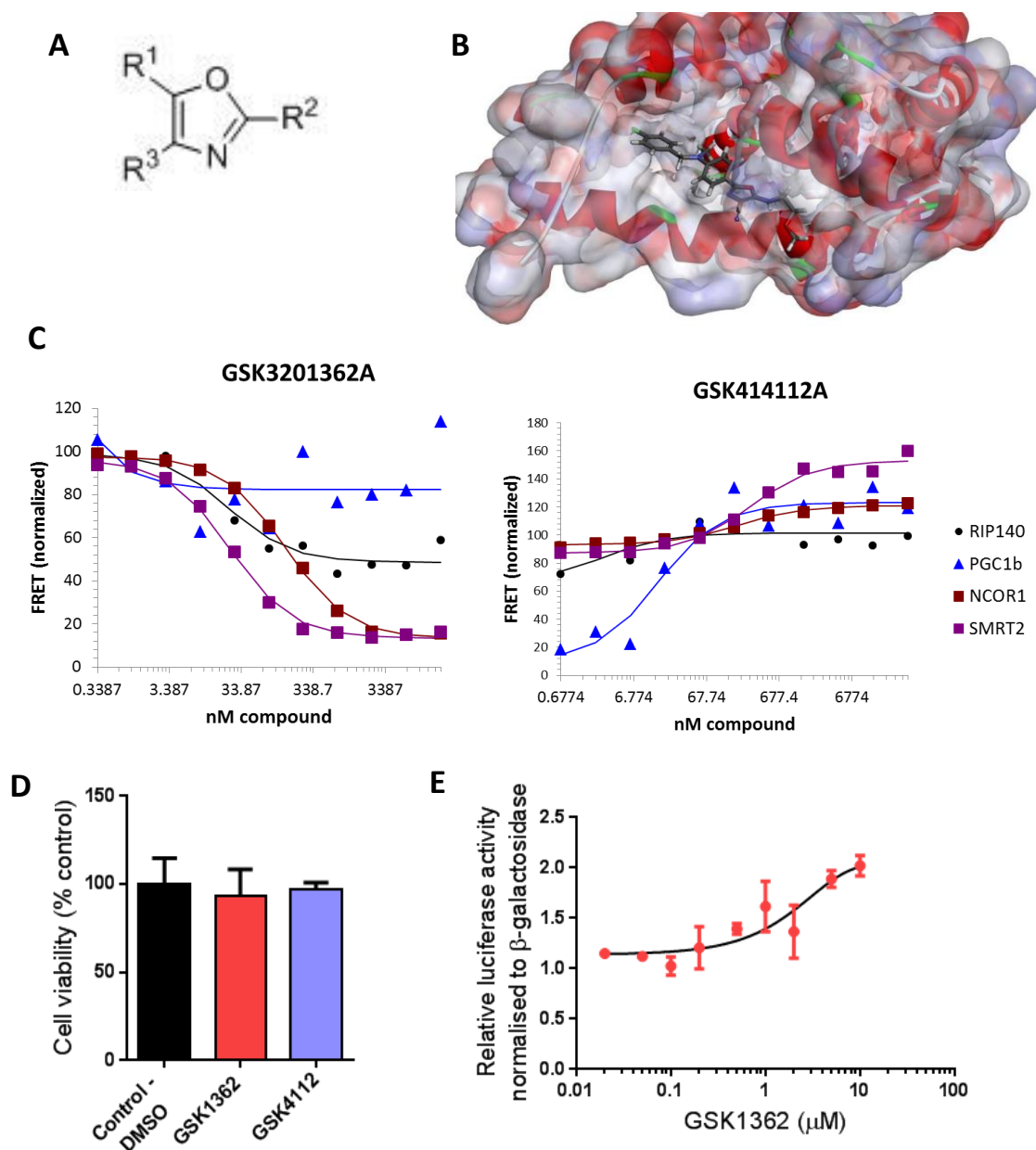
Figure 6.1: Characterisation of GSK1362

(A) Core scaffold of GSK1362. (B) Model representing GSK1362 docked in REV-ERBα LBD. (C) Effect of GSK1362 and GSK4112 compounds on peptide fragment recruitment to REV-ERBα. (D) HEK cells were treated with GSK1362 or GSK4112 at 10 μM or with 0.1% DMSO as control for 24 hours. Cell viability was determined using MTT protocol and data were normalized to control – 0.1% DMSO. Data are presented as mean ± SD; $n = 4$. (E) HEK cells were transfected with HA-REV-ERBα, a luciferase reporter driven by the *Bmal1* promoter and β-galactosidase as control of transfection efficiency. Cells were treated with GSK1362 at different concentrations or with 0.1% DMSO as control for 24 hours followed by the luciferase and β-galactosidase luminosity readings. Luciferase activity was normalised to β-galactosidase reading for each sample and values were plotted relatively to 0.1% DMSO. Errors bars indicate mean ± SD. Data are representative of $n = 3$.

dependent cytokine gene expression. It has been shown that lack of RIP140 leads to an inhibition of proinflammatory pathways in macrophages (Zschiedrich et al., 2008). However, the interaction of PGC-1b, a transcriptional coactivators involved in the control of cellular energy metabolic pathways and a potent inducer of heme synthesis, with REV-ERBα was not significantly affected by the addition of GSK1362. In contrast, compound GSK4112 allowed the recruitment of NCOR1, SMRT2 and PGC-1b consistently with its definition of REV-ERBα agonist. However, no difference in RIP140 recruitment was observed in presence of GSK4112.

Cytotoxicity of compound GSK1362 was tested in Human Embryonic Kidney (HEK) 293 cells along with compound GSK4112. Cells were treated with compounds at 10 µM or with 0.1% DMSO as control for 24 hours and cell viability was measured using MTT protocol. This assay showed that neither compound had cytotoxic effects in HEK 293 cells after a 24-hour treatment (Figure 6.1D).

Activity of GSK1362 was also examined using *Bmal1* reporter assay. HEK 293 cells were transfected with full-length REV-ERBα along with a luciferase reporter driven by the *Bmal1* promoter and β-galactosidase plasmid as transfection efficiency control. GSK1362 dose-dependently increased transcription driven by the *Bmal1* promoter ($EC_{50} = 2.5$ µM) (Figure 6.1E).

6.3.2 *Ex vivo* studies in murine macrophages

Macrophages are key immune surveillance cells. As this thesis is focused on lung inflammation, alveolar macrophages are the most suitable types of macrophages to test the ligands. However, getting enough alveolar macrophages to perform *ex vivo* studies requires a large number of mice whereas peritoneal macrophages can be extracted in greater amounts. Therefore, bearing in mind the 3Rs (replacement, reduction and refinement), experiments to assess the specificity of GSK1362 and its effect on PER2 rhythms were carried out in peritoneal macrophages.

6.3.2.1 GSK1362 increases amplitude of PER2 rhythms in peritoneal macrophages

The effect of GSK1362 on molecular clock responses was tested by measuring PER2::Luc bioluminescence signal from peritoneal exudate cells (PECs) treated *ex vivo* with GSK1362. The recording of bioluminescence, measured on photomultiplier tube (PMT), was started in absence of the ligand and then PECs were treated with GSK1362 at 10μM, or with DMSO as control, at different phase of phases of the circadian oscillation of PER2::Luc rhythms (indicated by black arrows on Figure 6.2). Cosinor analysis of the 48 hours post ligand addition revealed that at both treatment times, GSK1362 did not alter the period of PER2::Luc rhythm but increased its amplitude, in particular when ligand was applied on the descending phase of PER2::Luc rhythm.
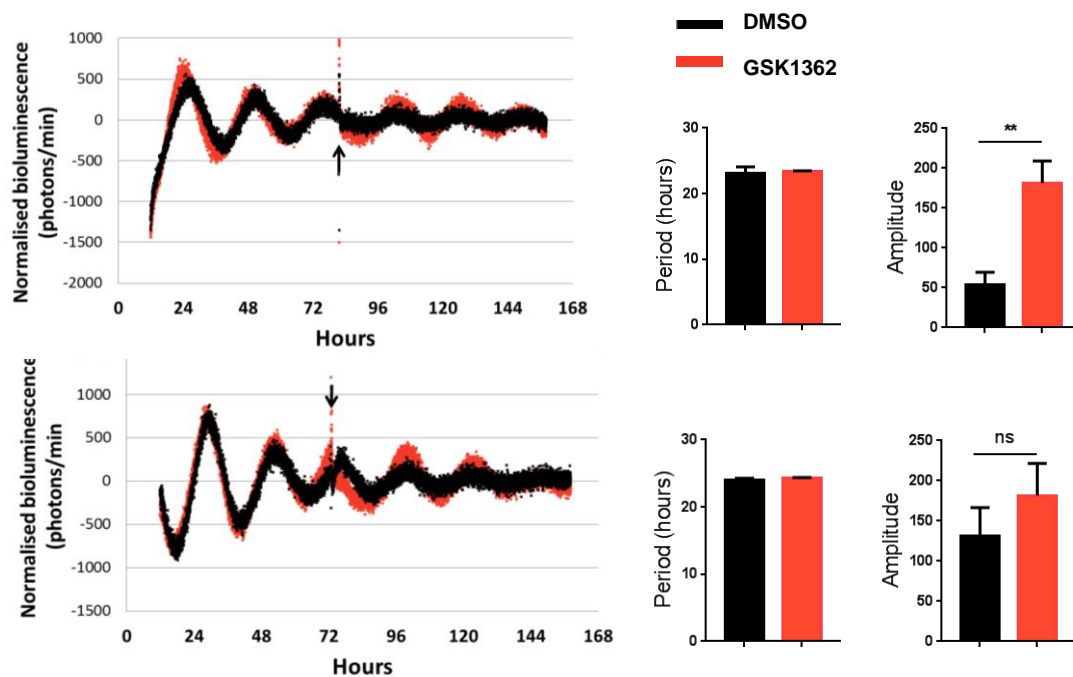
Figure 6.2: Effects of GSK1362 treatment on PER2::Luc rhythms in PECs

PECs from wild-type mice were synchronised by serum shock and PER2::Luc bioluminescence signal was recorded in PMTs. At different phases of PER2::Luc oscillations indicated by black arrows, GSK1362 (10 μM) was added. Photon counts per minutes were normalised to a 24 hour moving average and traces are representative of 3 biological replicates. Periods and amplitudes were determined by cosinor analyses of the 48 hours post ligand addition.

6.3.2.2 GSK1362 does not possess LXR activity but do not seem to be REV-ERBα specific in peritoneal macrophages

To verify the absence of LXR activity for GSK1362, PECs from wild-type mice were treated with GSK1362 at 10μM or with a commercial LXR agonist GW3965 at 2 μM as control for 4 hours. Levels of *Abca1* and *Abcg1*, two LXR targets, were indeed enhanced in presence of GW3965 but unchanged in presence of GSK1362 (Figure 6.3).
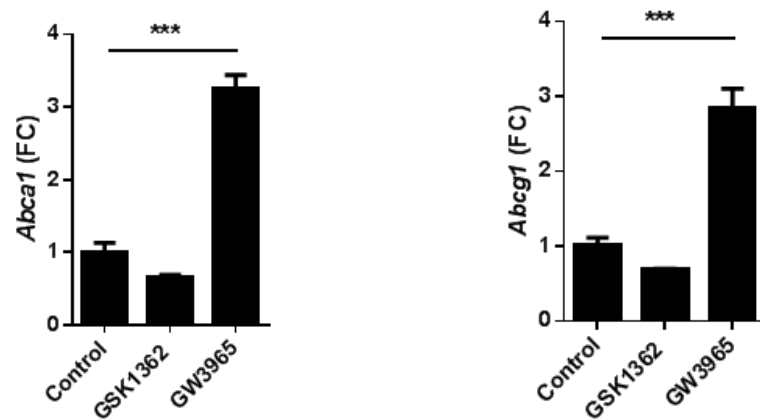
Figure 6.3: REV-ERBα ligand GSK1362 does not present LXR activity

PECs from wild type mice were treated with GSK1362 at 10 μM or with GW3965 at 2 μM for 4 hours. Gene expression was determined by Real-Time qPCR and normalized to DMSO-treated control cells. Data are presented as mean ± SD; n = 3. ***P <0.001 (One-way ANOVA, post hoc Bonferroni).

Then, to assess the specificity of GSK1362 to REV-ERBα, PECs from wild-type or *Rev-Erbα*$^{-/-}$ mice were treated with GSK1362 at 10 μM in presence of LPS at 100 ng/ml for 4 hours. Results from transcript level measurement were complex to interpret and the effects of GSK1362 were different depending on the cytokine or chemokine analysed (Figure 6.4).

In PECs from wild-type mice, no difference in *Il-6* mRNA levels was observed in presence of the ligand upon LPS challenge, whereas a significant decrease was seen in PECs from *Rev-Erbα*$^{-/-}$ mice. GSK1362 caused a significant decrease in *G-csf* transcript levels upon LPS challenge in PECs from both wild-type and *Rev-Erbα*$^{-/-}$
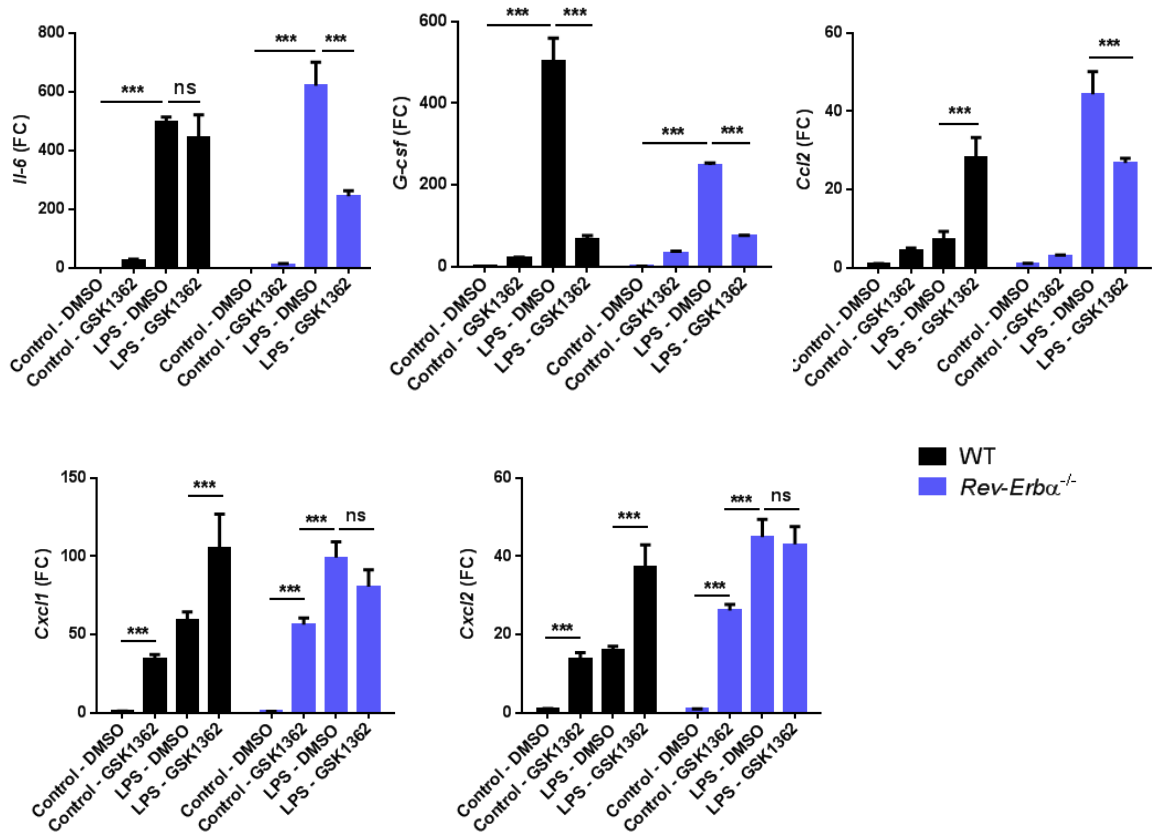
Figure 6.4: REV-ERBα ligand GSK1362 has divergent effects on different inflammatory genes in response to LPS in murine PECs

PECs from wild type or *Rev-Erbα*^{-/-} mice were treated with GSK1362 at 10 μM in presence or absence of LPS at 100 ng/ml for 4 hours. Gene expression was determined by Real-Time qPCR and normalized to un-treated control cells for both WT and *Rev-Erbα*^{-/-} groups. Data are presented as mean ± SD; *n* = 3. ***P <0.001 (One-way ANOVA, post hoc Bonferroni).

mice. *Ccl2* transcript levels were significantly elevated in presence of the ligand upon LPS challenge in PECs from wild-type mice, whereas they were significantly down-regulated in PECs from *Rev-Erbα*^{-/-} mice. Moreover, *Ccl2* response to LPS challenge was greater in PECs from *Rev-Erbα*^{-/-} mice than in PECs from wild-type mice, consistently with published findings showing a negative regulation of *Ccl2* expression by REV-ERBα in murine macrophage (Sato et al., 2014). Ligand GSK1362 also triggered a significant increase in *Cxcl1* and *Cxcl2* in un-stimulated PECs. However, upon LPS challenge, *Cxcl1* and *Cxcl2* were upregulated in presence of the ligand only in PECs from wild-type mice.

As GSK1362 elicited effects on inflammatory responses in PECs from *Rev-Erbα*^{-/-} mice, this compound could not be REV-ERBα specific. Moreover, the divergent effects of GSK1362 on the different cytokines or chemokines suggest that several and distinct pathways are involved in PECs.

6.3.2.3 GSK1362 displays anti-inflammatory properties in alveolar macrophages

Alveolar macrophages from control *Rev-Erbα*^{fl/fl} mice were collected around ZT8, seeding into plates and treated directly with GSK1362 at 10μM in presence of LPS at 100 ng/ml for 4 hours. A significant decrease of several cytokines was observed in presence of the ligand suggesting that GSK1362 has an anti-inflammatory action in alveolar macrophages (Figure 6.5). However, no significant effect was measured for the chemokines *Cxcl1* and *Cxcl2*.
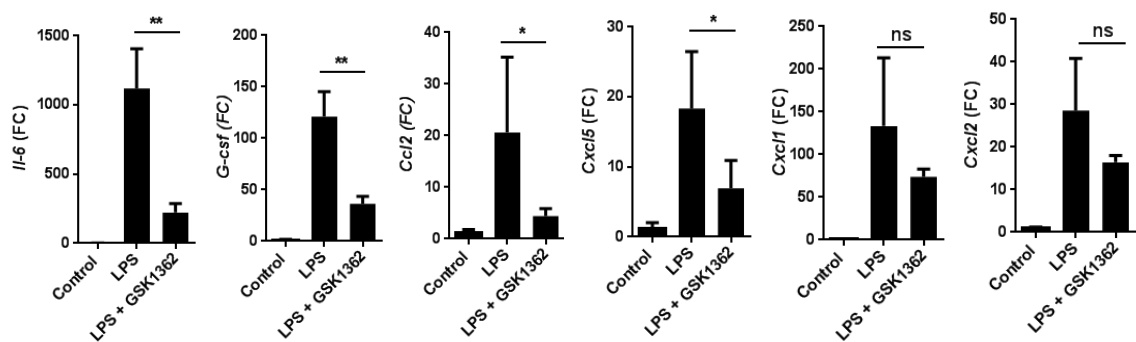
Figure 6.5: REV-ERBα ligand GSK1362 represses a selection of inflammatory genes in response to LPS in murine alveolar macrophages

Alveolar macrophages were collected at ZT8, seeded into plates and directly treated with GSK1362 at 10 μM in presence or absence of LPS at 100 ng/ml for 4 hours. Gene expression was determined by Real-Time qPCR and normalized to un-treated control cells. Data are presented as mean ± SD; n = 3. *$P<0.05$, **$P <0.01$, ***$P <0.001$ (One-way ANOVA, post hoc Bonferroni).

Based on evidence from the previous chapters showing the importance of the epithelium in regulating lung inflammation, effects of REV-ERBα ligands in bronchial epithelial cells upon inflammatory stimuli was also investigated.

6.3.3 *In vitro* studies in bronchial epithelial cells

Previous work has demonstrated that bronchiolar epithelial cells are a key cell type to sustain circadian rhythms in mice (Gibbs et al., 2009) and to regulate pulmonary inflammation via NF-κB pathway (Cheng et al., 2007). Primary human bronchial epithelial (NHBE) cells and murine LA-4 cell line were chosen as *in vitro* models.

6.3.3.1 Normal Human Bronchial Epithelial (NHBE) cells

NHBE cells are commonly used as a model to study pulmonary inflammation. However, no information about potential circadian rhythms in NHBE cells has been published so far. Therefore, the first objective was to determine whether these cells exhibited rhythmic variations in clock gene expression and then challenge them with inflammatory stimulus in presence of REV-ERBα ligands.

6.3.3.1.1 NHBE cells display circadian rhythms and respond to different stimuli

Different methods can be applied to synchronised cells *in vitro*. Serum shock, chemicals such as dexamethasone and forskolin, or temperature cycles have been shown to reset the phase of mammalian circadian oscillators by activating various signaling pathways triggering to circadian gene expression (Nagoshi et al., 2005). For this project, synchronisation was carried out by serum shock, the most common method used to assess molecular clock function in cultured cells. Any measurement was performed at least 16 hours after serum shock in order to let the cell clock system to be reset and potentially to oscillate in a daily fashion. Indeed, serum shock triggers induction of immediate-early genes such as *rper1* and *rper2* which results in the degradation of immediate-early repressors (*rev-erbα*, *dbp* and *tef*). This process which allows to restart circadian cycles in a synchronous fashion in all cells takes about 8 hours according to previous studies (Balsalobre et al., 1998).

NHBE cells, synchronised by serum shock, exhibited strong rhythms in clock gene transcript levels and in REV-ERBα protein levels (Figure 6.6). As in murine lung, rhythms at transcript and protein levels for REV-ERBα were in phase suggesting a rapid translation process and a quick turnover of the protein. NHBE cell synchronization using 100 nM dexamethasone was also performed and similar phase patterns of clock gene mRNA levels were revealed (Appendix 16, Figure A16). However, to prevent any anti-inflammatory effect due to residual dexamethasone, serum shock was chosen for cell synchronization in all the following experiments.
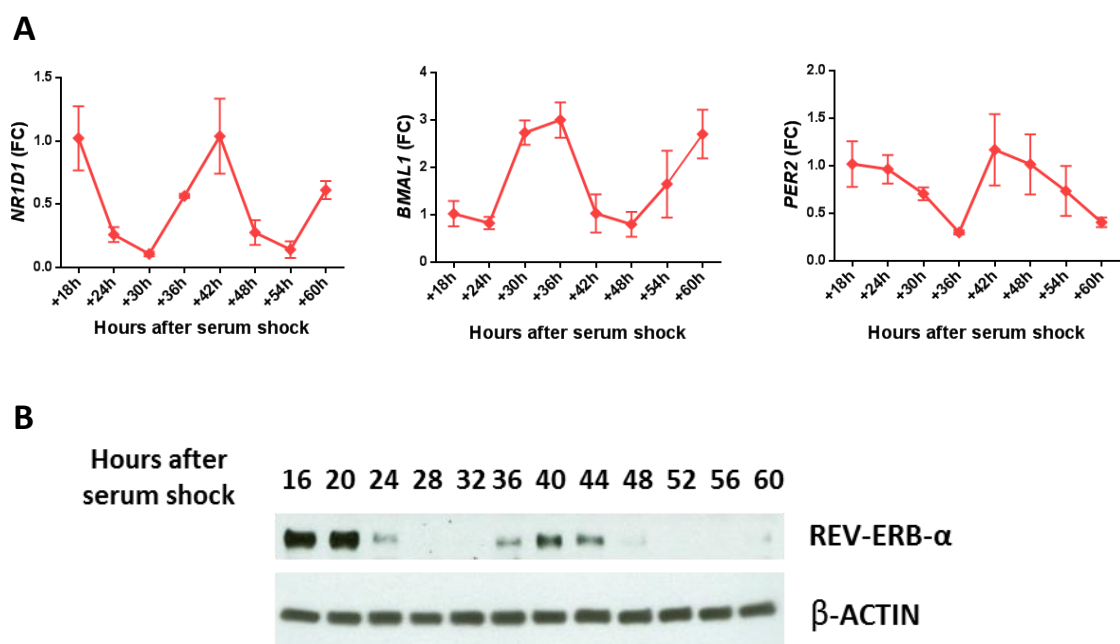
Figure 6.6: Rhythmic variations of clock genes and REV-ERBα protein in NHBE cells synchronised by serum shock

(A) mRNA levels of the clock genes were measured using Taqman Real-Time qPCR and normalized to the first time point. Data are presented as mean ± SD; n = 3. (B) Total cell lysates were analysed by Western blotting for REV-ERBα protein levels (15 µg total protein loaded per lane). Data representative of n = 3.

Previous studies have shown NHBE cells responded to different pro-inflammatory agents such as LPS (Helzer et al., 2015), IL-1β, TNF-α and IFN-γ (Wang and Dasso,

2009). However, the responses differ according to the length of treatment, the concentration of the agents and the cell culture method.

In this project, a short treatment was required in order to carry out experiments during peak or trough periods of clock genes. At the peak of REV-ERBα, 16 hours after synchronisation by serum shock, NHBE cells were treated with LPS at 1 μg/ml, TNF-α at 5 ng/ml or IL-1β at 1 ng/ml for 2 hours. LPS treatment had no effect on the cytokines and chemokines whereas TNF-α and IL-1β stimulation elicited strong and similar responses for *IL-6*, *IL-8* and *GM-CSF*. However, *CXCL5* transcript was significantly elevated only upon IL-1β challenge (Figure 6.7). For all the following experiments with epithelial cells, IL-1β was used as inflammatory stimulus.
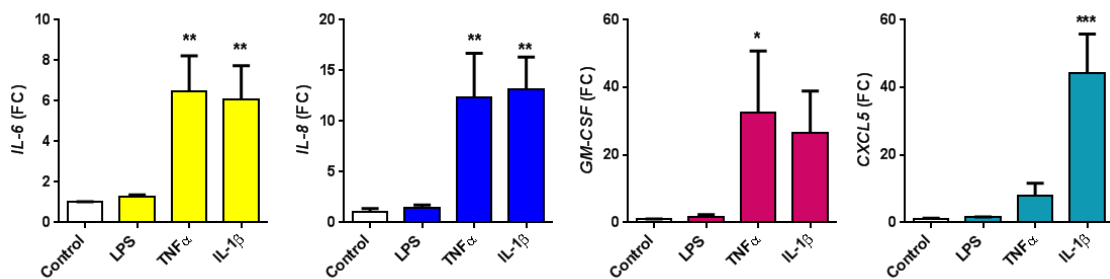
Figure 6.7: NHBE cell responses to LPS, TNF-α and IL-1β treatments

NHBE cells were synchronised by serum shock and stimulated 16 hours later with LPS at 1 μg/ml, TNF-α at 5ng/ml or IL-1β at 1 ng/ml for 2 hours. mRNA levels of *IL-6*, *IL-8*, *GM-CSF* and *CXCL5* were measured using Taqman Real-Time qPCR and normalized to un-stimulated control cells (fold change = 1). Data are presented as mean ± SD; n = 3. *P <0.05, **P <0.001, ***P <0.0001 compared to un-stimulated control cells (One-way ANOVA, post hoc Bonferroni).

In order to optimize inflammatory responses, NHBE cells were challenged with different doses of IL-1β and then for different lengths (Figure 6.8A,B). A dose-dependent increase of *IL-6*, *IL-8* and *CXCL5* was observed for IL-1β concentrations ranging from 0.1 to 1 ng/ml, with a plateau of responses for concentrations above 1 ng/ml. Moreover, responses to IL-1β challenge were more important after 2 hours

treatment than after 4 hours. Therefore, IL-1β was used at 1 ng/ml for 2 hours in all the following experiments.

Moreover, the effect of the time of treatment on inflammatory responses was investigated by challenging NHBE cells with IL-1β at 18 or 30 hours post serum shock. These two time points were chosen as they match peak and trough of REV-ERBα respectively. Inflammatory responses to IL-1β were similar at both time points (Figure 6.8C) except for *IL-8* of which the induction upon IL-1β stimulation was significantly greater when cells were challenged 30 hours post serum shock. However, basal levels of *IL-8* in un-stimulated cells were also greater at that time point.
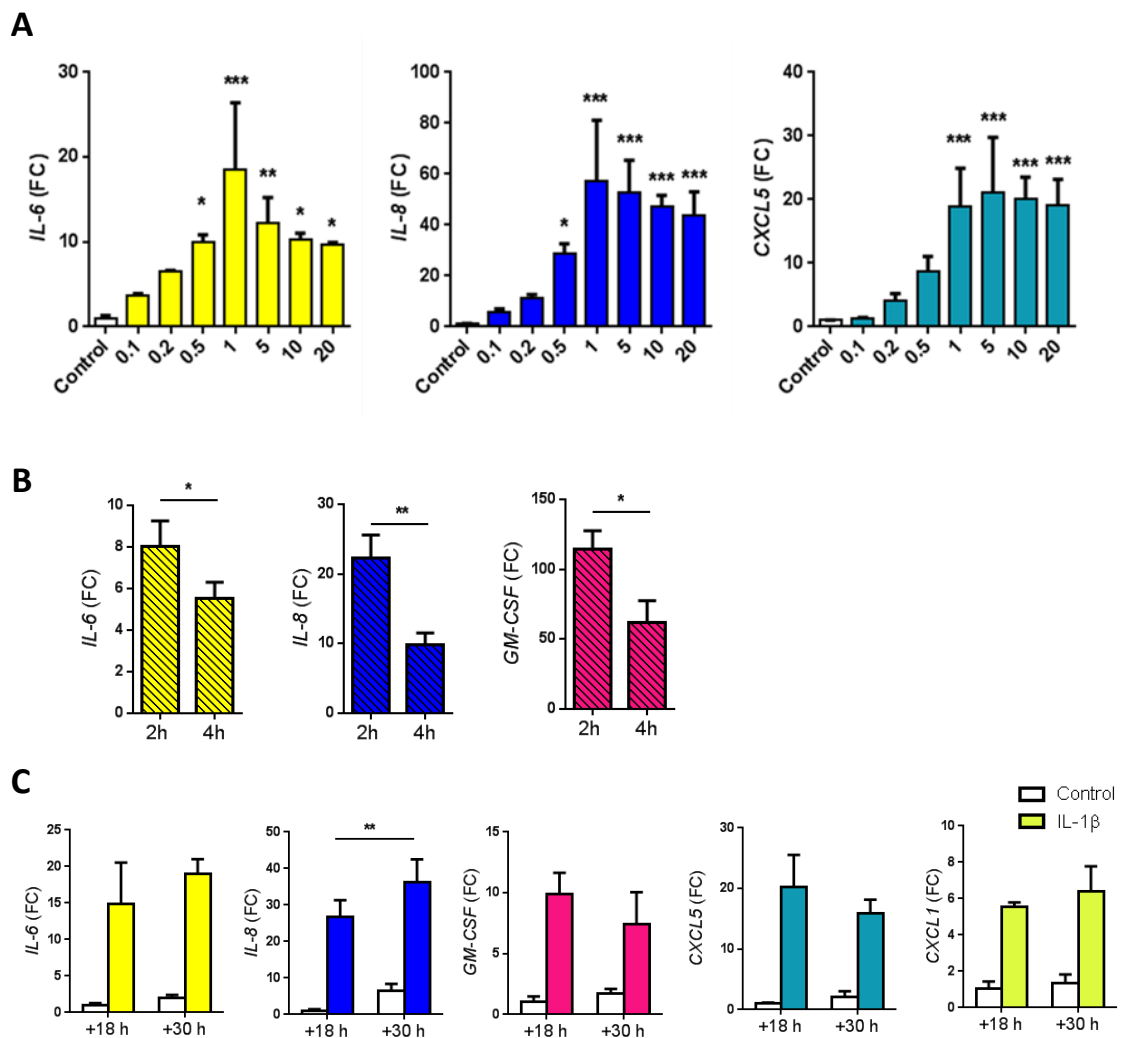
Figure 6.8: Inflammatory responses to IL-1β at different concentrations, different lengths or at different times in NHBE cells (legend on next page)

(A) NHBE cells were synchronised by serum shock and stimulated 18 hours later with IL-1β at different concentrations for 2 hours. mRNA levels were measured using Taqman Real-Time qPCR and normalized to un-stimulated control cells (PBS). Data are presented as mean ± SD; $n = 3$. *P <0.05, **P <0.01, ***P <0.001*, significant increase compared to control (One-way ANOVA, post hoc Bonferroni). (B) NHBE cells were synchronised by serum shock and stimulated 16 hours later with IL-1β at 1 ng/ml for 2 or 4 hours. mRNA levels were measured using Taqman Real-Time PCR and normalized to un-stimulated control cells for the same length of treatment. Data are presented as mean ± SD; $n = 3$. *P <0.05, **P <0.01* (Student's *t*-test). (C) NHBE cells were synchronised by serum shock and stimulated 18 or 30 hours later with IL-1β at 1 ng/ml for 2 hours. mRNA levels were measured using Taqman Real-Time qPCR and normalized to un-stimulated control cells at +18h. Data are presented as mean ± SD; n = 3. **P <0.01 (Two-way ANOVA, post hoc Bonferroni).

6.3.3.1.2   REV-ERBα ligands increase REV-ERBα protein levels in NHBE cells

NHBE cells were treated with GSK1362, GSK4112, Hemin or with two other REV-ERBα ligands, GSK2945 and GSK3824, at 10 μM for 4 hours, 16 or 28 hours after synchronisation by serum shock, peak and trough of REV-ERBα respectively. Increase of REV-ERBα protein levels were observed in presence of ligands, especially with GSK1362, when cells were treated 16 hours post serum shock (Figure 6.9A,B). As expected, no REV-ERBα protein could be detected 28 hours post serum shock. This result could suggest a stabilisation of the protein in presence of the ligands probably due to a change of the protein conformation that prevents from degradation. This hypothesis was investigated in chapter 7. Moreover, treatment with Hemin, GSK1362 and GSK3824 at the peak of REV-ERBα also induced a significant up-regulation of *REV-ERBα* transcription, suggesting that these ligands may act on different pathways which promote activation of *REV-ERBα* gene expression (Figure 6.9C).
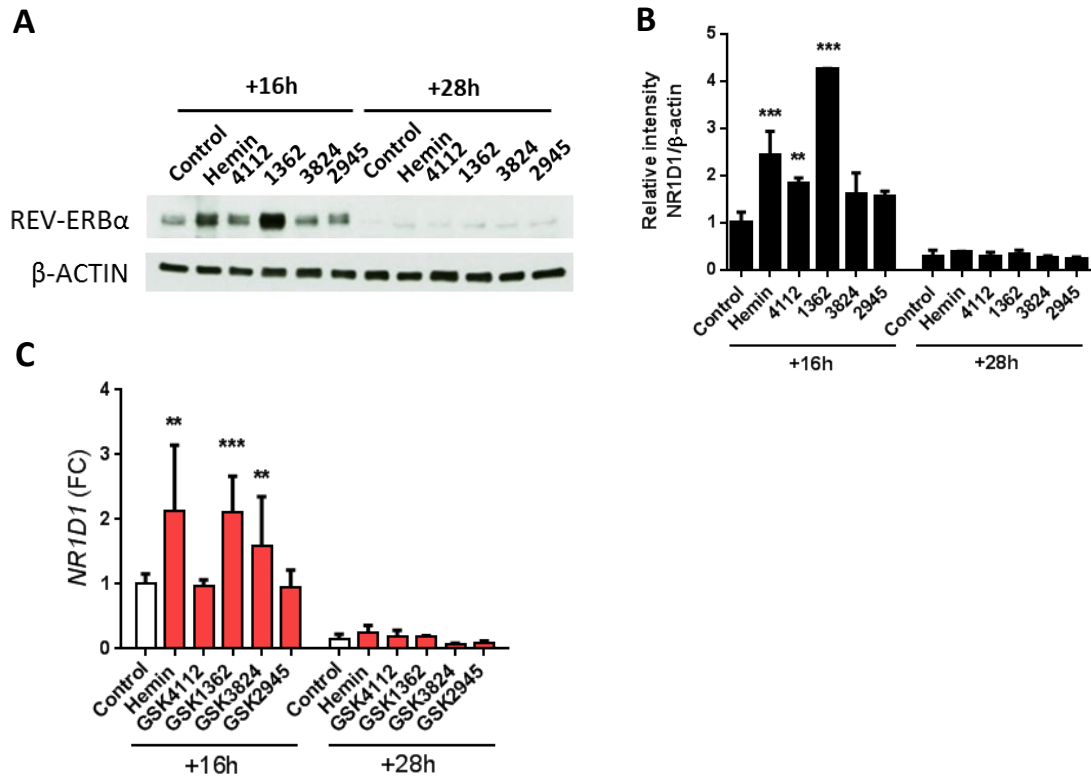
Figure 6.9: Ligand treatment effects on REV-ERBα at protein and transcript levels in NHBEs

NHBE cells were synchronised by serum shock and 16 or 28 hours later treated with natural or synthetic ligands at 10 μM for 4 hours. (A) REV-ERBα protein levels were assessed by Western blotting protein levels (6 μg total protein loaded per lane). (B) Relative intensity was obtained by dividing intensity of REV-ERBα bands by the corresponding β-ACTIN ones and results were normalised to control DMSO treated cells at +16h. (C) mRNA levels were measured using Taqman Real-Time qPCR and normalized control DMSO treated cells at +16h. Data are presented as mean ± SD; n = 3. **P <0.01, **P <0.001, significantly increased compared to control DMSO treated cells at +16h (Two-way ANOVA, post hoc Bonferroni).

6.3.3.1.3   REV-ERBα ligands exert divergent effects on different pro-inflammatory cytokines in NHBE cells

The role of GK1362 in regulating inflammation in NHBE cells was then investigated. Cells were pre-treated with GSK1362 and GSK4112 as comparison at 10 μM 16 hours after serum shock. Two hours later, IL-1β at 1 ng/ml was added to the cells for a 2-hour incubation time (Figure 6.10). Upon IL-1β stimulation,

treatment with GSK1362 and GSK4112 increased inflammatory mediator transcript levels for *IL-6* and *IL-8* whereas it down-regulated *CCL2* levels. *GM-CSF* was significantly elevated in presence of GSK1362 but not GSK4112 after challenge with IL-1β. However, GSK1362 had no effect on *CXCL5* levels in presence of IL-1β. These results indicated that REV-ERBα exert divergent effects on different cytokines/chemokines upon IL-1β stimulation in NHBE cells.
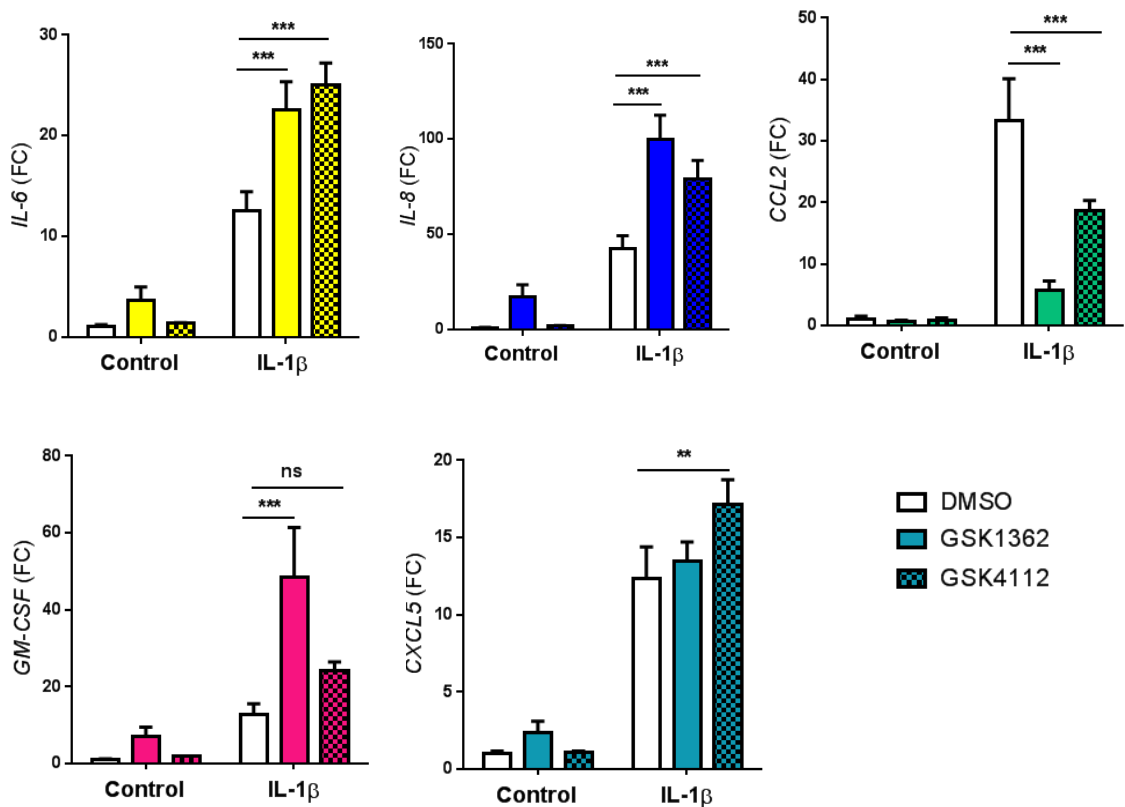
Figure 6.10: Effect of GSK1362 and GSK4112 treatment on responses to IL-1β stimulation at the peak of REV-ERBα

NHBE cells were synchronised by serum shock and 16 hours later treated with GSK1362 or GSK4112 at 10 μM followed 2 hours later by IL-1β at 1 ng/ml for 2 hours. Gene expression was determined by Real-Time qPCR and normalized to DMSO-treated control cells. White bars = 0.01% DMSO, plain colored bars = GSK1362 at 10 μM, hatched colored bars = GSK4112 at 10 μM. Data are presented as mean ± SD; n = 3. **P <0.01, ***P <0.001 (Two-way ANOVA, post hoc Bonferroni).

In order to assess the specificity of GSK1362 to REV-ERBα in NHBE cells, REV-ERBα knock-down was attempted using siRNA transfection. Different concentrations and lengths of siRNA treatment had been tested in order to optimize the efficiency of the transfection and best results were obtained when the cells were transfected for 48 hours with non-targeting or Rev-Erbα siRNA at 25 nM. However, the efficiency of the transfection remained low with about 60% reduction at transcript levels and 40% reduction at protein levels (Appendix 17 Figure A17). The knock-down was then not efficient enough to test the specificity of GSK1362 to REV-ERBα. Instead, I took advantage of the endogenous REV-ERBα rhythm by treating NHBE cells at the trough of the protein, 28 hours after serum synchronisation.

Cells were pre-treated with GSK1362 at 10 μM 28 hours after serum shock, followed by IL-1β at 1 ng/ml for additional 2 hours (Figure 6.11). Unlike treatment at the peak of REV-ERBα, GSK1362 treatment at its trough had no effect on *IL-6*, *IL-8* and *GM-CSF*. However, the repression of *CCL2* in presence of the ligand upon IL-1β challenge was still observed, suggesting that the ligand acts on another target which controls *CCL2* expression.
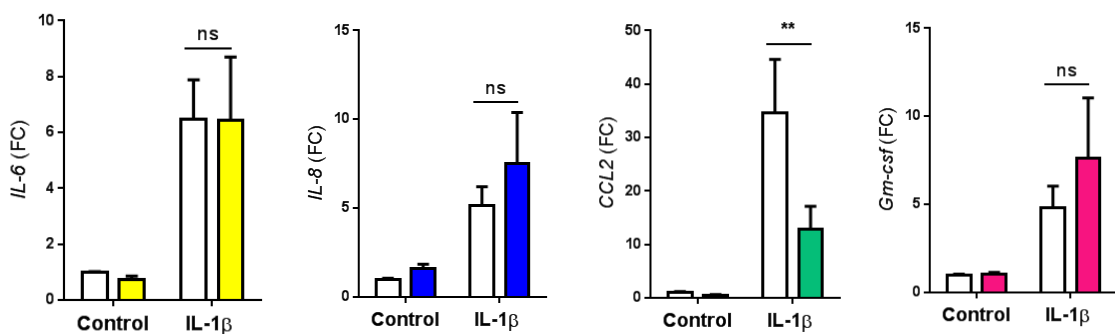
Figure 6.11: Effect of GSK1362 treatment on responses to IL-1β stimulation at the trough of REV-ERBα

NHBE cells were synchronised by serum shock and 28 hours later treated with GSK1362 at 10 μM followed 2 hours later by IL-1β at 1 ng/ml for 2 hours. Gene expression was determined by Real-Time qPCR and normalized to DMSO-treated control cells. White bars = 0.01% DMSO, plain colored bars = GSK1362 at 10 μM. Data are presented as mean ± SD; n = 3. **P <0.01 (Two-way ANOVA, post hoc Bonferroni).

6.3.3.2 LA-4 cells

As the effects of GSK1362 appeared to depend on the cell type, another lung epithelial cell model was applied. LA-4 cells are epithelial-like cells isolated from an urethan-induced lung adenoma of a 28 week old A/He strain mouse.

6.3.3.2.1 LA-4 cells display circadian rhythms

Rhythms in LA-4 cells were assessed at transcript and protein levels after serum shock synchronisation over 48 hours. As for NHBE cells, *Rev-Erbα* transcript and protein peaked around 18 hours post synchronisation and with a trough around 30 hours post synchronisation (Figure 6.12). However, the oscillations for the clock genes in LA-4 cells displayed low amplitude.
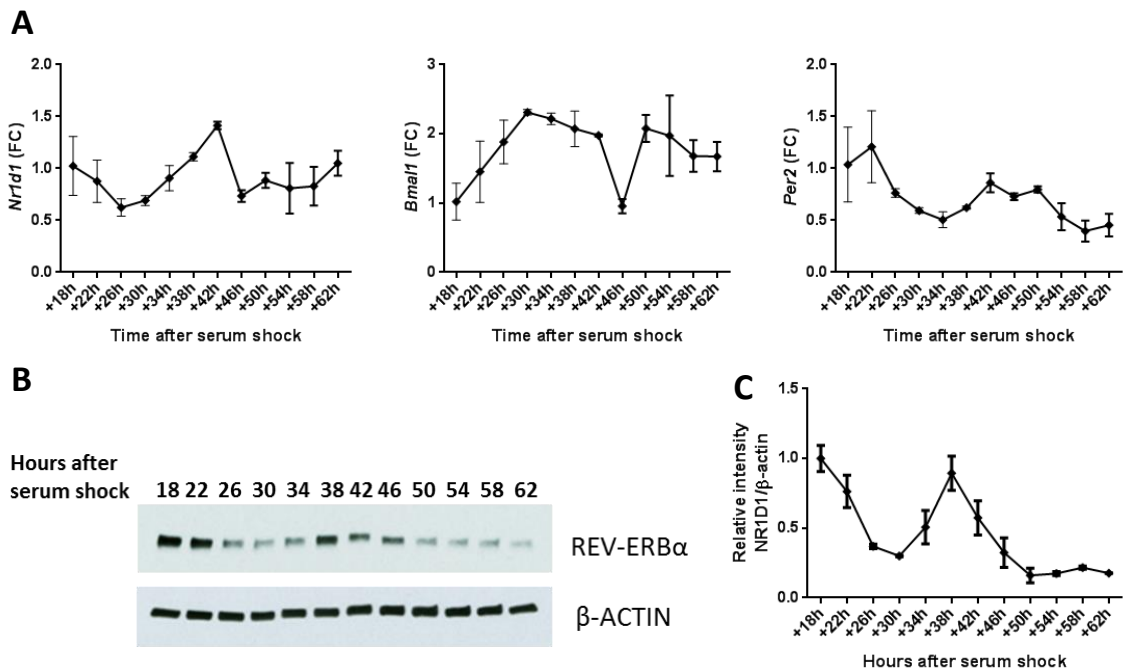
Figure 6.12: Circadian variations of clock genes and REV-ERBα in LA-4 cells synchronised by serum shock

(A) mRNA levels of the clock genes were measured using Taqman Real-Time qPCR and normalized to the first time point, 18h post serum shock. Data are presented as mean ± SD; n = 3. (B) Total cell lysates were analysed by Western blotting for REV-ERBα protein levels (7 µg total protein loaded per lane). (C) Relative intensity was obtained by dividing intensity of REV-ERBα bands by the corresponding β-ACTIN ones and results were normalised to the first time point. Data are presented as mean ± SD, n = 2.

6.3.3.2.2 REV-ERBα ligands increase REV-ERBα protein levels in LA-4 cells

LA-4 cells were treated with GSK1362, GSK4112 or Hemin at 10 µM for 4 hours, at the peak of REV-ERBα, 16 hours after synchronisation by serum shock. Increase of REV-ERBα protein levels were observed in presence of ligands, especially with GSK1362 (Figure 6.13A,B). Moreover, treatment with GSK1362 also induced a significant up-regulation of *REV-ERBα* transcription whereas GSK4112 and Hemin had no effect on the gene activation (Figure 6.13C).
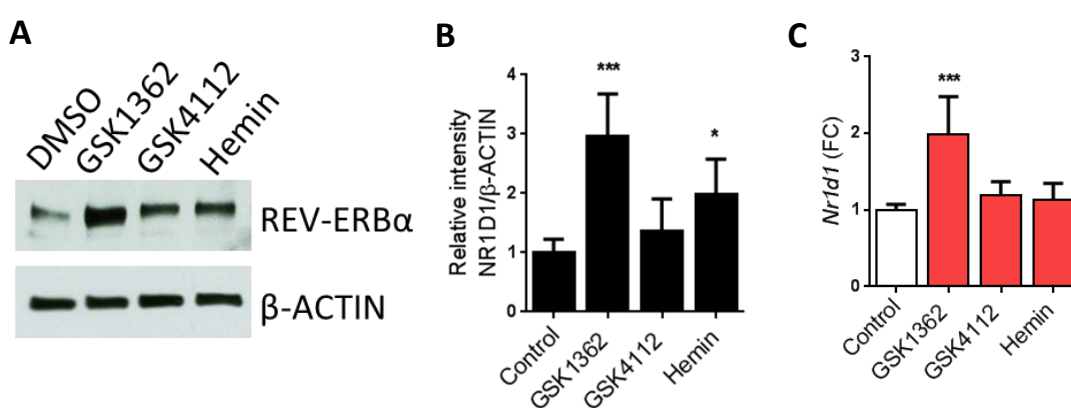
Figure 6.13: Effects of ligand treatment on REV-ERBα at protein and transcript levels in LA-4 cells

LA-4 cells were synchronised by serum shock and 16 hours later treated with the different ligands at 10 µM for 4 hours. (A) Total cell lysates were analysed by Western blotting for REV-ERBα protein levels (12 µg total protein loaded per lane). (B) Relative intensity was obtained by dividing intensity of REV-ERBα bands by the corresponding β-ACTIN ones and results were normalised to control DMSO treated cells at +16h. (C) mRNA levels were measured using Taqman Real-Time qPCR and normalized control DMSO treated cells at +16h. Data are presented as mean ± SD; n = 3. **P <0.01, **P <0.001, significantly increased compared to control DMSO treated cells at +16h (One-way ANOVA, post hoc Bonferroni).

6.3.3.2.3 REV-ERBα ligand GSK1362 represses *Cxcl5* expression upon IL-1β challenge

LA-4 cells were treated with GSK1362, GSK4112 or Hemin at 10 µM 16 hours after serum shock. Two hours later, IL-1β at 1 ng/ml was added to the cells for a 2-hour

incubation time. Overall, the different compounds had insignificant impact on the different cytokines/chemokines measured upon IL-1β stimulation; except for GSK1362 on *Cxcl5*. This ligand induced a significant down-regulation of *Cxcl5* transcript levels upon IL-1β challenge (Figure 6.14). To a lesser extent, *Cxcl5* and *Cxcl2* levels were also reduced in LA-4 cells treated with hemin upon IL-1β challenge.
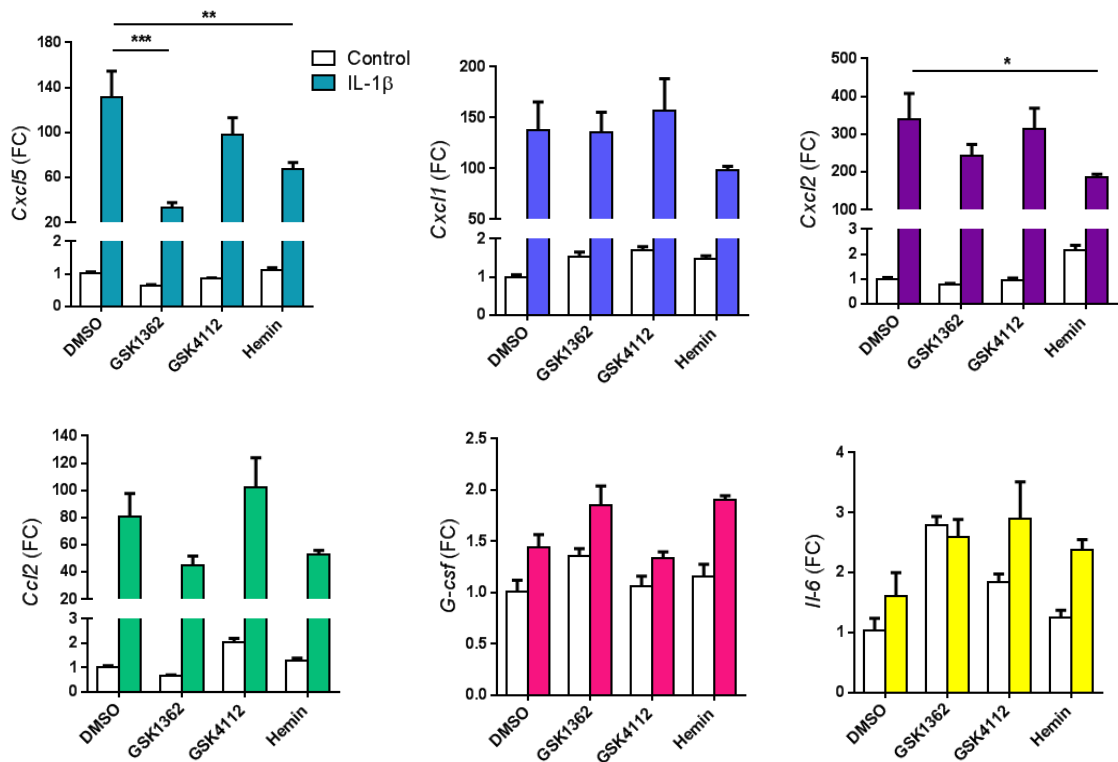
Figure 6.14: Effects of REV-ERBα ligands on responses to IL-1β stimulation in LA-4 cells

LA-4 cells were synchronised by serum shock and 16 hours later treated with the different ligands at 10 μM followed 2 hours later by IL-1β at 1 ng/ml for 2 hours. Gene expression was determined by Real-Time qPCR and normalized to DMSO control cells. White bars = PBS, colored bars = IL-1β at 1 ng/ml. Data are presented as mean ± SD; *n* = 3. *P < 0.05, **P < 0.01, ***P <0.001 (Two-way ANOVA, post hoc Bonferroni).

6.3.4 *In vivo* studies

Treatment with ligand GSK1362 induced a repression of inflammatory responses in murine alveolar macrophages *ex vivo* and in murine epithelial cells *in vitro*. Unfortunately, the pharmacology of this compound was not suitable for *in vivo* studies due to its high lipophilicity. However, chemists at GlaxoSmithKline suggested to test another compound GSK3824 *in vivo* as it had better a more suitable pharmacology.

Prior *in vitro* and *ex vivo* work revealed that treatment with GSK3824 increased protein levels in NHBE cells (Figure 6.9) and in LA-4 cells (Figure 6.15A). Moreover, it also repressed expression of pro-inflammatory cytokines in NHBE cells and murine PECs upon inflammatory stimuli (Figure 6.15B,C).
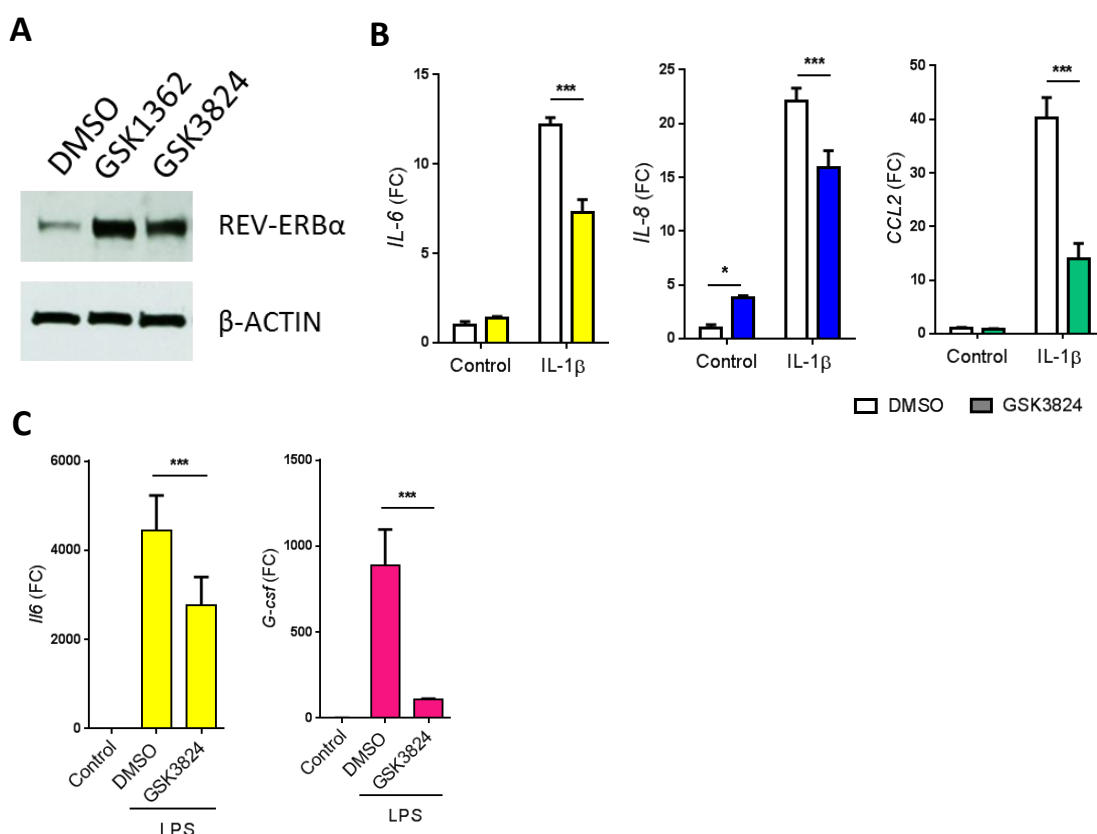
Figure 6.15: *In vitro* and *ex vivo* effects of GSK3824 in different cell types
(A) LA-4 cells were synchronised by serum shock and 16 hours later treated with the different ligands at 10 μM for 4 hours. Total cell lysates were analysed by Western blotting for REV-ERBα protein levels (12 μg total protein loaded per lane). (B) NHBE cells were synchronised by serum shock and 16 hours later treated with (legend continued on next page)

GSK3824 at 10 µM followed 2 hours later by IL-1β at 1 ng/ml for 2 hours. Gene expression was determined by Real-Time qPCR and normalized to DMSO-treated control cells. White bars = 0.01% DMSO, plain colored bars = GSK3824 at 10 µM. Data are presented as mean ± SD; n = 3. *P <0.05, ***P <0.001 (Two-way ANOVA, post hoc Bonferroni). (C) PECs from wild type mice were treated with LPS at 100 ng/ml in presence or absence of GSK3824 at 10 µM for 4 hours. Gene expression was determined by Real-Time qPCR and normalized to untreated control cells. Data are presented as mean ± SD; *n* = 3. ***P <0.001 (One-way ANOVA, post hoc Bonferroni).

Based on the encouraging results observed *in vitro* and a suitable pharmacology and toxicity, potential anti-inflammatory effects of GSK3824 were evaluated *in vivo*. Due to poor solubility, the compound solution to be administrated *in vivo* was in form of particles in suspension. The aim was to administrate first the compound into the animal followed by aerosolised LPS challenge in order to assess whether the ligand could regulate the endotoxin-induced inflammation. Timing of the compound administration and LPS challenge was difficult to decide. Indeed, best timing to give the compound to the mouse was when the receptor, REV-ERBα was present which is between CT8 and CT12. However, at this time of the day, neutrophil recruitment in response to aerosolised LPS is at its trough (Gibbs et al., 2014). Therefore, we compromised by administering the compound first at ZT10, peak of REV-ERBα, and again at ZT14 to give a maximal dose to the animal and then challenging the mice at ZT15 when neutrophil response should be rising again. GSK3828 was administered intranasally in order to target specifically the lung. BAL sample analyses revealed a significant increase in infiltration of inflammatory cells, predominantly neutrophils for mice which received GSK3824 compared to vehicle (Figure 6.16A). These results contradict *in vitro* and *ex vivo* data in NHBE cells and murine PECs respectively, showing an anti-inflammatory effect of this ligand. However, when measuring the drug amount in the lung and correlating it with neutrophil numbers, we observed a linear regression suggesting an anti-inflammatory effect of GSK3824 (Figure 6.16B). An explanation for these contradictory findings is that the particles in the compound solution may induce neutrophil recruitment but high dose of the compound reaching the lung could reduce it. Indeed, it has been previously reported that particles can cause lung inflammation (Donaldson and Tran, 2002). Further

studies would be warranted to test this hypothesis but more importantly, another more efficient route of administration of these ligands has to be developed.

A

B
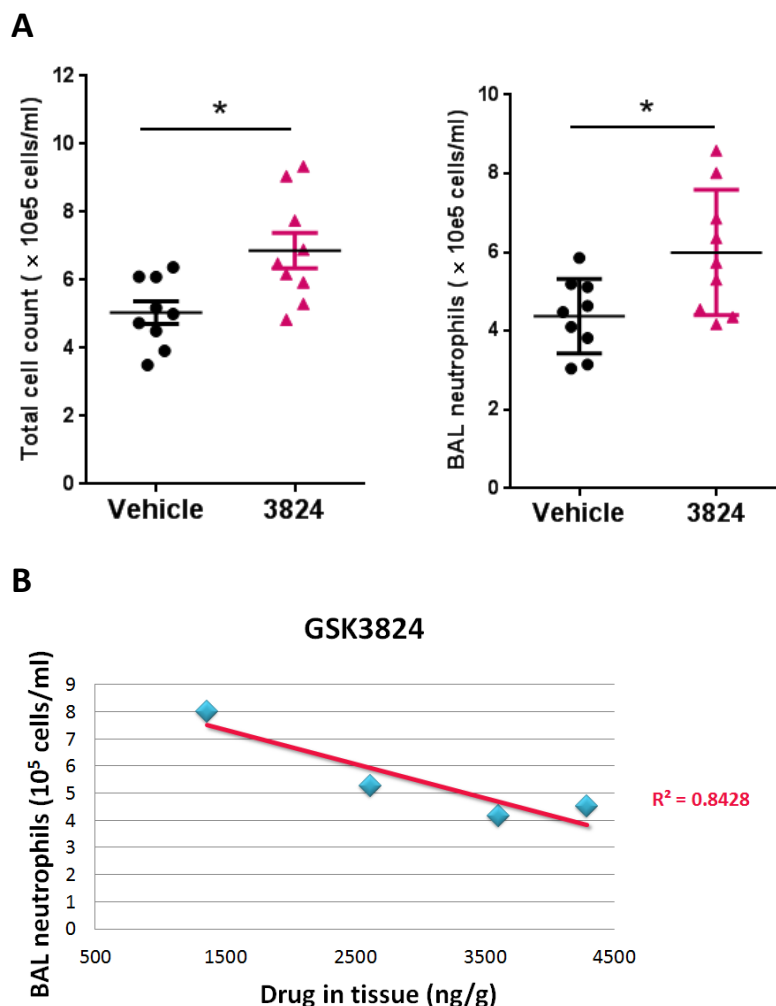
Figure 6.16: *In vivo* **effects of REV-ERBα ligand GSK3824 upon LPS challenge**

After two intra-nasal administrations of GSK3824 (4.96 mg/kg each) at ZT10 and ZT14, male C57BL6J mice were exposed for 20 min to aerosolized LPS at 2 mg/ml or to saline as control at ZT15, and sacrificed 5 hours later at ZT20. (A) Total cell counts per ml BAL and neutrophil counts performed by cytospin and Leishman's Eosin Methylene Blue staining. Data are presented as mean ± SEN; $n = 9$. *P <0.05 (Student's *t*-test). (B) Compound levels into the lung were determined by liquid chromatography-mass spectrometry (LC-MS) at GlaxoSmithKline, Stevenage.

6.4 Discussion

6.4.1 GSK1362: agonist, antagonist or inverse agonist of REV-ERBα?

Before trying to answer this question, it is worth reminding ourselves of some definitions. An agonist binds to the ligand binding domain (LBD) of a protein which induces a conformational change. This results in increased recruitment of cofactor proteins and enhanced repression or activation of target gene transcription. In contrast, an antagonist does not provoke a biological response of the receptor; rather it blocks or dampens the ability of an agonist to bind it. They are sometimes called blockers. An inverse agonist binds to the receptor binding-site but inhibits the constitutive activity of the receptor. An inverse agonist induces a conformational change within the receptor that decreases the affinity of the receptor for the co-factor proteins.

Peptide recruitment profiles showed decreased affinity of NCOR1 and SMRT2, two repressive coregulatory factors, for REV-ERBα in presence of GSK1362, in a dose-dependent manner, indicating an inverse agonist effect. Moreover, addition of GSK1362 enhanced *Bmal1* reporter gene expression (Figure 6.1). Other groups observed similar increase of *Bmal1* reporter gene expression using different small synthetic ligands and suggested the ligands could block the action of the endogenous agonist heme, thus defining these molecules as antagonists (Kojetin et al., 2011).

Therefore, results from these assays suggest that GSK1362 is either an inverse agonist or an antagonist of REV-ERBα and therefore, exaggerated responses were expected upon inflammatory challenges.

6.4.2 GSK1362 exerts divergent effects upon inflammatory challenges

In PECs, *ex vivo* treatment with GSK1362 prevented LPS-induced *G-csf* transcript activation but augmented *Ccl2*, *Cxcl1* and *Cxcl2* responses (Figure 6.4). In alveolar macrophages, the majority of pro-inflammatory gene transcripts measured were down-regulated in presence of GSK1362 after an *ex vivo* LPS challenge indicating an agonist effect in these cells (Figure 6.5). In contrast, in normal human bronchial epithelial cells, this compound induced an exaggerated response for *IL-6*, *IL-8* and *GM-CSF* but down-regulated *CCL2* expression upon IL-1β stimulation (Figure 6.10).

Finally, in murine epithelial-like lung LA-4 cells, GSK1362 treatment repressed *Cxcl5* expression upon IL-1β challenge (Figure 6.14). It is interesting to note that this down-regulation of *Cxcl5* transcription in LA-4 cells fits with my *in vivo* findings about an enhancement of CXCL5 expression in mice lacking REV-ERBα DBD in bronchiolar epithelial cells upon aerosolised LPS challenge, given that GSK1362 would, in that case, act as an agonist to strengthen REV-ERBα repressive activity. All together, these results, summarised in Table 6.1, indicate that GSK1362 exerts pro- or anti-inflammatory effects, depending on the cell type and the cytokine or chemokine analysed.

	LPS-stimulated macrophages		IL-1β-stimulated bronchial epithelial cells	
Cytokine	PECs (mouse)	AMs (mouse)	NHBEs (human)	LA-4 (mouse)
Il-6	—	↘	↗	—
G-csf	↘	↘	n.m	—
Gm-csf	n.m	n.m	↗	n.m
Ccl2	↗	↘	↘	—
Cxcl1	↗	—	n.m	—
Cxcl2/Il-8	↗	—	↗	—
Cxcl5	n.m	↘	—	↘

Table 6.1: Summary of ligand GSK1362 effects on pro-inflammatory cytokine and chemokine expression in different cell types

↘ : decreased expression ; ↗ : increased expression ; — : no difference in expression ; n.m : expression non measured.

Peptide profile recruitment revealed that addition of GSK1362 caused lower affinity of the repressive factors NCOR1 and SMRT2 for REV-ERBα, which could explained the pro-inflammatory effects of the ligand, but also lower affinity of RIP140, a coactivator for NF-κB/RelA-dependent cytokine gene expression, which could explain the anti-inflammatory effects of GSK1362. These divergent effects were also observed with GSK4112 as previous work in human macrophages challenged with LPS has demonstrated an anti-inflammatory effect of GSK4112

(Gibbs et al., 2012) whereas this compound induced a significant up-regulation of *IL-6* and *IL-8* in NHBE cells treated with IL-1β (Figure 6.10). Over the past few years, other nuclear receptor ligands have demonstrated divergent effects, between species but also between tissues from the same species, such as PPAR-γ ligands (Caldwell and Argo, 2007) and liver X receptor (LXR) agonists (Tsui et al., 2015). A reason for the complex effects of nuclear receptor ligands may lie on the involvement of different pathways depending on the cell type and the target. Moreover, it is important to consider that these ligands are rarely specific to the nuclear receptor of interest.

6.4.3 GSK1362: a ligand specific to REV-ERBα?

The commonly used REV-ERBα ligand GSK4112 is now known not to be specific to REV-ERBα and exhibits LXRα activities, making impossible to attribute the anti-inflammatory effects of GSK4112 to REV-ERBα or LXRα function. In contrast, by measuring LXR target gene expression, I demonstrated that GSK1362 has no effect on LXR activity (Figure 6.3). However, GSK1362 still displayed multiple effects on inflammatory gene expression upon *ex vivo* LPS challenge in *Rev-Erbα*^{-/-} PECs indicating that this compound is not specific to REV-ERBα (Figure 6.4). Moreover, GSK1362 treatment of *Rev-Erbα*^{-/-} PECs repressed the expression of most of the inflammatory genes measured, upon *ex vivo* LPS challenge. This may suggest that deletion of REV-ERBα would allow the expression of another element (normally repressed by REV-ERBα), to which GSK1362 would bind and then exert an anti-inflammatory effect.

6.4.4 GSK1362 alters REV-ERBα expression and PER2 rhythmic oscillations

Different groups have reported that REV-ERBα ligands modulate the circadian clock machinery itself. Meng et al. (2008) showed that treatment of primary lung fibroblasts and ectopic lung slices with synthetic REV-ERB agonist was able to reset the circadian rhythm in a phasic manner. Another study found that administration of synthetic REV-ERB ligands disrupts rhythmic wheel running behaviour and alters

the circadian pattern of core clock gene expression in the hypothalamic of mice (Solt et al., 2012).

My data showed that treatment with novel synthetic ligand GSK1362 increased amplitude of PER2::Luc rhythms in peritoneal exudate cells. Moreover, I found that addition of REV-ERBα ligands and especially with GSK1362 induced an increase in REV-ERBα protein and transcript levels in NHBE and LA-4 cells. Higher amounts of the protein could be explained by stabilisation of the receptor in presence of the ligand probably due to a change of the protein conformation that prevents from degradation. This hypothesis was investigated in chapter 7. GSK1362-induced increase in *Rev-Erbα* transcript levels suggests that this ligand may act on different components which promote activation of *Rev-Erbα* gene expression. However, it has been reported that REV-ERBα is able to repress its own transcription by binding a responsive element (RevRE) as an homodimer (Adelmant et al., 1996). Therefore, as an antagonist (or inverse agonist), GSK1362 would block (or decrease) the recruitment of co-repressor complexes preventing from repression of *Rev-Erbα* transcription. This also could explain the increase in *Rev-Erbα* mRNA levels upon GSK1362 treatment.

6.5 Conclusion

Over the past few years, REV-ERB ligands have emerged as powerful tools to regulate REV-ERB activity *in vitro* and more recently *in vivo*. In this chapter, I showed that novel synthetic compound GSK1362 appears to display high binding affinity to REV-ERBα and to exert antagonist effects on recruitment of co-factors. However, when assessing its effects on inflammatory responses, GSK1362 exhibits complex effects with enhanced or repressed pro-inflammatory mediator expression, depending on the inflammatory stimulus, on the cytokines/chemokines measured and on the cell type analysed. This highlights the importance to account for the local tissue and cellular context. Nonetheless, one of the biggest challenges for the synthesis of REV-ERB ligands is to find the right pharmacokinetics, which would allow to use them *in vivo*. Also, developing new routes of administration with tissue-specific delivery, taking into account the time of day of administration, would certainly contribute to a more efficient use of chrono-pharmaceuticals.

Chapter 7:   Consequences of inflammation

on REV-ERBα

7.1 Introduction

While studies have highlighted the importance of the clock in modulation of inflammation, there is evidence that this connection is bidirectional and the inflammatory response itself can affect molecular clock pathways (Arjona et al., 2012; Okada et al., 2008). For instance, the NF-κB subunit RelB interacts directly with BMAL1 in the presence of CLOCK to repress circadian gene expression at the promoter of the clock-controlled gene *Dbp* (Bellet et al., 2012). Post-translational modifications (PTMs) such as phosphorylation, sumoylation and ubiquitination, constitute an important regulatory system in clock protein and nuclear receptor function. PTMs regulate the dynamics of circadian clocks (period length and phase) by introducing delays in the transcriptional-translational feedback loops (Gallego and Virshup, 2007). Studies investigating the mechanisms of clock protein and nuclear receptor turnover have highlighted the role of proteasomes and, subsequently, ubiquitination, in targeting receptors for degradation (Helzer et al., 2015). My data indicates that REV-ERBα plays a major role in repressing lung inflammation. It is now hypothesised that, reciprocally, this nuclear receptor needs to be repressed at the site of infection or injury to allow a full immune response. In this chapter, effects of inflammatory stimuli on REV-ERBα protein levels and post-translational modifications were investigated.

7.2 Hypothesis tested and experimental approaches

Hypothesis: Inflammation degrades REV-ERBα.

Objectives:

- Employ different inflammatory stimuli *in vivo* and *in vitro* and measure levels of REV-ERBα proteins.

 - Dissect the degradation pathway by investigating post-translational modifications of REV-ERBα.

- Assess the effect of ligand binging on REV-ERBα degradation process.

7.3 Results

7.3.1 REV-ERBα levels are reduced by inflammatory stimuli *in vivo*

In experiments where C57BL6J mice were exposed to aerosolised LPS, REV-ERBα protein levels were dramatically decreased after 2 hours and even more after 4 hours (Figure 7.1A,B). Consistently, in all my experiments using genetically modified mouse models described in the previous chapters, decrease of REV-ERBα protein levels was observed, 5 hours after LPS challenge (Appendix 18, Figure A18). Moreover, reduction of *Rev-Erbα* mRNA levels was also measured in response to LPS (Figure 7.1C). This result was consistent with a recent study which has localised a NF-κB binding site on the mouse *Rev-Erbα* promoter repressing its activity (YangGuang, 2014). Endotoxin challenge may also degrade directly the protein via activation of inflammatory pathways and post-translational modification such as ubiquitination.

A 10-day cigarette smoke exposure induced a decrease in *Rev-Erbα* transcript levels (Figure 7.1D) but had no impact on protein levels (Figure 7.1E,F).
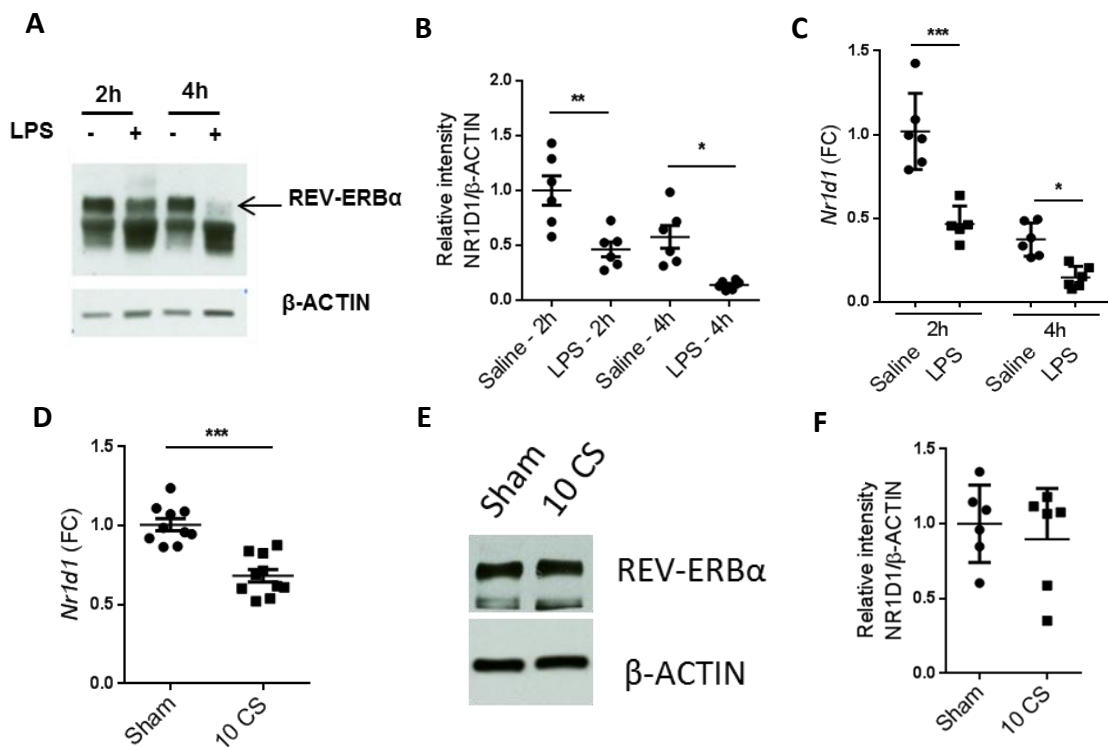
Figure 7.1: Reduced levels of REV-ERBα proteins and/or transcripts in murine lungs upon aerosolised LPS and cigarette smoke challenges (legend on next page)

(A,B,C) Male C57BL6J mice were challenged with aerosolised LPS at 2mg/ml for 20 min at CT8 and lungs were collected 2 or 4 hours later. (D,E,F) Mice were exposed to cigarette smoke between ZT8 and ZT10 for 10 days and culled 20 hours after the last exposure at ZT6. (A,E) Total lung tissues were analysed by Western blotting for REV-ERBα protein levels using GSK6F05 monoclonal antibody (20 µg total protein loaded per lane). (B,F) Relative intensity was obtained by dividing the intensity of REV-ERBα bands by their beta-actin ones and results were normalised to saline-2h group or sham group. Data are presented as mean ± SEM; *n=6, *P <0.05, ***P <0.001* (One-way ANOVA, post hoc Bonferroni). (C,D) Gene expression was determined by Real-Time qPCR and normalized to saline-2h group or sham group. Data are presented as mean ± SEM; *n = 6-10, **P <0.01, ***P <0.001* (One-way -way ANOVA, post hoc Bonferroni).

7.3.2 REV-ERBα levels are reduced by inflammatory stimuli *in vitro*

In both murine and human epithelial cells, LA-4 and NHBE cells respectively, IL-β or TNFα induced a moderate reduction of REV-ERBα proteins (Figure 7.2A,B). However, REV-ERBα protein levels were greatly increased when cells were treated with the proteasome inhibitor MG132, suggesting a key role for the 26S proteasome in the protein turnover.
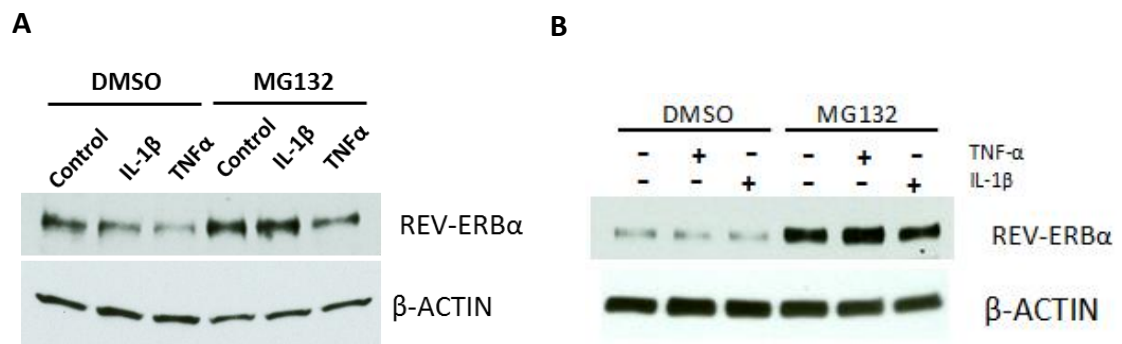
Figure 7.2: Effects of pro-inflammatory cytokines IL-β or TNFα and proteasome inhibition on REV-ERBα protein stability *in vitro*

(A) LA-4 cells were synchronised by serum shock and 18 hours later treated with MG132 at 5 µM and IL-1β or TNFα at 5 ng/ml for 2 hours. (B) NHBE cells were synchronised by serum shock and 18 hours later treated with MG132 at 5 µM and IL-β or TNFα at 10 ng/ml for 1 hour. Total cell lysates were analysed by Western blotting for REV-ERBα protein levels.

7.3.3 REV-ERBα ligand GSK1362 delays protein degradation

In chapter 6, I have demonstrated that treatment with different REV-ERBα ligands increased the protein levels in both murine and human epithelial cells but also activated *Rev-Erbα* transcription. In order to assess the effects of GSK1362 on REV-ERBα protein only, without confounding contributions from transcription or translation, NHBE cells were treated with cycloheximide (CHX) in a time-course experiment followed by Western blotting. In presence of GSK1362, the half-life of REV-ERBα protein was significantly prolonged, even when cells were challenged with IL-1β, which by itself accelerated the protein degradation (Figure 7.3). This clearly proved that both GSK1362 and IL-1β act on REV-ERBα protein itself and while GSK1362 delays the protein degradation, IL-1β accelerates it.
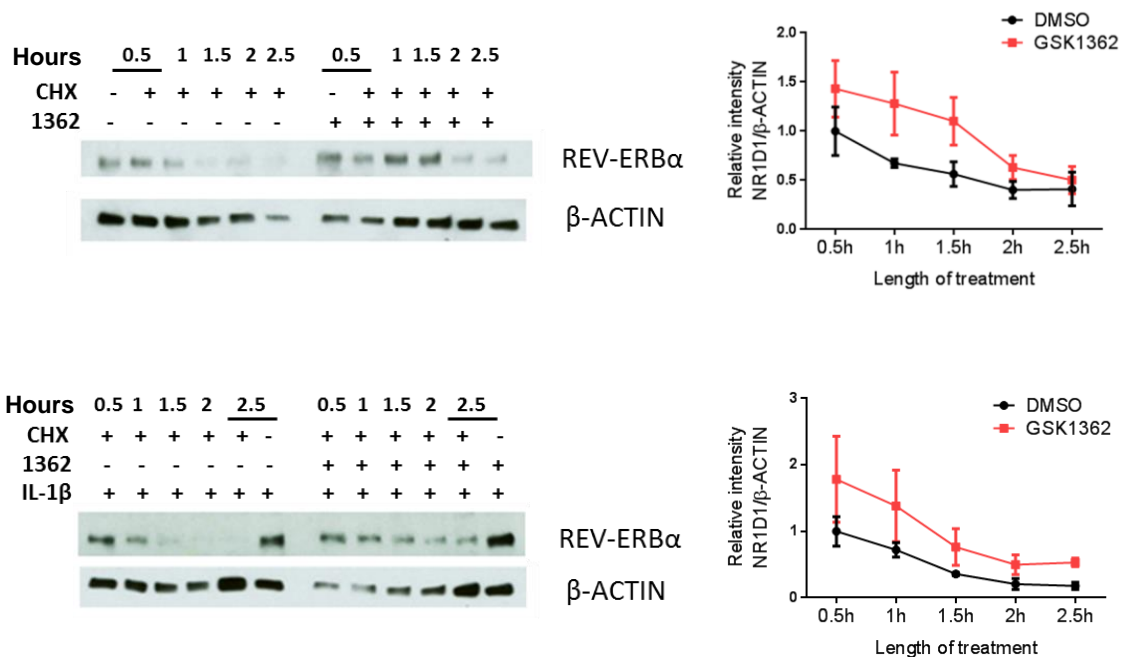
Figure 7.3: Delayed REV-ERBα protein degradation after GSK1362 treatment
NHBE cells cells were synchronised by serum shock and 18 hours later treated with GSK1362 at 10 µM followed 15 minutes later by CHX at 10 µM and IL-1β at 1 ng/ml for indicated times. Total cell lysates were analysed by Western blotting for REV-ERBα protein levels. Relative intensity was obtained by dividing the intensity of REV-ERBα bands by their beta-actin ones and results were normalised to DMSO - 0.5h treated group group. Data are presented as mean ± SD; *n* = 3.

7.3.4 Inflammatory stimuli promote REV-ERBα ubiquitination which can be blocked by GSK1362

Human embryonic kidney cells (HEK293T), an easy-to-transfect cell line, were chosen to investigate the mechanisms of ubiquitination and degradation. These cells were transfected with HA-Rev-Erbα and His-Ubiquitin, and then treated for 4 hours with REV-ERBα ligand GSK1362 and inflammatory mediators IL-1β or TNFα, in presence of MG132 to block any proteasomal degradation. After purification of the ubiqutinated fraction of REV-ERBα, purified and total lysates were run for Western blotting. As predicted, IL-1β or TNFα drove an increase in REV-ERBα ubiquitination. More interestingly, GSK1362 treatment blocked ubiquitination of the protein upon IL-1β or TNFα stimulation (Figure 7.4A). This might be explained by a modification of the protein conformation when the ligand binds the nuclear receptor, masking then crucial ubiquitination sites. In contrast, treatment with natural ligand Hemin or synthetic ligand GSK4112 did not impact on ubiquitination levels of REV-ERBα (Figure 7.4B).
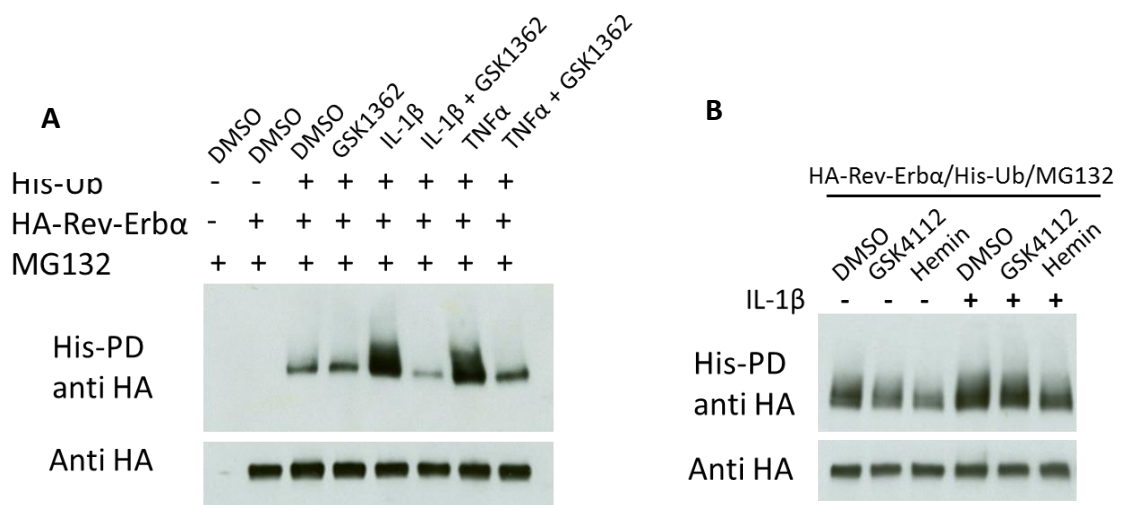
Figure 7.4: Effects of pro-inflammatory cytokines IL-1β or TNFα and REV-ERBα ligands on the protein ubiquitination

HEK293T cells were co-transfected with HA-Rev-Erbα and His-Ub plasmids. About 16h after transfection, the cells were treated with GSK1362 (A), GSK4112 or Hemin (B) at 10 μM and TNFα or IL-1β at 5 ng/ml for 4 hours in the presence of MG132 at 5 μM. Cells were lysed with total lysis buffer or guanidinium –HCl buffer for His-purification. His-purified protein and total lysates were used for running Western blot with Anti-HA monoclonal antibody.

7.3.5 CDK1 is involved in REV-ERBα ubiquitination process

Recently, a study reported that the cyclin-dependent kinase 1 (CDK1) mediates phosphorylation of REV-ERBα, allowing the consequent recruitment of the F-box protein FBXW7α which targets the protein for ubiquitination and subsequent degradation (Zhao et al., 2016). In order to assess whether this CDK1-FBXW7 pathway was implicated in IL-1β-driven ubiquitination of REV-ERBα described above, His-ubiquitin purification was performed on HEK293T cells treated with IL-1β in presence or absence of the CDK inhibitor, Roscovitine. Supporting Zhao et al. findings, Roscovitine addition reduced quantities of ubiquitinated REV-ERBα in both presence and absence of IL-1 stimulation (Figure 7.5).
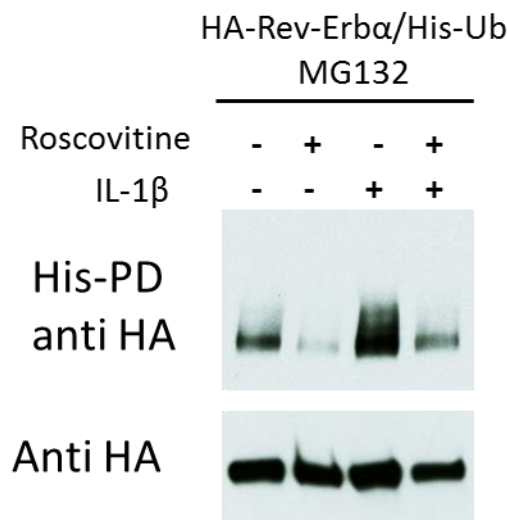
Figure 7.5: Reduction of REV-ERBα ubiquitination with CDK inhibitor Roscovitine
HEK293T cells were co-transfected with HA-Rev-Erbα and His-Ub plasmids. About 16h after transfection, the cells were treated with Roscovitive at 50 μM and IL-1β at 5 ng/ml for 4 hours in the presence of MG132 at 5 μM. Cells were lysed with total lysis buffer or guanidinium –HCl buffer for His-purification. His-purified protein and total lysates were used for running Western blot with Anti-HA monoclonal antibody.

7.3.6 Sumoylation of REV-ERBα is required for its ubiquitination

Small ubiquitin-related modifiers (SUMO), that are ubiquitin-like polypeptides, can covalently attach to proteins in a process similar to ubiquitination (Wang and Dasso, 2009). Expanding studies characterising proteins conjugated to ubiquitin or Ub-like peptides, such as SUMO have revealed an important point of crosstalk between the SUMO and ubiquitin pathways (Denuc and Marfany, 2010). Here, HEK293T cells were transfected with HA-Rev-Erbα, His-Ubiquitin and Senp-1 then treated with MG132 and inflammatory mediators before lysis and subsequent His-purification, as above. Again, inflammatory mediators IL-1β or TNFα drove higher levels of ubiquitinated proteins. The introduction of SENP-1 (Sentrin-specific Protease 1), an enzyme that blocks sumoylation, resulted in low levels of ubiquitinated proteins, even in the presence of inflammatory stimuli, suggesting that sumoylation is required for the ubiquitination process to take place (Figure 7.6).
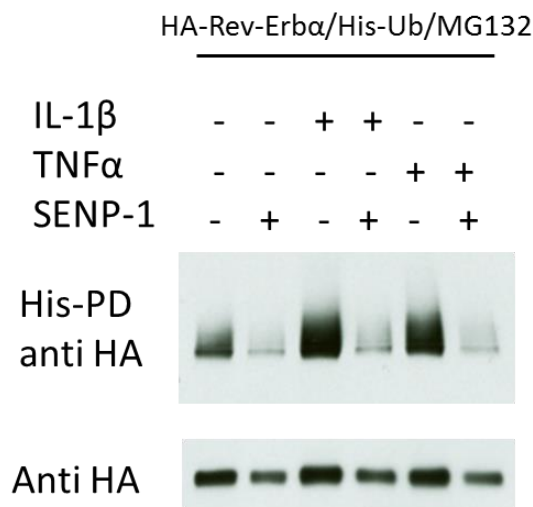
Figure 7.6: Impact of sumoylation inhibition on REV-ERBα ubiquitination

HEK293T cells were co-transfected with HA-Rev-Erbα, His-Ub and Senp-1 flag plasmids. About 16h after transfection, the cells were treated with TNFα or IL-1β at 5 ng/ml for 4 hours in the presence of MG132 at 5 μM. Cells were lysed with total lysis buffer or guanidinium –HCl buffer for His-purification. His-purified protein and total lysates were used for running Western blot with Anti-HA monoclonal antibody.

7.3.7 Inflammatory stimuli promote REV-ERBα sumoylation which can be blocked by GSK1362

As the cross-talk between sumoylation and ubiquitination pathways has been highlighted, it was then expected to investigate the sumoylation state of REV-ERBα. Mammalian cells express three major SUMO paralogues, called SUMO-1, SUMO-2 and SUMO-3. These SUMO paralogues have different targets, although SUMO-2 and SUMO-3 being ~95% identical to each other usually target the same proteins. Also, the overall cellular concentration of SUMO-2/3 is greater than that of SUMO-1. Therefore, it is likely that the bulk of sumoylation involves SUMO-2/3. Moreover, photobleaching experiments suggest that SUMO-1 is less dynamic than the other SUMO paralogues (Ayaydin and Dasso, 2004).

For my project, I focused on REV-ERBα sumoylation by SUMO-2. HEK293 cells were transfected with HA-Rev-Erbα, His-SUMO-2, Ubc9 and Senp-1, then treated with MG132 for 4 hours before cell lysis and His-purification. As expected, Ubc9 transfection induced an increase in sumoylated proteins whereas Senp-1 has the opposite effect (Figure 7.7A). Indeed, Ubc9 is an enzyme that catalyses covalent attachment of SUMOs to other proteins while Senp-1 blocks sumoylation. If proteasomal degradation was not prevented by adding MG132, no sumoylated REV-ERBα could be observed, indicating a rapid turnover of the protein after post translational modifications (Figure 7.7A).

Next, I found that treatment with pro-inflammatory cytokine IL-1β greatly increased sumoylation of REV-ERBα (Figure 7.7B). Again, when MG132 was not applied, the abundance of the sumoylated protein was less important, indicating a rapid degradation of the protein.

Then, I wanted to assess the effects of REV-ERBα ligands on sumoylation levels of the protein. HEK293 cells were transfected with HA-Rev-Erbα, His-SUMO-2 and Ubc9, and then treated with GSK1362, GSK4112 or Hemin at 10 μM and IL-1β in presence of MG132 for 4 hours before cell lysis and His-purification. While introduction of GSK1362 into the cells resulted in blocking sumoylation of REV-ERBα, GSK4112 treatment did not have any effect on sumoylation levels, whereas Hemin treatment induced formation of a poly-sumoylated high molecular complex around 250 kDa (Figure 7.7C). This result points out that these three ligands have different actions on REV-ERBα leading to different states of sumoylation. Finally, I

confirmed that GSK1362 treatment also blocked sumoylation of REV-ERBα upon IL-1β stimulation (Figure 7.7D).
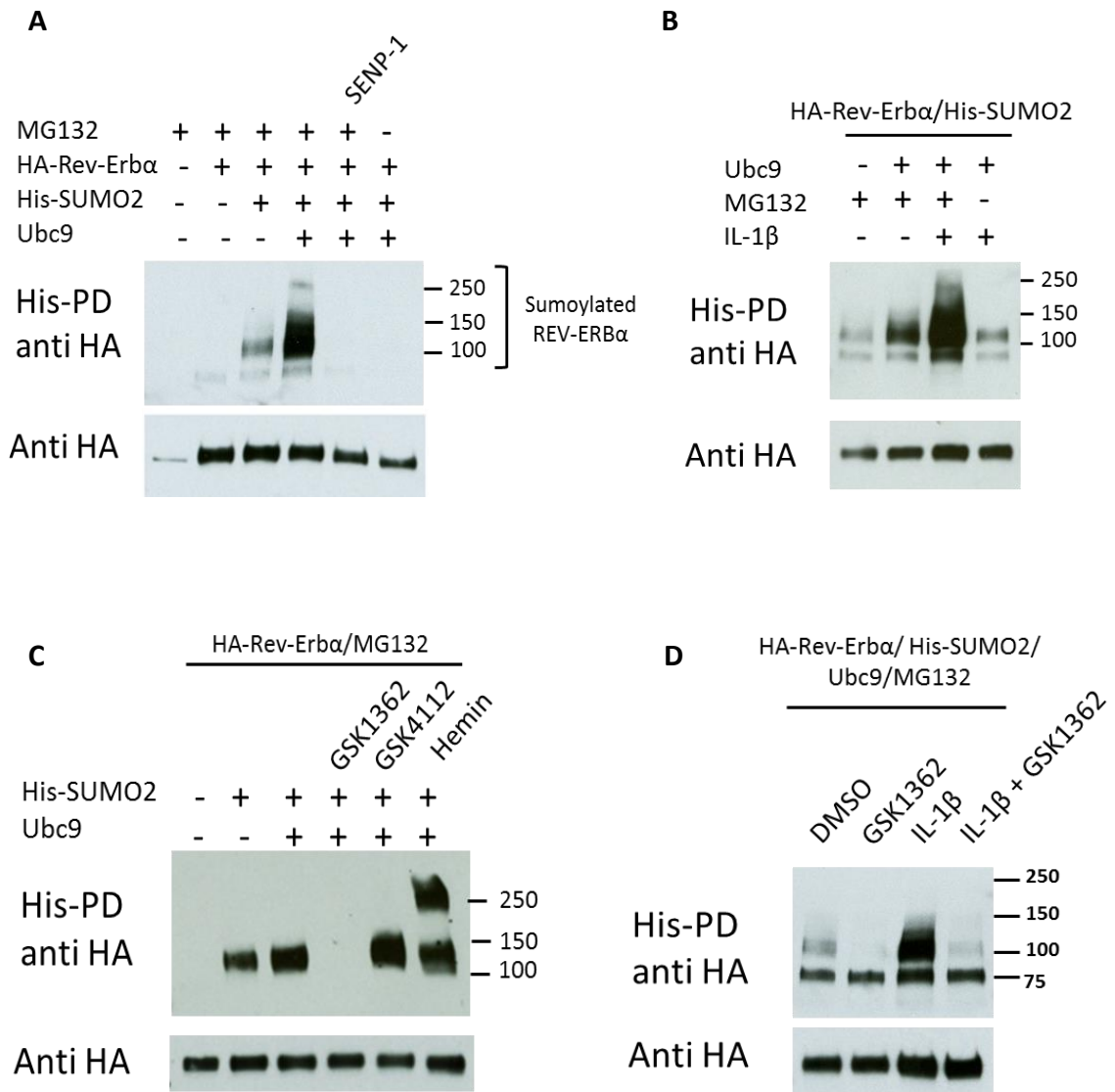
Figure 7.7: SUMO-2 targeting to REV-ERBα upon IL-1β and ligand treatment

(A-D) HEK293T cells were co-transfected with HA-Rev-Erbα, His-SUMO-2, Ubc9 and Senp-1 flag plasmids as indicated. About 16h after transfection, the cells were treated with MG132 at 5 μM, ligands at 10 μM and IL-1β at 5 ng/ml for 4 hours. Cells were lysed with total lysis buffer or guanidinium –HCl buffer for His-purification. His-purified protein and total lysates were used for running Western blot with Anti-HA monoclonal antibody.

7.3.8 Sumoylation of REV-ERBα facilitates HDAC3 recruitment

Studies have revealed that REV-ERBα exerts its repressive activity through the recruitment of the endogenous nuclear receptor corepressor (N-CoR)/histone deacetylase 3 (HDAC3) complex (Chandra et al., 2013; Yin and Lazar, 2005). Here, using a immunoprecipitation assay, I showed that IL-1β stimulation of HEK293T induced recruitment of HDAC3 to REV-ERBα (Figure 7.8). Moreover, HDAC3 recruitment was repressed when sumoylation was blocked by using SENP-1, suggesting that sumoylation of REV-ERBα is a critical post-translational modification for an efficient recruitment of the repressor complex. Finally, GSK1362 or Hemin treatment did not have a major impact on HDAC3 recruitment either in presence or absence of IL-1β stimulation. Interestingly, an additional band around 250 kDa can be observed when cells were treated with both IL-1β and Hemin, and in absence of SENP-1 (Figure 7.8B). This correlated with the poly-sumoylated high molecular complex observed when the sumoylated fraction of REV-ERBα was detected from cells treated with Hemin (Figure 7.7C).
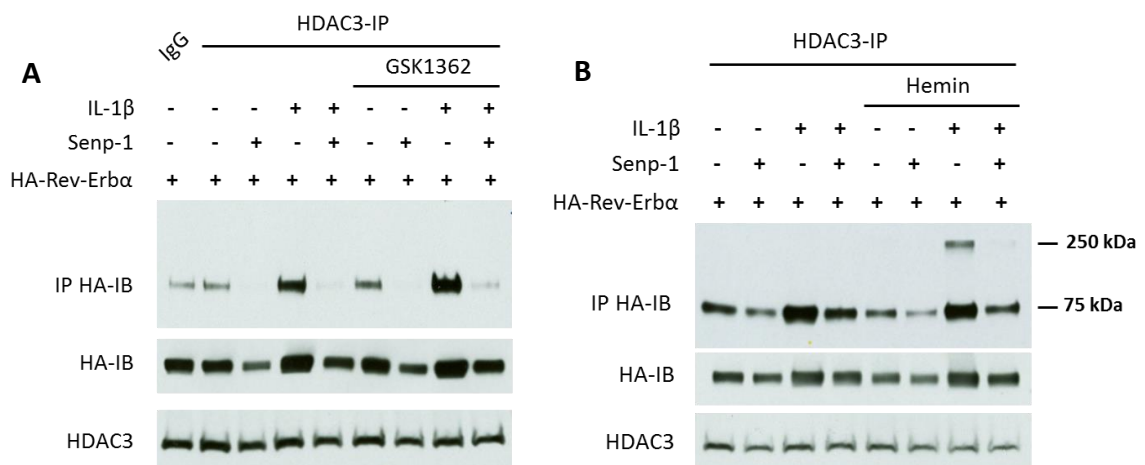
Figure 7.8: HDAC3 recruitment to REV-ERBα upon IL-1β stimulation, ligand treatment and sumoylation inhibition

HEK293T cells were transfected with HA-Rev-Erbα and Senp-1 plasmids. About 16 hours after transfection, cells were treated with GSK1362 (A) or Hemin (B) in presence of IL-1β for 4 hours. Cells were lysed with 1% Triton-X-100 lysis buffer containing NEM 10mM. In the upper panel, the cell lysates were immuno-precipitated with normal rabbit IgG or anti-HDAC3 antibody and the blot was probed with anti-HA antibody. In the middle and lower panels, cell lysates without undergoing immunoprecipitation were used as REV-ERBα or HDAC3 input with the blots probed with anti-HA or anti-HDAC3 antibodies respectively.

7.3.9 An attempt to elucidate the mechanism of action of GSK1362 when bound to REV-ERBα

In respect of my findings showing that GSK1362 stabilized REV-ERBα protein, exhibited effects upon inflammatory stimuli but did not affect recruitment of co-repressor HDAC3, I wanted to assess whether REV-ERBα bound to the DNA at different loci in presence of this compound. For that purpose, I decided to perform chromatin immunoprecipitation followed by high-throughput sequencing (ChIP-Seq) for REV-ERBα and also for histone 3 lysine 27 acetylation (H3K27ac), a histone modification associated with active enhancers and promoters (Creyghton et al., 2010), in LA-4 cells treated with GSK1362 in the presence or absence of IL-1β. The choice of LA-4 cells was made according to the down-regulation of *Cxcl5* transcription observed in these cells upon IL-1 β stimulation (Figure 6.12), which fitted with my *in vivo* findings about an enhancement of CXCL5 expression in mice lacking REV-ERBα DBD in bronchiolar epithelial cells upon endotoxin challenge. LA-4 cells were treated with GSK1362 at 10 μM (or DMSO as control) 17 hours after serum shock synchronization and one hour later cells were stimulated with IL-1 β at 1 ng/ml for one additional hour. Cells were the fixed and processed as described in Chapter 2.

Before sequencing, the immuno-precipitated DNA samples were analyzed by qPCR using one positive and one negative control target. For H3K27ac, a fragment in the promoter of *Gapdh* was used as positive control whereas a sequence containing two RORE elements in the promoter of *Bmal1* was used as positive control for REV-ERBα ChIP (Feng et al., 2011). Immuno-precipitated *Gapdh* represented around 2% of the DNA input against 0.15% for the negative control suggesting that H3K27ac ChIP had been efficient (Figure 7.9A) However, the proportions of immuno-precipitated *Bmal1* promoter and negative control were similar suggesting a non-specific immuno-precipitation (Figure 7.9B). These results were confirmed by ChIP-Seq analyses; no enrichment over the input samples was measured for REV-ERBα ChIP, indicating a non-specific pull-down. In contrast, strong enrichment was recorded for H3K27ac immuno-precipitated samples over the input samples.

A Anti-H3K27ac

B Anti-REV-ERBα

C

D
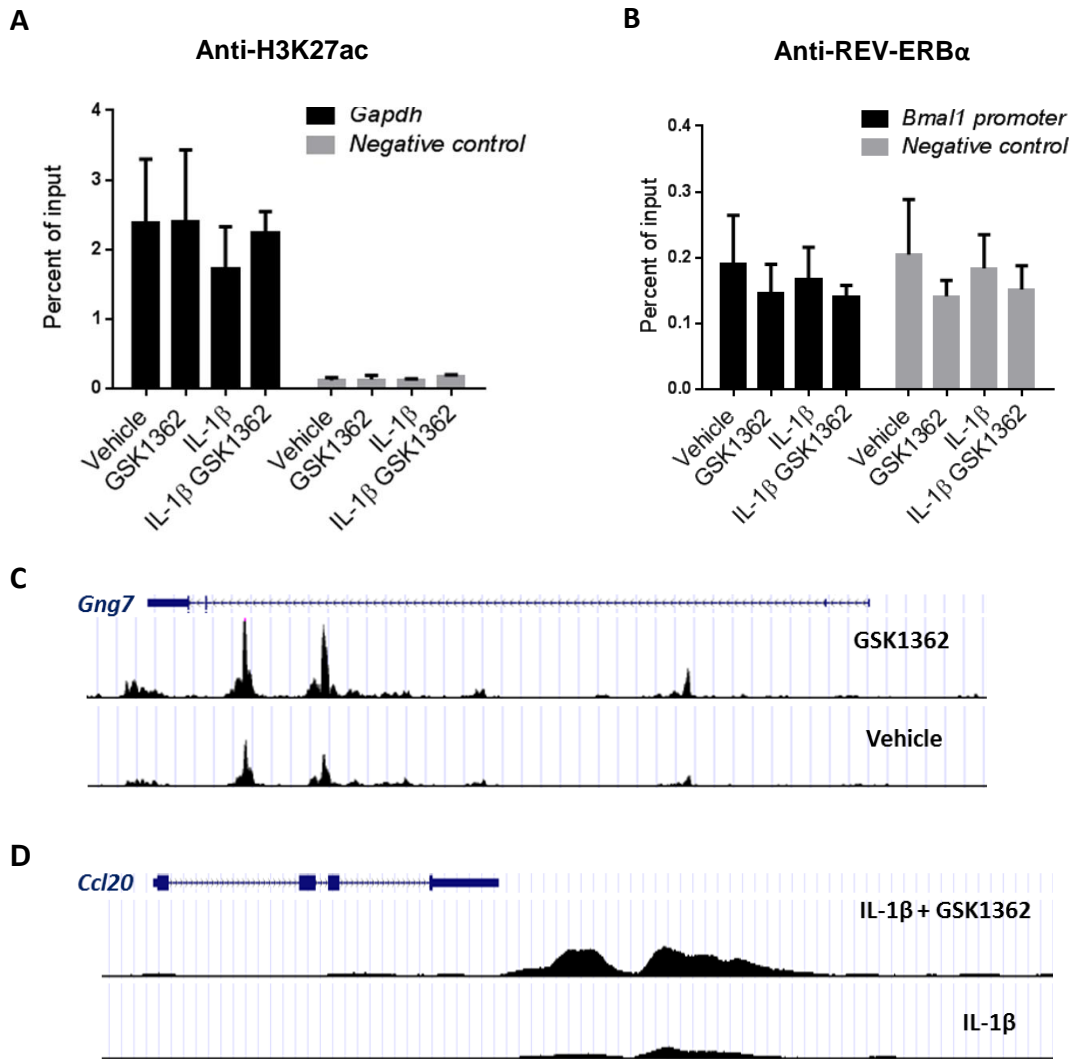
Figure 7.9: ChiP-seq for H3K27ac and REV-ERBα in LA-4 cells

LA-4 cells were treated with GSK1362 at 10 μM (or DMSO as control) 17 hours after serum shock synchronization and one hour later cells were stimulated with IL-1 β at 1 ng/ml for one additional hour. Cells were the fixed and processed as described in Chapter 2. (A,B) qPCR at the indicated genomic regions was performed using immuno-precipitated DNA to validate enrichment. The values indicate the percent of signal from immunospecific chromatin precipitates to signal from the input DNA. Technical duplicates and experimental duplicates are reflected in the errors bars indicating standard deviation. (C,D) Aligned peak tracks at selected loci for H3K27ac ChIP-Seq were taken from UCSC Genome browser.

Ligand treatment induced a two-fold H3K27ac binding increase at 130 regions and a two-fold H3K27ac binding decrease at 137 regions, compared to vehicle treatment. Gene ontology analyses revealed that an enriched part of the positively regulated

regions was involved in regulation of cyclic adenosine monophosphate (cAMP) biosynthetic and metabolic processes. cAMP is a second messenger, used for intracellular signal transduction, important in many biological processes. For instance, guanine nucleotide binding protein (G protein), gamma 7 (Gng7), one of the genes involved in cAMP biosynthetic and metabolic processes, had the highest increase in H3K27ac marks compared to vehicle (Figure 7.9C). On the other hand, an enriched part of the negatively regulated regions was involved in metal, ion binding. Repression of H3K27ac marks on such regions could be due a reduction of heme binding to REV-ERBα in presence of GSK1362.

In presence of IL-1β stimulation, ligand treatment caused a two-fold H3K27ac increase at 127 regions and a two-fold H3K27ac decrease at only 2 regions. Gene ontology analyses revealed that enriched portions of the positively regulated regions were involved in negative regulation of kinase activity such as the gene encoding for Homeodomain Interacting Protein Kinase 3 (HIPK3), known to negatively regulate apoptosis (Curtin and Cotter, 2004). Enriched regions were also involved in protein transport and trans-Golgi networks. In terms of inflammatory mediators (cytokines and chemokines), only Ccl20 showed increased H3K27ac marks upon ligand treatment and IL-1 β stimulation, probably on an enhancer regions.

Concerning the two regions showing decreased H3K27ac marks in presence of GSK1362 and IL-1 β, the first one overlapped with *Rnf115* gene which encodes for E3 ubiquitin ligase RING finger protein 115, suggesting that GSK1362 represses ubiquitination by reducing activation of this E3 ligase. It would be now interesting to assess whether this E3 ligase is involved in REV-ERBα ubiquitination. The second region overlapped with *Pepd* gene which encodes a member of the peptidase family. The enzyme serves an important role in the recycling of proline, and may be rate limiting for the production of collagen.

In summary, H3K27ac ChiP-Seq revealed some interesting differences in gene activation upon GSK1362 treatment but these acetylation marks were not specific enough to elucidate the mechanism of action of this ligand when bound to REV-ERBα. Further work is warranted to optimize experimental conditions and achieve efficient REV-ERBα ChiP-Seq.

7.4 Discussion

7.4.1 Reduction of REV-ERBα at transcript and protein levels by inflammation

Over the past few years, groups have reported that inflammation can affect the circadian clock. In cultured fibroblasts synchronized by serum shock, addition of TNF-α or IL-1β caused repressed expression of the period genes *Per1*, *Per2*, and *Per3* (Cavadini et al., 2007). Long-term treatment with IFN-γ in cultures obtained from a transgenic *Per1-luciferase* rat significantly reduced the *Per1-luc* rhythm amplitude in individual SCN neurons (Kwak et al., 2008). Similarly, intravenous injection of LPS in rats induced transient repression of *Per2* expression in the suprachiasmatic nucleus and liver (Okada et al., 2008).

My findings revealed that *in vivo* inflammatory challenges, using aerosolized LPS or cigarette smoke, caused a reduction in *Rev-Erbα* transcript levels in the lung. Previous reports support inflammation-induced suppression of *Rev-Erbα* transcription, by either cigarette smoke (Vasu et al., 2009) or aging and obesity (Sato et al., 2014). YangGuang et al. (2014) also found that LPS reduced *Rev-Erbα* promoter activity in a dose-dependent manner and they identified an unique sequence consisting of overlapping AP-1 and nuclear factor kappa B (NFκB) consensus sequences on the mouse *Rev-Erbα* promoter. However, they could not identify the mechanisms by which NFκB regulates *Rev-Erbα* promoter activity and they suggested that a higher-order regulation at the chromatin level might be involved.

My data showed that REV-ERBα was also down-regulated at the protein level when mice were subjected to LPS (Figure 7.1). *In vitro*, treatment with TNF-α or IL-1β induced a moderate reduction of REV-ERBα proteins in murine and human lung epithelial cells (Figure 7.2). Furthermore, blocking translation using cycloheximide revealed that IL-1β acted directly at the protein levels to reduce REV-ERBα in NHBE cells, as degradation of the protein was quicker in presence of IL-1 β than without inflammatory stimuli (Figure 7.3). To my knowledge, this direct REV-ERBα protein degradation by inflammatory stimuli has never been reported in the literature, probably due to the lack of a good anti-REV-ERBα antibody that we now possess.

However, thanks to REV-ERBα plasmid constructs containing tags such as FLAG, HA, mechanisms of REV-ERBα degradation have started to be elucidated.

7.4.2 REV-ERBα ubiquitination

The ubiquitin–proteasome pathway is responsible for the degradation of nearly all regulated proteins, including circadian clock proteins (Stojkovic et al., 2014). Using His-ubiquitin construct and his-purification method, I was able to show that inflammatory mediators IL-1β or TNFα induced REV-ERBα ubiquitination (Figure 7.4). The ubiquitin system requires the activity of three classes of proteins: E1 ubiquitin-activating enzymes, E2 ubiquitin-conjugating enzymes, and E3 ubiquitin ligases. Specificity of protein ubiquitination is conferred by E3 ubiquitin ligases. There are ∼600 mouse/human genes that encode E3 ligases, and there are thousands of potential E3 ligase substrates in any given cell (Li et al., 2008b), making difficult to identify which E3 ligases ubiquitinate which proteins for degradation. In this project, I did not focus on identifying the E3 ligases involved in inflammation-induced REV-ERBα ubiquitination. However, a few groups have tackled this task and started to identify E3 ligases which target REV-ERBα for degradation. Lazar's group was the first to report that two E3 ligases, Arf-bp1 and Pam (Myc-bp2) were required for REV-ERBα ubiquitination (Yin et al., 2010). Later, Hogenesch's group developed a screening approach aimed at identifying ubiquitin ligases that degrade proteins of interest and found the ubiquitin ligase Seven in absentia 2 (Siah2) as a key regulator of circadian REV-ERBα turnover (DeBruyne et al., 2015).

Moreover, a recent study reported a novel post-translational regulatory circuit in which cyclin-dependent kinase 1 (CDK1) phosphorylation of REV-ERBα was recognized by the F-box protein FBXW7α to target the protein for ubiquitination and subsequent degradation (Zhao et al., 2016). My data suggests involvement of this pathway in inflammation-induced REV-ERBα ubiquitination as using the CDK inhibitor Roscovitine decreased IL-1β ubiquitination of REV-ERBα (Figure 7.5).

7.4.3 REV-ERBα sumoylation

Previous studies have shown that the essential clock component BMAL1 is sumoylated on a highly conserved lysine residue (Lys259), predominantly by poly-SUMO-2/3 rather than SUMO-1 (Cardone et al., 2005; Lee et al., 2008). Both studies highlighted that sumoylation played an important role in BMAL1 circadian expression and clock rhythmicity and Lee et al. (2008) demonstrated that sumoylation was a prerequisite for ubiquitination of BMAL1. They found that mutation of the sumoylation site dramatically decreased the ubiquitination and proteasome degradation of BMAL1. Moreover, they showed that overexpression of SUMO proteases decreased the levels of sumoylated as well as ubiquitinated BMAL1, whereas when using Ubiquitin proteases only ubiquitinated BMAL1 was affected. Similarly, my data demonstrated that sumoylation of REV-ERBα is required for its ubiquination (Figure 7.6). I also showed that REV-ERBα can be conjugated to SUMO-2 and that pro-inflammatory mediator IL-1β induced exaggerated SUMO-2 attachment to REV-ERBα (Figure 7.7). The understanding of this pre-sumoylation/ubiqutination pathway mechanisms has begun to be elucidated thanks to the recent discovery of a functionally conserved family of enzymes known as SUMO-targeted ubiquitin ligases (STUbL) which catalyse the addition of ubiquitin to proteins that have been previously sumoylated (Prudden et al., 2007).

Therefore, my findings suggest that inflammation induces REV-ERBα sumoylation, which then drives the protein ubiquinitation and its subsequent proteosomal degradation. CDK1 phosphorylation of REV-ERBα appears to be a critical step of this pathway and it would be interesting to assess whether this step occurs beforehand sumoylation of the protein.

7.4.4 Sumoylation/ubiquitination pathway blocked by GSK1362

Building on the findings of chapter 6 revealing that treatment with GSK1362 increased protein levels in murine and epithelial cells, I showed in this chapter that this small tool compound acted on REV-ERBα protein itself, delaying the protein degradation (Figure 7.3). Further investigation on post-translational modifications of REV-ERBα revealed that GSK1362 was able to block SUMO-2 conjugation of the protein, even in presence of IL-1 β (Figure 7.7), and therefore the consequent

ubiquitination of the protein (Figure 7.4). This suggests that GSK1362, when binding to REV-ERBα, may change its conformation and mask the SUMO sites or may directly block these sites, protecting the protein from later degradation. In contrast, GSK4112 had no effect on post-translational modifications of REV-ERBα (Figure7.4, 7.7). Hemin had no impact on the protein ubiqutination but induced the formation of poly-sumoylated high molecular complex with REV-ERBα (Figure 7.7C).

Although it has been shown that heme binding increases REV-ERB LBD thermal stability (Raghuram, 2007), my findings constitute the first evidence that a synthetic ligand can stabilize REV-ERBα by preventing from degradation. However, glycogen synthase kinase 3β (GSK3β) has also been reported to stabilizes REV-ERBα through N-terminal phosphorylation preventing its rapid proteasomal degradation (Yin et al., 2006). Consistently, lithium, an inhibitor of GSK3β, leads to degradation of REV-ERBα and activation of the clock gene Bmal1. Lithium is commonly used in the treatment of bipolar disorder and several human genetic studies reported associations between polymorphisms at the Rev-Erbα locus and responsiveness to lithium treatment among patients exhibiting bipolar disorder (Campos-de-Sousa et al., 2010; McCarthy et al., 2011). This suggests that regulation of REV-ERBα activity through control of protein levels may be achieved with small molecules.

7.4.5 Recruitment of HDAC3 upon inflammation

Lazar and colleagues have demonstrated that REV-ERBα exerts its repressive activity through the recruitment of the nuclear co-repressor (NCoR)/HDAC3 complex to the RevRE/RORE present in target gene promoters (Feng et al., 2011; Yin and Lazar, 2005). My data clearly demonstrates that stimulation with pro-inflammatory cytokine IL-1β induced recruitment of HDAC3 to REV-ERBα (Figure 7.8), probably in the aim of repressing inflammatory gene expression. This result highlights the complexity of inflammatory pathways as HDAC3 has been shown to be required for inflammatory gene expression in macrophages (Chen et al., 2012) and that impairment of HDAC3 activity through pharmacological inhibition suppressed inflammatory gene expression in a model of rheumatoid arthritis (Angiolilli et al., 2015).

Moreover, I showed that sumoylation of REV-ERBα facilitated recruitment of HDAC3 (Figure 7.8). To my knowledge, this was the first time that post-translational modifications of REV-ERBα were reported to be critical steps for efficient recruitment of co-repressor complex. This finding also highlights the multiple functions of SUMO proteins as I also showed that SUMO-2 attachment targeted REV-ERBα for degradation (Figure 7.6).

Looking at the effects of ligand binding, GSK1362 had no major impact on HDAC3 recruitment to REV-ERBα, indicating that its main mechanism of action is through protein stabilization, rather than altered protein partner recruitment. In contrast, Hemin treatment induced the formation of a high molecular complex containing REV-ERBα on which HDAC3 was recruited. Studies have demonstrated that heme stabilizes interaction between REV-ERBα and NCoR-HDAC3 (Raghuram, 2007; Yin et al., 2007) and that two REV-ERBα molecules are required for an efficient interaction with NCoR (Everett and Lazar, 2014). Therefore, the high molecular complex observed in presence of Hemin could be constituted of two REV-ERBα molecules which are poly-sumoylated, as evidenced by Figure 7.7C.

7.5 Conclusions

In this chapter, I showed that inflammation *in vivo* and *in vitro* induced REV-ERBα degradation through successive post-translation modifications of the protein. Pro-inflammatory cytokine IL-1β caused sumoylation of REV-ERBα, driving its ubiquitination and subsequent proteosomal degradation. Phosphorylation of the protein by CDK(s) was also required to target REV-ERBα for ubiquitination. Addition of synthetic ligand GSK1362 delayed the degradation of REV-ERBα, acting to block protein sumoylation, and subsequent ubiquitination. On the other hand, IL-1β inflammatory challenge induced recruitment of HDAC3 to REV-ERBα, probably in the attempt of repressing inflammatory gene activation in order to control the immune reaction. These data highlights a new circuit linking inflammation and REV-ERBα, with the existence of two homeostatic arms; one implicated REV-ERBα repressive activity and the other one involving inflammation-induced REV-ERBα protein degradation. This homeostatic system is depicted in

Figure 7.10. Moreover, REV-ERBα degradation by inflammatory signaling offers a new mechanism to explain circadian disruption in chronic inflammatory diseases.
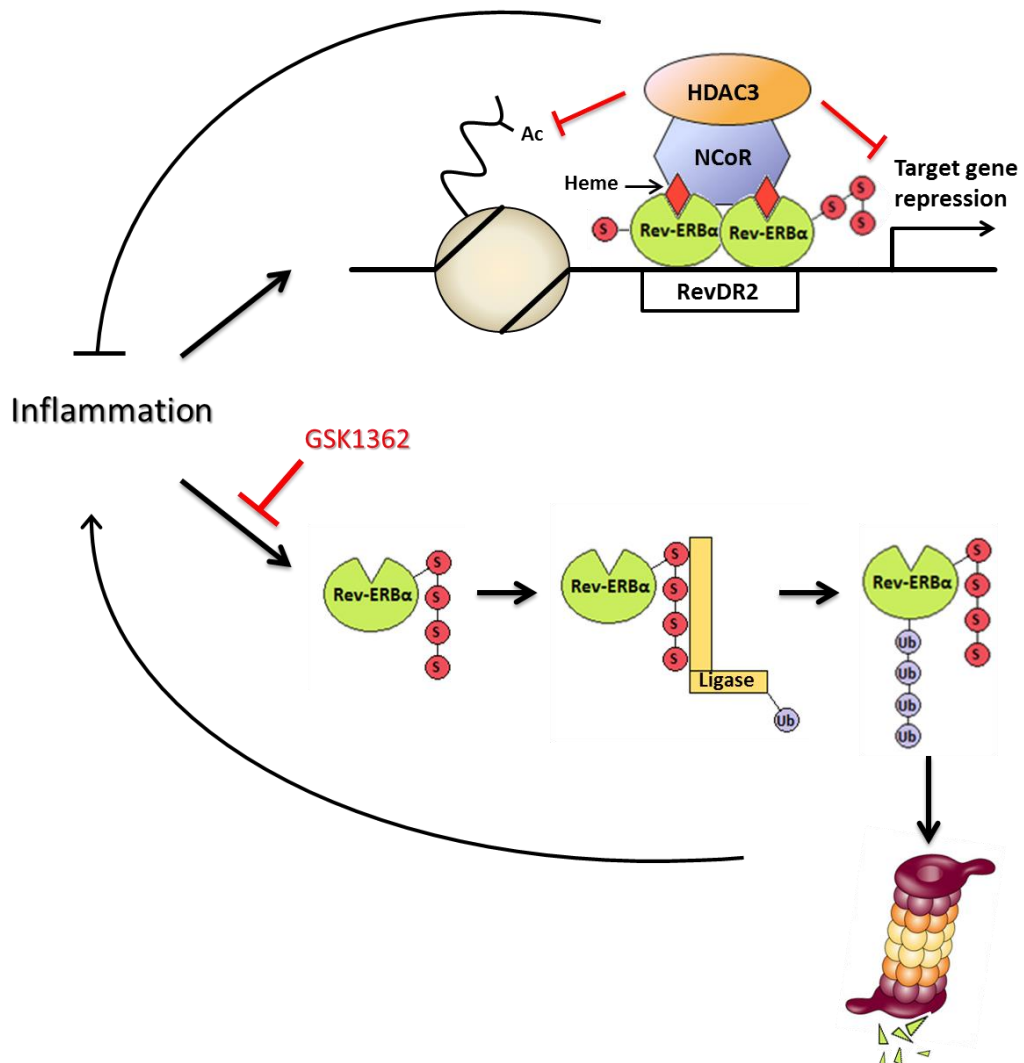
Figure 7.10: Schematic representation of new homeostatic circuit linking inflammation and REV-ERBα

On one arm of the circuit, inflammation induces the DNA binding of two molecules of REV-ERBα on RevDR2 elements which allows the recruitment of co-repressor NCoR/HDAC3 complex in a heme and sumoylation dependent manner. HDAC3 deacetylates surrounding histone tails and represses target gene transcription, probably participating to reduction of inflammation. On the second arm of the circuit, inflammation causes SUMO-2 attachment to REV-ERBα which drives the protein ubiquitination allowing the proteosomal degradation of a repressor and therefore development of a full immune response. Treatment with synthetic REV-ERBα ligand GSK1362 blocks this degradation pathway. A proper equilibrium has to be obtained between these two arms in order to determine the inflammatory set-point and to limit inflammatory activity under resting, non-stress conditions.

Chapter 8:   Discussion

8.1 Summary of key findings

The experiments contained within this thesis have been designed and performed with the aim of elucidating the role of the clock gene and nuclear receptor REV-ERBα in regulating pulmonary inflammation. The key findings are described below.

Rev-Erbα^{-/-} mice exhibit exaggerated pro-inflammatory responses in the lung upon endotoxin and cigarette smoke challenges.

Rev-Erbα^{-/-} mice lack time-of-day variation in neutrophil influx to the lung following endotoxin challenge.

Deletion of REV-ERBα does not disrupt clock gene oscillations in the lung (Figure 3.1), but does abolish the time-of-day variation in neutrophil invasion and pro-inflammatory mediator recruitment into the lung in response to aerosolised lipopolysaccharide challenge (Figures 3.3C, 3.4 and 3.5).

The bronchiolar epithelial cells, and not myeloid cells, are key cell type for REV-ERBα to repress pulmonary inflammation through its ability to bind DNA.

Deletion of REV-ERBα DNA binding domain (DBD) in _Ccsp_-expressing cells leads to exaggerated neutrophilic inflammation upon aerosolized LPS challenge, accompanied with enhanced Cxcl5 expression and release in the airway (Figure 4.4), in contrast to the relatively inconsequential impairment of REV-ERBα DBD function in myeloid cells (Figures 4.7, 4.8).

Impairment of both REV-ERBα and REV-ERBβ in bronchiolar epithelial cells results in a dramatic pulmonary pro-inflammatory phenotype.

Dual deletion of REV-ERBα DNA binding domain (DBD) and REV-ERBβ in _Ccsp_-expressing cells resulted in greatly exaggerated inflammatory responses to LPS, involving more chemokines than in the mouse model lacking REV-ERBα DBD only (Figures 5.3, 5.4, 5.5).

Time-of-day gating of pulmonary inflammation was lost in mice lacking REV-ERBα DBD and REV-ERBβ in bronchiolar epithelial cells.

Impairment of both REV-ERBα and REV-ERBβ function in *Ccsp*-expressing cells resulted in disrupted expression of core clock gene and proteins (Figures 5.1D, 5.2C, 5.5F) as well as loss of time-of-day gating of pulmonary neutrophilic inflammation (Figure 5.6).

Inflammatory stimuli *in vitro* and *in vivo* degraded REV-ERBα protein via post-translational modifications of the protein.

Significant loss of REV-ERBα protein was observed after nebulized LPS (Figure 7.1), which was also seen *in vitro* in response to inflammatory cytokine action, and which required sumoylation of the protein (Figures 7.6, 7.7) for subsequent ubiquitination (Figure 7.4) and proteasome degradation (Figures 7.2, 7.3).

GSK1362, a novel synthetic REV-ERBα ligand, stabilizes the protein by blocking post-translational modifications aimed to the protein degradation, but has divergent effect upon inflammation.

Small tool compound GSK1362 blocked SUMO-2 conjugation of REV-ERBα (Figure 7.7) and its subsequent ubiquitination (Figure 7.4), delaying its proteosomal degradation (Figure 7.3). However, GSK1362 exhibited complex effects upon inflammatory challenges with enhanced or repressed pro-inflammatory mediator expression, depending on the stimulus, on the cytokines/chemokines measured and on the cell type analysed (Figures 6.3, 6.4,6.8, 6.12).

8.2 General discussion

In mammals, the circadian clock is known to regulate multiple aspects of physiology and pathology, including hormone secretion, locomotor activity and response to inflammatory stimuli (Gibbs et al., 2012; Hastings et al., 2007; Keller et al., 2009). Circadian rhythms are thought to have evolved in aerobic organisms to anticipate environmental cycles in energy supply and oxidative stress (oxygen levels driven by photosynthetic bacteria and the solar cycles) (Edgar et al., 2012). They ensure that organisms handle their energy supply efficiently and enhance their ability to survive respiration-associated cycles of oxidative stress. Given the intense energy demands for mounting an immune response (transcription of cytokines and chemokines, cell migration and pathogen neutralisation all require energy), it is therefore not surprising that immunity is under circadian control. Appropriate timing of immune reactions would prevent energy and transcriptional machinery from being diverted away unnecessarily. Over the past few years, evidence has emerged showing that the immune system is regulated in a rhythmic manner, highlighting interactions between clock proteins and immune cell function and therefore suggesting a key role for circadian rhythms in affecting disease onset and therapies.

8.2.1 Evidence of daily variation in the immune response

As early as the 1960s, pioneering studies showed that survival to lethal doses of bacteria or bacterial products in mice varied significantly across a circadian cycle, with enhanced lethality when animals were challenged during the resting phase (light phase) (Halberg et al., 1960; Shackelford and Feigin, 1973). This has recently been investigated further at the cellular levels with experiments assessing isolated splenic and peritoneal macrophage responses to bacterial challenge (Keller et al., 2009). These studies revealed increased release of tumour necrosis factor α (TNFα) and interleukin-6 (IL-6) when cells were challenged with LPS at CT12, the beginning of the active phase for mice. Moreover, the authors performed a microarray analysis on peritoneal macrophages harvested from mice every 4 hours over 24 hours and found that 8% of the macrophage transcriptome was cycling with a circadian variation. When analyzing components of the TLR4 signalling pathway, they found circadian regulation of multiple factors, including regulatory components of NF-κB and

members of the mitogen-activated protein kinase (MAPK) pathways, which drive pro-inflammatory signaling. This indicates that TLR4 pathway in macrophages may be primed to respond more strongly at certain times of the circadian cycle. Gibbs et al. (2012) confirmed this higher sensitivity to LPS at CT12 by using intraperitoneal injection of LPS at either CT0 or CT12. In that experiment, whilst TNFα did not show a significant time-of-day variation, IL-6 and other cytokines such as CCL2 and CCL5 were significantly up-regulated when mice were challenged at CT12 compared to CT0. Moreover, this gating of inflammatory responses required a functional molecular oscillator as temporal variation in IL-6 production was lost in mice lacking BMAL1 in macrophages.

Host defense responses against pathogens also vary according to circadian time. Bellet et al. (2013) showed that circadian clock modulates the inflammatory response during acute intragastric infection with the pathogen *Salmonella enterica* serovar Typhimurium (S. Typhimurium). Mice infected with S. Typhimurium at ZT4 (day time and resting phase) were colonized to higher levels and developed a higher pro-inflammatory response than mice infected at ZT16 (night time and active phase). Moreover, the ability to clear the bacteria from the colon 72 hours post infection was greater in mice inoculated at ZT16 than at ZT4. The authors reported that *Salmonella* colonization over competing microbes in the gut is influenced by circadian expression of antimicrobial peptides. The antimicrobial peptide lipocalin-2, to which *Salmonella* is resistant, exhibits higher levels during the day than at night allowing suppression of susceptible microorganisms in competition with *Salmonella* and therefore better growth of *Salmonella* during the day that at night. Using *Clock* mutant mice, the authors also demonstrated that a functional clock is required for optimal *S*. Typhimurium colonization and maximal induction of several proinflammatory genes.

Adaptive immunity has also been shown to be influenced by the time of day. T cell proliferation after stimulation via the T cell receptor (TCR) vary in a circadian manner, which is blunted in *Clock* gene mutant mice (Fortier et al., 2011). The authors showed that this was not based on the daily variation in the number of T cell subsets in the lymph nodes nor on the expression level of the T cell receptor (TCR). Instead, they demonstrated a circadian variation in the protein levels of the tyrosine

kinase ZAP70, which is just downstream of the TCR in the T cell activation pathway and is crucial for T cell function, suggesting that ZAP70 was the molecular link between time of day and immune function. This study also revealed that the time of immunization has a strong impact on the magnitude of the adaptive immune response. T cell activation, proliferation, and acquisition of effector functions many days later were more important when mice were immunized in the middle of the day at ZT6 than in the middle of the night at ZT18. This provides clues for more efficient vaccination strategies by taking into account the time of administration.

Blood leukocyte numbers have long been known to exhibit circadian oscillations (Haus and Smolensky, 1999) and circadian rhythms in immune cell trafficking may explain temporal variations of immune responses. Leukocytes in the mouse circulation reach their highest levels at ZT5 which coincide with the increased vaccination efficacy seen at ZT6 by Fortier et al. In contrast to the day time peak of haematopoietic cell numbers in the blood, the migration of haematopoietic cells to tissues preferentially occurs during the night. In mice, the homing of neutrophils to the bone marrow, as well as monocyte recruitment to skeletal muscle peak at ZT13 and are thought to be regulated by rhythmic expression of endothelial cell adhesion molecules (e.g., ICAM-1 and VCAM-1) and chemokines (Scheiermann et al., 2012). This night-time leukocyte homing coincides with higher sensitivity to LPS with increased release of cytokines at CT12 (Gibbs et al., 2012; Keller et al., 2009).

This temporal increase in leukocyte trafficking in the hours around the beginning of the active phase is interpreted as being indicative of a clock-controlled enhanced sensitivity and immunosurveillance when the animals are active and more likely to encounter pathogens. However, this explanation does not fit the temporal variation of inflammatory responses observed in the lung. Indeed, the magnitude of neutrophilic inflammation within the lung is greater when mice were challenged with aerosolized LPS at CT0 or ZT0, the beginning of the resting phase, than at CT12 or ZT12 (Gibbs et al., 2014 and Figures 3.3, 5.6). The reason of why the lung is more susceptible to bacterial challenge at the onset of the day and resting phase is still elusive and would merit further investigation. It is important to stress that the lung is an unique site for neutrophil migration; in the lung parenchyma, neutrophils exit the pulmonary circulation at the capillary level, rather than via postcapillary venules, as in the

systemic circulation. Therefore, neutrophils must deform to pass through restrictions encountered in the pulmonary capillary bed, increasing neutrophil retention time within the lung which may be amenable to selective interventions (Doerschuk et al., 1993). More recently, this neutrophil retention in the lung has been found to facilitate neutrophil depriming mechanisms to release them back into the systemic circulation in a quiescent state (Summers et al., 2014).

Instead of correlating greater immune reactions to anticipation of the active phase and higher risk of infection, it would be interesting to consider linking temporal variation of immunity to circadian variation of energy metabolism. This would explain better the difference in timing of greater inflammatory responses across different tissues and organs as metabolic processes and energy supplies are handled differently through the body. Recently, this hypothesis has presented an accelerating interest, supported by growing body of evidence reporting multi-level interactions between the metabolic and immune systems (Delmastro-Greenwood and Piganelli, 2013; Mathis and Shoelson, 2011; Rathmell, 2012).

8.2.2 Clock proteins in immune cell function

Over the past few years, clock proteins have been shown to interact with key immune signalling molecules, either by modulating their transcription or via protein-protein interactions. In this section, impact of core clock components BMAL1, CLOCK, PERs, CRYs, REV-ERBs and RORs on the immune system is discussed.

8.2.2.1 BMAL1/CLOCK

The two basic helix-loop-helix (bHLH)-PAS domain transcription factors, CLOCK and BMAL1 form a heterodimer, which constitutes the positive arm of the molecular oscillator and binds to E-boxes to promote transcription. BMAL1 is a key clock component as it is the only clock gene of which global deletion renders mice arrhythmic at cellular and behavioral levels (Bunger et al., 2000). *Bmal1* knock-out mice also have reduced lifespans and display various symptoms of premature aging (Kondratov et al., 2006) as well as reproductive deficiencies (Alvarez et al., 2008) making them unsuitable for assessing immune function. However, by using mouse

models with cell specific knock-out of *Bmal1*, the role of BMAL1 in regulating immunity has been investigated. Deletion of *Bmal1* in myeloid cell lineage disrupts the gating of inflammatory responses upon *in vivo* LPS challenge and induced exaggerated IL-6 levels in peritoneal macrophages challenged with LPS at ZT0 compared to wild-type peritoneal macrophages (Gibbs et al., 2012). Curtis et al. (2015) also showed that mice deficient in myeloid BMAL1 have an increased risk of LPS-induced sepsis with heightened induction of the pro-inflammatory microRNA miR-155 and NF-κB activity. Another study found that mice with myeloid cell specific deletion of BMAL1 present a decreased survival rate during an infectious challenge with the gram-positive bacterium *Listeria monocytogenes* compared to wild-types (Nguyen et al., 2013). The authors showed that this specific deletion of *Bmal1* impaired diurnal variations in Ly6C^{hi} inflammatory monocyte numbers (first line defense against *L. monocytogenes)* in blood, spleen, and bone marrow. They suggested that BMAL1:CLOCK heterodimer negatively regulated expression of CCL2 in monocytes, which likely contributed to the circadian oscillations of Ly6C^{hi} inflammatory monocytes. Apart from *Ccl2*, Toll-like receptor TLR9, the pattern recognition receptor that recognizes bacterial and viral DNA, has also been shown to be regulated by BMAL1:CLOCK heterodimer (Silver et al., 2012). Conducting ChIP assays in serum-entrained peritoneal macrophages, the authors found that BMAL1:CLOCK heterodimer bound to the promoter of *Tlr9*, which contains two putative E-boxes, and promoted its expression and function in a circadian manner. The control of BMAL1:CLOCK on *Tlr9* expression has a strong impact on the adaptive immune system as mice immunized at the time of enhanced TLR9 responsiveness, at ZT19, presented strong innate immune reactions with an improved adaptive immune response. In the lung, deletion of BMAL1 in epithelial cells results in exaggerated neutrophilic inflammation at all time points measured (Gibbs et al., 2014). However, as described in this thesis in chapters 4 and 5, this pro-inflammatory phenotype was most likely a consequence of the consequent deletion of the REV-ERBs.

The BMAL1 binding partner CLOCK has also been shown to regulate immune signal. The Antoch group (Spengler et al., 2012) have reported a novel mechanism of rhythmic inflammatory signalling in which the daily variations in the intensity of the NF-κB response to a variety of immunomodulators were mediated by CLOCK,

independently of BMAL1. Using coimmunoprecipitation assays, CLOCK was found in protein complexes with the p65 subunit of NF-κB, and its overexpression leaded to an increase in specific phosphorylated and acetylated transcriptionally active forms of p65. Moreover, overexpression of BMAL1 counteracted the CLOCK-dependent increase in the activation of NF-κB–responsive genes probably by sequestering and degrading CLOCK (Spengler et al., 2009). Consistent with these findings, the authors showed that NF-κB activation was impaired in *Clock*-deficient cells and livers of *Clock* knock-out mice. Because expression of CLOCK is nearly constitutive during the circadian cycle at both the mRNA and protein levels (Lee et al., 2001), Spengler et al. hypothesized that CLOCK mediated NF-κB activity is rhythmically modulated by BMAL1 by mediating the nuclear translocation and then site-specific phosphorylation/degradation of CLOCK. This suggests another mechanism by which BMAL1 could limit inflammation.

8.2.2.2 PERs and CRYs

The PERIOD (PER) and CRYPTOCHROME (CRY) proteins constitute the negative arm of the 'core' feedback loop, each encoded by separate genes (Per1-3 and Cry1-2). In the molecular oscillator, these proteins form an heterodimer which suppresses the activity of the CLOCK:BMAL1 complex, but these proteins can also independently impact upon immune pathways.

Per2 knock-out mice exhibit elevated levels of c-myc (a proliferative gene) and reduced p53 (antiproliferative) expression concomitant with increased γ-irradiation-induced rates of cell proliferation and lymphoma (Fu et al., 2002). Another study reported that *Per2*-deficient mice were more resistant to lipopolysaccharide (LPS)-induced endotoxic shock than control wild-type mice at all time points analyzed, which could be explained by a dramatically reduced levels of the proinflammatory cytokines gamma interferon (IFN-γ) and interleukin-1β (IL-1β) in the serum of LPS-treated *Per2* knock-out mice (Liu et al., 2006). Moreover, deficiency in PER2 also reduces expression and function of the Toll-like receptor TLR9 (Silver et al., 2012). Therefore, PER2 may positively regulate pro-inflammatory cytokines at specific times of the circadian cycle and this potentially by repressing the activity of BMAL1.

Dual deletion of *Cry1* and *Cry2* in bone marrow-derived macrophages and fibroblats leads to constitutive elevation of pro-inflammatory cytokine expression such as *Il-6*, *Tnf-α*, and *Inos* (Narasimamurthy et al., 2012). This was explained by observation of exaggerated activation of protein kinase A (PKA) signalling, which increased phosphorylation of p65 and caused constitutive NF–κB stimulation in *Cry1*$^{-/-}$;*Cry2*$^{-/-}$ cells. The authors suggested that the increase in PKA signaling activity was likely induced by the significantly high basal level of cAMP detected in these cells. This hypothesis was verified by demonstrating that CRY1 binds to adenylyl cyclase to block its function and suppress the cAMP production. These results offer an additional mechanism linking the circadian clock to the NF-κB pathway where CRY, a component of the negative arm of the feedback loop, acts as an immuno-suppressor. This could explain that *Cry1*$^{-/-}$;*Cry2*$^{-/-}$ mice developed maximal exacerbation of joint swelling, and upregulation of TNF-α production in a model of collagen-induced arthritis (Hashiramoto et al., 2010). These findings has been supported by a recent study showing that CRY1 and 2 repressed inflammation within the fibroblast-like synoviocytes (FLSs) of the inflamed limbs in the same model of collagen-induced arthritis (Hand et al., 2016). The authors also provided novel evidence that a CRYPTOCHROME activator, KL001, has anti-inflammatory properties in murine and human FLSs, highlighting CRY activity as a novel avenue for therapeutic development in rheumatoid arthritis.

8.2.2.3 REV-ERBs and RORs

The REV-ERBs (α and β) and RORs (α, β and γ) form the auxiliary loop of the molecular clock machinery and both bind same retinoic acid-related orphan response elements (ROREs) while exerting opposite effects on transcription (REV-ERBs are repressors, RORs are activators). Both REV-ERBs and RORs are nuclear hormone receptors, and whilst heme has been identified as an endogenous ligand for REV-ERBs (Raghuram, 2007), the nature of endogenous ligands for the ROR family has yet to be elucidated. However, cholesterol derivatives were identified as RORα agonists (Kallen et al., 2004).

As described briefly in chapter 3, REV-ERBα has shown to be a critical intermediary between the core clock and inflammatory pathways, especially in macrophages.

REV-ERBα was first shown to block pro-inflammatory signals in macrophages by repressing the Toll-Like Receptor 4 (TLR4) gene, which triggers the innate immune response to LPS (Fontaine et al., 2008). More recently, a study reported that circadian gating of IL-6 response to endotoxin challenge was lost in mice lacking *Rev-Erbα* and in cultured macrophages from these animals (Gibbs et al., 2012). Moreover, the authors showed REV-ERBα synthetic agonist ligand GSK4112 reduced the expression of a set of cytokines in macrophages subjected to LPS. Although, the mechanism behind this pharmacological effect has yet to be elucidated, it is hypothesized that synthetic ligands facilitate the recruitment of the repressor complex NCoR-HDAC3 to pro-inflammatory gene promoters. Consistently, Sato et al. (2014), found that REV-ERBα repressed murine *Ccl2* promoter activity via direct binding to a RORE located in the proximal *Ccl2* promoter region in macrophages. Recent mapping of the macrophage Rev-Erbα and Rev-Erbβ cistromes suggests that Rev-Erbα controls gene expression in macrophages through the repression of enhancer-derived RNA (eRNA) transcription (Lam et al., 2013). eRNAs are short RNA strand produced from an enhancer site and play a role in the transcription of an adjacent gene. By performing ChIP-Seq, the authors found for example REV-ERB binding sites vicinal to the metalloproteinase *Mmp9* and the chemokine receptor *Cx3cr1* genes. This was confirmed by qPCR showing up-regulation of *Mmp9* and *Cx3cr1* mRNAs in macrophages lacking both REV-ERBs and repression of *Mmp9* and *Cx3cr1* in macrophages with overexpression of either Rev-Erbα or Rev-Erbβ. These findings suggest that the REV-ERBs can also repress inflammatory gene expression by binding not at the promoter but further downstream at enhancer regions, repressing then eRNA transcription which in turn would repress inflammatory gene expression. The work contained in this thesis constitutes an additional argument proving the critical role of the REV-ERBs to regulate immune responses with a focus on pulmonary inflammation.

RORs have been implicated in the regulation of thymopoiesis with RORγ showing to be essential for the development of several secondary lymphoid tissues, including lymph nodes (Eberl et al., 2004). Mice lacking RORα, also called *staggerer* mice, display a higher degree of LPS-induced inflammation than wild-type mice with enhanced levels of IL-1β, IL-6 CXCL2 in BAL fluids (Stapleton et al., 2005). RORα also contributes to immune function in the intestinal epithelium by controlling the

diurnal regulation of several pathogen recognition receptors, including Nod2 and various Toll-like receptors (Mukherji et al., 2013). A recent study has proposed a new "facilitated repression" model indicating that RORs promote REV-ERBs loading on DNA via chromatin decondensation and thus favour its repressive activity (Zhu et al., 2015). Therefore, effects of loss of RORs may be attributed to reduced REV-ERB DNA binding and consequent activity.

8.2.3 CXCL5, a key chemokine for neutrophil recruitment, regulated by REV-ERBα and REV-ERBβ

The CXCR2 receptor and its ligands are critical elements in the recruitment of neutrophils to sites of inflammation (Kobayashi, 2006). CXCR2 binds chemokines with the ELR motif (Glutamic acid-leucine-arginine), including CXCL1 (also named keratinocyte-derived chemokine, KC), CXCL2 (also known as macrophage inflammatory protein 2, MIP-2), CXCL5 (also named LPS-induced CXC chemokine, LIX) and CXCL15 (also known as lungkine). Because these chemokines target the same receptor, they were generally considered redundant. Yet, the different cellular sources of these chemokines suggested distinct spatial regulation and function. Indeed, CXCL1 and CXCL2 are secreted by myeloid cells such as macrophages and neutrophils, whereas CXCL15 is produced by bronchial epithelial cells (Bhatia et al., 2012). CXCL5 has been shown to be secreted by type I and II alveolar epithelial cells (Jeyaseelan et al., 2005) but also by bronchial and bronchiolar epithelial cells (Gibbs et al., 2014; Nouailles et al., 2014). My own work also showed that Normal Human Bronchial Epithelial (NHBE) cells express CXCL5 (Chapter 6). Therefore, the cellular source of CXCL5 appears to be the respiratory epithelium in general. Although the role of CXCL1 and CXCL2 in neutrophil recruitment to inflamed lungs is well appreciated in various infectious diseases (Moore et al., 2000; Tsai et al., 2000), the function of CXCL5 has started to be elucidated only recently.

In studies using specific blocking antibodies, Worthen group demonstrated a key role for CXCL5 for inducing neutrophil accumulation in the lungs upon LPS challenge (Jeyaseelan et al., 2005) and regulating consequent pulmonary inflammation (Mei et al., 2010). Moreover, another study has shown that upon *Mycobacterium tuberculosis* infection, CXCL5 was expressed earlier and more abundantly than other

chemokines (CXCL1 and CXCL2) and its expression correlated with M. tuberculosis infection dose (Nouailles et al., 2014). Using a *Cxcl5* knock-out mouse model, the authors showed that CXCL5 was largely responsible for neutrophil recruitment into the lungs upon tuberculosis. *Cxcl5$^{-/-}$* mice exhibited enhanced survival compared to wild-types following high dose *M. Tuberculosis* infection. This was not due to heightened bacterial clearance but was the result of impaired neutrophil recruitment and consequent reduced lung inflammation.

My thesis results confirmed the essential role of CXCL5 in recruiting neutrophils into the lungs upon aerosolized LPS challenge. Through all my experiments, the higher CXCL5 levels were measured either in BAL samples or lung homogenates at transcript levels, the more neutrophils were detected in BAL samples when mice were exposed to nebulized LPS. However, in homeostatic conditions, augmented CXCL5 in BAL samples was not always associated with increase in neutrophil numbers in the airways. Indeed, mice with dual impairment of REV-ERBα and β in bronchiolar epithelial cells exhibited a constant elevation (through the day) of CXCL5 at protein level in the airway space and at transcript level in the bronchioles in unchallenged conditions compared with their littermate controls. Yet, neutrophil numbers were increased in the double mutant mice compared with controls only at the onset of the day. This suggests that secretion of CXCL5 into the airway space is not sufficient for neutrophil invasion in homeostatic conditions and that another parameter is required. Identification of such parameter would warrant further investigation but it could be correlated to temporal differences in permeability of the endothelial barrier or in neutrophil numbers in the blood.

But one the main and novel findings of my thesis work was the identification of the nuclear receptors REV-ERBα and REV-ERBβ as regulator of CXCL5 expression in the respiratory epithelium. Although impairment of one paralog, REV-ERBα was sufficient for an up-regulation of CXCL5, a dual impairment of both REV-ERBs induced a dramatic up-regulation of the chemokine both in homeostatic and LPS-challenged conditions. Further work would be warranted to fully understand the underlying mechanisms but the ability of REV-ERBα to bind DNA appeared to be crucial (Chapter 4). A successful Chip-Seq study of REV-ERBα in the lung could allow to assess whether the nuclear receptor binds directly on *Cxcl5* gene (either at

the promoter or at an enhancer region) or binds to another gene which regulates *Cxcl5* expression.

8.2.4 The role of glucocorticoids and the glucocorticoid receptor in inflammation

Natural and synthetic glucocorticoids (Gc) are very potent anti-inflammatory molecules and remain at the forefront for treatment of chronic inflammatory diseases such as asthma, rheumatoid arthritis, inflammatory bowel disease and autoimmune diseases, all of which are associated with increased expression of inflammatory genes. Although much has been learnt about Gc mechanism of action over the 60 years since their discovery, much also remains unknown and the past few years have provided crucial mechanistic insights especially into the dynamic nature of the glucocorticoid receptor (GR) interactions with DNA.

Glucocorticoids bind to GRs in the cytoplasm which then dimerize and translocate to the nucleus, where they bind to positive glucocorticoid response elements (GRE) or negative glucocorticoid response elements (nGRE) on glucocorticoid-responsive genes, resulting in increased or repressed transcription respectively. GR can regulate transcription directly through recruitment of co-factors and chromatin remodelling complexes such as nuclear co-repressor 1 - NCoR (Chen and Evans, 1995) or indirectly through interacting with other transcription factors. As GREs are absent from the promoter regions of most inflammatory genes, the anti-inflammatory effects of GR signalling are thought to mainly be achieved by indirect repression between activated GRs and activated transcription factors, such as NF-κB and activator protein-1 (AP-1) which regulate inflammatory gene expression (Caldenhoven et al., 1995).

The findings contained in this thesis clearly demonstrate a critical role of the REV-ERBs in regulating lung inflammation and it would be legitimate to investigate whether any interaction exists between REV-ERBs and GR. It is interesting to note that concentrations of corticosterone, the endogenous Gc in rodents, vary across the day in the bloodstream, and peak around ZT12 (Malisch et al., 2008), therefore concomitant with REV-ERB zenith (Figure 3.1).

Moreover, genome-wide mapping of GR occupancy in relation to chromatin landscape has previously revealed binding sites in the proximal CXCL5 promoter on an enhancer element (John et al., 2008). This was confirmed recently by chromatin immunoprecipitation (ChIP) studies measuring GR occupancy at this element (Gibbs et al., 2014). The authors also found that GR occupancy at the *Cxcl5* locus showed circadian oscillations and as expected, the pattern of GR binding was in anti-phase to that of *Cxcl5* expression, peaking at CT12 when endogenous glucocorticoid production is most pronounced. My thesis results suggest that neutrophil recruitment to the lung upon bacterial challenge is driven by CXCL5 of which the expression may depend to the ability of REV-ERBα to bind DNA in the bronchiolar epithelial cells (Chapter 4). Therefore, CXCL5 expression appears to be regulated by both GR and REV-ERBα, highlighting a potential interaction, direct or indirect, between these two nuclear receptors, supported by the fact that the chromatin occupancy for GR and REV-ERBα protein levels both display circadian rhythms which are in phase. Furthermore, Gibbs et al. (2014) found that GR recruitment to *Cxcl5* locus was reduced and no longer rhythmic in mice with bronchiole-specific ablation of *Bmal1*, leading to enhanced CXCL5 expression. But as discussed previously (Chapter 5), some of the effects of this *Bmal1* cell specific knock-out appeared to be a result of the consequent deletion of the REV-ERBs suggesting again a possible interplay between REV-ERB and GR. Finally, work in the lab and under review for publication, has revealed a large overlap between GC-regulated genes and REV-ERBα (58%) and REVERBβ (53%) target genes. In support of this, GR and REVERBα were found in the same molecular complexes by co-immunoprecipitation in HEK cells (experiment carried out by myself), suggesting a direct modulatory effect of REVERBα in shaping GC-response. This study was mainly focused on offering new mechanisms of GR action on energy metabolism but a potential interaction between GR and REV-ERBs, controlling both time-of-day variation and also magnitude of pulmonary inflammation, would warrant further investigation.

8.2.5 Circadian component in human health and disease

In humans, the impact of disrupted rhythms on health has been relatively well described and is now generally accepted. Shift work and chronic jetlag are linked to

increased risk and progression of cancer (Filipski et al., 2004; Straif et al., 2007), diabetes (Axelsson and Puttonen, 2012) and stroke (Brown et al., 2009). Circadian rhythms may also influence the outcome of patients in the intensive care units (ICUs) with critical illnesses. In a rat model of sepsis, animals kept under constant conditions exhibited significant reduced survival compared to the animals maintained under a 12:12 hour light-dark cycle (Carlson and Chiu, 2008), suggesting that enforced increased light/dark contrast in the intensive care unit could improve the recovery of patients with sepsis. Awareness of the importance of minimizing circadian disruption and improving circadian system chronoenhancement in ICUs is now rising and some practical countermeasures are starting to be put in place to make these units optimal healing environments for patients (Engwall et al., 2015).

Moreover, it is now well known that inflammatory diseases such as asthma, rheumatoid arthritis (Buttgereit et al., 2015) and atherosclerosis (McAlpine and Swirski, 2016) display strong circadian components with exacerbations at night and in the early hours of the morning. Symptoms of asthma frequently show exacerbation at around 04:00. Sudden death in asthma also tends to occur at this time. In a survey of 7729 patients with asthma, 74% awoke at least once a week in the early morning hours with symptoms such as wheezing and shortness of breath and 40% reported having these symptoms on a nightly basis (Litinski et al., 2009). There are three defining components of asthma; chronic inflammation, airway hyper-responsiveness and reversible airway obstruction and each of these parameters exhibit 24-hour fluctuations with worsening around 4 AM compared to 4 PM. First, lung function follows a diurnal rhythm, with improved pulmonary function during the day and the amplitude of this rhythm is far more pronounced in patients with nocturnal asthma (Hetzel and Clark, 1980). Furthermore, patients with symptoms and signs of 'nocturnal asthma' exhibit significantly higher concentrations of inflammatory markers in the distal airways (such as leukocyte, neutrophil and eosinophil counts) at 4 AM compared to 4 PM (Kraft et al., 1996). Increase in neutrophils and eosinophils correlates with the overnight decrements in forced expiratory volume in 1 s (FEV_1). An important lesson to be learned from these studies is that asthma medication may be more effective at preventing attacks if it is given at certain times of day. Indeed, a series of investigations has confirmed the advantage of chronotherapy for asthma. For instance, a study showed that administration of the corticosteroid prednisone at 3

PM rather than 8 AM or 8 PM is more effective in preventing a nocturnal drop of FEV_1 and improving the respiratory inflammatory profile in patients with nocturnal asthma (Beam et al., 1992). Furthermore, the inhaled steroid Triamcinolone, given once a day between 3 PM and 5 PM had better effect on improvements in FEV_1 and nocturnal awakenings, than given once at 8 AM, and similar effect to a four-time a day dosing (Pincus et al., 1997).

Patients with Chronic Obstructive Pulmonary Disease (COPD) also exhibit exacerbated symptoms at night and early in the morning, contributing to sleep disturbance, limited morning activities, and poor health status (Lopez-Campos et al., 2013). Epidemiological data indicate that more than 75% of patients with COPD may experience nocturnal symptoms (Agusti et al., 2011). Another study showed that morning symptoms were also a burden to patients with COPD, with the majority reporting troublesome phlegm and cough upon waking or in the early morning (Kessler et al., 2011). While work has been done to characterize these nighttime and early morning symptoms among patients with COPD in various populations, the impact and factors associated with these symptoms is not well understood (Stephenson et al., 2015). A growing body of evidence suggests that COPD symptoms such as abnormal airway inflammation could be caused by disrupted circadian rhythms within the lung. A study reported that expression of the core clock genes *BMAL1*, *PER2*, *CRY1*, and *REV-ERBα* was reduced in peripheral blood mononuclear cells (PBMCs), sputum cells, and lung tissues from smokers and patients with COPD when compared with nonsmokers (Yao et al., 2015). This is believed to be due to the reduction of Sirtuin1 (SIRT1) in lungs of smokers and patients with COPD (Rajendrasozhan et al., 2008). SIRT1 is an NAD+-dependent deacetylase which affects clock function by binding with CLOCK:BMAL1 complexes and deacetylating BMAL1 and PER2 proteins (Belden and Dunlap, 2008; Nakahata et al., 2008). It has been showed that cigarette smoke (CS) induced post-translational carbonyl modifications on SIRT1 cysteine residues, decreasing its enzymatic activity and marking the protein for proteasomal degradation (Caito et al., 2010). Confirming these findings, a study showed that *BMAL1* was acetylated and degraded in the lungs of mice exposed to CS and in patients with COPD, compared with lungs of the nonsmoking controls, linking *BMAL1* reduction mechanistically to CS-induced reduction of SIRT1 (Hwang et al., 2014). Thus, my own data, showing

reduction of *Rev-Erbα* transcripts upon 10-day cigarette smoke exposures (Figure 7.1) could be explained by CS-induced SIRT1 degradation leading to acetylation and degradation of *Bmal1* and subsequent reduction of *Rev-Erbα* transcription. Moreover, Yao et al. (2015) found that treatment with SIRT1 activator SRT1720 attenuated LPS-mediated reduction of *BMAL1* and *REV-ERBα* in PBMCs from nonsmokers and inhibited LPS-induced cytokine release.

Overall, these data indicate that environmental CS affects molecular clock function in lung tissue via the reduction of SIRT1, which in turn leads to inflammatory responses. This pathway could explain the symptoms observed in the pathogenesis of COPD and emphysema.

Therefore, chronic airway inflammation, typical of asthma and COPD, might be caused through disruption of the molecular clock. To my knowledge, no genome wide association study (GWAS) has uncovered critical single nucleotide polymorphisms (SNPs) of clock genes associated with lung diseases, although one study showed a marginal association of a polymorphism in the CLOCK gene (rs1522113) with bronchodilator response in asthmatics (Duan et al., 2014). Future research using clock gene knockout mice, and studies in patients with asthma and COPD might provide insights to the role of molecular clock genes in the development and persistence of chronic inflammatory diseases.

8.2.6 Future work

Multiple lines of research directly follow on from the results presented in this thesis and it is anticipated that the investigations proposed below will enhance our knowledge about how both REV-ERBα and β control rhythmic pulmonary immune responses.

8.2.6.1 Role of REV-ERBβ in regulating pulmonary inflammatory responses upon aerosolised LPS challenge

In chapter 5, I clearly demonstrated a significant compensatory role of REV-ERBβ, in that impairment of both REV-ERBα and β in the bronchiolar epithelium resulted

in greatly exaggerated inflammatory responses to LPS, compared to effects of REV-ERBα mutation only. It will be now interesting to generate a new mouse model lacking only REV-ERBβ in bronchiolar cells and assess the responses of these mice to an aerosolized LPS challenge. As described in chapter 5, a prediction will be that this mutation would not result in a pro-inflammatory upon LPS as it would be compensate by REV-ERBα, which could form dimers, recruit NCoR and repress pulmonary inflammation. Performing that experiment would allow us to fully understand REV-ERBβ contribution in regulating lung inflammation.

8.2.6.2 Potential interplay between GR and REV-ERBs to control rhythmic pulmonary inflammatory responses

As described earlier, evidence suggests a potential interplay between GR and REVERBs, especially in regulating CXCL5 expression. It seems now important to further investigate the potential existence of such an interaction in the lung, which could control both time-of-day variation and magnitude of pulmonary inflammation.

A first experiment could be to assess the effect of dexamethasone (a synthetic Gc) pre-treatment on pulmonary inflammatory responses to aerosolized LPS challenge in mice lacking both REV-ERBβ and REVERBα DBD in bronchiolar epithelial cells (mouse model studied in chapter 5). If the REV-ERBs act as co-partners of GR, a prediction would be that the normal repression of LPS-induced inflammation by dexamethasone would be lost in these animals.

8.2.6.3 Role of REV-ERBα in regulating pulmonary chronic inflammatory diseases such as asthma and COPD

One of the difficulties of investigating this topic is to develop a decent model of chronic inflammation which accurately reflects disease pathophysiology of asthma and COPD, both very complex diseases in their heterogeneity.

At the moment, the best and most widely used mouse model of COPD remains cigarette smoke exposure, as long-term exposure to cigarette smoke is considered to

be the main risk factor for this disease. The main characteristic features of human COPD such as neutrophilia, production of cytokines, chemokines and proteases, oxidative stress, small airway fibrosis/remodelling, mucus hypersecretion, lung dysfunction and development of emphysema can all be replicated in mice exposed to cigarette smoke. Some variations on this cigarette smoke model, related to exposure time, the association of other inducers or inhibitors, exacerbations or the use of transgenic animals have been developed to facilitate the identification of pathogenic pathways. However, it is clear that no one animal model is an exact mimic of human COPD and each choice of an animal model has its own benefits and deficiencies (Vlahos and Bozinovski, 2014).

Most mouse models of asthma involve short-term challenge of sensitized mice with ovalbumin (OVA) as antigen delivered either by inhalational exposure or intratracheally. This primarily drives an eosinophilic, allergic inflammatory reaction. Before the start of my project, the role of REV-ERBα on responses to allergic inflammatory challenge using the OVA model was assessed by sensitizing $Rev\text{-}Erb\alpha^{-/-}$ mice with OVA and challenging them by intranasal administration. Although OVA challenge induced a significant increase in eosinophils in the lung, no differences were seen between $Rev\text{-}Erb\alpha^{-/-}$ mice and wild-type littermate controls.

This OVA model is experimentally convenient, but given the nature of the antigenic challenge, it is relevant only to allergic/eosinophilic asthma in humans. The majority of children with asthma have evidence of allergy/atopy, but asthma of adult onset is frequently non-eosinophilic (Bush and Menzies-Gow, 2009). To circumvent this issue, researchers recently switched to using topically delivered house dust mite allergen (HDM) to model allergic asthma, even if further characterization of this model is necessary (Phillips et al., 2013). In the near future, a colleague at University of Manchester is going to employ HDM model in $Rev\text{-}Erb\alpha^{-/-}$ mice, which will give us a more comprehensive picture of the role of REV-ERBα in regulating pulmonary chronic inflammatory diseases.

8.3 Conclusion

In summary, the work presented in this thesis constitutes novel findings highlighting a new circuit lying between the circadian clock and inflammation, involving major homeostatic networks targeting REV-ERBα protein. While I showed that REV-ERBα was a critical repressor of pulmonary inflammatory responses, the nuclear receptor was also targeted for degradation upon inflammatory stimuli. I also demonstrated that the bronchial epithelium plays a dominant role in the timing of pulmonary innate immunity by the actions of REV-ERBs. Identification of REV-ERBα degradation as a robust early response to inflammation supports a homeostatic role in determining the inflammatory set-point, and limiting inflammatory activity under resting, non-stress conditions, as evidenced by the constant high basal production of chemokines in the bronchial epithelium of double mutant mice. REV-ERBα has been proposed as a tractable drug target for metabolic disorders, and also possibly for inflammatory diseases. The highly variable responses seen with the new ligand GSK1362, with high binding affinity for REV-ERBα, suggest that any such therapeutic development would require careful consideration, not least as the pattern of response differs between cell-types. Therefore, the emerging role of REV-ERBs as cell-type specific mediators of timing information and control to inflammatory response gives new insights into an ancient homeostatic control system and REV-ERBα agonists could become potential human therapeutics once their molecular and physiological tissue-specific effects will be fully understood.

Appendices

Appendix 1 - Genotyping reactions, primer sequences and gel recipe

Rev-erb Alpha & Beta Floxed

Primers:

Name	Sequence
ALPHA Lf	5'CATTACCAGTAAGTCAATGCCCAGC3'
ALPHA Er	5' GAAGAGTGTGTGTTTGCCCAAGAGG 3'
BETA Lf	5'-TCATCGCTCCAGTCTCCTACATTTC 3'
BETA Er	5'GGAAGTGCTCCAACAAGGTAGTGCA3'

PCR Master Mix:

	Rev-erb Alpha & Beta Flox (25 µl reaction)				
	X 1	**X10**	**X 20**	**X 25**	**X 30**
Water	14.05	140.5	281	351.25	421.5
Buffer	5	50	100	125	150
$MgCl_2$	2	20	40	50	60
dNTP (10mM)	0.5	5	10	12.5	15
Primer 1 (100 µM)	0.125	1.25	2.5	3.125	3.75
Primer 2 (100 µM)	0.125	1.25	2.5	3.125	3.75
Go TAQ	0.2	2	4	5	6
gDNA	3	3	3	3	3

PCR Cycling Conditions:

Heated Lid = 110ºC

Temperature	Time
94°	3 mins
Start Cycle	
94°	1min
62°	1min
Repeat cycle x 2	
72°	5 mins
Start cycle	
94°	30s
62°	1 min
72°	1 min
Repeat cycle x 30	
72°	3 mins

Hold at 4ºC

Rev-Erbα WT band: 769bp   Rev-Erbβ WT band: 983bp
Rev-Erbα Floxed band: 956bp   Rev-Erbβ Floxed band: 1182bp
Rev-Erbα Null (knock-out) band: 420bp   Rev-Erbβ Null (knock-out) band: 443bp

CCSP^{iCre}

Primers:

Name	Sequence
iCre Forward	5'-TCTGATGAAGTCAGGAAGAACC-3'
iCre Reverse	5'-GAGATGTCCTTCACTCTGATT-3'

PCR Master Mix:

Ccsp^{iCre} genotyping (25 µl reaction)				
	X 1	**X 10**	**X 20**	**X 30**
Water	14.72	147.2	294.4	441.6
Buffer	5	50	100	150
MgCl$_2$	2	20	40	60
dNTP (2.5mM)	1.959	19.59	39.18	58.77
Primer 1 (100 µM)	0.098	0.98	1.96	2.94
Primer 2 (100 µM)	0.098	0.98	1.96	2.94
Go TAQ	0.125	1.25	2.5	3.75
gDNA	1.0	1.0	1.0	1.0

PCR Cycling Conditions:

Heated Lid = 110ºC

Temperature	Time
94º	2 mins
Start Cycle	
94º	30 secs
60º	1 min
72º	1 min
End Cycle	
Repeat cycle x 30	
72º	5 mins

Hold at 4ºC

iCre band ~ 500bp

LysM^{Cre}

Primers:

Name	Sequence
Lys WT Forward	5' –CTTGGGCTGCCAGAATTTCTC- 3'
Lys Cre Reverse	5' –CCCAGAAATGCCAGATTACG- 3'

PCR Master Mix:

LysM^{Cre} genotyping (25 µl reaction)				
	x 1	**x 10**	**x20**	**x 30**
Water	15.0288	150.288	300.576	450.864
Buffer	5	50	100	150
MgCl$_2$	2	20	40	60
dNTP (10mM)	0.6154	6.154	12.308	18.462
Primer 1 (20 µM)	0.6154	6.154	12.308	18.462
Primer 2 (20 µM)	0.6154	6.154	12.308	18.462
Go TAQ	0.125	1.25	2.5	3.75
gDNA	1.0	1.0	1.0	1.0

PCR Cycling Conditions:

Heated Lid = 110ºC

Temperature	Time
94°	2 mins
Start Cycle	
94°	30 secs
63°	30 secs
72°	1 min
End Cycle	
Repeat cycle x 30	
72°	5 mins

Hold at 4ºC

CRE band: 700 bp

Per2::Luc

Primers:

Name	Sequence
Common	5'- CTGTGTTTACTGCGAGAGT-3'
WT Reverse	5'- GGGTCCATGTGATTAGAAAC-3'
Mutant Reverse	5'- TAAAACCGGGAGGTAGATGAGA-3'

PCR Master Mix:

Per2::Luc genotyping (25 µl reaction)					
	1	**10**	**20**	**25**	**30**
Water	9.527	95.27	190.54	238.18	285.81
Buffer	5	50	100	125	150
MgCl$_2$	2	20	40	50	60
dNTP (2.5mM)	2.208	22.08	44.16	55.2	66.24
Primer 1 (20µM)	1.38	13.8	27.6	34.5	41.4
Primer 2 (20µM)	1.38	13.8	27.6	34.5	41.4
Primer 3 (20µM)	1.38	13.8	27.6	34.5	41.4
GoTAQ	0.125	1.25	2.5	3.125	3.75
gDNA	2	2	2	2	2

PCR Cycling Conditions:

Heated Lid = 110ºC

Temperature (ºC)	Time
94	2 mins
Start Cycle	
94	30s
58	30s
72	1 min
End Cycle	
Repeat cycle x 30	
72	5 mins

Hold at 4ºC

WT band: 230bp
Mutant band: 650bp

Agarose gels

For 100ml standard run:
2g LE agarose (for 2% gel)
100 ml 0.5x TBE
8 μl Safeview (NBS Biologicals)

Gels were run in electrophoresis tanks with 0.5x TBE as running buffer.

5x TBE

54g Tris Base
27.5g Boric Acid
20ml EDTA (0.5M)
1l dH$_2$O

0.5x TBE

100ml 5x TBE
900ml dH$_2$O

Appendix 2 – Media and buffer recipes

Recording media recipe

Makes 1L:

> 1 pot of DMEM powder (1000mg/l glucose – low glucose DMEM)
> 4g glucose powder (weigh out in bijou)
> 4.7ml sodium bicarbonate
> 10ml HEPES
> 2.5ml Pen/Strep

Make up to 1L with autoclaved water

Mix, filter through 0.22μM membrane and store at 4°C

Immediately prior to use:

Add 5% FBS (2.5 ml in 50 ml)
Add luciferin – 50 μl per 50 ml (one aliquot of 0.1M – final concentration 0.1mM)

Hybridisation buffer

To make 30ml hybridisation solution:

> 6ml 20x SSC pH7.0-----i.e. to give 4x
> 15ml Deionised formamide
> 7ml DEPC-treated water
> 600μl Transfer RNA (10.9mg/ml)
> 60μl 0.5M EDTA (pH8.0)

Stir to mix then add gently the following components to avoid bubbles

> 600μl 50x Denhart's solution
> 750μl 10% SDS
> 3g Dextran sulphate

Warm up to 55°C to facilitate the solubilisation of the dextran sulphate, aliquot in 6ml and store at -20°C (up to 6 months).

TEN Buffer

20ml Tris-HCl pH8 1M
4ml EDTA 0.5M
200ml NaCl 5M
Make up to 2l with ddH2O

His-purification buffer recipes

Buffer 1 (for 250 ml):
    6M Guanidinium/HCl (143.29g)
    0.1M Na_2HPO_4 /NaH2PO$_4$
        Na_2HPO_4: 46.6 ml of 0.5M
        NaH_2PO_4: 3.4 ml of 0.5M
    0.01M Tris – 2.5 ml of 1M
    Adjust to pH8

Buffer 3 (for 250 ml):
    8M Urea (120.12g)
    0.1M Na_2HPO_4 /NaH_2PO_4
        Na_2HPO_4: 10.84 ml of 0.5M
        NaH_2PO_4: 39.16 ml of 0.5M
    0.01M Tris – 2.5 ml of 1M
    Adjust to pH6.3

1M Imidazole
    0.85g in 12.5ml dH_2O (keep in foil paper)

0.5M Na_2HPO_4
    Na_2HPO_4, $12H_2O$ (MW: 358.14) 44.81 g for 250 ml

0.5M Na_2HPO_4
    NaH_2PO_4 (MW: 119.98) 15 g for 250 ml

IP lysis buffer
150 mM NaCl
20 mM Tris-HCl
10% glycerol
1% TritonX-100
1mM PMSF
10 mM NEM
1 tab PhosSTOP
1 tab Complete EDTA-free protease inhibitor
  cocktail

RIPA buffer
1% NP-40
0.1% SDS
50 mM Tris-HCl pH 7.4
150 mM NaCl
0.5% Sodium Deoxycholate
1 mM EDTA

SDS-PAGE Running buffer

$5 \times$ SDS-PAGE Running buffer
0.128 mol Tris Base
1.25 mol glycine
50 ml of 10% SDS
1 L distilled deionised water (ddH_2O).
Solution stored at room temperature.

To use, $1 \times$ SDS-PAGE Running buffer solution was made by diluting 200 ml of $5 \times$ SDS-PAGE Running buffer into 800 ml ddH_2O.

Transfer buffer

25 mmol Tris Base
0.192 mol glycine
800 ml ddH$_2$O
200 ml methanol
Solution stored at4°C.

Tris buffered saline (TBS) solution and TBS-Tween-20 (TBST)

10 × TBS (for 1L)
0.2 mol Tris Base
1.37 mol NaCl
1 L ddH$_2$O
Adjust to pH 7.6 with HCl.
Solution stored at room temperature.

To use, 1 × TBS-Tween-20 (TBST) solution was made by diluting 100 ml of 10 × TBS into 900 ml ddH$_2$O and adding 1 ml Tween-20. Solution was stored at room temperature.

Appendix 3 – Probe and primer sequences for *in situ* hybridisation

Nr1d1 **DBD – exons 2 to 5**
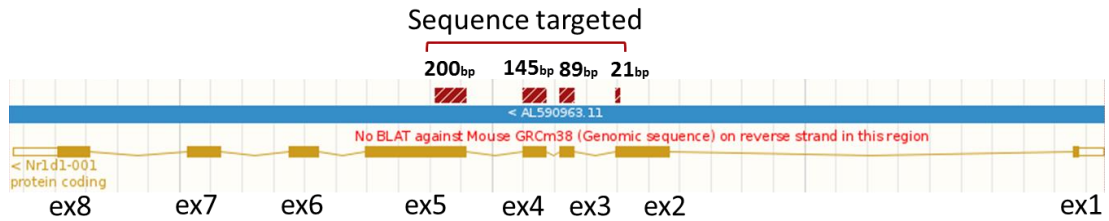
Primers used:

Forward 5'-CTGAGAGAAGCCCACCAAAG-3'
Reverse 5'-TAGGGCACAAGCAACATTACC -3'

Nr1d1 **LBD – exons 6 to 8**
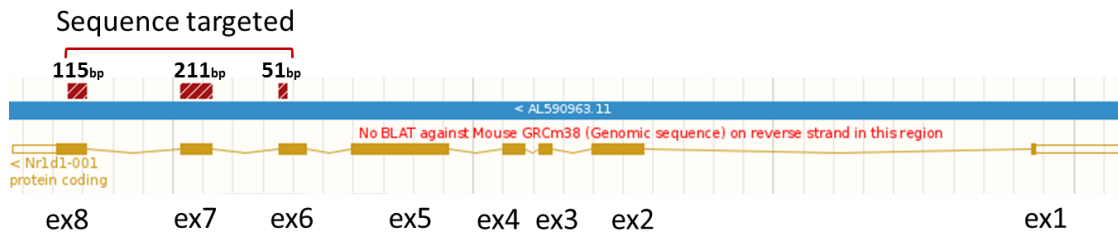
Primers used:

Forward 5'-TTGGTGAAGCGGGAAGTCTC -3'
Reverse 5'-GACCTTTCTCAGCACGACCA -3'

Nr1d2 **exon 8/3'UTR**
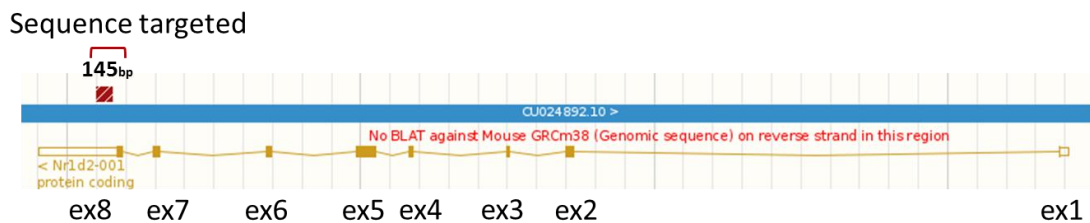
Primers used:

Forward 5'-CCCTACTTGAGCAGGAACCC -3'
Reverse 5'-TGTTAGACATTGGCCCACCC -3'

Cxcl5 exons 1 to 4
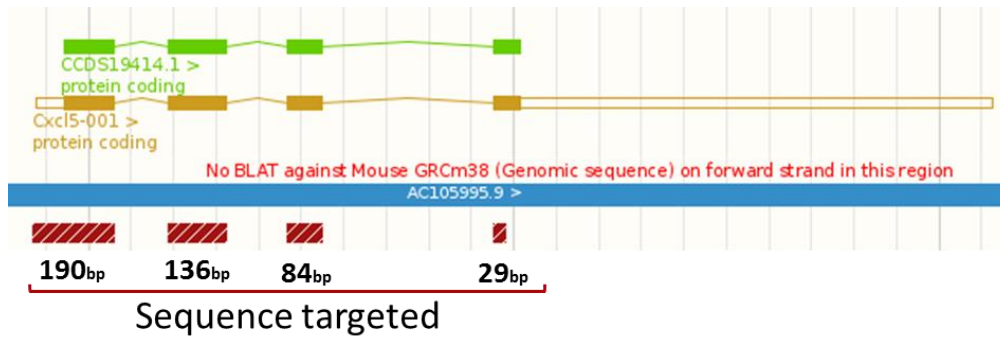
Primers used:

Forward 5'- TAGAGCCCCAATCTCCACAC -3'
Reverse 5'- GTGCATTCCGCTTAGCTTTC -3'

Appendix 4 – qPCR primer sequences and master mix recipes

Mouse primers

> **Taqman primers**

Bmal1
Forward 5'-CCAAGAAAGTATGGACACAGACAAA-3'
Reverse 5'-GCATTCTTGATCCTTCCTTGGT-3'
Probe 5' FAM -TGACCCTCATGGAAGGTTAGAATATGCAGAA-3' TAMRA

Per2
Forward 5'- GCCTTCAGACTCATGATGACAGA -3'
Reverse 5'- TTTGTGTGCGTCAGCTTTGG-3'
Probe 5' FAM-ACTGCTCACTACTGCAGCCGCTCGT -3' TAMRA

Il6
Forward 5'- CTATACCACTTCACAAGTCGGAGG-3'
Reverse 5'- TGCACAACTCTTTTCTCATTTCC-3'
Probe 5' FAM- TTAATTACACATGTTCTCTGGGAAATCG-3' TAMRA

Cxcl1
Forward 5'- CTGCACCCAAACCGAAGTC -3'
Reverse 5'- AGCTTCAGGGTCAAGGCAAG -3'
Probe 5' FAM- CACTCAAGAATGGTCGCGAGGC -3' TAMRA

Cxcl2
Forward 5'- TGTGACGCCCCCAGGA -3'
Reverse 5'- AACTTTTTGACCGCCCTTGAG -3'
Probe 5' FAM- TGCGCCCAGACAGAAGTCATAGCCA -3' TAMRA

G-csf
Forward 5'- GCTGCTGCTGTGGCAAAGT -3'
Reverse 5'- AGCCTGACAGTGACCAGG -3'
Probe 5' FAM- CACTATGGTCAGGACGAGAGGCCGTT -3' TAMRA

Primers from Life technologies were FAM-labeled with MGB probes:

Nr1d1 (exons 1-2): Mm00520708_m1	*Nrf2*: Mm00477784_m1
Nr1d1 (exons 4-5): Mm00520711_g1	*Nqo1*: Mm01253561_m1
Nr1d2: Mm01310356_g1	*Hmox1*: Mm00516005_m1
Cxcl5: Mm00436451_g1	*Gclc*: Mm00802655_m1
Abcg1: Mm00437390_m1	*Txnrd1*: Mm00443675_m1
Abca1: Mm00442646_m1	*Scgb1a1*: Mm00442046_m1

SYBR Green primers

Bmal1 **promoter**
Forward 5'- AATTGGTTTGGGTTGTCCGCCAAG -3'
Reverse 5'- AACCTACTTTCCGACCAATCCGCT -3'

Gapdh Mouse Positive Control Primer Set 2, Active Motif #71018
Mouse Negative Control Primer Set 2, Active Motif # 71012

Human primers

Taqman primers

BMAL1
Forward 5'- TGCCTCGTCGCAATTGG -3'
Reverse 5'- ACCCTGATTTCCCCGTTCA-3'
Probe 5' FAM - CGACTGCATTCTCATGTAGTTCCACAACCA -3' TAMRA

REV-ERBα
Forward 5'- CTTCAATGCCAACCATGCAT -3'
Reverse 5'- CCTGATTTTCCCAGCGATGT -3'
Probe 5' FAM - AGGTAGCCCTCCAGCCACCACCC -3' TAMRA

PER2
Forward 5'- GTCCAGCCCCCACCTTTC -3'
Reverse 5'- GGGAAGGAATAACTGGGTAGCA -3'
Probe 5' FAM - CTGCCCCTTTGGCGCCTGTCAT -3' TAMRA

IL6
Forward 5'- GGTACATCCTCGACGGCATCT -3'
Reverse 5'- GTGCCTCTTTGCTGCTTTCAC -3'
Probe 5' FAM - TGTTACTCTTGTTACATGTCTCCTTTCTCAGGGCT -3' TAMRA

GM-CSF
Forward 5'- CCTGAAGGACTTTCTGCTTGTCA -3'
Reverse 5'- CTCATCTGGCCGGTCTCACT -3'
Probe 5' FAM - CCCCTTTGACTGCTGGGAGCCAG -3' TAMRA

CXCL1
Forward 5'- CGAAGTCATAGCCACACTCAAGAA -3'
Reverse 5'- GTTCAGCATCTTTTCGATGATTTTC -3'
Probe 5' FAM - TGCCTCAATCCTGCATCCCCCAT-3' TAMRA

HMOX1

Forward 5'- CCAGCAACAAAGTGCAAGATTC-3'
Reverse 5'- TCACATGGCATAAAGCCCTACAG -3'
Probe 5' FAM - TCTCCGATGGGTCCTTACACTCAGCTTTCT -3' TAMRA

Primers from Life technologies were FAM-labeled with MGB probes:

IL8: Hs00174103_m1   *NR1D2*: Hs00233309_m1
CXCL2: Hs00601975_m1   *NQO1*: Hs01045994_m1
CXCL5: Hs00171085_m1   *NRF2*: Hs00232352_m1
CCL2: Hs00234140_m1

Reaction recipes

Total volume reaction: 20 µl

Taqman with MWG primers	x1 (µl)
Mastermix	10
Forward primer (10 µM)	0.4
Reverse primer (10 µM)	0.4
Probe (10 µM)	0.4
18s rRNA primer	1
dH$_2$O	6.8
cDNA	1

Taqman with Life technologies primers	x1 (µl)
Mastermix	10
Gene of interest primer	1
18s rRNA primer	1
dH$_2$O	7
cDNA	1

Mastermix – Eurogentec Efficiensee FAST + dTTP RT-QP2X-03+WOUNFB

SYBR Green with MWG primers	x1 (µl)
Mastermix	10
Forward primer (10 µM)	0.4
Reverse primer (10 µM)	0.4
ROX	0.2
dH$_2$O	8
cDNA	1

SYBR Green with Active motif primers	x1 (µl)
Mastermix	10
Active Motif primer	1.6
ROX	0.2
dH$_2$O	7.2
cDNA	1

Mastermix - 2× SYBR Green master mix (Promega)

Appendix 5 – Characterisation of antibody GSK6F05
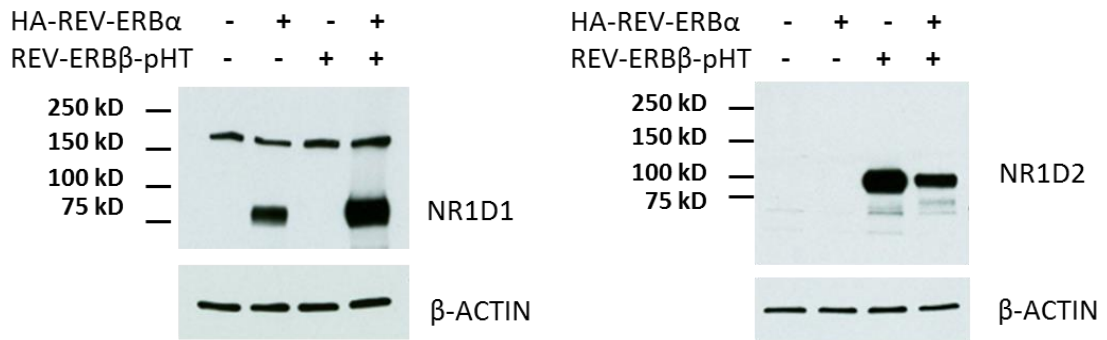
Figure A5. 1: Specificity of antibody GSK6F05 for REV-ERBα

HEK 293 cells were transfected with HA-REV-ERBα and REV-ERBβ-Halotag. Total cell lysates were analysed by Western blotting for REV-ERBα protein levels using mouse monoclonal antibody GSK6F05 and for REV-ERBβ protein levels using rabbit polyclonal antibody (Proteintech, # 13906-1-AP). (4 μg total protein loaded per lane).
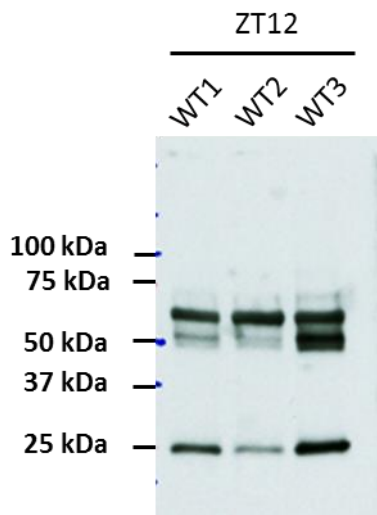
Figure A5. 2: Non-specific bands detected from murine whole lung

Lysates from whole lung collected at ZT12 was run on a Western blot. The membrane was then probed directly with mouse secondary antibody. (18 μg total protein loaded per lane).

Appendix 6 – Diurnal expression of inflammatory genes in wild-type and *Rev-Erbα* knock-out mice
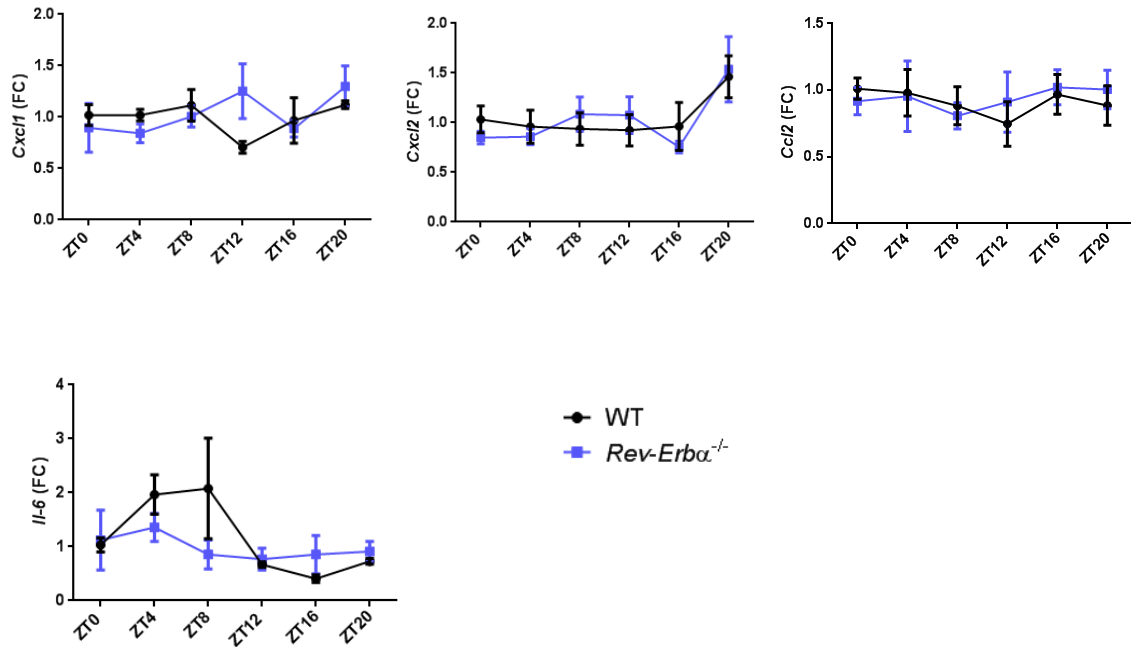
Figure A6. 1: Profile of inflammatory gene expression across a diurnal period in wild-type and *Rev-Erbα*-/- mice

Lung tissues from *Rev-Erbα*-/- and wild-type littermate control mice were collected at different time points across the day. mRNA levels in total lung tissues were determined by Real-Time qPCR and normalized to WT at ZT0. Data are presented as mean ± SEM; $n = 5$-6 for WT and $n = 3$-5 for KO.

Appendix 7 – Cytokine/chemokine secretion into the lung upon aerosolised LPS challenge at ZT0 and ZT12 in wild-type and *Rev-Erbα* knock-out mice
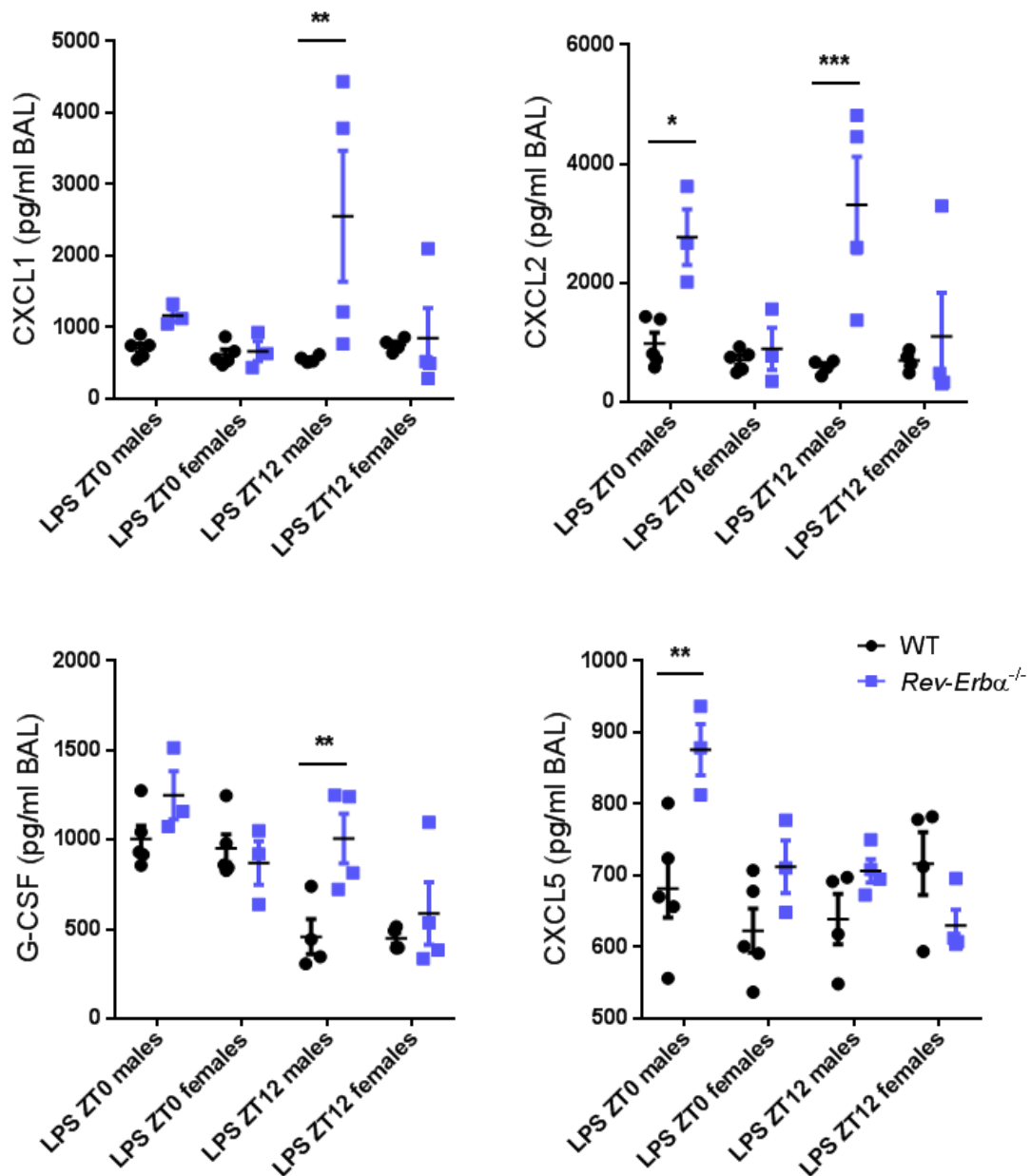
Figure A7. 1: Gender analysis of cytokines and chemokines recovered by BAL after LPS challenge at ZT0 or ZT12 in wild-type and *Rev-Erbα*^{-/-} mice

Mice were exposed to aerosolised LPS at 2mg/ml or to saline for 20 minutes at ZT0 or ZT12 and culled 5 hours later. Broncho-alveolar lavage (BAL) fluid was analysed for 23 cytokines simultaneously via multiplex. Data are presented as mean ± SEM; *n* = 6-10, *P <0.05, ***P <0.001* (Two-way ANOVA, post hoc Bonferroni).

Cytokine/Chemokine	ZT0			ZT12		
	WT	Rev-Erbα$^{-/-}$	Significance	WT	Rev-Erbα$^{-/-}$	Significance
IL-1α	OOR <	OOR <		OOR <	OOR <	
IL-1β	OOR <	OOR <		OOR <	OOR <	
IL-2	OOR <	OOR <		OOR <	OOR <	
IL-5	OOR <	OOR <		OOR <	OOR <	
IL-6	772.4 ± 40.49	690.8 ± 70.91	ns	598.2 ± 48.75	644.7 ± 86.64	ns
IL-10	OOR <	OOR <		OOR <	OOR <	
IL-12p70	OOR <	OOR <		OOR <	OOR <	
IL-13	OOR <	OOR <		OOR <	OOR <	
IL-17	OOR <	OOR <		OOR <	OOR <	
G-CSF	978.2 ± 51.69	1059 ± 117.5	ns	454.2 ± 47.65	797.8 ± 130.3	*
GM-CSF	77.70 ± 11.43	77.43 ± 17.28	ns	83.53 ± 10.80	103.4 ± 19.78	ns
IFN-γ	OOR <	OOR <		OOR <	OOR <	
CXCL1 (KC)	663.7 ± 46.19	916.3 ± 134.3	0.0506	655.0 ± 44.63	1701 ± 566.4	*
CXCL2	844.0 ± 103.2	1830 ± 495.4	*	640.7 ± 50.94	2206 ± 654.8	*
CXCL5	652.3 ± 25.89	794.2 ± 43.27	***	677.8 ± 29.92	668.3 ± 19.22	ns
CXCL10 (IP10)	202.5 ± 30.78	191.6 ± 30.35	ns	187.2 ± 15.85	240.6 ± 63.20	ns
CCL2 (MCP-1)	1512 ± 54.98	1330 ± 76.66	ns	1524 ± 62.94	1383 ± 115.7	ns
CCL3 (MIP-1α)	2348 ± 197.7	1706 ± 208.3	ns	2298 ± 165.4	1647 ± 203.3	ns
CCL4 (MIP-1β)	8922 ± 575.4	6968 ± 742.7	ns	9434 ± 720.3	7648 ± 1088	ns
CCL5 (RANTES)	383.3 ± 31.53	276.2 ± 18.70	*	453.4 ± 33.50	340.7 ± 36.24	*
CCL11 (EOTAXIN)	OOR <	OOR <		OOR <	OOR <	
TNF-α	110.1 ± 5.476	103.9 ± 10.17	ns	84.01 ± 5.339	75.62 ± 9.763	ns
M-CSF	OOR <	OOR <		OOR <	OOR <	

Table A7. 1: Summary of cytokine analysis via multiplex of BAL samples from *Rev-Erbα$^{-/-}$* and WT mice exposed to LPS at ZT0 and ZT12

Rev-Erbα$^{-/-}$ and wild-type littermate control mice were exposed to aerosolised LPS at 2mg/ml or to saline for 20 minutes at ZT0 or ZT12 and culled 5 hours later. Broncho-alveolar lavage (BAL) fluid was analysed for 23 cytokines simultaneously via multiplex. Where differences are significant, the row corresponding to the analyte is highlighted. OOR< = Out of Range Below. Values are mean ± SEM, *n* = 6-10, *P <0.05, ***P <0.001 (Student's *t*-test).

Appendix 8 – Cytokine/chemokine secretion into the lung upon 10-day cigarette smoke exposure in wild-type and *Rev-Erbα* knock-out mice

| Cytokine/Chemokine | 10-day smoke | | | | | |
| | BALs | | | Lung homogenates | | |
	WT	*Rev-Erbα*$^{-/-}$	Significance	WT	*Rev-Erbα*$^{-/-}$	Significance
IL-1α	OOR <	OOR <		1037 ± 118.0	1596 ± 170.5	*
IL-1β	OOR <	OOR <		206.7 ± 5.873	229.4 ± 12.39	ns
IL-2	OOR <	OOR <		OOR <	OOR <	
IL-5	OOR <	OOR <		OOR <	OOR <	
IL-6	OOR <	OOR <		233.8 ± 21.83	381.9 ± 67.45	*
IL-10	OOR <	OOR <		OOR <	OOR <	
IL-12p70	OOR <	OOR <		OOR <	OOR <	
IL-13	OOR <	OOR <		OOR <	OOR <	
IL-17	OOR <	OOR <		OOR <	OOR <	
G-CSF	OOR <	OOR <		OOR <	OOR <	
GM-CSF	OOR <	OOR <		OOR <	OOR <	
IFN-γ	OOR <	OOR <		15.15 ± 0.9235	19.84 ± 3.959	ns
CXCL1 (KC)	20.88 ± 1.851	32.04 ± 3.199	**	86.88 ± 7.283	122.8 ± 18.24	*
CXCL2	3.841 ± 0.4166	4.398 ± 1.103	ns	26.35 ± 1.599	42.71 ± 6.315	***
CXCL5	152.6 ± 7.556	208.5 ± 51.07	ns	714.5 ± 14.48	719.1 ± 23.03	ns
CXCL10 (IP10)	OOR <	OOR <		OOR <	OOR <	
CCL2 (MCP-1)	OOR <	OOR <		242.5 ± 8.441	216.1 ± 14.90	ns
CCL3 (MIP-1α)	OOR <	OOR <		101.8 ± 5.999	113.9 ± 9.889	ns
CCL4 (MIP-1β)	OOR <	OOR <		OOR <	OOR <	
CCL5 (RANTES)	OOR <	OOR <		353.7 ± 25.55	331.6 ± 30.07	ns
CCL11 (EOTAXIN)	OOR <	OOR <		980.9 ± 41.75	1032 ± 43.58	ns
TNF-α	OOR <	OOR <		OOR <	OOR <	
M-CSF	OOR <	OOR <		38.42 ± 1.066	35.64 ± 1.660	ns

Table A8. 1: Summary of cytokine analysis via multiplex of BAL samples from *Rev-Erbα*$^{-/-}$ and WT mice exposed to cigarette smoke for 10 days

Rev-Erbα$^{-/-}$ and wild-type littermate control mice were exposed to cigarette smoke between ZT8 and ZT10 for 10 days and culled 20 hours after the last exposure. Broncho-alveolar lavage (BAL) fluid and lung homogenates were analysed for 23 cytokines simultaneously via multiplex. Where differences are significant, the row corresponding to the analyte is highlighted. OOR< = Out of Range Below. Values are mean ± SEM, *n* = 6-10, *P <0.05, **P <0.01, ***P <0.001 (Two-way ANOVA, post hoc Bonferroni).

Appendix 9 – Antioxidant gene *Nqo1* transcript levels in whole lung after 22-month cigarette smoke exposure in wild-type mice
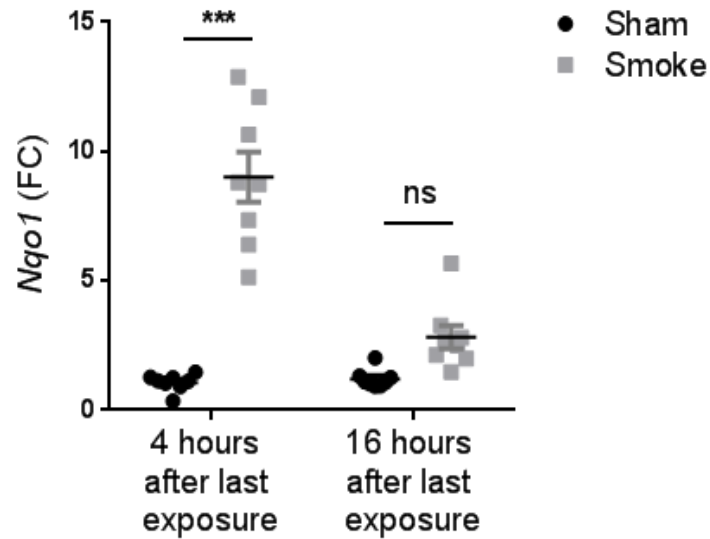
Figure A9. 1: *Nqo1* transcript levels in whole lung after 22-month cigarette smoke exposure in wild-type mice

C57BL/6 mice were exposed to cigarette smoke or air daily, five days a week, for 22 months. Daily exposures occurred between ZT2 and ZT4. Cull was processed either 4 or 16 hours after the last exposure at ZT8 or ZT20 respectively and lung tissues were collected. Gene expression was determined by Real-Time qPCR and normalized to sham group culled 4 hours after exposure. Data are presented as mean ± SEM; $n = 8$, ****P <0.001* (Two-way ANOVA, post hoc Bonferroni).

Appendix 10 – Responses to aerosolised LPS at ZT4 in *Ccsp*^{icre/+} mice and *Ccsp*^{+/+} littermate controls
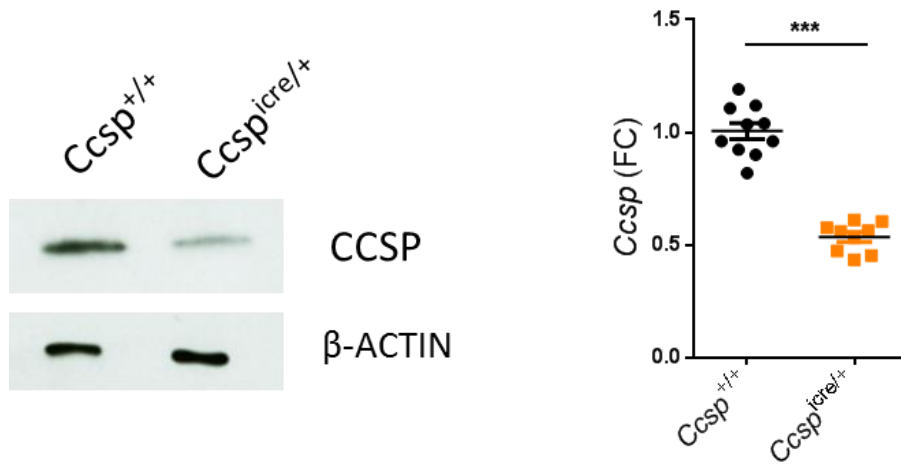
Figure A10. 1: Reduction of CCSP at protein and transcript levels in *Ccsp*^{icre/+} mice.
Lungs from *Ccsp*^{icre/+} mice and *Ccsp*^{+/+} littermate controls were collected at ZT9. (A) Levels of CCSP proteins were measured by Western blotting using anti-uteroglobin rabbit polyclonal antibody (18 μg total protein loaded per lane). (B) mRNA levels in total lung tissues were determined by Real-Time qPCR and normalized to *Ccsp*^{icre/+} mice. Data are presented as mean ± SEM; *n* = 9-10, ****P <0.001* (Student's *t*-test).

Figure A11. 1: Transcript levels of inflammatory genes in response to LPS challenge at ZT4 in *Ccsp-Rev-Erbα*-DBD^m mice and *Rev-Erbα*$^{fl/fl}$ littermate controls

Mice were exposed to aerosolised LPS at 2mg/ml or to saline for 20 minutes at ZT4 and culled 5 hours later. RNA was extracted from whole lung and transcript levels were measured by Taqman Real-Time qPCR and normalized to *Rev-Erbα*$^{fl/fl}$ saline group. Data are presented as mean ± SEM; n = 7-9, *P <0.05 (Two-way ANOVA, post hoc Bonferroni).

Cytokine/Chemokine	Rev-Erbα$^{fl/fl}$	Ccsp-Rev-Erbα-DBD^m	Significance
IL-1α	57.77 ± 7.822	62.65 ± 7.644	ns
IL-1β	OOR<	OOR<	ns
IL-2	OOR<	OOR<	ns
IL-5	OOR<	OOR<	ns
IL-6	859.7 ± 95.86	731.7 ± 104.8	ns
IL-10	OOR<	OOR<	
IL-12p70	OOR<	OOR<	ns
IL-13	OOR<	OOR<	ns
IL-17	OOR<	OOR<	
G-CSF	923.9 ± 40.57	915.0 ± 89.11	ns
GM-CSF	75.35 ± 8.890	47.92 ± 8.625	*
IFN-γ	OOR<	OOR<	
CXCL1 (KC)	232.3 ± 35.96	202.7 ± 25.14	ns
CXCL2	415.5 ± 53.11	324.1 ± 22.67	ns
CXCL5	422.5 ± 34.40	705.4 ± 35.26	***
CXCL10 (IP10)	1031 ± 172.1	475.5 ± 95.55	*
CCL2 (MCP-1)	3030 ± 397.9	2683 ± 372.6	ns
CCL3 (MIP-1α)	3080 ± 553.9	1691 ± 280.0	ns (0.0521)
CCL4 (MIP-1β)	7653 ± 1714	5615 ± 1340	ns
CCL5 (RANTES)	445.7 ± 92.24	402.8 ± 91.48	ns
CCL11 (EOTAXIN)	25.79 ± 6.811	17.73 ± 5.736	ns
TNF-α	104.2 ± 13.94	113.8 ± 19.25	ns
M-CSF	OOR<	OOR<	ns

Table A11. 1: Summary of cytokine analysis via multiplex of BAL samples from *Ccsp-Rev-Erbα*-DBD^m mice and *Rev-Erbα*$^{fl/fl}$ mice exposed to LPS at ZT4

Ccsp-Rev-Erbα-DBD^m mice and *Rev-Erbα*$^{fl/fl}$ littermate controls were exposed to aerosolised LPS at 2mg/ml or to saline for 20 minutes at ZT4 and culled 5 hours later. Broncho-alveolar lavage (BAL) fluid was analysed for 23 cytokines simultaneously via multiplex. Where differences are significant, the row corresponding to the analyte is highlighted. OOR< = Out of Range Below, ns = non significant. Values are mean ± SEM, *n* = 7-9, *P <0.05, ***P <0.001* (Student's *t*-test).

Appendix 12 – Responses to aerosolised LPS at ZT0 and ZT12 in *Ccsp-Rev-Erbα*-DBD^m mice and *Rev-Erbα*^fl/fl littermate controls

Cytokine/Chemokine	ZT0 *Rev-Erb α*^fl/fl	ZT0 *Ccsp-Rev-Erb α*-DBD^m	ZT0 Significance	ZT12 *Rev-Erb α*^fl/fl	ZT12 *Ccsp-Rev-Erb α*-DBD^m	ZT12 Significance
IL-1α	OOR <	OOR <		OOR <	OOR <	
IL-1β	OOR <	OOR <		OOR <	OOR <	
IL-2	OOR <	OOR <		OOR <	OOR <	
IL-5	OOR <	OOR <		OOR <	OOR <	
IL-6	659.9 ± 102.9	713.8 ± 101.8	ns	250.2 ± 59.45	175.0 ± 45.36	ns
IL-10	OOR <	OOR <		OOR <	OOR <	
IL-12p70	OOR <	OOR <		OOR <	OOR <	
IL-13	OOR <	OOR <		OOR <	OOR <	
IL-17	OOR <	OOR <		OOR <	OOR <	
G-CSF	975.0 ± 156.3	1267 ± 162.0	ns	305.3 ± 30.56	294.9 ± 47.99	ns
GM-CSF	24.58 ± 4.480	19.62 ± 6.950	ns	45.60 ± 12.16	31.90 ± 6.553	ns
IFN-γ	OOR <	OOR <		OOR <	OOR <	
CXCL1 (KC)	528.3 ± 79.01	487.8 ± 46.29	ns	644.4 ± 74.42	500.8 ± 37.63	ns
CXCL2	622.6 ± 99.43	641.9 ± 74.34	ns	575.7 ± 102.6	408.6 ± 80.62	ns
CXCL5	664.4 ± 39.24	886.2 ± 63.18	*	801.3 ± 99.89	755.4 ± 46.42	ns
CXCL10 (IP10)	OOR <	OOR <		OOR <	OOR <	
CCL2 (MCP-1)	1799 ± 382.5	2180 ± 307.2	ns	946.8 ± 300.7	573.6 ± 213.9	ns
CCL3 (MIP-1α)	1348 ± 248.9	1253 ± 264.2	ns	1002 ± 213.1	1081 ± 210.4	ns
CCL4 (MIP-1β)	2811 ± 792.5	4403 ± 848.4	ns	1738 ± 718.0	772.9 ± 381.7	ns
CCL5 (RANTES)	271.5 ± 77.78	342.8 ± 66.85	ns	156.75 ± 25.77	OOR <	
CCL11 (EOTAXIN)	OOR <	OOR <		OOR <	OOR <	
TNF-α	87.69 ± 14.74	115.6 ± 12.68	ns	33.00 ± 6.348	30.22 ± 7.513	ns
M-CSF	OOR <	OOR <		OOR <	OOR <	

Table A12. 1: Summary of cytokine analysis via multiplex of BAL samples from *Ccsp-Rev-Erbα*-DBD^m mice and *Rev-Erbα*^fl/fl mice exposed to LPS at ZT0 and ZT12

Ccsp-Rev-Erbα-DBD^m mice and *Rev-Erbα*^fl/fl littermate controls were exposed to aerosolised LPS at 2mg/ml or to saline for 20 minutes at ZT0 or ZT12 and culled 5 hours later. Broncho-alveolar lavage (BAL) fluid was analysed for 23 cytokines simultaneously via multiplex. Where differences are significant, the row corresponding to the analyte is highlighted. OOR< = Out of Range Below, ns = non significant. Values are mean ± SEM, n = 7-9, *P <0.05 (Student's t-test).
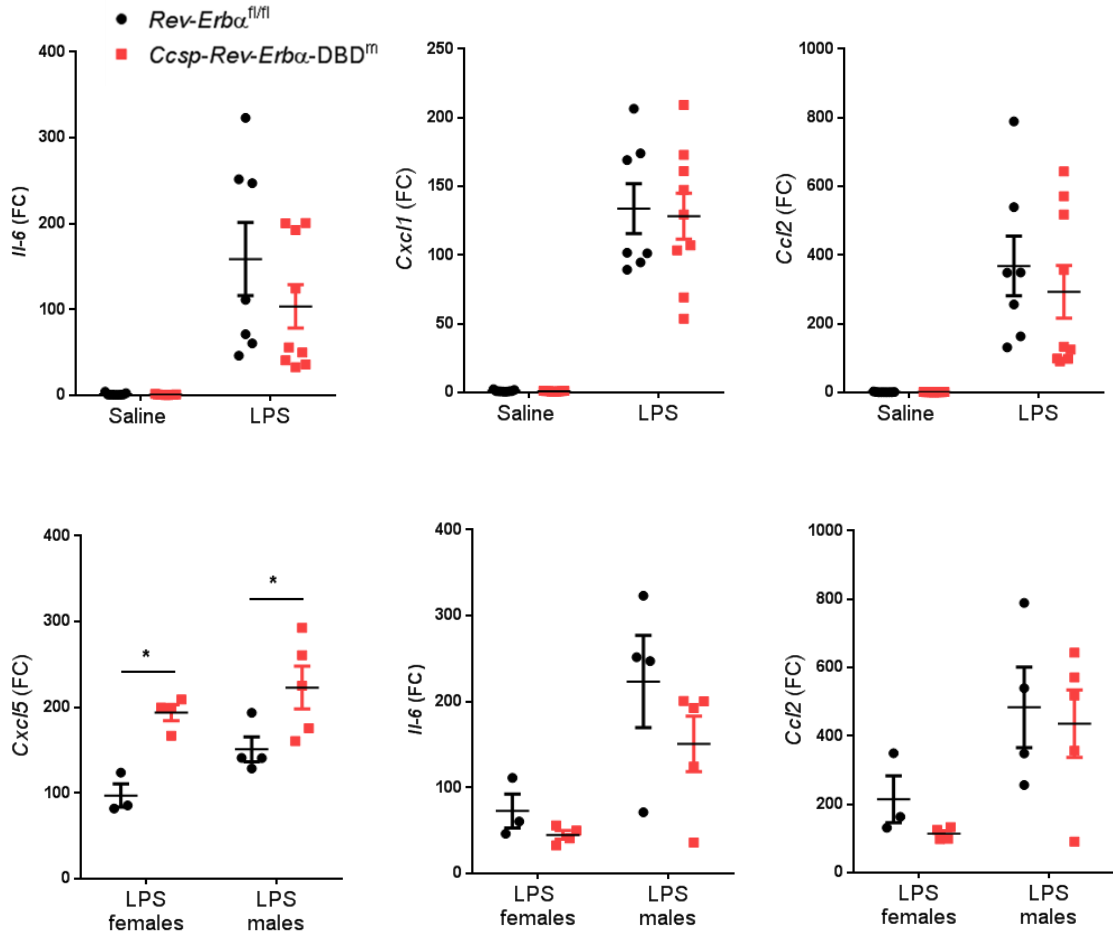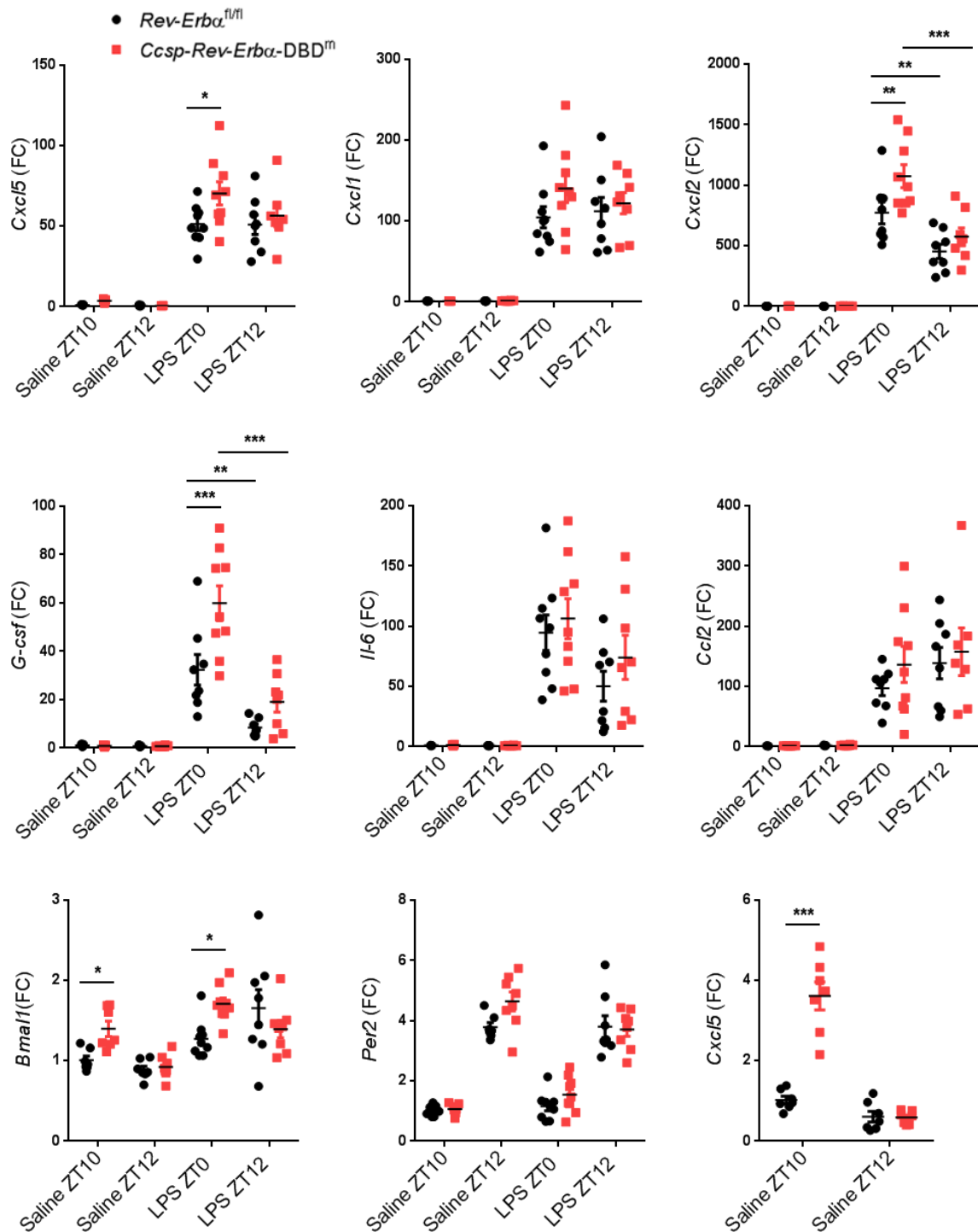
Figure A12. 1: Transcript levels of inflammatory genes in response to LPS challenge at ZT0 and ZT12 in *Ccsp-Rev-Erbα*-DBD[m] mice and *Rev-Erbα*^{fl/fl} littermate controls

Mice were exposed to aerosolised LPS at 2mg/ml or to saline for 20 minutes at ZT0 or ZT12 and culled 5 hours later. RNA was extracted from whole lung and transcript levels were measured by Taqman Real-Time qPCR and normalized to *Rev-Erbα*^{fl/fl} saline group at ZT0. Data are presented as mean ± SEM; n = 7-9, *P <0.05, **P <0.01, ***P <0.001 (Two-way ANOVA, post hoc Bonferroni).

Appendix 13 – Responses to aerosolised LPS at ZT4 in *LysM-Rev-Erbα*-DBD^m mice and *Rev-Erbα*^{fl/fl} littermate controls

Cytokine/Chemokine	ZT4 *Rev-Erbα*^{fl/fl}	*LysM-Rev-Erbα*-DBD^m	Significance
IL-1α	OOR <	OOR <	
IL-1β	OOR <	OOR <	
IL-2	OOR <	OOR <	
IL-5	OOR <	OOR <	
IL-6	906.9 ± 101.7	1015 ± 168.9	ns
IL-10	OOR <	OOR <	
IL-12p70	OOR <	OOR <	
IL-13	OOR <	OOR <	
IL-17	OOR <	OOR <	
G-CSF	843.5 ± 102.2	1101 ± 170.0	ns
GM-CSF	96.56 ± 16.07	75.45 ± 15.35	ns
IFN-γ	OOR <	OOR <	
CXCL1 (KC)	478.1 ± 79.90	633.8 ± 92.35	ns
CXCL2	642.5 ± 94.40	816.7 ± 86.00	ns
CXCL5	453.1 ± 12.99	473.6 ± 37.64	ns
CXCL10 (IP10)	208.3 ± 37.20	260.4 ± 54.21	ns
CCL2 (MCP-1)	1689 ± 179.3	1774 ± 182.8	ns
CCL3 (MIP-1α)	2263 ± 222.8	1875 ± 326.1	ns
CCL4 (MIP-1β)	7050 ± 1234	7396 ± 1270	ns
CCL5 (RANTES)	459.9 ± 92.16	643.9 ± 102.6	ns
CCL11 (EOTAXIN)	OOR <	OOR <	
TNF-α	81.76 ± 10.97	100.6 ± 13.06	ns
M-CSF	OOR <	OOR <	

Table A13. 1: Summary of cytokine analysis via multiplex of BAL samples from *LysM-Rev-Erbα*-DBD^m mice and *Rev-Erbα*^{fl/fl} mice exposed to LPS at ZT4

LysM-Rev-Erbα-DBD^m mice and *Rev-Erbα*^{fl/fl} littermate controls were exposed to aerosolised LPS at 2mg/ml or to saline for 20 minutes at ZT4 and culled 5 hours later. Broncho-alveolar lavage (BAL) fluid was analysed for 23 cytokines simultaneously via multiplex. OOR< = Out of Range Below, ns = non significant. Values are mean ± SEM, *n* = 8 (Student's *t*-test).
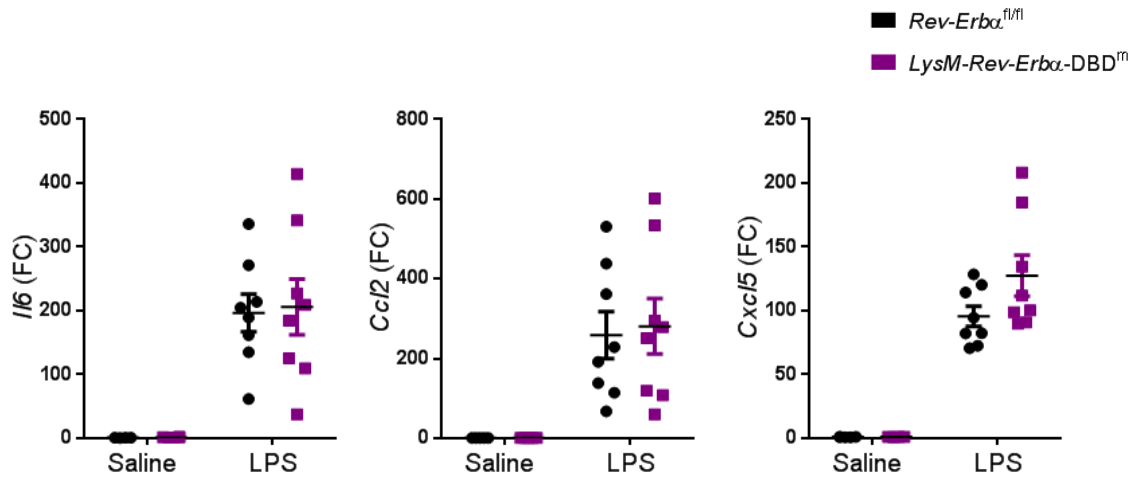
Figure A13. 1: Transcript levels of inflammatory genes in response to LPS challenge at ZT4 in *LysM-Rev-Erbα*-DBD^m mice and *Rev-Erbα*^fl/fl littermate controls

Mice were exposed to aerosolised LPS at 2mg/ml or to saline for 20 minutes at ZT4 and culled 5 hours later. RNA was extracted from whole lung and transcript levels were measured by Taqman Real-Time qPCR and normalized to *Rev-Erbα*^fl/fl saline group. Data are presented as mean ± SEM; $n = 8$, (Two-way ANOVA, post hoc Bonferroni).

Appendix 14 – Responses to aerosolised LPS at ZT4 in *Ccsp-Rev-Erbα*-DBD^m, *Ccsp-Rev-erbα*-DBD^m/*Rev-Erbβ*^{-/-} mice and *Rev-Erbα*^{fl/fl}, *Rev-Erbα/β*^{fl/fl} littermate controls

Cytokine/Chemokine	*Rev-Erb α* $^{fl/fl}$	*Ccsp-Rev-Erb* α- DBD^m	Significance	*Rev-Erb α/ β* $^{fl/fl}$	*Ccsp-Rev-Erb α -DBD^m/Rev-Erb β* $^{-/-}$	Significance
IL-1α	45.83 ± 5.291	39.12 ± 4.465	ns	68.65 ± 9.544	83.90 ± 12.60	ns
IL-1β	OOR <	OOR <		OOR <	OOR <	
IL-2	OOR <	OOR <		OOR <	OOR <	
IL-5	OOR <	OOR <		OOR <	OOR <	
IL-6	487.1 ± 131.8	672.4 ± 119.9	ns	1862 ± 194.3	1110 ± 82.62	**
IL-10	OOR <	OOR <		OOR <	OOR <	
IL-12p70	OOR <	OOR <		OOR <	OOR <	
IL-13	OOR <	OOR <		OOR <	OOR <	
IL-17	OOR <	OOR <		OOR <	OOR <	
G-CSF	426.0 ± 85.57	717.9 ± 151.2	ns	1309 ± 177.9	2031 ± 108	**
GM-CSF	37.76 ± 8.484	27.46 ± 4.782	ns	95.09 ± 12.62	40.14 ± 9.888	**
IFN-γ	OOR <	OOR <		OOR <	OOR <	
CXCL1 (KC)	385.7 ± 79.86	541.6 ± 48.15	ns	874.3 ± 108.9	3353 ± 414.6	***
CXCL2	398.4 ± 82.25	571.7 ± 64.50	ns	953.0 ± 140.6	2240 ± 197.9	***
CXCL5	450.5 ± 80.58	874.1 ± 124.1	***	556.1 ± 37.05	1812 ± 39.65	***
CXCL10 (IP10)	OOR <	OOR <		291.1 ± 51.17	235.0 ± 32.55	ns
CCL2 (MCP-1)	728.3 ± 233.2	987.1 ± 374.1	ns	3169 ± 156.5	3589 ± 214.3	ns
CCL3 (MIP-1α)	1295 ± 369.7	913.8 ± 254.6	ns	2075 ± 220.2	2069 ± 315.4	ns
CCL4 (MIP-1β)	1081 ± 417.0	1659 ± 890.1	ns	7340 ± 551.1	9051 ± 1008	ns
CCL5 (RANTES)	93.42 ± 28.78	208.2 ± 106.1	ns	505.5 ± 51.63	265.1 ± 37.57	*
CCL11 (EOTAXIN)	OOR <	OOR <		12.99 ± 1.479	27.12 ± 3.572	**
TNF-α	26.18 ± 6.645	47.59 ± 13.63	ns	107.9 ± 11.25	131.1 ± 9.459	ns
M-CSF	OOR <	OOR <		OOR <	OOR <	

Table A14. 1: Summary of cytokine analysis via multiplex of BAL samples from *Ccsp-Rev-Erbα*-DBD^m, *Ccsp-Rev-erbα*-DBD^m/*Rev-Erbβ*^{-/-} mice and *Rev-Erbα*^{fl/fl}, *Rev-Erbα/β*^{fl/fl} littermate controls exposed to LPS at ZT4

Mice were exposed to aerosolised LPS at 2mg/ml or to saline for 20 minutes at ZT4 and culled 5 hours later. Broncho-alveolar lavage (BAL) fluid was analysed for 23 cytokines simultaneously via multiplex. OOR< = Out of Range Below, ns = non significant. Values are mean ± SEM, *n* = 5-8, **P <0.01, ***P <0.001 (Student's *t*-test).

**Appendix 15 – Responses to aerosolised LPS at ZT0 and ZT12 in *Ccsp-Rev-Erbα*-DBD^m/*Rev-Erbβ^{-/-}* mice and *Rev-Erbα/β*^{fl/fl} littermate controls**

Cytokine/Chemokine	ZT0			ZT12		
	Rev-Erb α/β^{fl/fl}	*Ccsp-Rev-Erbα-DBDm-Rev-Erbβ*^{-/-}	Significance	*Rev-Erb α/β*^{fl/fl}	*Ccsp-Rev-Erbα-DBDm-Rev-Erbβ*^{-/-}	Significance
IL-1α	30.47 ± 4.859	34.76 ± 7.309	ns	62.00 ± 4.557	49.54 ± 5.587	ns
IL-1β	OOR <	OOR <		OOR <	OOR <	
IL-2	OOR <	OOR <		OOR <	OOR <	
IL-5	OOR <	OOR <		OOR <	OOR <	
IL-6	1208 ± 120.1	940.5 ± 113.1	ns	842.7 ± 96.62	822.7 ± 128.6	ns
IL-10	OOR <	OOR <		OOR <	OOR <	
IL-12p70	OOR <	OOR <		OOR <	OOR <	
IL-13	OOR <	OOR <		OOR <	OOR <	
IL-17	OOR <	OOR <		OOR <	OOR <	
G-CSF	1977 ± 214.6	1769 ± 152.2	ns	845.2 ± 131.0	1488 ± 123.5	**
GM-CSF	25.21 ± 5.518	9.617 ± 2.116	*	41.16 ± 5.367	48.47 ± 9.601	ns
IFN-γ	OOR <	OOR <		OOR <	OOR <	
CXCL1 (KC)	2404 ± 451.6	3482 ± 741.9	ns	1877 ± 442.9	5045 ± 406.7	***
CXCL2	1476 ± 195.8	1676 ± 337.4	ns	1175 ± 243.9	2973 ± 141.2	***
CXCL5	619.5 ± 56.06	1085 ± 12.13	***	448.3 ± 34.48	1132 ± 21.11	***
CXCL10 (IP10)	195.0 ± 23.27	149.9 ± 16.86	ns	238.7 ± 59.80	179.0 ± 13.00	ns
CCL2 (MCP-1)	2259 ± 172.6	1983 ± 253.2	ns	2010 ± 102.3	2044 ± 88.66	ns
CCL3 (MIP-1α)	2017 ± 369.9	1546 ± 466.1	ns	1765 ± 272.9	1842 ± 227.5	ns
CCL4 (MIP-1β)	12586 ± 2099	11088 ± 3372	ns	10133 ± 986.2	10344 ± 866.9	ns
CCL5 (RANTES)	330.6 ± 86.79	171.1 ± 11.48	ns	377.8 ± 74.96	186.7 ± 16.34	*
CCL11 (EOTAXIN)	18.59 ± 4.075	18.56 ± 4.343	ns	9.499 ± 1.038	16.52 ± 2.249	*
TNF-α	184.1 ± 22.62	136.8 ± 27.07	ns	115.7 ± 14.86	138.9 ± 9.172	ns
M-CSF	OOR <	OOR <		OOR <	OOR <	

Table A15. 1: Summary of cytokine analysis via multiplex of BAL samples from *Ccsp-Rev-Erbα*-DBD^m/*Rev-Erbβ^{-/-}* mice and *Rev-Erbα/β*^{fl/fl} littermate controls exposed to LPS at ZT0 and ZT12

Mice were exposed to aerosolised LPS at 2mg/ml or to saline for 20 minutes at ZT0 or ZT12 and culled 5 hours later. Broncho-alveolar lavage (BAL) fluid was analysed for 23 cytokines simultaneously via multiplex. OOR< = Out of Range Below, ns = non significant. Values are mean ± SEM, *n* = 7-9, **P < 0.01, ***P < 0.001 (Student's *t*-test).
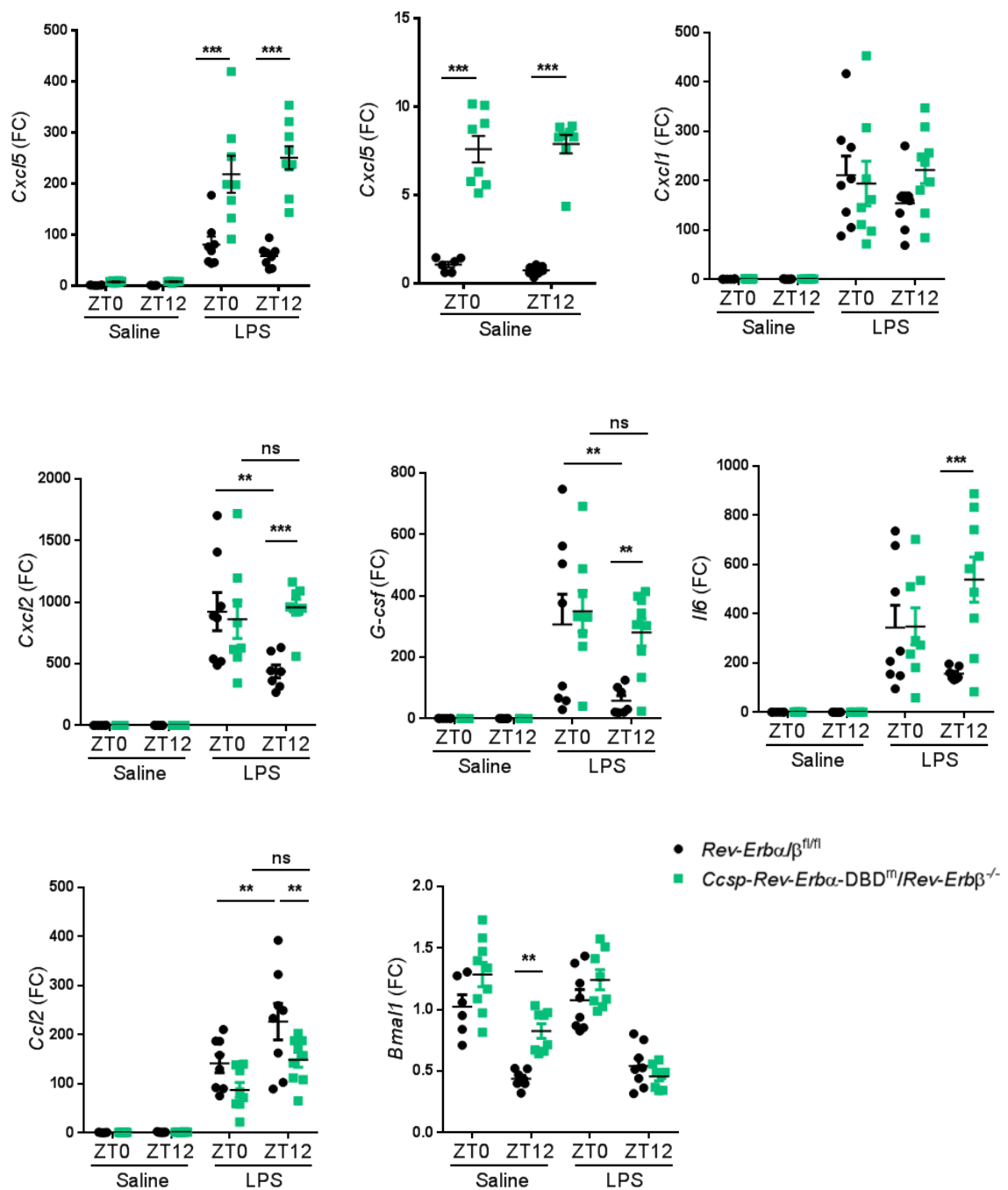
Figure A15. 1: Transcript levels of inflammatory genes in response to LPS challenge at ZT0 and ZT12 in *Ccsp-Rev-Erbα*-DBD^m/*Rev-Erbβ^-/-*mice and *Rev-Erbα/β*^fl/fl littermate controls

Mice were exposed to aerosolised LPS at 2mg/ml or to saline for 20 minutes at ZT0 or ZT12 and culled 5 hours later. RNA was extracted from whole lung and transcript levels were measured by Taqman Real-Time qPCR and normalized to ZT0 *Rev-Erbα/β*^fl/fl saline group. Data are presented as mean ± SEM; *n* = 7-9, (Two-way ANOVA, post hoc Bonferroni).

Appendix 16 – Comparison of cell synchronisation by serum shock or dexamethasone
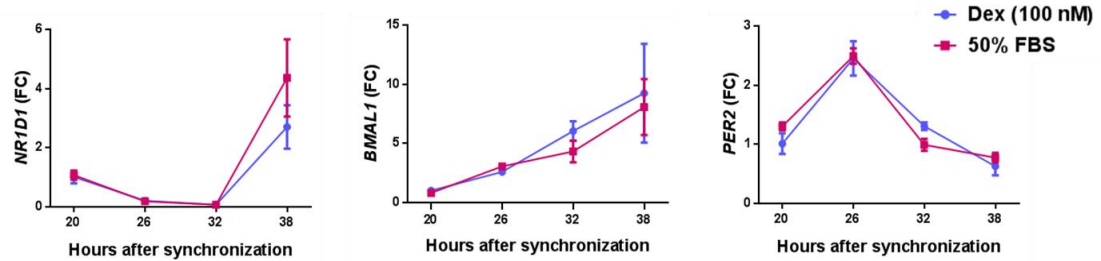
Figure A16. 1: Rhythmic variations of clock genes in NHBE cells synchronised by serum shock or dexamethasone

NHBE cells were synchronised by incubation with 50% FBS or dexamethasone at 100 nM for one hour. mRNA levels of the clock genes were measured using Taqman Real-Time qPCR and normalized to the first time point. Data are presented as mean ± SD; n = 3.

Appendix 17 – REV-ERBα knock-down by siRNA in NHBE cells
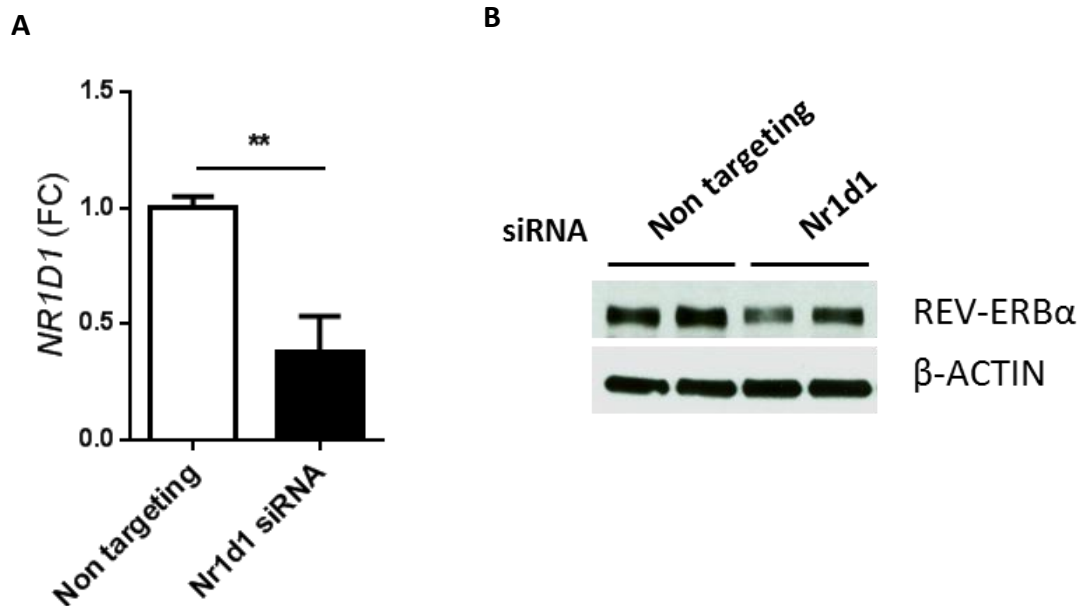
Figure A17. 1: Efficiency of Rev-Erbα siRNA transfection on mRNA and protein levels NHBE cells were transfected for 48 hours with Rev-Erbα siRNA at 25 nM. Then, cells were synchronised by serum shock and 18 hours later cells were lysed for RNA extraction or protein quantification. (A) *REV-ERBα* expression was determined by Real-Time qPCR and normalized to non targeting siRNA transfected cells. Data are presented as mean ± SD; n = 3. **P <0.01 (Student's *t*-test). (B) Total cell lysates were analysed by Western blotting for REV-ERBα protein levels (15 µg total protein loaded per lane).

Appendix 18 – Reduction of REV-ERBα protein levels upon aerosolised LPS in genetic targeted mouse models

A

B
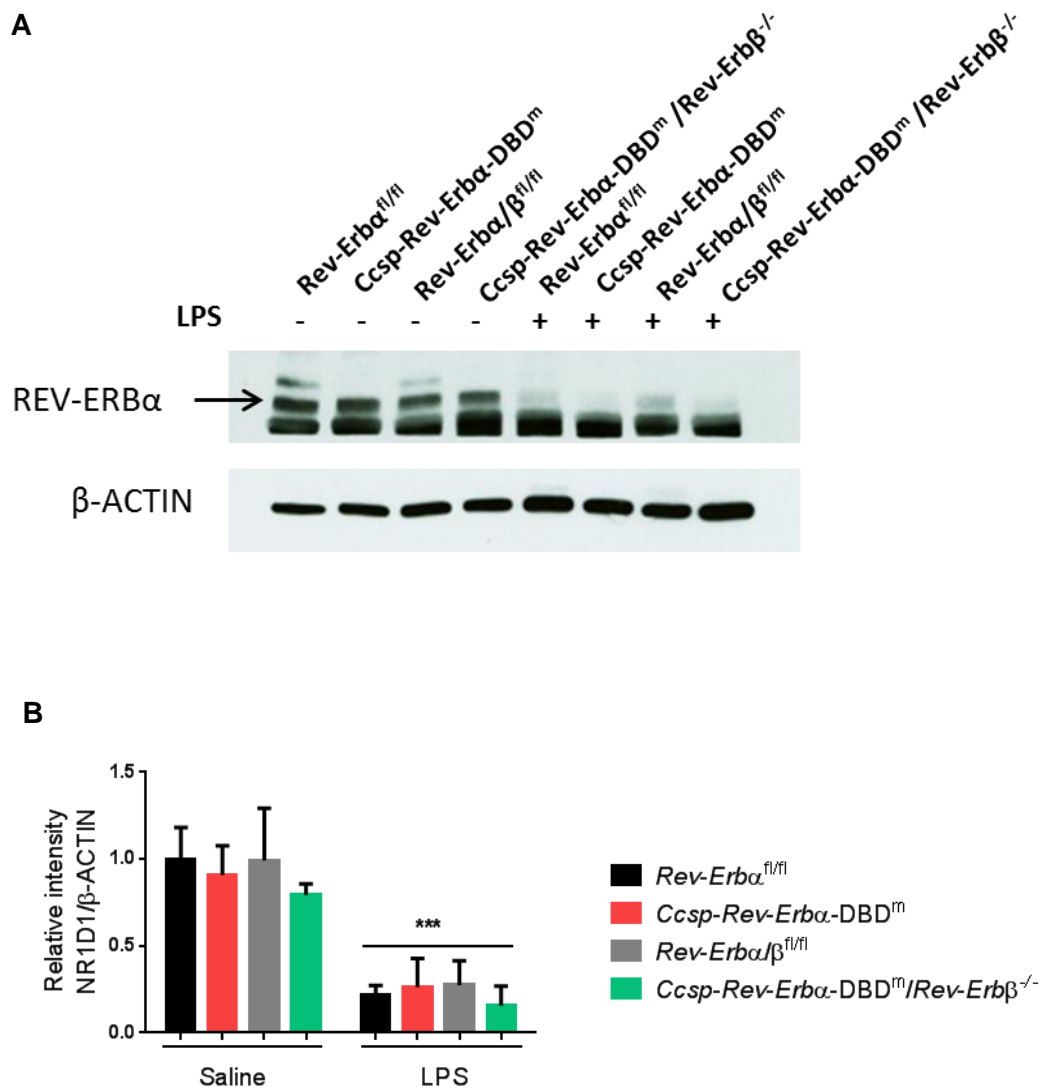
Figure A18. 1: Aerosolised LPS reduces levels of REV-ERBα protein in murine lungs

Ccsp-Rev-Erbα-DBD[m], *Ccsp-Rev-erbα*-DBD[m]*/Rev-Erbβ*^{-/-} mice and *Rev-Erbα*^{fl/fl}, *Rev-Erbα/β*[fl/fl] littermate controls were exposed to aerosolised LPS at 2mg/ml or to saline for 20 minutes at ZT4 and culled 5 hours later. (A) Total lung tissues were analysed by Western blotting for REV-ERBα protein levels using GSK6F05 monoclonal antibody (20 µg total protein loaded per lane). (B) Relative intensity was obtained by dividing the intensity of REV-ERBα bands by their beta-actin ones and results were normalised to *Rev-Erbα*^{fl/fl} saline group, $n=3$; ***$P < 0.001$, significantly reduced compared to saline groups (One-way ANOVA, post hoc Bonferroni).

References

Adelmant, G., Bègue, A., Stéhelin, D., Laudet, V., 1996. A functional Rev-erb alpha responsive element located in the human Rev-erb alpha promoter mediates a repressing activity. Proceedings of the National Academy of Sciences of the United States of America 93, 3553-3558.

Agusti, A., Hedner, J., Marin, J.M., Barbé, F., Cazzola, M., Rennard, S., 2011. Night-time symptoms: a forgotten dimension of COPD. European Respiratory Review 20, 183-194.

Alvarez, J.D., Hansen, A., Ord, T., Bebas, P., Chappell, P.E., Giebultowicz, J.M., Williams, C., Moss, S., Sehgal, A., 2008. The Circadian Clock Protein BMAL1 Is Necessary for Fertility and Proper Testosterone Production in Mice. Journal of Biological Rhythms 23, 26-36.

Angiolilli, C., Kabala, P., Grabiec, A., Malvar-Fernández, B., Baeten, D., Reedquist, K., 2015. A2.19 HDAC3 is required for the inflammatory gene expression program in fibroblast-like synoviocytes. Annals of the Rheumatic Diseases 74, A23.

Arjona, A., Sarkar, D.K., 2005. Circadian Oscillations of Clock Genes, Cytolytic Factors, and Cytokines in Rat NK Cells. The Journal of Immunology 174, 7618-7624.

Arjona, A., Silver, A.C., Walker, W.E., Fikrig, E., 2012. Immunity's fourth dimension: approaching the circadian-immune connection. Trends in Immunology.

Arrigoni, L., Richter, A.S., Betancourt, E., Bruder, K., Diehl, S., Manke, T., Bönisch, U., 2015. Standardizing chromatin research: a simple and universal method for ChIP-seq. Nucleic Acids Research.

Arsalane, K., Broeckaert, F., Knoops, B., Wiedig, M., Toubeau, G., Bernard, A., 2000. Clara Cell Specific Protein (CC16) Expression after Acute Lung Inflammation Induced by Intratracheal Lipopolysaccharide Administration. American Journal of Respiratory and Critical Care Medicine 161, 1624-1630.

Axelsson, J., Puttonen, S., 2012. Night shift work increases the risk for type 2 diabetes. Evidence Based Medicine 17, 193-194.

Ayaydin, F., Dasso, M., 2004. Distinct In Vivo Dynamics of Vertebrate SUMO Paralogues. Molecular Biology of the Cell 15, 5208-5218.

Balsalobre, A., Damiola, F., Schibler, U., 1998. A Serum Shock Induces Circadian Gene Expression in Mammalian Tissue Culture Cells. Cell 93, 929-937.

Bando, H., Nishio, T., van der Horst, G.T.J., Masubuchi, S., Hisa, Y., Okamura, H., 2007. Vagal Regulation of Respiratory Clocks in Mice. The Journal of Neuroscience 27, 4359-4365.

Beam, W.R., Weiner, D.E., Martin, R.J., 1992. Timing of Prednisone and Alterations of Airways Inflammation in Nocturnal Asthma. American Review of Respiratory Disease 146, 1524-1530.

Beck-Schimmer, B., Schwendener, R., Pasch, T., Reyes, L., Booy, C., Schimmer, R.C., 2005. Alveolar macrophages regulate neutrophil recruitment in endotoxin-induced lung injury. Respiratory Research 6, 1-14.

Belden, W.J., Dunlap, J.C., 2008. SIRT1 Is a Circadian Deacetylase for Core Clock Components. Cell 134, 212-214.

Bellet, M.M., Deriu, E., Liu, J.Z., Grimaldi, B., Blaschitz, C., Zeller, M., Edwards, R.A., Sahar, S., Dandekar, S., Baldi, P., George, M.D., Raffatellu, M., Sassone-Corsi, P., 2013. Circadian clock regulates the host response to Salmonella. Proceedings of the National Academy of Sciences 110, 9897-9902.

Bellet, M.M., Zocchi, L., Sassone-Corsi, P., 2012. The RelB subunit of NFκB acts as a negative regulator of circadian gene expression. Cell Cycle 11, 3304-3311.

Bendall, L.J., Bradstock, K.F., 2014. G-CSF: From granulopoietic stimulant to bone marrow stem cell mobilizing agent. Cytokine & Growth Factor Reviews 25, 355-367.

Benowitz, N.L., Hansson, A., Jacob, P., 2002. Cardiovascular Effects of Nasal and Transdermal Nicotine and Cigarette Smoking. Hypertension 39, 1107-1112.

Bhalla, D.K., Hirata, F., Rishi, A.K., Gairola, C.G., 2008. Cigarette Smoke, Inflammation, and Lung Injury: A Mechanistic Perspective. Journal of Toxicology and Environmental Health, Part B 12, 45-64.

Bhatia, M., Zemans, R.L., Jeyaseelan, S., 2012. Role of Chemokines in the Pathogenesis of Acute Lung Injury. American Journal of Respiratory Cell and Molecular Biology 46, 566-572.

Bollinger, T., Leutz, A., Leliavski, A., Skrum, L., Kovac, J., Bonacina, L., Benedict, C., Lange, T., Westermann, J.r., Oster, H., Solbach, W., 2011. Circadian Clocks in Mouse and Human CD4+ T Cells. PLoS ONE 6, e29801.

Bonnelye, E., Vanacker, J., Desbiens, X., Begue, A., Stehelin, D., Laudet, V., 1994. Rev-erb beta, a new member of the nuclear receptor superfamily, is expressed in the nervous system during chicken development. Cell Growth Differ 5, 1357-1365.

Brown, D.L., Feskanich, D., Sánchez, B.N., Rexrode, K.M., Schernhammer, E.S., Lisabeth, L.D., 2009. Rotating Night Shift Work and the Risk of Ischemic Stroke. American Journal of Epidemiology 169, 1370-1377.

Bugge, A., Feng, D., Everett, L.J., Briggs, E.R., Mullican, S.E., Wang, F., Jager, J., Lazar, M.A., 2012. Rev-erbα and Rev-erbβ coordinately protect the circadian clock and normal metabolic function. Genes & Development 26, 657-667.

Buijs, R.M., van Eden, C.G., Goncharuk, V.D., Kalsbeek, A., 2003. The biological clock tunes the organs of the body: timing by hormones and the autonomic nervous system. Journal of Endocrinology 177, 17-26.

Bunger, M.K., Wilsbacher, L.D., Moran, S.M., Clendenin, C., Radcliffe, L.A., Hogenesch, J.B., Simon, M.C., Takahashi, J.S., Bradfield, C.A., 2000. Mop3 Is an Essential Component of the Master Circadian Pacemaker in Mammals. Cell 103, 1009-1017.

Burke, L., Downes, M., Carozzi, A., Giguère, V., Muscat, G.E.O., 1996. Transcriptional Repression by the Orphan Steroid Receptor RVR/Rev-erbβ Is Dependent on the Signature Motif and Helix 5 in the E Region: Functional Evidence for a Biological Role of RVR in Myogenesis. Nucleic Acids Research 24, 3481-3489.

Bush, A., Menzies-Gow, A., 2009. Phenotypic Differences between Pediatric and Adult Asthma. Proceedings of the American Thoracic Society 6, 712-719.

Buttgereit, F., Smolen, J.S., Coogan, A.N., Cajochen, C., 2015. Clocking in: chronobiology in rheumatoid arthritis. Nat Rev Rheumatol 11, 349-356.

Caito, S., Rajendrasozhan, S., Cook, S., Chung, S., Yao, H., Friedman, A.E., Brookes, P.S., Rahman, I., 2010. SIRT1 is a redox-sensitive deacetylase that is post-translationally modified by oxidants and carbonyl stress. The FASEB Journal 24, 3145-3159.

Caldenhoven, E., Liden, J., Wissink, S., Van de Stolpe, A., Raaijmakers, J., Koenderman, L., Okret, S., Gustafsson, J.A., Van der Saag, P.T., 1995. Negative cross-talk between RelA and the glucocorticoid receptor: a possible mechanism for the antiinflammatory action of glucocorticoids. Molecular Endocrinology 9, 401-412.

Caldwell, S.H., Argo, C.K., 2007. Divergent effects of peroxisome proliferator–activated receptor-γ ligands in human and mouse nonalcoholic steatohepatitis. Hepatology 46, 285-287.

Campos-de-Sousa, S., Guindalini, C., Tondo, L., Munro, J., Osborne, S., Floris, G., Pedrazzoli, M., Tufik, S., Breen, G., Collier, D., 2010. Nuclear Receptor Rev-Erb-α Circadian Gene Variants and Lithium Carbonate Prophylaxis in Bipolar Affective Disorder. Journal of Biological Rhythms 25, 132-137.

Cardone, L., Hirayama, J., Giordano, F., Tamaru, T., Palvimo, J.J., Sassone-Corsi, P., 2005. Circadian Clock Control by SUMOylation of BMAL1. Science 309, 1390-1394.

Cardoso, W.V., Whitsett, J.A., 2008. Resident Cellular Components of the Lung. Proceedings of the American Thoracic Society 5, 767-771.

Carlson, B.A., Yoo, M.-H., Conrad, M., Gladyshev, V.N., Hatfield, D.L., Park, J.M., 2011. Protein kinase-regulated expression and immune function of thioredoxin reductase 1 in mouse macrophages. Molecular Immunology 49, 311-316.

Carlson, D.E., Chiu, W.C., 2008. THE ABSENCE OF CIRCADIAN CUES DURING RECOVERY FROM SEPSIS MODIFIES PITUITARY-ADRENOCORTICAL FUNCTION AND IMPAIRS SURVIVAL. Shock 29, 127-132.

Castanon-Cervantes, O., Wu, M., Ehlen, J.C., Paul, K., Gamble, K.L., Johnson, R.L., Besing, R.C., Menaker, M., Gewirtz, A.T., Davidson, A.J., 2010. Dysregulation of Inflammatory Responses by Chronic Circadian Disruption. The Journal of Immunology 185, 5796-5805.

Cavadini, G., Petrzilka, S., Kohler, P., Jud, C., Tobler, I., Birchler, T., Fontana, A., 2007. TNF-α suppresses the expression of clock genes by interfering with E-box-mediated transcription. Proceedings of the National Academy of Sciences of the United States of America 104, 12843-12848.

Chandra, V., Mahajan, S., Saini, A., Dkhar, H.K., Nanduri, R., Raj, E.B., Kumar, A., Gupta, P., 2013. Human IL10 repression by Reverb alpha ameliorates Mycobacterium tuberculosis clearance. Journal of Biological Chemistry.

Chen, J.D., Evans, R.M., 1995. A transcriptional co-repressor that interacts with nuclear hormone   receptors. Nature 377, 454-457.

Chen, X.-L., Dodd, G., Thomas, S., Zhang, X., Wasserman, M.A., Rovin, B.H., Kunsch, C., 2006. Activation of Nrf2/ARE pathway protects endothelial cells from oxidant injury and inhibits inflammatory gene expression. American Journal of Physiology - Heart and Circulatory Physiology 290, H1862-H1870.

Chen, X., Barozzi, I., Termanini, A., Prosperini, E., Recchiuti, A., Dalli, J., Mietton, F., Matteoli, G., Hiebert, S., Natoli, G., 2012. Requirement for the histone deacetylase Hdac3 for the inflammatory gene expression program in macrophages. Proceedings of the National Academy of Sciences of the United States of America 109, E2865-E2874.

Cheng, D.-s., Han, W., Chen, S.M., Sherrill, T.P., Chont, M., Park, G.-Y., Sheller, J.R., Polosukhin, V.V., Christman, J.W., Yull, F.E., Blackwell, T.S., 2007. Airway Epithelium Controls Lung Inflammation and Injury through the NF-κB Pathway. The Journal of Immunology 178, 6504-6513.

Cho, H., Zhao, X., Hatori, M., Yu, R.T., Barish, G.D., Lam, M.T., Chong, L.-W., DiTacchio, L., Atkins, A.R., Glass, C.K., Liddle, C., Auwerx, J., Downes, M., Panda, S., Evans, R.M., 2012. Regulation of circadian behaviour and metabolism by REV-ERB-α and REV-ERB-β. Nature 485, 123-127.

Clausen, B.E., Burkhardt, C., Reith, W., Renkawitz, R., Förster, I., 1999. Conditional gene targeting in macrophages and granulocytes using LysMcre mice. Transgenic Research 8, 265-277.

Creyghton, M.P., Cheng, A.W., Welstead, G.G., Kooistra, T., Carey, B.W., Steine, E.J., Hanna, J., Lodato, M.A., Frampton, G.M., Sharp, P.A., Boyer, L.A., Young, R.A., Jaenisch, R., 2010. Histone H3K27ac separates active from poised enhancers and predicts developmental state. Proceedings of the National Academy of Sciences 107, 21931-21936.

Crystal, R.G., Randell, S.H., Engelhardt, J.F., Voynow, J., Sunday, M.E., 2008. Airway Epithelial Cells. Proceedings of the American Thoracic Society 5, 772-777.

Curtin, J.F., Cotter, T.G., 2004. JNK Regulates HIPK3 Expression and Promotes Resistance to Fas-mediated Apoptosis in DU 145 Prostate Carcinoma Cells. Journal of Biological Chemistry 279, 17090-17100.

Curtis, Anne M., Bellet, Marina M., Sassone-Corsi, P., O'Neill, Luke A.J., 2014. Circadian Clock Proteins and Immunity. Immunity 40, 178-186.

Cutolo, M., Straub, R.H., Buttgereit, F., 2008. Circadian rhythms of nocturnal hormones in rheumatoid arthritis: translation from bench to bedside. Annals of the Rheumatic Diseases 67, 905-908.

Davidson, A.J., Sellix, M.T., Daniel, J., Yamazaki, S., Menaker, M., Block, G.D., 2006. Chronic jet-lag increases mortality in aged mice. Current Biology 16, R914-R916.

DeBruyne, J.P., Baggs, J.E., Sato, T.K., Hogenesch, J.B., 2015. Ubiquitin ligase Siah2 regulates RevErbα degradation and the mammalian circadian clock. Proceedings of the National Academy of Sciences of the United States of America 112, 12420-12425.

DeLeo, F.R., Renee, J., McCormick, S., Nakamura, M., Apicella, M., Weiss, J.P., Nauseef, W.M., 1998. Neutrophils exposed to bacterial lipopolysaccharide upregulate NADPH oxidase assembly. The Journal of Clinical Investigation 101, 455-463.

Delmastro-Greenwood, M.M., Piganelli, J.D., 2013. Changing the energy of an immune response. American journal of clinical and experimental immunology 2, 30-54.

Denuc, A., Marfany, G., 2010. SUMO and ubiquitin paths converge, pp. 34-39.

Doerschuk, C.M., Beyers, N., Coxson, H.O., Wiggs, B., Hogg, J.C., 1993. Comparison of neutrophil and capillary diameters and their relation to neutrophil sequestration in the lung. Journal of Applied Physiology 74, 3040-3045.

Donaldson, K., Tran, C.L., 2002. INFLAMMATION CAUSED BY PARTICLES AND FIBERS. Inhalation Toxicology 14, 5-27.

Downes, M., Burke, L.J., Bailey, P.J., Muscat, G.E., 1996. Two receptor interaction domains in the corepressor, N-CoR/RIP13, are required for an efficient interaction with Rev-erbA alpha and RVR: physical association is dependent on the E region of the orphan receptors. Nucleic Acids Research 24, 4379-4386.

Downs, S., Brandli, O., Zellweger, J.-P., Schindler, C., Kunzli, N., Gerbase, M., Burdet, L., Bettschart, R., Zemp, E., Frey, M., Keller, R., Tschopp, J.-M., Leuenberger, P., Ackermann-Liebrich, U., the, S.t., 2005. Accelerated decline in lung function in smoking women with airway obstruction: SAPALDIA 2 cohort study. Respiratory Research 6, 45.

Duan, Q.L., Lasky-Su, J., Himes, B.E., Qiu, W., Litonjua, A.A., Damask, A., Lazarus, R., Klanderman, B., Irvin, C.G., Peters, S.P., Hanrahan, J.P., Lima, J.J., Martinez, F.D., Mauger, D., Chinchilli, V.M., Soto-Quiros, M., Avila, L., Celedón, J.C., Lange, C., Weiss, S.T., Tantisira, K.G., 2014. A genome-wide association study of bronchodilator response in asthmatics. The pharmacogenomics journal 14, 41-47.

Duez, H., Staels, B., 2009. Rev-erb-α: an integrator of circadian rhythms and metabolism. Journal of Applied Physiology 107, 1972-1980.

Dumas, B., Harding, H.P., Choi, H.S., Lehmann, K.A., Chung, M., Lazar, M.A., Moore, D.D., 1994. A new orphan member of the nuclear hormone receptor superfamily closely related to Rev-Erb. Molecular Endocrinology 8, 996-1005.

Eastman, C.I., Mistlberger, R.E., Rechtschaffen, A., 1984. Suprachiasmatic nuclei lesions eliminate circadian temperature and sleep rhythms in the rat. Physiology & Behavior 32, 357-368.

Eberl, G., Marmon, S., Sunshine, M.-J., Rennert, P.D., Choi, Y., Littman, D.R., 2004. An essential function for the nuclear receptor ROR[gamma]t in the generation of fetal lymphoid tissue inducer cells. Nat Immunol 5, 64-73.

Edgar, R.S., Green, E.W., Zhao, Y., van Ooijen, G., Olmedo, M., Qin, X., Xu, Y., Pan, M., Valekunja, U.K., Feeney, K.A., Maywood, E.S., Hastings, M.H., Baliga, N.S., Merrow, M., Millar, A.J., Johnson, C.H., Kyriacou, C.P., O/'Neill, J.S., Reddy, A.B., 2012. Peroxiredoxins are conserved markers of circadian rhythms. Nature advance online publication.

Eide, E.J., Woolf, M.F., Kang, H., Woolf, P., Hurst, W., Camacho, F., Vielhaber, E.L., Giovanni, A., Virshup, D.M., 2005. Control of Mammalian Circadian Rhythm by CKIepsilon-

Regulated Proteasome-Mediated PER2 Degradation. Molecular and Cellular Biology 25, 2795-2807.

Elizur, A., Adair-Kirk, T.L., Kelley, D.G., Griffin, G.L., deMello, D.E., Senior, R.M., 2007. Clara cells impact the pulmonary innate immune response to LPS. American Journal of Physiology - Lung Cellular and Molecular Physiology 293, L383-L392.

Elizur, A., Adair-Kirk, T.L., Kelley, D.G., Griffin, G.L., deMello, D.E., Senior, R.M., 2008. Tumor Necrosis Factor-α from Macrophages Enhances LPS-Induced Clara Cell Expression of Keratinocyte-Derived Chemokine. American Journal of Respiratory Cell and Molecular Biology 38, 8-15.

Engwall, M., Fridh, I., Johansson, L., Bergbom, I., Lindahl, B., 2015. Lighting, sleep and circadian rhythm: An intervention study in the intensive care unit. Intensive and Critical Care Nursing 31, 325-335.

Everett, L.J., Lazar, M.A., 2014. Nuclear Receptor Rev-erbα: Up, Down, and All Around. Trends in endocrinology and metabolism: TEM 25, 586-592.

Feng, D., Liu, T., Sun, Z., Bugge, A., Mullican, S.E., Alenghat, T., Liu, X.S., Lazar, M.A., 2011. A Circadian Rhythm Orchestrated by Histone Deacetylase 3 Controls Hepatic Lipid Metabolism. Science 331, 1315-1319.

Filipski, E., Delaunay, F., King, V.M., Wu, M.-W., Claustrat, B., Gréchez-Cassiau, A., Guettier, C., Hastings, M.H., Lévi, F., 2004. Effects of Chronic Jet Lag on Tumor Progression in Mice. Cancer Research 64, 7879-7885.

Fontaine, C., Rigamonti, E., Pourcet, B., Duez, H., Duhem, C., Fruchart, J.-C., Chinetti-Gbaguidi, G., Staels, B., 2008. The Nuclear Receptor Rev-erbα Is a Liver X Receptor (LXR) Target Gene Driving a Negative Feedback Loop on Select LXR-Induced Pathways in Human Macrophages. Molecular Endocrinology 22, 1797-1811.

Fortier, E.E., Rooney, J., Dardente, H., Hardy, M.-P., Labrecque, N., Cermakian, N., 2011. Circadian Variation of the Response of T Cells to Antigen. The Journal of Immunology 187, 6291-6300.

Fu, L., Pelicano, H., Liu, J., Huang, P., Lee, C.C., 2002. The Circadian Gene Period2 Plays an Important Role in Tumor Suppression and DNA Damage Response In Vivo. Cell 111, 41-50.

Gallego, M., Virshup, D.M., 2007. Post-translational modifications regulate the ticking of the circadian clock. Nat Rev Mol Cell Biol 8, 139-148.

Gaultier, C., Reinberg, A., Girard, F.o., 1977. CIrcadian rhythms in lung resistance and dynamic lung compliance of healthy children. Effects of two bronchodilators. Respiration Physiology 31, 169-182.

Gebel, S., Gerstmayer, B., Kuhl, P., Borlak, J., Meurrens, K., Müller, T., 2006. The kinetics of transcriptomic changes induced by cigarette smoke in rat lungs reveals a specific program of defense, inflammation, and circadian clock gene expression. Toxicological sciences : an official journal of the Society of Toxicology 93, 422-431.

Geyfman, M., Kumar, V., Liu, Q., Ruiz, R., Gordon, W., Espitia, F., Cam, E., Millar, S.E., Smyth, P., Ihler, A., Takahashi, J.S., Andersen, B., 2012. Brain and muscle Arnt-like protein-1 (BMAL1) controls circadian cell proliferation and susceptibility to UVB-induced DNA damage in the epidermis. Proceedings of the National Academy of Sciences 109, 11758-11763.

Gibbs, J., Ince, L., Matthews, L., Mei, J., Bell, T., Yang, N., Saer, B., Begley, N., Poolman, T., Pariollaud, M., Farrow, S., DeMayo, F., Hussell, T., Worthen, G.S., Ray, D., Loudon, A., 2014. An epithelial circadian clock controls pulmonary inflammation and glucocorticoid action. Nat Med 20, 919-926.

Gibbs, J.E., Beesley, S., Plumb, J., Singh, D., Farrow, S., Ray, D.W., Loudon, A.S.I., 2009. Circadian Timing in the Lung; A Specific Role for Bronchiolar Epithelial Cells. Endocrinology 150, 268-276.

Gibbs, J.E., Blaikley, J., Beesley, S., Matthews, L., Simpson, K.D., Boyce, S.H., Farrow, S.N., Else, K.J., Singh, D., Ray, D.W., Loudon, A.S.I., 2012. The nuclear receptor REV-ERBα mediates circadian regulation of innate immunity through selective regulation of inflammatory cytokines. Proceedings of the National Academy of Sciences 109, 582-587.

Glass, C.K., Saijo, K., 2010. Nuclear receptor transrepression pathways that regulate inflammation in macrophages and T cells. Nat Rev Immunol 10, 365-376.

Godinho, S.I.H., Maywood, E.S., Shaw, L., Tucci, V., Barnard, A.R., Busino, L., Pagano, M., Kendall, R., Quwailid, M.M., Romero, M.R., O'Neill, J., Chesham, J.E., Brooker, D., Lalanne, Z., Hastings, M.H., Nolan, P.M., 2007. The After-Hours Mutant Reveals a Role for Fbxl3 in Determining Mammalian Circadian Period. Science 316, 897-900.

Grant, D., Yin, L., Collins, J.L., Parks, D.J., Orband-Miller, L.A., Wisely, G.B., Joshi, S., Lazar, M.A., Willson, T.M., Zuercher, W.J., 2010. GSK4112, a Small Molecule Chemical Probe for the Cell Biology of the Nuclear Heme Receptor Rev-erbα. ACS Chemical Biology 5, 925-932.

Greenberg, H., Cohen, R.I., 2012. Nocturnal asthma. Current Opinion in Pulmonary Medicine 18, 57-62 10.1097/MCP.1090b1013e32834d32098e.

Guilding, C., Scott, F., Bechtold, D.A., Brown, T.M., Wegner, S., Piggins, H.D., 2013. Suppressed cellular oscillations in after-hours mutant mice are associated with enhanced circadian phase-resetting. The Journal of Physiology 591, 1063-1080.

Guillaumond, F., Dardente, H., Giguère, V., Cermakian, N., 2005. Differential Control of Bmal1 Circadian Transcription by REV-ERB and ROR Nuclear Receptors. Journal of Biological Rhythms 20, 391-403.

Hadden, H., Soldin, S.J., Massaro, D., 2012. Circadian disruption alters mouse lung clock gene expression and lung mechanics. Journal of Applied Physiology 113, 385-392.

Halberg, F., Johnson, E.A., Brown, B.W., Bittner, J.J., 1960. Susceptibility Rhythm to E. coli Endotoxin and Bioassay. Experimental Biology and Medicine 103, 142-144.

Hand, L.E., Hopwood, T.W., Dickson, S.H., Walker, A.L., Loudon, A.S.I., Ray, D.W., Bechtold, D.A., Gibbs, J.E., 2016. The circadian clock regulates inflammatory arthritis. The FASEB Journal.

Harding, H.P., Lazar, M.A., 1995. The monomer-binding orphan receptor Rev-Erb represses transcription as a dimer on a novel direct repeat. Molecular and Cellular Biology 15, 4791-4802.

Harrod, K.S., Mounday, A.D., Stripp, B.R., Whitsett, J.A., 1998. Clara cell secretory protein decreases lung inflammation after acute virus infection, pp. L924-L930.

Hashiramoto, A., Yamane, T., Tsumiyama, K., Yoshida, K., Komai, K., Yamada, H., Yamazaki, F., Doi, M., Okamura, H., Shiozawa, S., 2010. Mammalian Clock Gene Cryptochrome Regulates Arthritis via Proinflammatory Cytokine TNF-α. The Journal of Immunology 184, 1560-1565.

Haspel, J.A., Chettimada, S., Shaik, R.S., Chu, J.-H., Raby, B.A., Cernadas, M., Carey, V., Process, V., Hunninghake, G.M., Ifedigbo, E., Lederer, J.A., Englert, J., Pelton, A., Coronata, A., Fredenburgh, L.E., Choi, A.M.K., 2014. Circadian rhythm reprogramming during lung inflammation. Nat Commun 5.

Hastings, M., O'Neill, J.S., Maywood, E.S., 2007. Circadian clocks: regulators of endocrine and metabolic rhythms. Journal of Endocrinology 195, 187-198.

Haus, E., Smolensky, M.H., 1999. Biologic Rhythms in the Immune System. Chronobiology International 16, 581-622.

Hayashi, M., Shimba, S., Tezuka, M., 2007. Characterization of the Molecular Clock in Mouse Peritoneal Macrophages. Biological and Pharmaceutical Bulletin 30, 621-626.

He, B., Chen, Z., 2016. Molecular Targets for Small-Molecule Modulators of Circadian Clocks. Current Drug Metabolism 17, 503-512.

Helzer, K.T., Hooper, C., Miyamoto, S., Alarid, E.T., 2015. Ubiquitylation of nuclear receptors: new linkages and therapeutic implications. Journal of Molecular Endocrinology 54, R151-R167.

Hetzel, M.R., Clark, T.J., 1980. Comparison of normal and asthmatic circadian rhythms in peak expiratory flow rate. Thorax 35, 732-738.

Hu, X., Lazar, M.A., 1999. The CoRNR motif controls the recruitment of corepressors by nuclear hormone receptors. Nature 402, 93-96.

Hwang, J.-W., Sundar, I.K., Yao, H., Sellix, M.T., Rahman, I., 2014. Circadian clock function is disrupted by environmental tobacco/cigarette smoke, leading to lung inflammation and injury via a SIRT1-BMAL1 pathway. The FASEB Journal 28, 176-194.

Iizuka, T., Ishii, Y., Itoh, K., Kiwamoto, T., Kimura, T., Matsuno, Y., Morishima, Y., Hegab, A.E., Homma, S., Nomura, A., Sakamoto, T., Shimura, M., Yoshida, A., Yamamoto, M., Sekizawa, K., 2005. Nrf2-deficient mice are highly susceptible to cigarette smoke-induced emphysema. Genes to Cells 10, 1113-1125.

Jeyaseelan, S., Manzer, R., Young, S.K., Yamamoto, M., Akira, S., Mason, R.J., Worthen, G.S., 2005. Induction of CXCL5 During Inflammation in the Rodent Lung Involves Activation of Alveolar Epithelium. American Journal of Respiratory Cell and Molecular Biology 32, 531-539.

John, S., Sabo, P.J., Johnson, T.A., Sung, M.-H., Biddie, S.C., Lightman, S.L., Voss, T.C., Davis, S.R., Meltzer, P.S., Stamatoyannopoulos, J.A., Hager, G.L., 2008. Interaction of the Glucocorticoid Receptor with the Chromatin Landscape. Molecular Cell 29, 611-624.

Kaasik, K., 2004. Reciprocal regulation of haem biosynthesis and the circadian clock in mammals. Nature 430, 467-471.

Kallen, J., Schlaeppi, J.-M., Bitsch, F., Delhon, I., Fournier, B., 2004. Crystal Structure of the Human RORα Ligand Binding Domain in Complex with Cholesterol Sulfate at 2.2 Å. Journal of Biological Chemistry 279, 14033-14038.

Karatsoreos, I.N., Bhagat, S., Bloss, E.B., Morrison, J.H., McEwen, B.S., 2011. Disruption of circadian clocks has ramifications for metabolism, brain, and behavior. Proceedings of the National Academy of Sciences 108, 1657-1662.

Keller, M., Mazuch, J., Abraham, U., Eom, G.D., Herzog, E.D., Volk, H.-D., Kramer, A., Maier, B., 2009. A circadian clock in macrophages controls inflammatory immune responses. Proceedings of the National Academy of Sciences 106, 21407-21412.

Kelly, E.A.B., Houtman, J.J., Jarjour, N.N., 2004. Inflammatory changes associated with circadian variation in pulmonary function in subjects with mild asthma. Clinical & Experimental Allergy 34, 227-233.

Kessler, R., Partridge, M.R., Miravitlles, M., Cazzola, M., Vogelmeier, C., Leynaud, D., Ostinelli, J., 2011. Symptom variability in patients with severe COPD: a pan-European cross-sectional study. European Respiratory Journal 37, 264-272.

Kida, H., Yoshida, M., Hoshino, S., Inoue, K., Yano, Y., Yanagita, M., Kumagai, T., Osaki, T., Tachibana, I., Saeki, Y., Kawase, I., 2005. Protective effect of IL-6 on alveolar epithelial cell death induced by hydrogen peroxide. American Journal of Physiology - Lung Cellular and Molecular Physiology 288, L342-L349.

Kirkham, P., Rahman, I., 2006. Oxidative stress in asthma and COPD: Antioxidants as a therapeutic strategy. Pharmacology & Therapeutics 111, 476-494.

Kobayashi, Y., 2006. Neutrophil Infiltration and Chemokines. 26, 307-316.

Kojetin, D., Wang, Y., Kamenecka, T.M., Burris, T.P., 2011. Identification of SR8278, a Synthetic Antagonist of the Nuclear Heme Receptor REV-ERB. ACS Chemical Biology 6, 131-134.

Kondratov, R.V., Kondratova, A.A., Gorbacheva, V.Y., Vykhovanets, O.V., Antoch, M.P., 2006. Early aging and age-related pathologies in mice deficient in BMAL1, the core componentof the circadian clock. Genes & Development 20, 1868-1873.

Kraft, M., Djukanovic, R., Wilson, S., Holgate, S.T., Martin, R.J., 1996. Alveolar tissue inflammation in asthma. American Journal of Respiratory and Critical Care Medicine 154, 1505-1510.

Krishnan, N., Davis, A.J., Giebultowicz, J.M., 2008. Circadian regulation of response to oxidative stress in Drosophila melanogaster. Biochemical and Biophysical Research Communications 374, 299-303.

Kwak, Y., Lundkvist, G.B., Brask, J., Davidson, A., Menaker, M., Kristensson, K., Block, G.D., 2008. Interferon-γ Alters Electrical Activity and Clock Gene Expression in Suprachiasmatic Nucleus Neurons. Journal of Biological Rhythms 23, 150-159.

Lai, A.G., Doherty, C.J., Mueller-Roeber, B., Kay, S.A., Schippers, J.H.M., Dijkwel, P.P., 2012. CIRCADIAN CLOCK-ASSOCIATED 1 regulates ROS homeostasis and oxidative stress responses. Proceedings of the National Academy of Sciences.

Lam, M.T.Y., Cho, H., Lesch, H.P., Gosselin, D., Heinz, S., Tanaka-Oishi, Y., Benner, C., Kaikkonen, M.U., Kim, A.S., Kosaka, M., Lee, C.Y., Watt, A., Grossman, T.R., Rosenfeld, M.G., Evans, R.M., Glass, C.K., 2013. Rev-Erbs repress macrophage gene expression by inhibiting enhancer-directed transcription. Nature 498, 511-515.

Langmesser, S., Albrecht, U., 2006. Life time-circadian clocks, mitochondria and metabolism. Chronobiology International 23, 151-157.

Lee, C., Etchegaray, J.-P., Cagampang, F.R.A., Loudon, A.S.I., Reppert, S.M., 2001. Posttranslational Mechanisms Regulate the Mammalian Circadian Clock. Cell 107, 855-867.

Lee, J., Lee, Y., Lee, M.J., Park, E., Kang, S.H., Chung, C.H., Lee, K.H., Kim, K., 2008. Dual Modification of BMAL1 by SUMO2/3 and Ubiquitin Promotes Circadian Activation of the CLOCK/BMAL1 Complex. Molecular and Cellular Biology 28, 6056-6065.

Lee, J.M., Johnson, J.A., 2004. An important role of Nrf2-ARE pathway in the cellular defense mechanism. Journal of biochemistry and molecular biology 37, 139-143.

Leys, C., Ley, C., Klein, O., Bernard, P., Licata, L., 2013. Detecting outliers: Do not use standard deviation around the mean, use absolute deviation around the median. Journal of Experimental Social Psychology.

Li, H., Cho, S.N., Evans, C.M., Dickey, B.F., Jeong, J.-W., DeMayo, F.J., 2008a. Cre-mediated recombination in mouse Clara cells. genesis 46, 300-307.

Li, W., Bengtson, M.H., Ulbrich, A., Matsuda, A., Reddy, V.A., Orth, A., Chanda, S.K., Batalov, S., Joazeiro, C.A.P., 2008b. Genome-Wide and Functional Annotation of Human E3 Ubiquitin Ligases Identifies MULAN, a Mitochondrial E3 that Regulates the Organelle's Dynamics and Signaling. PLoS ONE 3, e1487.

Librodo, P., Buckley, M., Luk, M., Bisso, A., 2015. Chronotherapeutic Drug Delivery. Journal of Infusion Nursing 38, S18-S23.

Litinski, M., Scheer, F.A.J.L., Shea, S.A., 2009. Influence of the Circadian System on Disease Severity. Sleep medicine clinics 4, 143-163.

Liu, J., Mankani, G., Shi, X., Meyer, M., Cunningham-Runddles, S., Ma, X., Sun, Z.S., 2006. The Circadian Clock Period 2 Gene Regulates Gamma Interferon Production of NK Cells in Host Response to Lipopolysaccharide-Induced Endotoxic Shock. Infection and Immunity 74, 4750-4756.

Logan, R.W., Zhang, C., Murugan, S., O'Connell, S., Levitt, D., Rosenwasser, A.M., Sarkar, D.K., 2012. Chronic Shift-Lag Alters the Circadian Clock of NK Cells and Promotes Lung Cancer Growth in Rats. The Journal of Immunology 188, 2583-2591.

Longo, P.A., Kavran, J.M., Kim, M.-S., Leahy, D.J., 2013. Chapter Eighteen - Transient Mammalian Cell Transfection with Polyethylenimine (PEI). In: Jon, L. (Ed.), Methods in Enzymology, Academic Press, pp. 227-240.

Lopez-Campos, J.L., Calero, C., Quintana-Gallego, E., 2013. Symptom variability in COPD: a narrative review. International Journal of Chronic Obstructive Pulmonary Disease 8, 231-238.

MacNee, W., 2005. Pathogenesis of Chronic Obstructive Pulmonary Disease. Proceedings of the American Thoracic Society 2, 258-266.

Malisch, J.L., Breuner, C.W., Gomes, F.R., Chappell, M.A., Garland Jr, T., 2008. Circadian pattern of total and free corticosterone concentrations, corticosteroid-binding globulin, and physical activity in mice selectively bred for high voluntary wheel-running behavior. General and Comparative Endocrinology 156, 210-217.

Mangelsdorf, D.J., Thummel, C., Beato, M., Herrlich, P., Schütz, G., Umesono, K., Blumberg, B., Kastner, P., Mark, M., Chambon, P., Evans, R.M., 1995. The nuclear receptor superfamily: The second decade. Cell 83, 835-839.

March, T.H., Wilder, J.A., Esparza, D.C., Cossey, P.Y., Blair, L.F., Herrera, L.K., McDonald, J.D., Campen, M.J., Mauderly, J.L., Seagrave, J., 2006. Modulators of Cigarette Smoke–Induced Pulmonary Emphysema in A/J Mice. Toxicological Sciences 92, 545-559.

Mathis, D., Shoelson, S.E., 2011. Immunometabolism: an emerging frontier. Nature reviews. Immunology 11, 81-81.

McAlpine, C.S., Swirski, F.K., 2016. Circadian Influence on Metabolism and Inflammation in Atherosclerosis. Circulation Research 119, 131-141.

McCarthy, M.J., Nievergelt, C.M., Shekhtman, T., Kripke, D.F., Welsh, D.K., Kelsoe, J.R., 2011. Functional genetic variation in the Rev-Erbα pathway and lithium response in the treatment of bipolar disorder. Genes, Brain and Behavior 10, 852-861.

Medzhitov, R., Horng, T., 2009. Transcriptional control of the inflammatory response. Nat Rev Immunol 9, 692-703.

Mei, J., Liu, Y., Dai, N., Favara, M., Greene, T., Jeyaseelan, S., Poncz, M., Lee, J.S., Worthen, G.S., 2010. CXCL5 Regulates Chemokine Scavenging and Pulmonary Host Defense to Bacterial Infection. Immunity 33, 106-117.

Meng, Q.J., McMaster, A., Beesley, S., Lu, W.Q., Gibbs, J., Parks, D., Collins, J., Farrow, S., Donn, R., Ray, D., Loudon, A., 2008. Ligand modulation of REV-ERBα function resets the peripheral circadian clock in a phasic manner. Journal of Cell Science 121, 3629-3635.

Mohawk, J.A., Green, C.B., Takahashi, J.S., 2012. Central and Peripheral Circadian Clocks in Mammals. Annual Review of Neuroscience 35, 445-462.

Moore, J.T., Collins, J.L., Pearce, K.H., 2006. The Nuclear Receptor Superfamily and Drug Discovery. ChemMedChem 1, 504-523.

Moore, T.A., Newstead, M.W., Strieter, R.M., Mehrad, B., Beaman, B.L., Standiford, T.J., 2000. Bacterial Clearance and Survival Are Dependent on CXC Chemokine Receptor-2 Ligands in a Murine Model of Pulmonary Nocardia asteroides Infection. The Journal of Immunology 164, 908-915.

Mukherji, A., Kobiita, A., Ye, T., Chambon, P., 2013. Homeostasis in Intestinal Epithelium Is Orchestrated by the Circadian Clock and Microbiota Cues Transduced by TLRs. Cell 153, 812-827.

Nagoshi, E., Brown, S.A., Dibner, C., Kornmann, B., Schibler, U., 2005. Circadian Gene Expression in Cultured Cells. In: Michael, W.Y. (Ed.), Methods in Enzymology, Academic Press, pp. 543-557.

Nakahata, Y., Kaluzova, M., Grimaldi, B., Sahar, S., Hirayama, J., Chen, D., Guarente, L.P., Sassone-Corsi, P., 2008. The NAD+-Dependent Deacetylase SIRT1 Modulates CLOCK-Mediated Chromatin Remodeling and Circadian Control. Cell 134, 329-340.

Narasimamurthy, R., Hatori, M., Nayak, S.K., Liu, F., Panda, S., Verma, I.M., 2012. Circadian clock protein cryptochrome regulates the expression of proinflammatory cytokines. Proceedings of the National Academy of Sciences 109, 12662-12667.

Nguyen, K.D., Fentress, S.J., Qiu, Y., Yun, K., Cox, J.S., Chawla, A., 2013. Circadian gene Bmal1 regulates diurnal oscillations of Ly6C(hi) inflammatory monocytes. Science (New York, N.Y.) 341, 10.1126/science.1240636.

Nguyen, T., Nioi, P., Pickett, C.B., 2009. The Nrf2-Antioxidant Response Element Signaling Pathway and Its Activation by Oxidative Stress. The Journal of Biological Chemistry 284, 13291-13295.

Nouailles, G., Dorhoi, A., Koch, M., Zerrahn, J., Weiner, J., 3rd, Fa, xE, C., K., Arrey, F., Kuhlmann, S., Bandermann, S., Loewe, D., Mollenkopf, H.-J., Vogelzang, A., Meyer-Schwesinger, C., Mittr, xFc, cker, H.-W., McEwen, G., Kaufmann, S.H.E., 2014. CXCL5-secreting pulmonary epithelial cells drive destructive neutrophilic inflammation in tuberculosis. The Journal of Clinical Investigation 124, 1268-1282.

O'Neill, J.S., Reddy, A.B., 2011. Circadian clocks in human red blood cells. Nature 469, 498-503.

Okada, K., Yano, M., Doki, Y., Azama, T., Iwanaga, H., Miki, H., Nakayama, M., Miyata, H., Takiguchi, S., Fujiwara, Y., Yasuda, T., Ishida, N., Monden, M., 2008. Injection of LPS Causes Transient Suppression of Biological Clock Genes in Rats. Journal of Surgical Research 145, 5-12.

Panda, S., Antoch, M.P., Miller, B.H., Su, A.I., Schook, A.B., Straume, M., Schultz, P.G., Kay, S.A., Takahashi, J.S., Hogenesch, J.B., 2002. Coordinated Transcription of Key Pathways in the Mouse by the Circadian Clock. Cell 109, 307-320.

Paranjpe, D.A., Sharma, V.K., 2005. Evolution of temporal order in living organisms. Journal of Circadian Rhythms 3, 7-7.

Pardee, K.I., Xu, X., Reinking, J., Schuetz, A., Dong, A., Liu, S., Zhang, R., Tiefenbach, J., Lajoie, G., Plotnikov, A.N., Botchkarev, A., Krause, H.M., Edwards, A., 2009. The Structural Basis of Gas-Responsive Transcription by the Human Nuclear Hormone Receptor REV-ERBβ. PLoS Biology 7, e1000043.

Pekovic-Vaughan, V., Gibbs, J., Yoshitane, H., Yang, N., Pathiranage, D., Guo, B., Sagami, A., Taguchi, K., Bechtold, D., Loudon, A., Yamamoto, M., Chan, J., van der Horst, G.T.J., Fukada, Y., Meng, Q.-J., 2014. The circadian clock regulates rhythmic activation of the NRF2/glutathione-mediated antioxidant defense pathway to modulate pulmonary fibrosis. Genes & Development 28, 548-560.

Peschke, E., Peschke, D., 1998. Evidence for a circadian rhythm of insulin release from perifused rat pancreatic islets. Diabetologia 41, 1085-1092.

Phillips, J.E., Peng, R., Harris, P., Burns, L., Renteria, L., Lundblad, L.K.A., Fine, J.S., Bauer, C.M.T., Stevenson, C.S., 2013. House dust mite models: Will they translate clinically as a superior model of asthma? Journal of Allergy and Clinical Immunology 132, 242-244.

Pincus, D.J., Humeston, T.R., Martin, R.J., 1997. Further studies on the chronotherapy of asthma with inhaled steroids: The effect of dosage timing on drug efficacy. Journal of Allergy and Clinical Immunology 100, 771-774.

Piotrowski, W., 2000. Cellular sources of oxidants in the lung. Int J Occup Med Environ Health 13, 369-385.

Pittendrigh, C.S., 1993. Temporal Organization: Reflections of a Darwinian Clock-Watcher. Annual Review of Physiology 55, 17-54.

Plopper, C.G., Hill, L.H., Mariassy, A.T., 1980. Ultrastructure of the Nonciliated Bronchiolar Epithelial (Clara) Cell of Mammalian Lung. III. A Study of Man with Comparison of 15 Mammalian Species. Experimental Lung Research 1, 171-180.

Podolin, P.L., Foley, J.P., Carpenter, D.C., Bolognese, B.J., Logan, G.A., Long, E., Harrison, O.J., Walsh, P.T., 2013. T cell depletion protects against alveolar destruction due to chronic cigarette smoke exposure in mice. American Journal of Physiology - Lung Cellular and Molecular Physiology 304, L312-L323.

Preitner, N., Damiola, F., Luis Lopez, M., Zakany, J., Duboule, D., Albrecht, U., Schibler, U., 2002. The Orphan Nuclear Receptor REV-ERBα Controls Circadian Transcription within the Positive Limb of the Mammalian Circadian Oscillator. Cell 110, 251-260.

Preuss, F., Tang, Y., Laposky, A.D., Arble, D., Keshavarzian, A., Turek, F.W., 2008. Adverse effects of chronic circadian desynchronization in animals in a "challenging" environment. American Journal of Physiology - Regulatory, Integrative and Comparative Physiology 295, R2034-R2040.

Prudden, J., Pebernard, S., Raffa, G., Slavin, D.A., Perry, J.J.P., Tainer, J.A., McGowan, C.H., Boddy, M.N., 2007. SUMO-targeted ubiquitin ligases in genome stability. The EMBO Journal 26, 4089-4101.

Raghuram, S., 2007. Identification of heme as the ligand for the orphan nuclear receptors REV-ERB[alpha] and REV-ERB[beta]. Nat Struct Mol Biol 14, 1207-1213.

Rahman, I., Adcock, I.M., 2006. Oxidative stress and redox regulation of lung inflammation in COPD. European Respiratory Journal 28, 219-242.

Rajendrasozhan, S., Yang, S.-R., Kinnula, V.L., Rahman, I., 2008. SIRT1, an Antiinflammatory and Antiaging Protein, Is Decreased in Lungs of Patients with Chronic Obstructive Pulmonary Disease. American Journal of Respiratory and Critical Care Medicine 177, 861-870.

Ralph, M.R., Foster, R.G., Davis, F.C., Menaker, M., 1990. Transplanted suprachiasmatic nucleus determines circadian period. Science 247, 975-978.

Rathmell, J.C., 2012. Metabolism and autophagy in the immune system: immunometabolism comes of age. Immunological reviews 249, 5-13.

Rea, M.A., 1998. Photic Entrainment of Orcadian Rhythms in rodents. Chronobiology International 15, 395-423.

Refinetti, R., 1993. Laboratory instrumentation and computing: Comparison of six methods for the determination of the period of circadian rhythms. Physiology & Behavior 54, 869-875.

Reppert, S.M., Weaver, D.R., 2002. Coordination of circadian timing in mammals. Nature 418, 935-941.

Roberts, A.W., 2005. G-CSF: A key regulator of neutrophil production, but that's not all! Growth Factors 23, 33-41.

Rochelle, L.G., Fischer, B.M., Adler, K.B., 1998. Concurrent Production of Reactive Oxygen and Nitrogen Species by Airway Epithelial Cells In Vitro. Free Radical Biology and Medicine 24, 863-868.

Roos, A.B., Berg, T., Ahlgren, K. M., Grunewald, J., Nord, M., 2014. Method for Generating Pulmonary Neutrophilia Using Aerosolized Lipopolysaccharide. J. Vis. Exp.

Rutter, J., Reick, M., Wu, L.C., McKnight, S.L., 2001. Regulation of Clock and NPAS2 DNA Binding by the Redox State of NAD Cofactors. Science 293, 510-514.

Sato, S., Sakurai, T., Ogasawara, J., Takahashi, M., Izawa, T., Imaizumi, K., Taniguchi, N., Ohno, H., Kizaki, T., 2014. A Circadian Clock Gene, Rev-erbα, Modulates the Inflammatory Function of Macrophages through the Negative Regulation of Ccl2 Expression. The Journal of Immunology 192, 407-417.

Scheiermann, C., Kunisaki, Y., Lucas, D., Chow, A., Jang, J.-E., Zhang, D., Hashimoto, D., Merad, M., Frenette, Paul S., 2012. Adrenergic Nerves Govern Circadian Leukocyte Recruitment to Tissues. Immunity 37, 290-301.

Schmidt, T.M., Chen, S.-K., Hattar, S., 2011. Intrinsically photosensitive retinal ganglion cells: many subtypes, diverse functions. Trends in neurosciences 34, 572-580.

Sender, V., Stamme, C., 2014. Lung cell-specific modulation of LPS-induced TLR4 receptor and adaptor localization. Communicative & Integrative Biology 7, e29053.

Shackelford, P.G., Feigin, R.D., 1973. Periodicity of Susceptibility to Pneumococcal Infection: Influence of Light and Adrenocortical Secretions. Science 182, 285-287.

Shin, Y., Noel, R., Banerjee, S., Kojetin, D., Song, X., He, Y., Lin, L., Cameron, M.D., Burris, T.P., Kamenecka, T.M., 2012. Small molecule tertiary amines as agonists of the nuclear hormone receptor Rev-erbα. Bioorganic & Medicinal Chemistry Letters 22, 4413-4417.

Shu, S., Ling, Z., Ye, M., Bo, L., Wang, L., Zhang, T., Chen, J., Li, T., 2011. Polydatin up-regulates clara cell secretory protein to suppress phospholipase A2 of lung induced by LPS in vivo and in vitro. BMC Cell Biology 12, 31-31.

Sibille, Y.R.H., 1990. Macrophages and polymorphonuclear neutrophils in lung disease and injury: State of the Art. Am Rev Respir Dis 144, 471–501.

Silver, Adam C., Arjona, A., Walker, Wendy E., Fikrig, E., 2012. The Circadian Clock Controls Toll-like Receptor 9-Mediated Innate and Adaptive Immunity. Immunity 36, 251-261.

Smolensky, M.H., Haus, E., 2001. Circadian rhythms and clinical medicine with applications to hypertension. American Journal of Hypertension 14, S280-S290.

Snyder, J.C., Reynolds, S.D., Hollingsworth, J.W., Li, Z., Kaminski, N., Stripp, B.R., 2010. Clara Cells Attenuate the Inflammatory Response through Regulation of Macrophage Behavior. American Journal of Respiratory Cell and Molecular Biology 42, 161-171.

Solt, L.A., Wang, Y., Banerjee, S., Hughes, T., Kojetin, D.J., Lundasen, T., Shin, Y., Liu, J., Cameron, M.D., Noel, R., Yoo, S.-H., Takahashi, J.S., Butler, A.A., Kamenecka, T.M., Burris, T.P., 2012. Regulation of circadian behaviour and metabolism by synthetic REV-ERB agonists. Nature 485, 62-68.

Spengler, M.L., Kuropatwinski, K.K., Comas, M., Gasparian, A.V., Fedtsova, N., Gleiberman, A.S., Gitlin, I.I., Artemicheva, N.M., Deluca, K.A., Gudkov, A.V., Antoch, M.P., 2012. Core circadian protein CLOCK is a positive regulator of NF-κB–mediated transcription. Proceedings of the National Academy of Sciences 109, E2457–E2465.

Spengler, M.L., Kuropatwinski, K.K., Schumer, M., Antoch, M.P., 2009. A serine cluster mediates BMAL-dependent CLOCK phosphorylation and degradation. Cell cycle (Georgetown, Tex.) 8, 4138-4146.

Stapleton, C.M., Jaradat, M., Dixon, D., Kang, H.S., Kim, S.-C., Liao, G., Carey, M.A., Cristiano, J., Moorman, M.P., Jetten, A.M., 2005. Enhanced susceptibility of staggerer (RORαsg/sg) mice to lipopolysaccharide-induced lung inflammation. American Journal of Physiology - Lung Cellular and Molecular Physiology 289, L144-L152.

Stephenson, J.J., Cai, Q., Mocarski, M., Tan, H., Doshi, J.A., Sullivan, S.D., 2015. Impact and factors associated with nighttime and early morning symptoms among patients with chronic obstructive pulmonary disease. International Journal of Chronic Obstructive Pulmonary Disease 10, 577-586.

Stojkovic, K., Wing, S.S., Cermakian, N., 2014. A central role for ubiquitination within a circadian clock protein modification code. Frontiers in Molecular Neuroscience 7, 69.

Straif, K., Baan, R., Grosse, Y., Secretan, B., Ghissassi, F.E., Bouvard, V., Altieri, A., Benbrahim-Tallaa, L., Cogliano, V., 2007. Carcinogenicity of shift-work, painting, and fire-fighting. The Lancet Oncology 8, 1065-1066.

Sukumaran, S., Jusko, W.J., DuBois, D.C., Almon, R.R., 2011. Light-dark oscillations in the lung transcriptome: implications for lung homeostasis, repair, metabolism, disease, and drug action. Journal of Applied Physiology 110, 1732-1747.

Summers, C., Singh, N.R., White, J.F., Mackenzie, I.M., Johnston, A., Solanki, C., Balan, K.K., Peters, A.M., Chilvers, E.R., 2014. Pulmonary retention of primed neutrophils: a novel protective host response, which is impaired in the acute respiratory distress syndrome. Thorax.

Sun, J., Brand, M., Zenke, Y., Tashiro, S., Groudine, M., Igarashi, K., 2004. Heme regulates the dynamic exchange of Bach1 and NF-E2-related factors in the Maf transcription factor network. Proceedings of the National Academy of Sciences of the United States of America 101, 1461-1466.

Takahashi, J.S., 1995. Molecular Neurobiology and Genetics of Circadian Rhythms in Mammals. Annual Review of Neuroscience 18, 531-553.

Takizawa, H., 1998. Airway epithelial cells as regulators of airway inflammation (Review). International Journal of Molecular Medicine 1, 367-445.

Talhout, R., Schulz, T., Florek, E., Van Benthem, J., Wester, P., Opperhuizen, A., 2011. Hazardous Compounds in Tobacco Smoke. International Journal of Environmental Research and Public Health 8, 613-628.

Tomita, T., Sakurai, Y., Ishibashi, S., Maru, Y., 2011. Imbalance of Clara cell-mediated homeostatic inflammation is involved in lung metastasis. Oncogene 30, 3429-3439.

Trump, R.P., Bresciani, S., Cooper, A.W.J., Tellam, J.P., Wojno, J., Blaikley, J., Orband-Miller, L.A., Kashatus, J.A., Boudjelal, M., Dawson, H.C., Loudon, A., Ray, D., Grant, D., Farrow, S.N., Willson, T.M., Tomkinson, N.C.O., 2013. Optimized Chemical Probes for REV-ERBα. Journal of Medicinal Chemistry 56, 4729-4737.

Tsai, W.C., Strieter, R.M., Mehrad, B., Newstead, M.W., Zeng, X., Standiford, T.J., 2000. CXC Chemokine Receptor CXCR2 Is Essential for Protective Innate Host Response in Murine Pseudomonas aeruginosaPneumonia. Infection and Immunity 68, 4289-4296.

Tsui, K.-H., Chung, L.-C., Feng, T.-H., Lee, T.-Y., Chang, P.-L., Chen, W.-T., Juang, H.-H., 2015. Divergent effect of liver X receptor agonists on prostate-specific antigen expression is dependent on androgen receptor in prostate carcinoma cells. The Prostate 75, 603-615.

Vasu, V.T., Cross, C.E., Gohil, K., 2009. Nr1d1, an important circadian pathway regulatory gene, is suppressed by cigarette smoke in murine lungs. Integrative cancer therapies 8, 321-328.

Vlahos, R., Bozinovski, S., 2014. Recent advances in pre-clinical mouse models of COPD. Clinical Science (London, England : 1979) 126, 253-265.

Wang, X.-Y., Keefe, K.M., Jensen-Taubman, S.M., Yang, D., Yan, K., Linnoila, R.I., 2012. Novel Method for Isolation of Murine Clara Cell Secretory Protein-Expressing Cells with Traces of Stemness. PLoS ONE 7, e43008.

Wang, Y., Dasso, M., 2009. SUMOylation and deSUMOylation at a glance. Journal of Cell Science 122, 4249-4252.

Watson, T.M., Reynolds, S.D., Mango, G.W., Boe, I.-M., Lund, J., Stripp, B.R., 2001. Altered lung gene expression in CCSP-null mice suggests immunoregulatory roles for Clara cells, pp. L1523-L1530.

Webb, D.R., 2014. Animal models of human disease: Inflammation. Biochemical Pharmacology 87, 121-130.

Welsh, D.K., Takahashi, J.S., Kay, S.A., 2010. Suprachiasmatic Nucleus: Cell Autonomy and Network Properties. Annual Review of Physiology 72, 551-577.

Westphalen, K., Gusarova, G.A., Islam, M.N., Subramanian, M., Cohen, T.S., Prince, A.S., Bhattacharya, J., 2014. Sessile alveolar macrophages communicate with alveolar epithelium to modulate immunity. Nature 506, 503-506.

Xu, Y.-Q., Zhang, D., Jin, T., Cai, D.-J., Wu, Q., Lu, Y., Liu, J., Klaassen, C.D., 2012. Diurnal Variation of Hepatic Antioxidant Gene Expression in Mice. PLoS ONE 7, e44237.

Yan, J., Wang, H., Liu, Y., Shao, C., 2008. Analysis of Gene Regulatory Networks in the Mammalian Circadian Rhythm. PLoS Comput Biol 4, e1000193.

Yang, S.-R., Wright, J., Bauter, M., Seweryniak, K., Kode, A., Rahman, I., 2007. Sirtuin regulates cigarette smoke-induced proinflammatory mediator release via RelA/p65 NF-κB in macrophages in vitro and in rat lungs in vivo: implications for chronic inflammation and aging. American Journal of Physiology - Lung Cellular and Molecular Physiology 292, L567-L576.

YangGuang, W.J., HinsonMaurice D., FernandoAmal P., SenguptaShaon, BiswasChhanda, LaPing, and DenneryPhyllis A., 2014. Oxidative Stress and Inflammation Modulate Rev-erbα Signaling in the Neonatal Lung and Affect Circadian Rhythmicity. Antioxidants & Redox Signaling 21, 17-32.

Yao, H., Sundar, I.K., Huang, Y., Gerloff, J., Sellix, M.T., Sime, P.J., Rahman, I., 2015. Disruption of Sirtuin 1–Mediated Control of Circadian Molecular Clock and Inflammation in Chronic Obstructive Pulmonary Disease. American Journal of Respiratory Cell and Molecular Biology 53, 782-792.

Yin, L., Joshi, S., Wu, N., Tong, X., Lazar, M.A., 2010. E3 ligases Arf-bp1 and Pam mediate lithium-stimulated degradation of the circadian heme receptor Rev-erbα. Proceedings of the National Academy of Sciences of the United States of America 107, 11614-11619.

Yin, L., Lazar, M.A., 2005. The Orphan Nuclear Receptor Rev-erbα Recruits the N-CoR/Histone Deacetylase 3 Corepressor to Regulate the Circadian Bmal1 Gene. Molecular Endocrinology 19, 1452-1459.

Yin, L., Wang, J., Klein, P.S., Lazar, M.A., 2006. Nuclear Receptor Rev-erbα Is a Critical Lithium-Sensitive Component of the Circadian Clock. Science 311, 1002-1005.

Yin, L., Wu, N., Curtin, J.C., Qatanani, M., Szwergold, N.R., Reid, R.A., Waitt, G.M., Parks, D.J., Pearce, K.H., Wisely, G.B., Lazar, M.A., 2007. Rev-erbα, a Heme Sensor That Coordinates Metabolic and Circadian Pathways. Science 318, 1786-1789.

Yona, S., Kim, K.-W., Wolf, Y., Mildner, A., Varol, D., Breker, M., Strauss-Ayali, D., Viukov, S., Guilliams, M., Misharin, A., Hume, D.A., Perlman, H., Malissen, B., Zelzer, E., Jung, S., 2013. Fate mapping reveals origins and dynamics of monocytes and tissue macrophages under homeostasis. Immunity 38, 79-91.

Yoo, S.-H., Yamazaki, S., Lowrey, P.L., Shimomura, K., Ko, C.H., Buhr, E.D., Siepka, S.M., Hong, H.-K., Oh, W.J., Yoo, O.J., Menaker, M., Takahashi, J.S., 2004. PERIOD2::LUCIFERASE real-time reporting of circadian dynamics reveals persistent circadian oscillations in mouse peripheral tissues. Proceedings of the National Academy of Sciences of the United States of America 101, 5339-5346.

Yoshida, K., Hashimoto, T., Sakai, Y., Hashiramoto, A., 2014. Involvement of the Circadian Rhythm and Inflammatory Cytokines in the Pathogenesis of Rheumatoid Arthritis. Journal of Immunology Research 2014, 6.

Zamir, I., Zhang, J., Lazar, M.A., 1997. Stoichiometric and steric principles governing repression by nuclear hormone receptors. Genes & Development 11, 835-846.

Zhang, R., Lahens, N.F., Ballance, H.I., Hughes, M.E., Hogenesch, J.B., 2014. A circadian gene expression atlas in mammals: Implications for biology and medicine. Proceedings of the National Academy of Sciences 111, 16219-16224.

Zhang, Y., Fang, B., Emmett, M.J., Damle, M., Sun, Z., Feng, D., Armour, S.M., Remsberg, J.R., Jager, J., Soccio, R.E., Steger, D.J., Lazar, M.A., 2015. Discrete functions of nuclear receptor Rev-erbα couple metabolism to the clock. Science.

Zhao, X., Hirota, T., Han, X., Cho, H., Chong, L.-W., Lamia, K., Liu, S., Atkins, Annette R., Banayo, E., Liddle, C., Yu, Ruth T., Yates, John R., III, Kay, Steve A., Downes, M., Evans, Ronald M., 2016. Circadian Amplitude Regulation via FBXW7-Targeted REV-ERBα Degradation. Cell 165, 1644-1657.

Zhu, B., Gates, Leah A., Stashi, E., Dasgupta, S., Gonzales, N., Dean, A., Dacso, Clifford C., York, B., O'Malley, Bert W., 2015. Coactivator-Dependent Oscillation of Chromatin Accessibility Dictates Circadian Gene Amplitude via REV-ERB Loading. Molecular Cell 60, 769-783.

Zschiedrich, I., Hardeland, U., Krones-Herzig, A., Berriel Diaz, M., Vegiopoulos, A., Müggenburg, J., Sombroek, D., Hofmann, T.G., Zawatzky, R., Yu, X., Gretz, N., Christian, M., White, R., Parker, M.G., Herzig, S., 2008. Coactivator function of RIP140 for NFκB/RelA-dependent cytokine gene expression. Blood 112, 264-276.

Zylka, M.J., Shearman, L.P., Weaver, D.R., Reppert, S.M., 1998. Three period Homologs in Mammals: Differential Light Responses in the Suprachiasmatic Circadian Clock and Oscillating Transcripts Outside of Brain. Neuron 20, 1103-1110.